A REVISED MODEL FOR RADIATION DOSIMETRY IN THE HUMAN GASTROINTESTINAL TRACT

A Dissertation

by

MD. NASIR UDDIN BHUIYAN

Submitted to the Office of Graduate Studies of
Texas A&M University
in partial fulfillment of the requirements for the degree of

DOCTOR OF PHILOSOPHY

August 2003

Major Subject: Nuclear Engineering

A REVISED MODEL FOR RADIATION DOSIMETRY IN THE HUMAN GASTROINTESTINAL TRACT

A Dissertation

by

MD. NASIR UDDIN BHUIYAN

Submitted to Texas A&M University
in partial fulfillment of the requirements
for the degree of

DOCTOR OF PHILOSOPHY

Approved as to style and content by:

John W. Poston, Sr. (Chair of Committee)	John R. Ford, Jr. (Member)
Ian Scott Hamilton (Member)	Michael Walker (Member)
	William E. Burchill (Head of Department)

August 2003

Major Subject: Nuclear Engineering

ABSTRACT

A Revised Model for Radiation Dosimetry in the Human Gastrointestinal Tract.

(August 2003)

Md. Nasir Uddin Bhuiyan, B.Sc.; M.Sc., University of Dhaka;

M.S., Texas A&M University

Chair of Advisory Committee: Dr. John W. Poston, Sr.

A new model for an adult human gastrointestinal tract (GIT) has been developed for use in internal dose estimations to the wall of the GIT and to the other organs and tissues of the body from radionuclides deposited in the lumenal contents of the five sections of the GIT. These sections were the esophagus, stomach, small intestine, upper large intestine, and the lower large intestine. The wall of each section was separated from its lumenal contents. Each wall was divided into many small regions so that the histologic and radiosensitive variations of the tissues across the wall could be distinguished. The characteristic parameters were determined based on the newest information available in the literature. Each of these sections except the stomach was subdivided into multiple subsections to include the spatiotemporal variations in the shape and characteristic parameters. This new GIT was integrated into an anthropomorphic phantom representing both an adult male and a larger-than-average adult female. The current phantom contains 14 different types of tissue. This phantom was coupled with the MCNP 4C Monte Carlo simulation package. The initial design and coding of the phantom and the Monte Carlo treatment employed in this study were

validated using the results obtained by Cristy and Eckerman (1987). The code was used for calculating specific absorbed fractions (SAFs) in various organs and radiosensitive tissues from uniformly distributed sources of fifteen monoenergetic photons and electrons, 10 keV - 4 MeV, in the lumenal contents of the five sections of the GIT. The present studies showed that the average photon SAFs to the walls were significantly different from that to the radiosensitive cells (stem cells) for the energies below 50 keV. Above 50 keV, the photon SAFs were found to be almost constant across the walls. The electron SAF at the depth of the stem cells was a small fraction of the SAF routinely estimated at the contents-mucus interface. Electron studies showed that the "self-dose" for the energies below 300 keV and the "cross-dose" below 2 MeV were only from bremsstrahlung and fluorescent radiations at the depth of the stem cells and were not important.

DEDICATION

To my parents,

Ali Ahmed Bhuiyan and Salma Ali,

to my wife,

Beethi,

to my children,

Sadia and Naif,

and

to my friend and mentor,

Dr. John W. Poston, Sr.

ACKNOWLEDGEMENTS

I wish to express my appreciation to Dr. John W. Poston, Sr., committee chairman, for his confidence in my abilities. He encouraged me, supported me, and allowed me to go ahead with this research and guided me during its planning and execution. His suggestions, criticisms, corrections, and compliments made this endeavor possible.

I would like to thank Dr. John R. Ford, Jr., member of my graduate committee, whose comments and constructive criticisms were important contributions to this research work.

I would like to thank Dr. Ian Scott Hamilton, member of my graduate committee, for his comments and support throughout my doctoral studies.

I would like to thank Dr. Michael Walker, member of my graduate committee, for his comments and suggestions regarding this dissertation.

I would like to thank Dr. Stewart C. Bushong, professor, Baylor College of Medicine, for his support and encouragement toward the successful completion of this work. Thanks to him for reading and criticizing an early draft of this dissertation.

Special thanks to Jennifer Watson, an undergraduate student, for helping me to arrange and process the data.

Thanks to my colleague David Hearne, Baylor College of Medicine, for assisting me with the typing of this manuscript.

TABLE OF CONTENTS

Page

Page

LIST OF FIGURES

Page

Page

LIST OF TABLES

Page

Page

LIST OF ACRONYMS

AC	Ascending Colon
AF	Absorbed Fraction
ALI	Annual Limit on Intake
CSDA	Continuous Slowing Down Approximation
DAC	Derived Air Concentration
DC	Descending Colon
EGS	Electron Gamma Shower
ESP	Esophagus
ETRAN	Electron Transport
GIT	Gastrointestinal Tract
HAT	Human Alimentary Tract
ICRP	International Commission on Radiological Protection
ICRU	International Commission on Radiation Units and Measurements
ITS	Integrated TIGER Series
LES	Lower Esophageal Sphincter
LI	Large Intestine
LLI	Lower Large Intestine
MCNP	Monte Carlo N-Particle
MIRD	Medical Internal Radiation Dose
MPBB	Maximum Permissible Body Burden

MPC	Maximum Permissible Concentration
NBS	National Bureau of Standards
ORNL	Oak Ridge National Laboratory
RSC	Recto-Sigmoid Colon
SAF	Specific Absorbed Fraction
SI	Small Intestine
ST	Stomach
TC	Transverse Colon
TTB	Thick-Target Bremsstrahlung
ULI	Upper Large Intestine

INTRODUCTION

HISTORICAL PERSPECTIVE

Evaluation of radiation dose due to internally deposited radionuclides involves careful specification of the exposure geometry (e.g., the human body) and the irradiation conditions. Because of their complexity, radiation transport and energy deposition in the body are usually simulated using a Monte Carlo computer code. The accuracy of these calculations depends upon the ability to model accurately the body and the radiation environment, and the Monte Carlo treatment employed.

Internal dosimetry calculations have traditionally used simple models of organs and the whole body when attempting to assess doses from internally deposited radionuclides. The first models reported widely were those used in the calculations of maximum permissible body burden (MPBB) and maximum permissible concentration (MPC) values found in ICRP Publication 2 (ICRP 1959) and National Bureau of Standards Handbook 69 (NBS 1959). In these models, the whole body and organs within were represented by a number of spheres of different radii. The ICRP specified 30 cm for the radius of the whole body. It is interesting to note that the same 30 cm radius is used for the entire gastrointestinal tract (GIT), the small intestine (SI), and muscle. The other three sections of the GIT — the stomach (ST), the upper large intestine (ULI), and the lower large intestine (LLI) were the spheres with effective radii of 10, 5, and 5 cm, respectively. Later the radii of the GIT and the SI were reduced to 10 cm based on Eve's review (1966). A monoenergetic photon source was assumed to be at the center of each

This dissertation follows the style and format of Health Physics.

of these spheres in the calculation of "effective absorbed energy" for photons. By placing the source at the center of the spherical organ, the calculation was simplified but the absorbed energy was over estimated.

There was need for a more detailed description of the organs in which specific regions or structures within the organ were delineated as radiation use increased and as more was understood about the biodistribution of radioactive materials in an organ. In the late 1950's and 1960's, high-speed digital computers empowered many research groups to develop simple phantoms to be used in internal dose estimations in conjunction with Monte Carlo computer codes for photon irradiation (Ellet et al. 1964, 1965; Fisher and Snyder 1966, 1967; Snyder 1967; Brownell et al. 1968; Snyder et al. 1969). W. S. Snyder at the Oak Ridge National Laboratory (ORNL) led a major effort. In the 1960's, he and his colleagues developed a number of phantoms for use in dose calculations using Monte Carlo techniques. Although he was specifically interested in internal radiation, his models were useful for external radiation sources as well. The early models were right circular cylinders representing the trunk of an adult male. As capabilities developed, they added a few regions inside the cylinder representing specific organs. For example, representations of the ovaries and the thyroid gland were two of the first organs added to the cylindrical phantom. These phantoms were homogenous in terms of mass density and elemental composition. The skeleton and the lungs were not defined in terms of their different mass densities and elemental compositions.

Snyder and coworkers developed the first heterogeneous phantom in 1969 at ORNL. This phantom consisted of three tissue types representing the tissues of the

skeleton, the lung, and the remainder (soft tissue); each type was assigned a different mass density and elemental composition. Twenty-two homogeneous internal organs were included in the design. The regions/organs within the phantom were described as mathematical regions, and were fashioned as simple geometrical shapes approximating the real shapes. The organs were located at the approximately correct locations in the body. Even though the organ volumes and the structural parameters were selected to simulate the data of Reference Man in ICRP publication 23 (1975), Snyder chose to call the phantom a "standard man approximation." This phantom ultimately became known as the "MIRD phantom." This phantom, in conjunction with a Monte Carlo transport code, was used in many dose calculations that included the calculations performed for the International Commission on Radiological Protection (ICRP) and the Medical Internal Radiation Dose (MIRD) Committee (Snyder et al. 1969; Snyder et al. 1974; ICRP 1975; ICRP 1979). In those calculations, twelve monoenergetic photons with energies ranging from 0.01 to 4 MeV were considered. The photons were distributed uniformly in selected organs termed source organs.

In the first heterogeneous phantom, each of the four sections of the GIT was modeled as a soft tissue region without separating the contents from the wall. Later, in 1974, Snyder et al. (1974) made significant improvements in the phantom. In this improved phantom, the ST, ULI, and the LLI were modeled as "organs with walls and contents" but no change was made to the SI. Improvements also were made to the head section, the leg regions, the male genitalia, the scapulae and the clavicles. The skin was added to this phantom. Over the years, several organs and body regions of this phantom

have been modified to support new developments in diagnostic and therapeutic nuclear medicine. However, the Snyder phantom (1974) remains the standard for internal dose estimations.

The "adult male" phantom described by Cristy (1980) is essentially the Snyder adult phantom (1974) and includes several modifications. Female breasts were added to the trunk; thus the Cristy phantom represents both adult male and a larger than average adult female (i.e., the Cristy phantom is hermaphroditic). The improved heart model of Coffey (1978) was fitted into the trunk. The lungs were redesigned to accommodate the new heart; the difference in size between right and left lungs—not represented in the Snyder phantom—was incorporated into the new design. The head model was made more realistic by using the ideas of Hwang, Shoup, and Poston (1976). The gall bladder designed by Hwang et al. (1976) was added. The entire GIT remained unchanged except in the descending colon to eliminate a small overlap with the pelvic skeleton and to make the wall thickness uniform. Other minor changes were made, not based on the anatomic data but for maintaining consistencies with pediatric phantoms modeled by Cristy (1980). The tissue types for skeletal, lung, and soft tissue, and the elemental composition and the mass density of each were kept unchanged.

In 1987, Cristy and Eckerman made small changes in the volumes of the breasts and the uterus of the Cristy phantom (1980). They used the same tissue types but employed different elemental compositions and mass densities for skeletal tissue and the soft tissue on the basis of the data in Table 105 of ICRP Publication 23. The lung was unchanged. As a result of these changes, the organ masses and the whole-body mass

were slightly different from those in the Cristy phantom (1980). This phantom was used with a Monte Carlo transport code for calculating "specific absorbed fractions" (SAFs) in various target organs from the same 12 monoenergetic photon sources in various source organs. The calculation methods were similar to those used in Snyder et al. (1978) for an adult but the dosimetry for radiosensitive tissues in the skeleton was different. Cristy and Eckerman applied the dosimetry methods developed by Spiers and coworkers for beta-emitting radionuclides deposited in bone. The latest ICRP recommendations on radiation protection published in ICRP publication 60 (1991) are based on Cristy and Eckerman calculations (1987).

A BRIEF REVIEW OF THE GASTROINTESTINAL TRACT (GIT) MODEL

Over the years, many changes have been made to the individual organ models of the Snyder phantom (1974) to make the models more realistic. But the GIT model remains the same since the model developed by Snyder et al. in 1974. As mentioned before, the SI was modeled as a solid soft tissue region without delineation of the wall and its contents. Many folds found in the SI were not considered in this model. The other three sections of the GIT were modeled as "organs with walls and contents." The entire wall of each of these sections was treated as a single tissue layer. Thus, only average quantities (e.g., average dose, average SAF, etc.) to the wall can be obtained using this model. These calculations were incapable of providing a distribution across the wall. The distribution information was desired for two reasons: tissues forming the wall have varying degrees of radiosensitivity and the locations of these tissues vary within and between individuals.

The epithelial cells, lining the GIT mucosa, are believed to be at risk for radiation induced malignancy as these cells are the most radiosensitive cells in the wall. The distinction among the tissue types in the wall may not have been important in the earlier models because those were used only for photon dose calculations. Dose variations across the wall were not significant for photons if the wall thickness was smaller than the mean free paths of the photons under consideration, i.e., for the photon energies >15 keV. But for the weakly-penetrating radiations (beta, conversion electrons, Auger electrons, low-energy x-rays)[*], the dose varies largely because of their limited range in tissue. Bhuiyan (2000) showed that the dose varies by several orders of magnitude over a small fraction of a centimeter of wall thickness for low-energy electrons. Obviously, the earlier models are not suitable for electron dose calculations. It should be noted that the photon-induced electrons (secondary electrons) were not transported in the early calculations with photon sources. The energies of the secondary electrons were assumed to be locally deposited. Poston et al. (1996b) showed that electron transport was not important to those calculations.

Until recently, no attempt has been made to perform calculations with electron emitting sources deposited in the lumen contents of the GIT because of the difficulties in modeling the complex structure of GIT and the complexity in the electron transport calculations. The ICRP "one-half approximation" (1979) continues to be used for estimates of dose from weakly penetrating sources deposited internally in the walled

[*]The ICRP (1979) calls these radiations "non-penetrating" but we have chosen another term that more clearly express the penetrating nature of beta radiation.

organs. Many calculations, including those performed for the ICRP and MIRD Committee, were based on this assumption. Recent calculations using the GIT models with Monte Carlo electron transport codes showed that this assumption for the walled organs is overly simplified for many useful electron energies (< 500 keV) (Poston et al. 1996b, Stubbs et al. 1998, Bhuiyan 2000). With the development of improved radiation transport codes, especially those available to transport beta and electron radiation, many difficult modeling tasks have been revisited.

Poston et al. (1996a) described a model of the GIT for use in dose calculations for radiation uniformly distributed in the contents of the GIT. The goal of their research was to define the sensitive cell region in the tract. This simple model was comprised of right circular cylinders representing sections of the tract located inside the heterogeneous phantom. Sections of the tract wall were defined by 10 regions, each of 100-μm thickness, over the region from the wall-contents interface to 1,000 μm. These models were used in the calculation of photon and electron absorbed fractions for a number of discrete energies. The annual limit on intake (ALI) for a single radionuclide was recalculated to demonstrate the effect of the improved absorbed fraction values on internal dose assessment. In this specific case, the revised ALI was a factor of three higher (less restrictive) than the value in ICRP Publication 30 (1979). However, even though there were a number of radionuclides for which the committed dose equivalent to a section of the GIT was the controlling organ, no additional calculations have been made. The effects of this GIT model on the other organs were not investigated.

There are a number of shortcomings of this model. The characteristic parameters, such as the length, wall thickness, and lumen radius, were very different from the real anatomic data. For example, The SI was modeled as a right circular cylinder of length 21 cm with a total volume of 265 cm^3 and contents volume of 102.5 cm^3, equivalent to one-fourth of the total small intestine. Thus, a wall thickness of 0.754 cm and a lumen radius of 1.246 cm were estimated. In reality, the *in-vivo* length and the wall thickness of the SI are about 300 cm and 0.3 cm, respectively. The results were not adjusted for these deviations. The lumens were modeled as full of contents. In reality, a portion of the lumen contains contents, while the rest is empty. Empty lumen is closed as the wall collapses under pressure. Obviously, the dose to the surrounding wall of a full lumen is higher than that of a partially-filled or empty lumen. Multiple folds in the SI were not considered. The effect of these folds to the wall dose may be ignored for electrons. However for photons, the "cross-doses" from the sources in the nearby folds may be significant.

Stubbs et al. (1998) modeled the GIT for use in calculating radiation absorbed dose to the wall. In this model, the GIT was composed of three isolated sections — the ST, SI, and large intestine or colon — surrounded by vacuum. The contents and the wall of each section were defined. The wall plus contents of the SI and the colon were represented as two coaxial circular cylinders 10 cm in length. The volume within the inner cylinder represented the lumen. The volume between the inner and the outer cylinders represented the wall. The lumen radii and the wall thicknesses were taken from the anatomical data for the ICRP Reference Man (1975). The same Cristy and Eckerman

adult ST model (1987) was used for the ST. The ST was described by two upright concentric ellipsoids, with the inner representing the lumen and the shell volume between the two representing the ST wall. Each of the organ walls were divided into many small segments so that Monte Carlo simulation result could be obtained practically at every point in the wall. The stem cells found lining either glands (ST, colon) or the base of villi (SI) were recognized to be the cells at risk to radiation. The position of the stem cells was determined based on anatomical data available in the literature. The absorbed dose at the position of the stem cells was regarded as the dose to the wall, instead of dose at the contents-wall interface which is normally reported. Stubbs et al. concluded, as did Poston et al. (1996a, 1996b), that the ICRP assumption for weakly-penetrating radiations for hollow organs is overly conservative. They used this model to calculate the "S values" (in units of Gy/Bq-s) as a function of distance from the contents-mucus interface only for four radionuclides important in nuclear medicine. The radionuclides were Y-90, Tc-99m, I-123, and I-131. Except for Y-90, the remaining three emit both penetrating and the weakly-penetrating radiations.

The Stubbs et al. (1998) model lacked the ability to account for the doses from scattered radiation and from sources in the nearby folds as each GIT section was modeled as an isolated segment surrounded by void. The scattered doses and the "cross-doses" may be insignificant when compared to the "self-doses" for electron sources but become significant for photon sources. Thus, this model was not suitable for radionuclides emitting photons. The lumens were full of contents in this model.

Adjustments were not made for the lack of appropriate source concentrations and for other deviations, such as length, diameter, and wall thickness.

More recently, an improved, but very simple, geometric model for the SI has been developed and used in the study of electron energy deposition in the wall of the GIT (Bhuiyan 2000). Results were obtained using this model for more than 50 monoenergetic electron energies in the range 10 keV to 500 keV. The wall was divided into many small regions. Depth-dose profiles were developed for each of the energies studied. The results could be used to determine doses practically at any location in the wall for any electron energy between 10 and 500 keV. Electron transport studies using the MCNP4A Monte Carlo simulation package (Briesmeister 1993) and a new model of the SI showed that only a small fraction of the available energy reaches the critical cells for monoenergetic electron sources in the contents of the tract ranging in energy from 10-500 keV. Normally, the absorbed dose at the wall-contents interface is reported as the dose to the wall. The results of these calculations indicated this practice should be discontinued and should be replaced by reporting the dose to the stem cell population. For electron energies below about 330 keV, the only contribution to the absorbed dose at the stem cell position came from bremsstrahlung. For higher energy electrons (i.e., 330 keV – 500 keV), the dose distribution curves were dominated by monoenergetic electrons at the depth of stem cells.

The effects on the dose due to the variations, observed within and between individuals, in the characteristic parameters of the SI, namely lumen radius and wall-thickness, also were studied using this model. The study showed that the effect of the

wall-thickness variations on the doses is indiscernible but the effect of the variation in the lumen radius is significant to the wall doses. This implies that the dosimetric quantities such as S values in units of Gy/Bq-s, SAF values in kg^{-1}, and absorbed fractions (AFs), depend strongly on source concentration (Bq/cm^3) or on the volume of the contents. Very often, in dosimetric calculations, the volume of the contents is ignored.

Bhuiyan (2000) modeled the SI as a 10 cm long isolated segment surrounded by void and described the SI model by a set of right circular cylinders. The structural parameters were determined from literature review. The lumen was assumed to be full of contents. Corrections were not made for the high source concentrations in the lumen. However, this model could not be used for photons and high-energy electrons with ranges greater than the wall thickness.

Jönsson et al. (2002) presented an improved model of the SI for calculation of the absorbed dose to the radiosensitive crypt cells in the SI wall from sources in the wall and the contents. The absorbed dose calculation included contributions of both self-dose and cross-dose from neighboring loops, factors not incorporated before into dosimetric models of the SI. They simulated the SI by using 19 circular cylinders. These cylinders were hexagonally arranged. Each cylinder consisted of two concentric cylinders, where the inner cylinder, 2.5 cm in diameter, represented the contents and the volume between the inner and the outer represented the wall. They used two wall thicknesses, 0.3 cm and 0.6 cm, for the calculations. Each cylinder, except the cylinder located at the center of the hexagon, was 20 cm in length. The central cylinder was taken to be 3 m in length.

Sources were uniformly distributed in the contents and the walls. Total absorbed dose, obtained by adding the self-dose and the cross-dose from the sources in both wall and contents, were calculated only for the central cylinder. The calculations were performed, using EGS4 Monte Carlo simulation package, for 10 monoenergetic electrons, 50 keV–10 MeV, and for radionuclides ^{99m}Tc, ^{111}In, ^{131}I, ^{67}Ga, ^{90}Y, and ^{211}At. They found that the self-dose from the wall was considerably greater than the self-dose from the contents and the cross-dose from the wall and the contents except for high electron energies. For the radionuclides investigated and the electrons in the range 100-200 keV and 8-10 MeV, the cross-dose was found to be higher than the self-dose from the contents. As in earlier models, the lumens were full of contents in this model. Adjustments were not made for the lack of appropriate source concentrations. Except for ^{90}Y, all other radionuclides investigated have photon components in their emission spectra. This model was not suitable for photon dosimetry as the SI was surrounded by void. Energy from alpha particles emitted from ^{211}At was considered to be locally absorbed.

The models described above have not provided a satisfactory rendition of the GIT. While the results obtained from these calculations provide significant insight into energy deposition in the wall, the fact remains that there is no comprehensive model of the GIT, especially the SI, for use in internal dose assessments for both electrons and photons for a broad spectrum of energy.

The calculations described above simulated only a small segment of the SI and ignored the influence of the "folded nature" of this section of the GIT. Therefore, a more complete model of the SI, as well as of the other sections of the GIT, is needed to bring

dosimetry of these walled organs to the same level as that of other organs of the body. It is noted that the esophagus (ESP) has not been considered as a section of the GIT in any of the GIT models developed thus far. The latest ICRP recommendations introduced specific risk estimates and tissue weighting factors, w_T, for radiation-induced cancer of the ES, ST and colon (ULI and LLI) (ICRP 1991), requiring dose estimations for these organs. Thus, a careful effort has been undertaken to remodel the entire GIT with all histologic, anatomic, and physiologic features pertinent to both photon and electron dosimetry for all energies.

The new GIT model developed in this study is suitable for the dose estimation of all organs, including the GIT-wall and -contents, from radioactive sources, emitting penetrating and/or weakly penetrating radiations having any energy, deposited internally in the lumen of the GIT. This GIT is positioned at the right place in a phantom which is similar to the adult phantom of Cristy and Eckerman (1987) but with different elemental compositions and mass densities for almost all of the organs.

This new GIT model has five sections representing the ES, ST, SI, ULI, and LLI. The wall of each section is separated from its lumen contents. Sources are uniformly distributed in the contents. The contents and wall of each are divided into many small regions so that the dose distribution inside and outside of the source contents of various geometric shapes can be obtained. The analytical calculation of the dose distribution of a complex geometric shape in a complex exposure geometry such as the human body may be impossible, especially for electrons. The shape, size, and the location for each section are more anatomically structured in this model. The characteristic parameters are

determined based on the newest information available to better approximate the true anatomic values. Each section except the ST consists of a number of subsections so that the spatiotemporal variations in the structure can be delineated in the model. The model is described in detail in the next section.

THE REVISED GASTROINTESTINAL TRACT (GIT) MODEL

INTRODUCTION

A new model for an adult human gastrointestinal tract (GIT) has been developed for use in internal dose assessments for the body organs including the GIT from radioactive sources in the lumen contents. The new GIT model is intended for use in the Monte Carlo transport calculations of both penetrating (gamma, x-rays) and weakly-penetrating radiations (beta, conversion electrons, Auger electrons) having any energy. The histologic, anatomic, and physiologic features of the GIT have been investigated. The features pertinent to both photon and electron dosimetry have been delineated in this GIT model. This model is a significant improvement on the earlier models, discussed in the previous section. In those models, many relevant features had been omitted due to difficulties in modeling those features.

The new GIT model is integrated into an anthropomorphic adult phantom which is similar but not identical to the adult male phantom of Cristy and Eckerman (1987). There are a number of differences between these two phantoms: (1) the new phantom is composed of fourteen different tissue types including the same three tissues used in Cristy and Eckerman adult phantom (1987) for lung, skeleton and soft tissue; (2) a small portion of the heart that is intercepted by the esophagus is excluded, and the pancreas is slightly shifted to accommodate the duodenum; (3) the GIT is redesigned to include more structural details pertinent to both photon and electron dosimetry for all energies. This phantom (Figs. 1-6) is surrounded by air instead of void for the Cristy and

Eckerman phantom (1987). Adrenals, thymus, gall bladder, and spleen are not included in this phantom as these organs are not important for internal dose estimations.

Frontal and lateral views of the phantom sectioned along the midlines (y = 0 and x = 0) are shown in Fig. 1 and Fig. 2, respectively. Transverse views of the phantom sectioned along different transverse planes are shown in the Figs. 3-6.

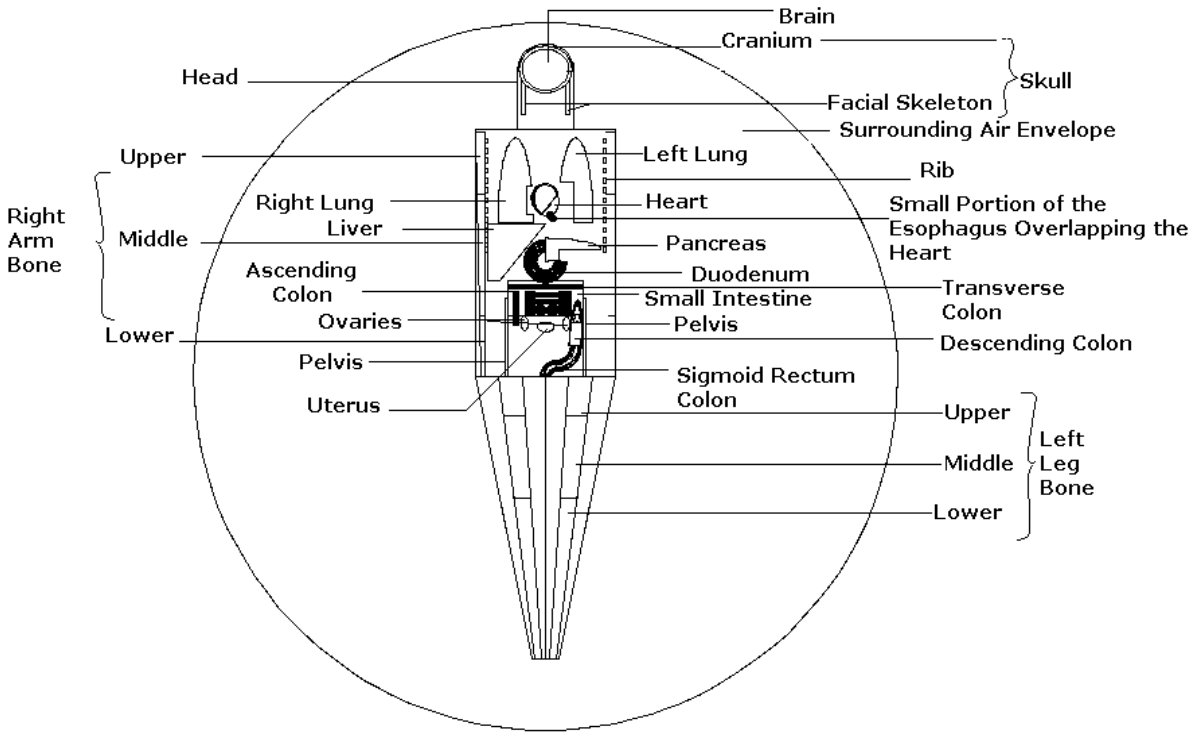

Fig. 1. Frontal view of the principal organs in the head, trunk, and the legs of the adult phantom developed in this study. The phantom was sectioned along the coronal plane y = 0 in a reference frame centered at the base of the trunk. The y-axis directed towards the posterior side of the phantom and the x-axis directed to the phantom's left (the reader's right in the figure).

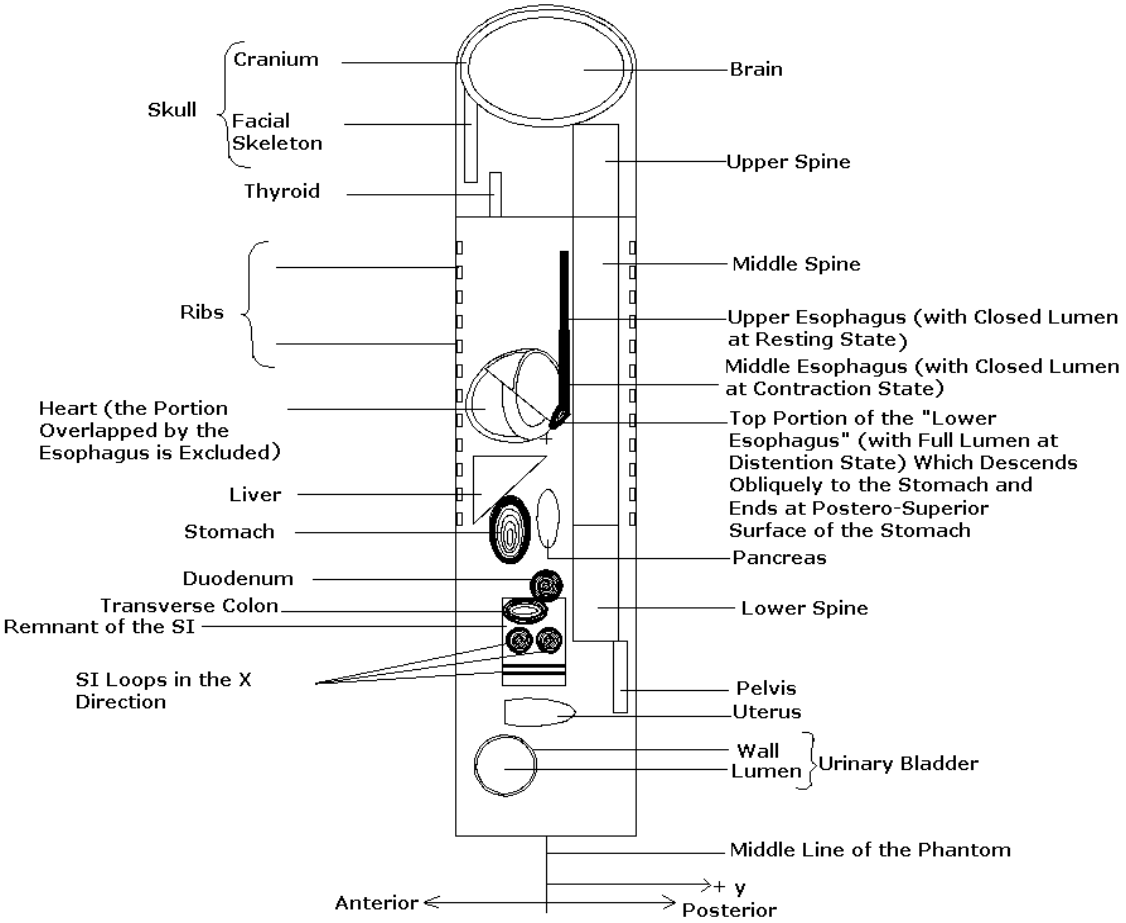

Fig. 2. Lateral view of the phantom sectioned along the sagittal plane x = 0.

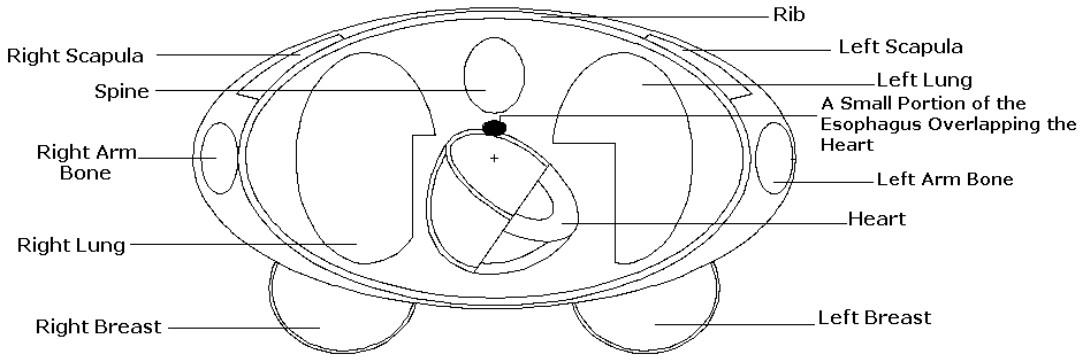

Fig. 3. Major organs/regions in the upper trunk region, sectioned along the transverse plane z = 52 cm, of the phantom representing adult male and larger-than-average adult female.

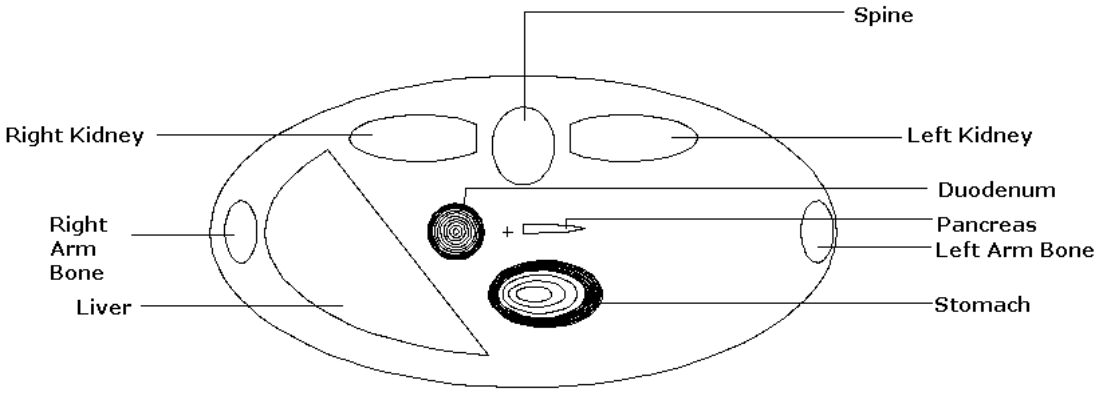

Fig. 4. Major organs/regions in the middle trunk sectioned along the transverse plane z = 32.7 cm.

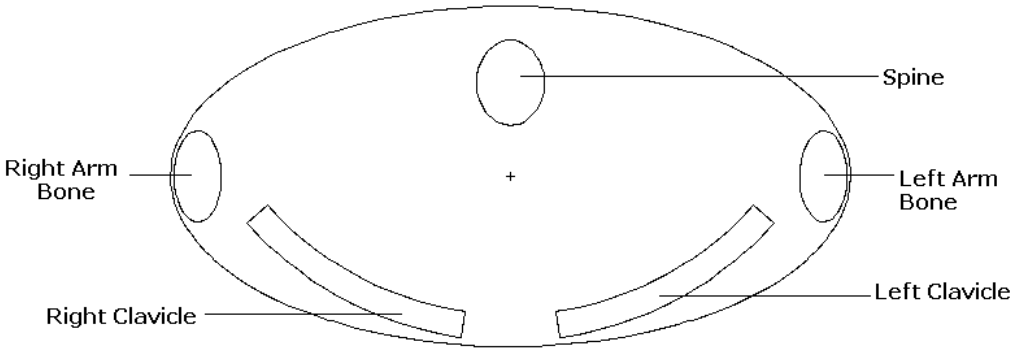

Fig. 5. Transverse view of the upper trunk region of the adult phantom.

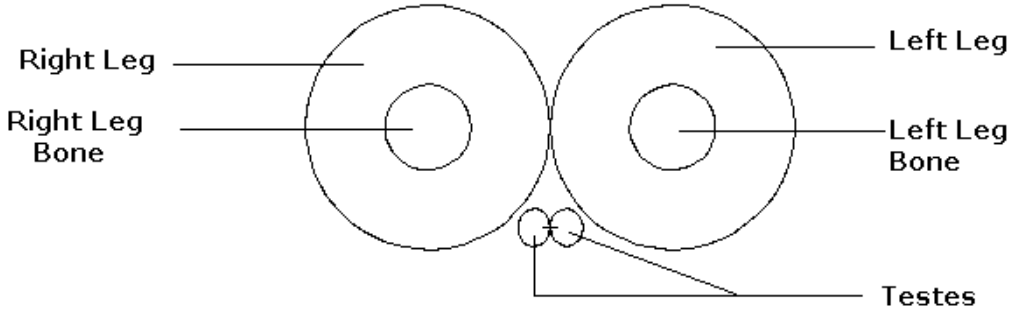

Fig. 6. Transverse view of the phantom sectioned along the transverse plane z = -2.3 cm with the testes identified at ± 1.3 cm, -8 cm, -2.3 cm.

The major difference between the two phantoms is in the GIT. The GIT model of Cristy and Eckerman (1987) is identical to that of Snyder (1978) in which the small intestine (SI) was modeled as a solid soft tissue region without delineating the wall and the contents, and the folds that this organ takes in its position in the abdomen. The other sections — stomach (ST), upper large intestine (ULI) consisting of ascending colon (AC) and transverse colon (TC), and lower large intestine (LLI) consisting of descending colon (DC) and sigmoid-rectum colon (SRC) — were modeled as organs with walls and contents. Each wall was treated as a single tissue layer. The distinction among the tissue types within the wall was not made because the Cristy and Eckerman phantom was designed for the dosimetry from photon sources, not for the dosimetry from electron sources. The wall tissues with different radiosensitivity should be distinguished in the GIT model for the electron dosimetry. Cristy and Eckerman considered primarily the total mass (wall plus contents) of a section in their model design. The individual detail of the characteristic parameters such as the length, lumen diameter, wall thickness, and masses of the wall and contents were ignored. These values differ largely from the true anatomic data. It is noted that the characteristic parameters may have little effect on the energy deposition pattern for photons. But for the weakly-penetrating radiations, the effects are strong enough to require real anatomic data to be incorporated into the model (Bhuiyan 2000).

The new GIT model developed in this study was suitable for both electron and photon transport calculations. There were five sections, namely the esophagus (ESP), ST, SI, ULI, and LLI. The wall of each section was separated from its lumen contents.

Each wall was divided into many small regions so that the more radiosensitive tissues could be distinguished from the less radiosensitive tissues. The epithelial cells, lining the GIT mucosa, were recognized as the cells at risk to radiation as these cells were the most radiosensitive cells in the wall and the epithelium was the location of radiation-induced malignant growths. The average depth, measured from the wall-contents interface, of stem cells for each section was determined by reviewing the histologic data. The shapes, sizes, and the locations of these sections were more anatomically structured. The characteristic parameters were determined based on the newest information available to better approximate the actual anatomic values. Each section, except the ST, consisted of a number of subsections so that the spatiotemporal variations in the structure could be delineated in the model.

The spatiotemporal behavior of the ES has been captured by dividing the section into three subsections — upper esophagus with closed lumen, middle esophagus with closed lumen, and lower esophagus being full of food — representing the states of the ESP at resting, contraction, and distension, respectively, observed during a passage of a food bolus through the ESP (Fig. 2).

This was the first GIT model that included the ESP as a section of the GIT. A number of different models for the GIT for use in internal dose assessments have been proposed since the first GIT model developed by the ICRP in 1959. The ESP was not included in any of those models. The ESP was not considered as an organ at risk to radiation-induced cancer in the early ICRP recommendations. This might be the reason for not including the ESP as part of the GIT model for internal dosimetry. A relatively

small transit time (~ 40 s per bolus) for lumenal contents of the ESP might be another reason. The latest ICRP recommendations introduced specific risk estimates and tissue (ULI and LLI) (ICRP 1991), requiring dose estimations for all these organs.

Anatomically, a full ST assumes an oblique position between the ESP and the duodenum in erect posture (Warren 2000). Cristy and Eckerman (1987) modeled the ST as full but the organ was positioned upright on the left side of the transverse colon (TC) in their phantom standing erect. The ST in the revised model inclines to the left side at an angle of 45 degrees and reaches as far as the bottom of the left lung. It is moved to a new position between the ESP and the duodenum. The postero-superior surface of the stomach is in contact with the bottom of the ESP while the postero-inferior surface touches the antero-superior surface of the duodenum. The liver is on the right side of the ST. The wall and the contents of the stomach are defined by two concentric ellipsoids with the geometric factors identical to the Cristy and Eckerman ST model (1987).

The SI consists of four regions. They are different in shape and size and represent the duodenum, jejunum, and ileum with full lumens, and the remnant of the jejuno-ileum region with empty lumen. The wall of the SI with empty lumen cannot withstand external pressure. As a result the wall collapses closing the lumen. The “remnant” is modeled as a solid region without lumen and represents that part of the SI where the lumen is empty and closed. So there is no source in the remnant. The radiation sources are homogenously distributed in the contents of the other three subsections. The folds are considered to be only in the jejuno-ileum region with full lumen. The folds are not considered in the remnant as the cross-dose to the remnant without folds is not

considerably different from the dose with the folds. The folds are delineated by repeating the basic structures of jejunum and ileum in the x-, y- and z-directions. The jejuno-ileum region, bounded by the ULI and the LLI, occupies the same space defined by Snyder (1974) and later adopted by Cristy and Eckerman (1987) for the SI in their phantoms. The characteristic parameters for each subsection are set based on anatomic data. Dose calculations are corrected for any deviation from true anatomic data.

The ULI consists of the ascending colon (AC) and transverse colon (TC) while the LLI consists of the descending colon (DC) and recto-sigmoid colon (RSC). As indicated before, Cristy and Eckerman (1987) considered only the organ masses in their model. They ignored the other structural parameters such as length, wall thickness, and lumen diameter. The lumens were full in their model. The masses of the contents were different from the real masses. The Monte Carlo simulation results were not corrected for these deviations. In the current model, all colon lumens, except the lumen of the RSC, are partly filled and partly empty. The RSC lumen is entirely filled in this model. Except for the length, the other structural parameters and the masses of the wall and the contents are based on the anatomic data available in the literature. Though the lengths used in the Cristy and Eckerman colon models (1987) are smaller than the real anatomic lengths, the same lengths are used in the revised model to fit the colon in the correct anatomic space. Appropriate factors are applied to the simulation results to correct for deviations in the length as well as in the other parameters. Transit times are taken into account in the calculations.

The characteristic parameters describing the sections of the GIT in the current model are presented along with those in various other references and models, e.g., ICRP Reference Man (1975), MIRD model (Snyder et al. 1978), ICRP model (1979), Cristy and Eckerman model (1987), Poston et al. model (1996a, 1996b), Stubbs et al. model (1998), Bhuiyan model (2000), Jönsson et al. model (2001), and the ICRP Human Alimentary Tract (HAT) document (2001). The HAT document prepared for the newest ICRP GIT model which is expected to be published in the year 2004. The model values were based on data obtained from review of various books, references and journal articles.

The phantom developed in the research was coupled with the MCNP 4C Monte Carlo simulation package (Briesmeister 2000). The code was used for calculating specific absorbed fractions (SAFs) in various organs and radiosensitive tissues from fifteen uniformly distributed sources of monoenergetic photons and electrons, 10 keV - 4 MeV, in the lumen contents of the five GIT sections.

To facilitate the description of the new GIT model, a brief description of the principal regions of the phantom is included in this section. The heart and the pancreas are described here. The other organs are not described as they are identical to those of the Cristy-Eckerman adult phantom (1987). Interested readers are referred to the relevant reference. The elemental compositions and densities of the organs and tissues also are presented in this section.

ELEMENTAL COMPOSITION OF THE TISSUES

The first heterogeneous phantom, developed by Snyder et al. (1969), contained three types of materials; each type was assigned a different mass density and elemental composition. These materials represented the tissues of the skeleton, the lung, and the remainder (soft tissue). The elemental compositions were obtained from Tipton, Snyder, and Cook (1966), who analyzed tissue specimens obtained from autopsies of 150 grossly normal U.S. adults. Cristy and Eckerman (1987) used the same three tissue types but with slightly different elemental compositions and mass densities in the revised Snyder phantom. The changes were made on the basis of data in Table 105 of ICRP Publication 23 (1975).

The current phantom contains 14 different types of tissue that include the tissues of skeleton, lung and soft tissue defined by Cristy and Eckerman (1987) and 11 other tissue types listed in the International Commission on Radiation Units and Measurements (ICRU) Report 44 (1989). The ICRU recommended elemental compositions and the mass densities were derived from the Report on ICRP Reference Man (1975) and from the work of Woodard and White (1986) on body tissue compositions. The soft tissue defined by Cristy and Eckerman (1987) is used for the GIT contents while the ICRU (1989) recommended tissue is used for the GIT wall, except the wall of the esophagus. In the absence of more appropriate of data, as recommended by ICRU (1989), ICRU skeletal muscle tissue was used for the esophageal wall and the urinary bladder wall.

Table 1 presents the elemental compositions and the densities of different tissues used in the current model, the Cristy and Eckerman model (1987) and the Snyder et al. (1969).

Table 1. The elemental compositions and the mass densities of adult human organs and tissues used in the current model and in other models.[a]

Model and reference	Tissue	Elemental composition (percentage by mass)					Density ($g\ cm^{-3}$)
		H	C	N	O	Other	
ICRU Report (1989)	Brain[b]	10.7	14.5	2.2	71.2	0.2 Na, 0.4 P, 0.2 S, 0.3 Cl, 0.3 K	1.04
	Breast[c]	10.6	33.2	3.0	52.7	0.1 Na, 0.1 P, 0.2 S, 0.1 Cl	1.02
	GIT wall	10.6	11.5	2.2	75.1	0.1 Na, 0.1 P, 0.1 S, 0.2 Cl, 0.1 K	1.03
	Heart (blood filled)	10.3	12.1	3.2	73.4	0.1 Na, 0.1 P, 0.2 S, 0.3 Cl, 0.2 K, 0.1 Fe	1.06
	Kidney	10.3	13.2	3.0	72.4	0.2 Na, 0.2 P, 0.2 S, 0.2 Cl, 0.2 K, 0.1 Ca	1.05
	Liver	10.2	13.9	3.0	71.6	0.2 Na, 0.3 P, 0.3 S, 0.2 Cl, 0.3 K	1.06
	Muscle (skeletal)[d]	10.8	4.1	1.1	83.2	0.3 Na, 0.1 S, 0.4 Cl	1.05
	Ovary	10.5	9.3	2.4	76.8	0.2 Na, 0.2 P, 0.2 S, 0.2 Cl, 0.2 K	1.05
	Pancreas	10.6	16.9	2.2	69.4	0.2 Na, 0.2 P, 0.1 S, 0.2 Cl, 0.2 K	1.04
	Testes	10.6	9.9	2.0	76.6	0.2 Na, 0.1 P, 0.2 S, 0.2 Cl, 0.2 K	1.04
	Thyroid	10.4	11.9	2.4	74.5	0.2 Na, 0.1 P, 0.1 S, 0.2 Cl, 0.1 K, 0.1 I	1.04
Crsity and Eckerman (1987)[e]	Soft tissue[f]	10.5	22.7	2.5	63.5	0.1 Na, 0.1 P, 0.2 S, 0.1 Cl, 0.2 K	1.04
	Skeleton	7.4	25.5	3.1	47.9	0.3 Na, 0.1 Mg, 5.1 P, 0.2 S, 0.1 Cl, 0.2 K, 10.2 Ca	1.40
	Lung	10.1	10.2	2.9	75.8	0.2 Na, 0.1 P, 0.2 S, 0.3 Cl, 0.2 K	0.296
Snyder et al. (1974)[e]	Soft tissue	10.0	23.0	2.3	63.0	0.1 Na, 0.2 P, 0.2 S, 0.1 Cl, 0.2 K	0.9869
	Skeleton	7.0	23	3.9	49.0	0.3 Na, 0.1 Mg, 6.9 P, 0.2 S, 0.1 Cl, 0.2 K, 9.9 Ca	1.4862
	Lung	10	10	2.8	76	0.2 Na, 0.1 P, 0.2 S, 0.3 Cl, 0.2 K	0.296

[a] The current phantom contains 14 different types of tissue that include the tissues of skeleton, lung and soft tissue defined by Cristy and Eckerman (1987) and 11 other tissue types listed in the ICRU Report 44 (1989).

[b] Brain composed of grey and white material 50:50, by mass

[c] Mammary glands constitutes the breast.

[d] ICRU skeletal muscle tissue is used for the esophageal wall and the urinary bladder wall, as recommended by ICRU.

[e] The values of the elemental compositions given by Cristy and Eckerman (1987) and the Snyder et al. (1974) are rounded to one significant digit in this table. These tissues also contain trace amounts of other elements such as Mg, Si, Ca, Fe, Zn, Rb.

[f] The soft tissue defined by Cristy and Eckerman (1987) is used for the remainder of the body organs, tissues or masses (GIT contents) those are not listed in this table.

PHANTOM

The phantom used in this research was modeled as erect with three major sections (Fig. 1): (1) an elliptical cylinder representing the trunk that includes the arms and the pelvic region to the crotch; (2) two truncated circular cones representing the legs and feet; and (3) an elliptical cylinder capped by half an ellipsoid representing the head and neck. The origin of the coordinate system is located at the center of the base of the trunk section. The positive z-axis extends upward through the head. The positive x and y axes extend to the phantom's left (the reader's right in Fig. 1) and the posterior side of the phantom. All dimensions given below are in centimeters.

The trunk of the phantom was described by

$$\left(\frac{x}{20}\right)^2 + \left(\frac{y}{10}\right)^2 \le 1 \text{ and } 0 \le z \le 70 .$$

The legs were described by

$$5\left(x^2 + y^2\right) \le \pm x(100 + z) \text{ and } -80 \le z \le 0 ,$$

where the "±" sign was taken as plus for the left leg and the minus for the right leg. The head was given by

$$\left(\frac{x}{8}\right)^2 + \left(\frac{y}{10}\right)^2 \le 1 \text{ and } 70 \le z \le 86.85 ,$$

$$\text{or } \left(\frac{x}{8}\right)^2 + \left(\frac{y}{10}\right)^2 + \left(\frac{z-86.85}{7.15}\right)^2 \le 1 \text{ and } z > 86.86 .$$

REVISED GIT MODEL

The revised GIT model consisted of five sections — the esophagus, stomach, small intestine, upper large intestine, and lower large intestine. Prior to the description of

the each section, the anatomic and histologic features of each section pertinent to photon and electron dosimetric modeling will be described to provide the basis for the model.

Esophagus

Anatomic and histologic information. The esophagus, the narrowest and proximal tubular part of the GIT, is a collapsible muscular tube that, in humans, extends—about 21-30 cm with mean 25 cm in the adult male and 20-26 cm with mean 23 cm in the adult female—from the laryngopharynx to the stomach. The esophageal wall weighs about 23-50 g with mean 37 g in the adult male and about 25-50 g with mean 34 g in the adult female (Tipton and Cook 1969, ICRP 23 1975, ICRP HAT document). The esophageal structure varies spatially along its length. There is a temporal variation in the esophageal structure as well. At a given location along the length, the esophagus assumes three distinct structures at three states of peristalsis which is produced by coordinated waves of circular muscle contraction and local longitudinal muscle shortening made in reflex response to the distension of the GIT walls by a swallowed bolus of food. The peristalsis, triggered by swallowing or deglutition, propagates distally and propels the bolus downward along the length of the GIT. The three peristaltic states—distension, contraction, and resting—were detected by high-frequency intralumenal ultrasonography techniques in a number of recent studies (Taniguchi et al. 1993; Miller et al. 1995; Yamamoto et al. 1998; Balaban et al. 1999; Pehlivanov et. el. 2001; Nicosia et. al. 2001). The esophageal wall thickness decreases as intralumenal contents distend the wall in the distension state. The distension state is followed by the contraction state in which the wall muscles are contracted transversely and are shortened longitudinally in a reflex

response to the distension, thus increasing the wall thickness. The lumen is closed at the peak contractions (Pehlivanov et al. 2001). The esophagus structure returns to the resting state (before swallowing or the distension) with the muscle layer that is thicker than that at the distension and is thinner than that at the contraction state. When the esophagus is empty at the resting state, the mucosa and submucosa are thrown into longitudinal folds thus closing its lumen (Pehlivanov et. el. 2001; Bolch et al. 2002).

Pehlivanov et al. (2001) recorded ultrasound images of the esophagus of 15 healthy adult humans. The recordings were made in resting state and at the peak of swallow-induced contraction in the lower esophageal sphincter (LES), which opens into the ST, and at 2, 4, 6, 8, and 10 cm above the LES. The esophageal muscle in the resting state was measured to be significantly higher in the LES compared with the rest of the esophagus where it was somewhat thicker in the distal compared with the proximal esophagus, as shown in Table 2. The muscle was significantly thicker at peak contraction than in the resting state at each level (see Table 2).

Using the same ultrasonography technique, Nicosia et al. (2001) studied *in vivo* the temporal variations in esophageal muscle thickness and geometry during peristalsis. They recorded muscle thicknesses (circular plus longitudinal) in the middle esophagus at the three states. The recorded minimum was 0.9 mm at the distension while the maximum was 3 mm at the peak contraction. At the resting state, the mean thickness was found to be 1.38 ± 0.07 mm. They did not mention the total wall thickness of the esophagus.

Table 2. Muscle layer thickness at three different states at different levels of the esophagus (Pehlivanov et al. 2001).

Level	Thickness in resting (mm)[a]		Thickness at peak contraction (mm) [a]	
	Mean		Mean	
LES[b]	1.92 ± 0.14	1.13 ± 0.16	2.54 ± 0.13	2.17 ± 0.32
2 cm	1.28 ± 0.09		2.31 ± 0.17	
4 cm	1.14 ± 0.09		2.16 ± 0.16	
6 cm	1.09 ± 0.06		2.20 ± 0.15	
8 cm	1.07 ± 0.07		2.15 ± 0.15	
10 cm	1.06 ± 0.06		2.04 ± 0.14	

[a] Values are means ± SE
[b] LES stands for lower esophageal sphincter

In a critical review, ICRP (1975) reported that the esophagus in adult human is 3.5-5.6 mm in wall thickness, 13-19 mm in diameter at the contraction state and 16-22 mm in diameter at distension state.

Ultrasound images showed that the geometry of the esophagus was almost circular or elliptical during peak contraction and "slit-like" in appearance in the resting and distended states (Pehlivanov et al. 2001; Nicosia et al. 2001). In conclusion, esophagus is elliptical in shape with varying major-to-minor-axes-ratio depending on the peristaltic states.

The esophageal wall contains all four of the basic alimentary canal tissue layers. From the lumen outward, these layers are the mucosa, submucosa, muscularis externa, and serosa (or adventitia). As discussed before, the esophageal wall thickness varies due to the spatiotemporal variation within an individual. There is a variation between individuals as well. The wall in the adult is about 3.5-5.6 mm thick in which the mucosa is about 500-800 μm (ICRP 23 1975). The mucosal epithelium is composed of nonkeratinized stratified squamous cells and is relatively thick, about 300 μm in the adult (ICRP HAT document 2001). The basement membrane (basal layer) of the

epithelium consists of the most radiosensitive stem cells that give rise to the epithelium. Overlying the epithelium, there is a thick coating of mucus that serves as a protective barrier and makes the esophageal lumen slippery that helps the passage of a food bolus.

Despite the actual variability in the stem cell depth due to the variation in the thicknesses of the mucus layer and epithelium lining, for dosimetry purposes we consider the depth of the stem cells to be 500 μm as an average, and, therefore, define the absorbed dose to the esophagus as the absorbed dose at a depth of 500 μm. The mucus thickness 200 μm is added to the average epithelium thickness of 300 μm (ICRP HAT document 2001) to obtain the mean stem cells depth of 500 μm.

Esophagus model. The esophagus model in this study represents an adult male esophagus 27 cm in length with a food bolus in the distal region which is at distension state. The model includes the resting state in the proximal region and the contraction state in the middle region as well. These three peristaltic states in three regions are modeled by dividing the entire esophageal length into three segments, each 9 cm in length but with different diameter. From the proximal to distal, these segments are: (i) "upper esophagus", an elliptical solid cylinder with radii of 0.9 cm and 0.4 cm representing a slit-like appearance of the proximal esophagus with closed lumen at resting state, (ii) "middle esophagus", an elliptical solid cylinder with radii of 0.8 cm and 0.5 cm representing the middle esophagus with closed lumen at contraction state, (iii) "lower esophagus", consisting of two concentric elliptical cylinders with the inner radii of 0.7 cm and 0.4 cm, and the outer radii of 1.1 cm and 0.8 cm representing the lumen and the wall of the distal esophagus at distension state. Note that contents are only in the

lower esophagus as this segment has a lumen while the other two segments are solid regions without lumen. The same wall thickness, 0.4 cm, is used for both the upper esophagus at resting and the lower esophagus at distension because the decrease in the wall thickness caused by changing the states from resting to distension is compensated by the increase in the thickness along the length from proximal to distal. The wall of the middle esophagus at contraction is thicker and is assumed to be 0.5 cm. The characteristic parameters of each segment in the current ESP model, presented in the table on page 34, describe an average structure of one of the three peristaltic states. The variation during the period of a particular state is not considered in this model.

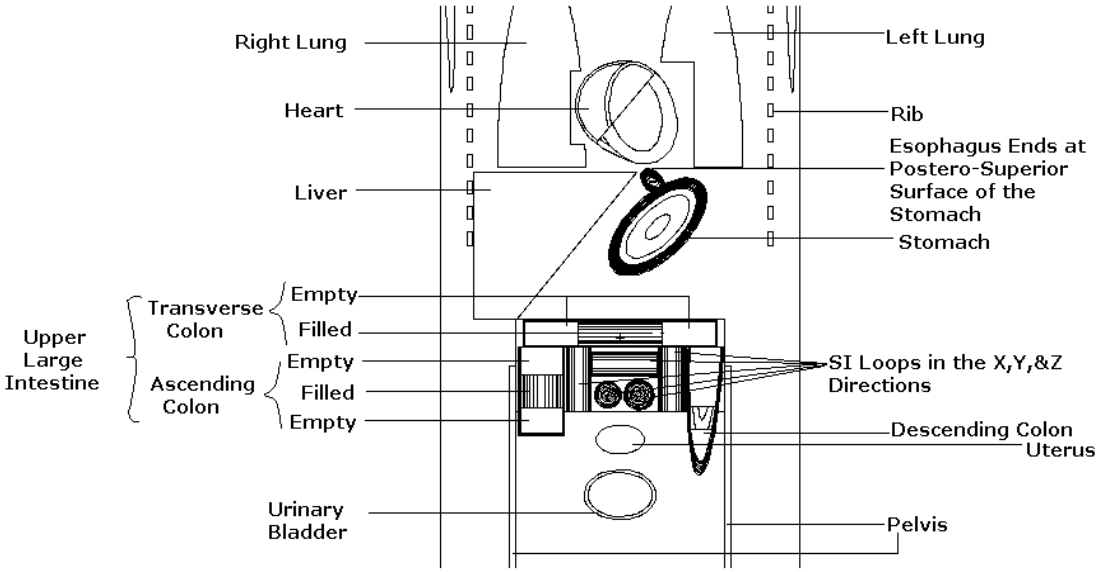

Fig. 7. Frontal view of the trunk sectioned along the coronal plane y = -2.36 cm in a reference frame centered at the base of the trunk. The y-axis is directed towards the posterior side of the phantom and the x-axis is directed to the phantom's left.

The esophagus, in relation to other organs, is placed in the phantom in an approximately true anatomic position (Warren 2000). As illustrated in Fig. 2, the upper

and the middle esophagus run vertically downward along the front of the middle spine, slightly behind the middle line of the phantom. The lower esophagus passes the middle line and deviates to the left as it descends obliquely from posterior to anterior and ends at the postero-superior surface of the stomach (Figs. 2 and 7). A small portion of the middle and lower esophagus intercepts the heart.

The upper and middle esophagus are defined by

$$\left(\frac{x-x_0}{a}\right)^2+\left(\frac{y-y_0}{b}\right)^2 \le 1,$$

$$\text{and } z_1 \le z \le z_2 .$$

The wall plus contents of the lower esophagus are represented by two coaxial elliptical cylinders. The wall is defined by the space between the two cylinders:

$$\left(\frac{x'}{a}\right)^2+\left(\frac{y'}{b}\right)^2 \le 1,$$

$$\left(\frac{x'}{a-d}\right)^2+\left(\frac{y'}{b-d}\right)^2 \ge 1,$$

$$\text{and } z_1 \le z' \le z_2 .$$

The contents are defined by the space within the inner cylinder:

$$\left(\frac{x'}{a-d}\right)^2+\left(\frac{y'}{b-d}\right)^2 \le 1,$$

$$\text{and } z_1 \le z' \le z_2 .$$

The $(x', y', z')-$coordinate system is related to the phantom's (x, y, z)-coordinate system by the following rotation-translation equation, given in matrix form:

$$\begin{bmatrix} x' \\ y' \\ z' \end{bmatrix} = \begin{bmatrix} 0.9063 & 0.2424 & 0.3462 \\ 0.0 & 0.8192 & -0.5736 \\ -0.4226 & 0.5198 & 0.7424 \end{bmatrix} \begin{bmatrix} x - x_0 \\ y - y_0 \\ z - z_0 \end{bmatrix}.$$

The above coordinate transformation as a result of the combination of a translation of the origin to $(x_0, y_{0,} z_0)$ and two rotations, the first being clockwise rotation about *x*-axis through an angle 35° and the second being counterclockwise rotation about the new y'-axis through an angle 25°.

The constants used in the above expressions are presented in Table 3.

Table 3. Characteristic parameters describing the adult human esophagus in the current dosimetry model.

Sub-section	x_0	y_0	z_0	a	b	d	z_1	z_2	Mass (g)	
									Wall	Contents
Upper Esophagus	0.0	2.0	-	0.9	0.4	-	57.2	66.2	10.69	-
Middle Esophagus	0.0	2.0	-	0.8	0.5	-	48.2	57.2	11.88	-
Lower Esophagus	0.0	2.0	48.2	1.1	0.8	0.4	-9.0	0.0	17.81	8.23

Each of the three esophageal sections is divided into many shell volumes by using many closely spaced coaxial elliptical cylinders. The thicknesses of these shell volumes are in the range of 1-1000 μm depending on the location of the shells and on the energy of the radiation to be transported.

The characteristic parameters that describe the esophagus in the current dosimetry model as well as in the ICRP Reference Man (1975) and in the ICRP HAT document (2001) are presented in Table 4.

Table 4. Characteristic parameters describing the adult human esophagus in the current dosimetry model and in other references.

Characteristic Parameters	Reference				
	ICRP Reference Man (1975)	HAT (2001)	Current Model		
			Upper Esophagus at Resting	Middle Esophagus at Contraction	Lower Esophagus at Distension
Geometry	—	—	Elliptical Cylinder	Elliptical Cylinder	Elliptical Cylinder
Length (cm)	25 (23-30)[1]	25 (21-30)[1]	9.0	9.0	9.0
Outer Radius/Radii (cm)	0.65-0.95[2] 0.80-1.10[3]	—	0.9, 0.4	0.8, 0.5	1.1, 08
Lumen Radius/Radii (cm)	—	—	Closed	Closed	0.7, 0.4
Wall Mass (g)	40	37±6[4]	10.69	11.88	17.81
Wall Thickness (cm)	0.35-0.56	0.35-0.56[5]	—	—	0.4
Contents' Mass (g)	—	—	—	—	8.23[6]
Transit Time (s)[7]	—	47/10.3	—	—	—
Mucus Thickness (μm)[8]	—	—	200	200	200
Epithelium Thickness (μm)	—	300	300	300	300
Stem Cell Depth (μm)[8]	—	—	500	500	500
Mucosal Layer Thickness (μm)	500-800	—	—	—	—

[1] Average length with the range in parenthesis is presented.
[2] At contraction state.
[3] At distension state.
[4] In the ICRP HAT document (2001), the reference esophageal wall mass in adult males is based on data of Tipton and Cook (1969).
[5] Esophageal wall thickness mentioned in the HAT document (2001) is taken from ICRP Publication on Reference Man (1975).
[6] Esophageal Contents' mass in the current model is chosen arbitrarily as no information is available.
[7] The esophageal transit times are on the order of 5 to 30 s (NCRP 1998). Transit time of 90% food through esophagus is 7 s. The residual 10% food through esophagus is 40 s (HAT 2001). Based on the HAT (2001) data, the total transit time comes to be 47 s and the effective transit time is 10.3 s = ((7 × 0.9) s + (40 × 0.1) s).
[8] The epithelium of the mucosa is stratified squamous and relatively thick, about 300 μm in the adult (21). The esophageal stem cells are located in the basal layer of the epithelium. The mucus thickness is arbitrarily chosen to be 200 μm as no information about esophageal mucus thickness is available. This 200 μm for the mucus layer is added to the epithelium thickness (300 μm) to obtain the distance or depth of the stem cells (500 μm) measured from the lumenal surface.

Stomach

Anatomic and histologic information. The stomach, the most distensible part of the GIT, is a J-shaped pouch that provides a temporary storage area of the ingested food where chemical digestion of proteins begins. It is located left of the midline of the trunk of the

body and is immediately inferior to the diaphragm which separates it from the base of the left lung. The stomach is connected at its proximal end to the esophagus by the lower esophageal sphincter (or cardiac orifice) and at the distal end to the duodenum of the small intestine via the pylorus sphincter, but it is quite flexible in between. The shape, size and position of the stomach vary largely with the posture, with the amount of the stomach contents and with the condition of the intestines on which it rests. The stomach may be cylindrical or roughly crescent shaped when empty of food or pear-shaped when partially distended, but the most common form in the erect posture is the fish-hook or J-shape. A full ST assumes an oblique position between the ES and the duodenum in erect posture (ICRP 23 1975; NCRP 15 1998; Graaff and Fox 1999; Warren 2000; ICRP HAT document 2001; Bolch 2002).

The stomach wall is made up of the same four basic layers of tissues, as is the majority of the GIT, with some differences in the microscopic anatomy that allow its unique digestive functions. For example, the additional third layer of smooth muscle in the muscularis externa enables the stomach to churn, mix, and pummel ingested food, as well as propel the ingesta along the length of the organ through peristalsis. The mucosa of the stomach wall is covered by a single layer of columnar epithelium 20 to 40 μm thick (Trier and Winter 1989; NCRP 1998). The surface epithelium is entirely composed of mucus secreting goblet cells. The surface epithelium is indented by millions of pits, called gastric pits, each about 200 μm deep and 70 μm in diameter (Trier and winter 1989). These gastric pits are invaginations of the surface epithelium into the submucosa. At the bottom of each gastric pit are one or more secreting glands resembling cylinders

with inner diameters in the range of 5 to 10 μm and inner lengths in the range of 200 to 500 μm (Allen 1989). The gland contains radiosensitive stem cells at a depth of approximately 200 μm (Trier and Winter 1989). The secreting glands are divided into three categories based on their role in stomach digestion: the cardiac glands occurring in the region just below the cardiac orifice secrete mucus; the pyloric glands occurring near the duodenum secrete mainly mucus but also gastrin and pepsinogen; and the gastric glands occurring between these two extremities host a number of different cells that secrete various enzymes and hormones, hydrochloric acid, mucus and other products such as gastrin, histamine, endorphins, serotonin, etc.

The surface epithelium of the mucosa is exposed to a very corrosive and acidic mixture of the gastric secretions. The epithelial cells are worn out and are constantly replaced through cell division of undifferentiated stem cells that reside within the glands located at the base of the gastric pits. The entire surface epithelium is replaced in every 2-6 days while the turnover time for the glandular cells is longer.

The mucus thickness varies along the length of the stomach. A large variation is observed in the measured values of the thickness as well. Measurement techniques considerably influence the measurement result. Two techniques are commonly used for measuring the thickness of the adherent mucus layer on unfixed, fresh mucosa: 1) an indirect method in which a slit lamp and pachymeter are used to measure the mucus thickness over a mucosa bathed with solution and 2) direct observation of unfixed sections of mucosa by light microscope. The pachymeter is an image-splitting device that allows the measurement of optically distinct objects (i.e., the objects with different

refractive indexes) to an accuracy of ± 20 μm. The mucus layer is translucent, thus readily distinguishable from the underlying mucosa. But the site of the mixing boundary between the insoluble mucus gel phase and the bulk lumenal fluid phase is not clearly observed by the pachymeter because their refractive indexes are almost equal. So a component of the bathing solution could be added to the mucus layer in the pachymeter measurement. As a result, the measured value might be greater than the actual thickness. Direct observation by light microscope is relatively simple and more reliable method of the two because the contours of the two phases are clearly observed in the later method (Allen 1989).

The mucus thickness was reported to be 192-652 μm (Bickel and Kauffman 1981; Kerss et al. 1982) and 50-450 μm with an average 180 μm (Allen 1989). Stubbs et al. (1998) assigned 180 μm for the mucus thickness in their stomach model.

Underlying the mucus layer is the mucosa with a thickness of 0.3-2.5 mm (ICRP 23 1975; ICRP HAT 2001). The stomach wall is 0.6-1.3 cm thick (ICRP 23 1975) and with a mass of 110-450 g and an average 150 g for the adult male and 140 g for the adult female (ICRP 23 1975; Tipton and Cook 1969). The mass of the contents of the ICRP Reference Man was 250 g taken directly from Eve's review work (1966). The reference value for the mass of the contents in the HAT document (2001) was based largely on autopsy measurements on 15 accident victims (Eve 1966) and was taken to be 175 g for the adult male and 160 g for the adult female. These values are lower than those derived by Eve, who relied more on theoretical considerations than autopsy measurements and who assumed considerably longer transit time for fluids than those considered in the

HAT document (30-45 m for adult male) (HAT 2001). The total transit time for stomach contents was taken to be 70 m for the adult male and 95 m for the adult female in the HAT document (2001).

The characteristic parameters describing the stomach in the current dosimetric model, and in various other models and references are presented in Table 5.

Table 5. Characteristic parameters describing the adult human stomach in the current model and in various other dosimetry models and references.

Characteristic Parameters	Reference							
	ICRP Reference Man (1975)	MIRD Model (Snyder et al. 1978)	ICRP Model (1979)	Cristy & Eckerman (1987)	Poston et al. (1996)	Stubbs et al. (1998)	HAT (2001)	Current Model
Model Geometry	—	Ellipsoid/ Cylinder(1)	Ellipsoid/ Cylinder(1)	Ellipsoid	Ellip-soid	Ellip-soid	—	Ellip-soid
Outer Dimensions (cm)	37, 15, 11	8, 4, 3	8, 4, 3	8, 4, 3	8, 4, 3	8, 4, 3	—	8, 4, 3
Wall Mass (g)(2)	150	148	148	158	158	158	150±46	156.5
Wall Thickness (cm)	0.6-1.3	0.613	0.613	0.613	0.613	0.613	—	0.613
Contents Mass (g)(2)	250(3)	247	247	260	260	260	175(3)	260
Transit Time (h)(4)	—	—	1	—	—	—	1.17	1.17
Mucus Thickness (μm)(5)	—	—	—	—	—	180	—	300±100
Gastric Pit Height (μm)(6)	—	—	—	—	—	200	—	200
Stem Cell Depth (μm)(7)	—	—	—	—	100-300	600	—	730±100
Mucosal Layer Thickness (μm)	500-2500	—	—	—	0-300	—	300-1500	—

(1) Ellipsoid for penetrating radiations and cylinder for weakly penetrating radiations (beta, conversion electron, Auger electron, etc.).

(2) The volumes of the stomach in all these models are identical as the same ellipsoids are used to represent the stomach in those models but the masses are different because different mass densities are used. The soft tissue with mass density 0.9869 g cm^{-3} defined by Snyder et al. (1974) was used both for the wall and for the contents of the GIT of the ICRP (1979) and MIRD (1978) models. Cristy & Eckerman (1987) change the mass density to 1.04 g cm^{-3} as well as change the elemental composition of the soft tissue on the basis of the data in Table 105 of ICRP Publication 23 (Table 1). This soft tissue was used for the wall and for the contents of the GIT models of Cristy & Eckerman (1987), Poston et al. (1996),

Table 5. Continued.

and Stubbs et al. (1998). In the current GIT model, the ICRU recommended elemental composition and mass density 1.03 g cm^{-3} (1989) of the GIT derived from the ICRP Report on Reference Man (ICRP 23 1975) are used for the walls of the GIT-sections, except the esophagus, but the Cristy & Eckerman soft tissue with density 1.04 g cm^{-3} is used for the contents.

In the ICRP HAT document (2001), the reference mass of the stomach wall in adult males is based on data of Tipton and Cook (1969).

(3) The contents' mass of the ICRP reference man was taken 250 g directly from Eve's review work (1966). The reference value for the contents' mass in the HAT document (2001) was based largely on autopsy measurements on 15 accident victims (Eve 1966) and was taken to be 175 g for adult male and 160 g for adult female. These values are lower than those derived by Eve, who relied more on theoretical considerations than autopsy measurements and who assumed considerably longer transit time for fluids than those considered in the HAT document (30-45 m for adult male) (HAT 2001).

(4) The mean transit time for stomach contents was taken to be 1 h for adult male based on Eve's recommendation (1966). Transit time for the current stomach model is taken from the ICRP HAT document (2001).

(5) The mucus thickness of the stomach was reported to be 192-652 μm (Bickel and Kauffman 1981; Kerss et al. 1982) and 50-450 μm with an average 180 μm (Allen 1989). Stubbs et al considered 180 μm for the mucus thickness based on the later study (Allen 1989). Instead of taking a single value, we consider that 95% of the measured data on the mucus thickness are distributed normally between 100 μm and 500 μm around a mean 300 μm with one standard deviation 100 μm.

(6) Stubbs et al. has taken the pit's height from the value given by Sleisenger et al (1983). The same pit's height is also used in this model as no other data is available.

(7) The stem cell depth is the distance measured from the wall-contents interface to the location of the stem cells that reside at some depth in the glands. So the stem cell depth 730 μm is obtained by adding the thicknesses of the mucus layer (300 μm), single cell thick layer of epithelium (30 μm), pit's height (200 μm) and the stem position in the glands (200 μm).

Stomach model. The stomach was modeled as a full stomach. As illustrated in Figs. 7 and 8, the stomach is located left of the midline of the trunk of the body with the long axis inclined left by making a 45 degree angle with the phantom's z-axis. As the stomach is inclined, it reaches as far as the bottom of the left lung. The postero-superior surface of the stomach is in contact with the bottom of the ES while the postero-inferior surface touches antero-superior surface of the duodenum. The liver is on the right side of the ST.

The wall and the contents of the stomach are represented by two concentric ellipsoids with the centroid at (4.05, -4.0, 37.1) and with the radii 4.0 cm, 3.0 cm and 8.0 cm for the outer ellipsoid, and 3.387 cm, 2.387 cm and 7.387 cm for the inner ellipsoid.

As mentioned before, the dimensions of the ellipsoids are the same as those used for the Cristy and Eckerman ST model (1987).

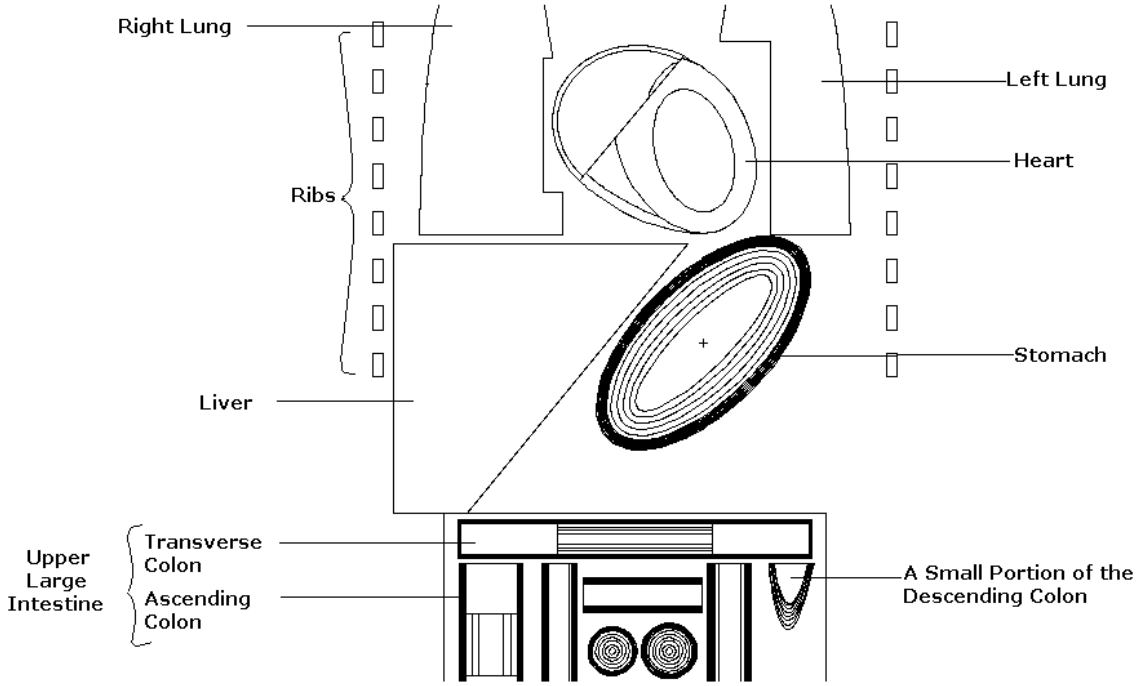

Fig. 8. Frontal view of the stomach inclined to the left by 45° with spatial relation to the lungs, liver, heart, ribs, and the intestine. The trunk sectioned along the coronal plane y = -4 cm in a reference frame centered at the base of the trunk. The y-axis directed toward the posterior side of the phantom and the x-axis directed to the phantom's left. The centroid of the ellipsoidal stomach is at 4.05 cm, -4 cm, 37.1 cm.

The stomach wall was represented by the volume between the two concentric ellipsoids. The contents were represented by the volume within the inner ellipsoid. The wall was defined by

$$\left(\frac{x'}{4.0}\right)^2+\left(\frac{y'}{3.0}\right)^2+\left(\frac{z'}{8.0}\right)^2\le 1,$$

$$\text{and } \left(\frac{x'}{3.387}\right)^2+\left(\frac{y'}{2.387}\right)^2+\left(\frac{z'}{7.387}\right)^2\ge 1.$$

The contents were defined by

$$\left(\frac{x'}{3.387}\right)^2+\left(\frac{y'}{2.387}\right)^2+\left(\frac{z'}{7.387}\right)^2<1.$$

The primed coordinate system, (x', y', z'), is related to the phantom's (x, y, z)-coordinate system by the following rotation-translation equation, given in matrix form:

$$\begin{bmatrix} x' \\ y' \\ z' \end{bmatrix} = \begin{bmatrix} 0.7071 & 0.0 & -0.7071 \\ 0.0 & 1.0 & 0.0 \\ 0.7071 & 0.0 & 0.7071 \end{bmatrix} \begin{bmatrix} x-4.05 \\ y+4.0 \\ z-37.1 \end{bmatrix}.$$

The above coordinate transformation as a result of the combination of a translation of the origin to $(4.05,–4.0,37.1)$ and a clockwise rotation about *y*-axis through a 45° angle.

Thus, the stomach wall is 0.613 cm thick and has a 152 cm^3 volume. The volume of the contents is 250 cm^3.

The wall and contents, each is divided into many shell volumes by using many closely spaced concentric ellipsoids. The space between two adjacent ellipsoids gives the thicknesses of these shell volumes that are in the range of 1-1000 μm depending on the location of the shells as well as on the energy of the radiation to be transported.

Small Intestine

Anatomic and histologic information. The SI is a convoluted tube that in adult humans extends—about 3 m in living persons (~ 6 m in cadavers due to muscle relaxation)—from the pyloric sphincter of the ST to the ileocecal valve, which opens into the LI. Based on function and histologic structure, it is divided into three regions: the duodenum, jejunum and ileum. The duodenum (~25 cm), the first portion of the SI, is a relatively fixed C-shaped tube facing the concave surface to the left around the head of

the pancreas. The jejunum and ileum (~110 cm and ~165 cm long, respectively) hang within the central and lower part of the abdominal cavity suspended by extensions (mesentery) of the peritoneum (serous membrane covering the abdominal cavity), and are bounded by the large intestine laterally and superiorly. The attachment of mesentery to the SI allows peristaltic movement with little chance of becoming twisted and kinked.

The SI wall is made up of the same four basic layers of tissues, as is the majority of the GIT, with certain modifications to allow the processes of digestion and absorption. From the lumen outward, these layers are the mucosa, submucosa, muscularis externa, and serosa (or adventitia). Each layer, or tunic, of the wall has a predominant tissue type that performs specific functions in the digestive processes. The mucosa, or mucous membrane, has three components: a single cell thick surface epithelium that lines the lumen, an underlying stroma composed of a vascularized, highly cellular, reticular connective tissue (lamina propia), and a thin layer of smooth muscle (mascularis mucosae). The surface epithelium, which is the site of secretion and absorption, and serves as a protective barrier, is folded to form millions of finger- or leaf-like projections (areal density = 20 to 40 per mm^2) called villi into the lumen. The epithelium at the base of each villus invaginates downward to form narrow pouches that open through pores to the lumen. These structures are called the intestinal crypts (crypts of Lieberkühn). The epithelial cells of the villi are predominantly columnar cells specialized for nutrient absorption, and interspersed among these are the mucus-secreting goblet cells. The epithelial cells that line the crypts secrete intestinal juice, a mixture of water and mucus, and antibacterial enzyme lysozome. A large surface area of the epithelium is made

available, for digestive and absorptive activities, by the mucosal circular folds (plicae circulares), by crypts, by villi, and by microvilli (thousands of tiny fingerlike projections formed by foldings of the cell membrane of each absorptive cell on the villous epithelium).

All the differentiated cell lineages of the intestinal epithelium are derived from common multipotent stem cells located near the base of each crypt (Cheng and Leblond 1974). A stem cell in the crypt divides in the normal intestine to produce a daughter stem cell (self renewal) and a more rapidly replicating transit cell. The transit cell, in turn, undergoes four to six rapid cell divisions in the proliferative zone located in the lower half of each crypt. These nascent cells undergo terminal differentiation as they migrate upward from the zone of proliferation onto the villus epithelium. Eventually, the differentiated epithelial cells are sloughed off as they reach the villus tip, whereby homeostasis of the normal adult intestinal epithelium is maintained (Cheng and Leblond 1974; Gordon and Hermiston 1994; Potten et al. 1997a, 1997b). The undifferentiated cells, especially the stem cells, in the crypts are the most radiosensitive. Hence, the stem cell region is considered to be the critical region for radiation damage to the small intestine.

The anatomic and histologic information required for constructing the geometry of the SI has been gleaned from currently available textbooks and journal articles, ICRP Publication 23 (1975) on Reference Man and Eve's review work (1966). Wide variability in the data was observed for some parameters such as lumen diameter, wall thickness and villus height.

A marked structural variation is observed along the length of the small intestine within an individual and between individuals. The variations are in the range of 0.2-0.4 cm in wall thickness and of 1.9-3.1 cm in lumen diameter (Golden 1959; Eve 1966; Gray 1974; ICRP 1975; Solomon and Davis 1978; Tortora and Evans 1986; Haubrich et al. 1995; Marieb 1998). The small intestine gradually diminishes in size from its commencement to its end. The duodenum wall is the thickest and the lumen is the widest while the ileum is the thinnest and the narrowest. Based on this review, the duodenum is 3.0 cm in lumen diameter and 0.3 cm in wall thickness, the jejunum is 2.7 cm in lumen diameter and 0.3 cm in wall thickness, and the ileum is 2.4 cm in lumen diameter and 0.25 cm in wall thickness.

No quantitative information is available on the mucus thickness of the SI. There are a few qualitative analyses found in the open literature. McClean et al. (1996) reported that about half of the mucosal surface of the SI is covered by a mucus gel of variable thickness. The mucus thickness in the duodenum is, despite the marked differences in epithelial surface topology, similar to that in the ST (Flemstrom et al. 1999). The mucus thickness of the stomach was reported to be 192-652 μm (Bickel and Kauffman 1981; Kerss et al. 1982) and 50-450 μm with an average 180 μm (Allen 1989). As discussed before, the mucus thickness of the stomach is taken to be 300±100 μm in the current model. Thus the mucus thickness of the duodenum is 300±100 μm. For the jejunum and ileum, the average mucus thickness is assigned to be 150±50 μm, which is half the stomach mucus thickness, since half of the SI length is devoid of mucus.

The villi appear in different shapes, sizes and numbers in the three regions of the small intestine. In the duodenum the villi are short, leaflike folds; the villi in the jejunum are rounded, fingerlike projections; and those in the ileum tend to have a clublike form. Villi typically are taller and more numerous in the jejunum than in the ileum (ICRP HAT document 2001). The literature suggests that a mean villus height of 500±45 μm is a good average over the range of 300-1500 μm for an adult human SI (Eve 1966; ICRP 1975; Penna et al. 1981; Stenling et al. 1984; Leeson et al. 1985; Tortora and Evans 1986; Johnson et al. 1987; Trier and Winter 1989; Fawcett 1994; Haubrich et al. 1995; Guyton 1996).

Based on the information on the crypts of Lieberkühn, it was concluded that 150 ± 12 μm was reasonable for the mean crypt depth of an adult human with a range of 120-170 μm; 45 ± 7 μm was the mean crypt width; 143 ± 25 μm was the mean height from Paneth to top (crypt-villi junction); and 135 ± 20 μm was the mean height of the stem cells measured from the junction (Eve 1966; Penna et al. 1981; Stenling et al. 1984; Potten and Booth 2000). The descriptive parameters of the SI obtained in the review are summarized in Table 6.

Distance from contents to the critical cells. A definite distance between the stem cells and the contents is difficult to specify because of the irregularities of the lumenal surface caused by the presence of protruding villi and indented crypts of Lieberkuhn on the internal surface of the SI, and the considerable variations in the number and size of these structures along the SI length. If it is assumed that the crypt space and the space between the villi is filled with material of similar scattering and energy-absorbing properties as

that of the wall material, and no contents or more specifically, no source, is present therein, the stem cell distance from the contents is the summation of mucus thickness, villus height and the depth of the stem cells in the crypt measured from the villi-crypt junction. A representative total distance can be obtained from the corresponding mean values of these parameters. Indeed, the crypt lumen is filled with exocrine secretions and mucus, and overflows into the intestinal lumen via the crypt lumen. The scattering and energy-absorbing properties are almost the same, except for mucus, as the soft tissues comprising the SI wall (ICRP 1975). If the ICRP (1975) values for the villus diameter of 130 μm and the number of villi per square millimeter of 75 are used to estimate the gaps between villi, one can show that the villi are closely packed without gaps. However, many of the reported values for the number of villi per unit area vary from 10 to 40 per square millimeter (Eve 1966; Fawcett 1994; Guyton 1996). Nevertheless, the 150 μm mucus thickness on each of the nearer sides of the adjacent villi, along with the exocrine secretions and mucus overflowing from the crypt seems to be sufficient material to fill the space between villi. Eve (1966), quoting Creamer, mentioned that all solid and insoluble materials in the lumen contents are separated from the mucosa by a sheet of mucus. He added that a soluble substance might flow through the mucus and up the crypts to arrive in the mitotic stem cell area. However, it may be necessary to take into account the irregularities of the surface and the small fraction of the source getting into the crypts (ICRP 1975). Since the objective was to calculate an average dose to the critical region, a “representative distance” may be chosen and the small fraction of the source that might be present in the crypt and between the villi may be ignored.

Table 6. Parameters describing the adult human small intestine in the current dosimetry model, and in other models and references.[a]

Characteristic Parameters	Reference									
	ICRP Reference Man (1975)	MIRD Model (Snyder et al. 1978)	ICRP Model (1979)	Cristy & Eckerman (1987)	Poston et al. (1996a)	Stubbs et al. (1998)	Bhuiyan (2000)	ICRP HAT Model (2001)	Jönsson et al. (2001)	Current Model
Model Geometry	—	Cylinder/ Solid Region[b]	Cylinder/ Solid Region[b]	Solid Region	Cylinder	Cylinder	Cylinder	—	Cylinder	D: Torus J-IL: Cylinder R: Solid Region[c]
Length (cm)	D: 25 J: 190 IL: 285 Total: 500	—	—	—	21	10	10	300	300	D: 20.26 J: 104.90 IL: 174.84[c] Total: 300
Lumen Radius (cm)	D: 2 J: 1.25-2 IL: 1-1.9	—	1.0	—	1.246	1.0	1.4 (0.95-1.55)[d]	1.5	1.25	D: 1.5 J: 1.35 IL:1.20 R: Closed Lumen[c]
Wall Mass (g)[e]	D: 60 J: 280 IL: 300 Total: 640	Total Mass (wall+contents): 1046	640	Total Mass (wall+contents): 1102.4	168	40.1	30.4	D: 56±9 J: 280±39 IL: 310±33 Total: 650	—	D: 64.9 J-IL: 535.1 Total: 650
Wall Thickness (cm)	D: 0.3-0.5 J: 0.3 IL: 0.2-0.5	0.3-0.4	0.2-0.3	—	0.754	0.5	0.3 (0.2-0.4)[d]	—	0.3 & 0.6	D: 0.30 J: 0.30 IL: 0.25
Contents Mass (g)[f]	400	400	400	—	106.5	32.7	64.0	280	—	D: 10.98 J-IL: 269.02 Total: 280
Transit Time(h)[h]	—	—	4.0	—	—	—	—	4.0	—	4.0

Table 6. Continued.

Characteristic Parameters	Reference									
	ICRP Reference Man (1975)	MIRD Model (Snyder et al. 1978)	ICRP Model (1979)	Cristy & Eckerman (1987)	Poston et al. (1996a)	Stubbs et al. (1998)	Bhuiyan (2000)	HAT (2001)	Jönsson et al. (2001)	Current Model
Mucus Thickness (μm)[(i)]	—	—	—	—	—	200	210±57	—	5-200	D: 300±100 J-IL: 150±50
Villus Height (μm)[(j)]	700	—	500-1500	—	—	500	500±45	—	500	500±45
Crypt Depth (μm)[(k)]	—	—	20-450	—	—	150	150±12	—	150	150±12
Stem Cell Position (μm)[(l)]	—	—	—	—	300-600	150	135±20	—	—	135±20
Stem Cell Depth[(m)] (μm)	—	—	—	—	—	850	845±75	—	—	D: 935±111 J-IL: 785±70 Avg.: 790
Mucosal Layer Thickness (μm)	—	—	—	—	449±141	—	—	—	—	—

[(a)] In the table, D stands for duodenum; J stands for jejunum, IL stands for Ileum; J-IL stands for Jejuno-ileum region; R stands for remnant.

[(b)] Solid region for strongly penetrating radiations (e.g., photon) and cylinder for weakly penetrating radiations (e.g., beta, electron, etc.).

[(c)] The structural and functional variations along the length of the small intestine (SI) are incorporated into the SI model by using three different geometries. Three-fourth of two concentric circular tori represents the wall plus lumen of the C-shaped duodenum. Eight circular cylinders, each 7 cm in length with closed ends, with the axes directed in x, y, and z-directions represent the convoluted part of the J-IL region with contents in the lumen. Each cylinder consists of two coaxial cylinders where the inner cylinder represents the lumen and the space between the cylinders represents the wall. Of eight, three cylinders with 21 cm in total length represent the jejunum with filled lumen and the remaining five cylinders with smaller radii but each with the same 7 cm in length represent the ileum with thinner wall and narrower lumen with full of contents. The rest of the tabulated length, which is 223.74 (=300-20.26-21-35) cm, represents that part of the J-IL region where the lumen is empty and closed. The fact is that the majority of the J-IL region is with empty and closed lumen and that has been taken into account in this model. This part is termed as the "remnant" of the J-IL region. The remnant is modeled as a solid soft tissue region.

[(d)] Bhuiyan (2000) calculated absorbed doses in the SI from the electron sources distributed uniformly in the lumenal contents. He modeled the SI as two coaxial circular cylinders with radii 1.4 cm and 1.7 cm, respectively. The volume between the two cylinders represented the wall while the inner cylinder represented the lumen. He also studied the effect of the lumen radius and the wall thickness on the absorbed dose.

Table 6. Continued.

[(e)] The volume of the small intestine in the MIRD model (Snyder et al. 978) and the Cristy and Eckerman model (1987) are the same but the masses are different because different mass densities are used. The soft tissue with mass density 0.9869 g cm^{-3} defined by Snyder et al. (1974) was used both for the wall and for the contents of the MIRD (Snyder et al. 978) model. Cristy and Eckerman (1987) change the mass density to 1.04 g cm^{-3} as well as change the elemental composition of the soft tissue on the basis of the data in Table 105 of ICRP Publication 23 (Table 1). In the current GIT model, the ICRU recommended elemental composition and mass density 1.03 g cm^{-3} (1989) of the GIT derived from the ICRP Report on Reference Man (ICRP 23 1975) are used for the walls of the GIT-sections, except the esophagus, but the Cristy & Eckerman soft tissue with density 1.04 g cm^{-3} is used for the contents as well as for the remnants of the jejuno-ileum region.
In the ICRP HAT document (2001), the reference mass of the small intestine wall is based on data of Tipton and Cook (1969) who measured the small intestine masses in 49 adult males.

[(f)] The contents' mass of the ICRP Reference Man was taken 400 g directly from Eve's review work (1966). The reference value for the contents' mass in the HAT document (2001) was based largely on autopsy measurements on 15 accident victims described by Eve 1966) and was taken to be 280 g for adult male. This value is lower than that derived by Eve, who relied more on theoretical considerations than autopsy measurements and who assumed considerably longer transit time for fluids than those considered in the HAT document (HAT 2001). The small intestine contents' mass in the current model is taken from the HAT document (2001). Stubbs et al. (1998) and Bhuiyan (2000) used 32.7 g and 64.0 g as the contents' mass, respectively. With lower contents' mass, the source concentration (number of particles per unit volume) becomes higher. Their calculation must have resulted in higher absorbed doses per source particle than the doses with actual concentration. Stubbs et al. (1998) did not adjust their Monte Carlo simulation results to the actual source concentration. Such an adjustment was not needed in the derivation of relative quantities, such as absorbed fraction (AF), ratio of the surface dose to the dose at any depth in the wall, made by Bhuiyan (2000). Poston et al. (1996) also used the contents' mass different from the actual mass in the derivation of AF as well as other quantities such as specific effective energy (SEE) and annual limit on intake (ALI) where the contents' mass adjustment was needed but it was not obvious whether such corrections were made. The Monte Carlo calculation with the current small intestine model is performed using higher than the actual contents' mass but the results were adjusted to the actual contents' mass which is considered to be as 280 g in this model (see Table).

[(h)] The mean transit time was taken to be 4 h for adult male based on Eve's recommendation (1966). Transit time for the current small intestine model is taken from the ICRP HAT model (2001).

[(i)] In the current model, the mucus thickness of the duodenum is taken to be 300±100 μm, same as that of the stomach. For the jejunum and ileum, the average mucus thickness is assigned to be 150±50 μm, which is half the stomach mucus thickness, since the studies showed that half of the SI length is devoid of mucus. Stubbs et al. (1998) has arbitrarily taken 200 μm as no data on SI mucus was available. Bhuiyan (2000) assigned 210±57 μm for the SI mucus thickness based on the data on the stomach.

[(j)] Villus height is measured from the villus' bottom to the top.

[(k)] Crypt depth measures the distance between villus-crypt junction and the bottom of the crypt. The crypt depth is provided by Potten and Booth (2000).

[(l)] Stem cell position measures the distance between villus-crypt junction and the location of the stem cells near the bottom of the crypt. The Stem cell position is provided by Potten and Booth (2000).

[(m)] The stem cell depth is the distance measured from the wall-contents interface to the location of the stem cells in the crypt. So the stem cell depth is obtained by adding the mucus thickness, villus' height, and the stem position in the crypts. The error or standard deviation associated with the stem cell depth is obtained using the "error propagation formula" for normal distribution.

As outlined earlier, the "representative distances" from contents-wall interface to the critical cells are, 935 μm for the duodenum, obtained by adding 300, 500 and 135 μm, and 785 μm for jejuno-ileum region, obtained by adding 150, 500 and 135 μm (see Table 6). The error or standard deviations associated with these distances are obtained using the "error propagation formula" for a normal distribution.

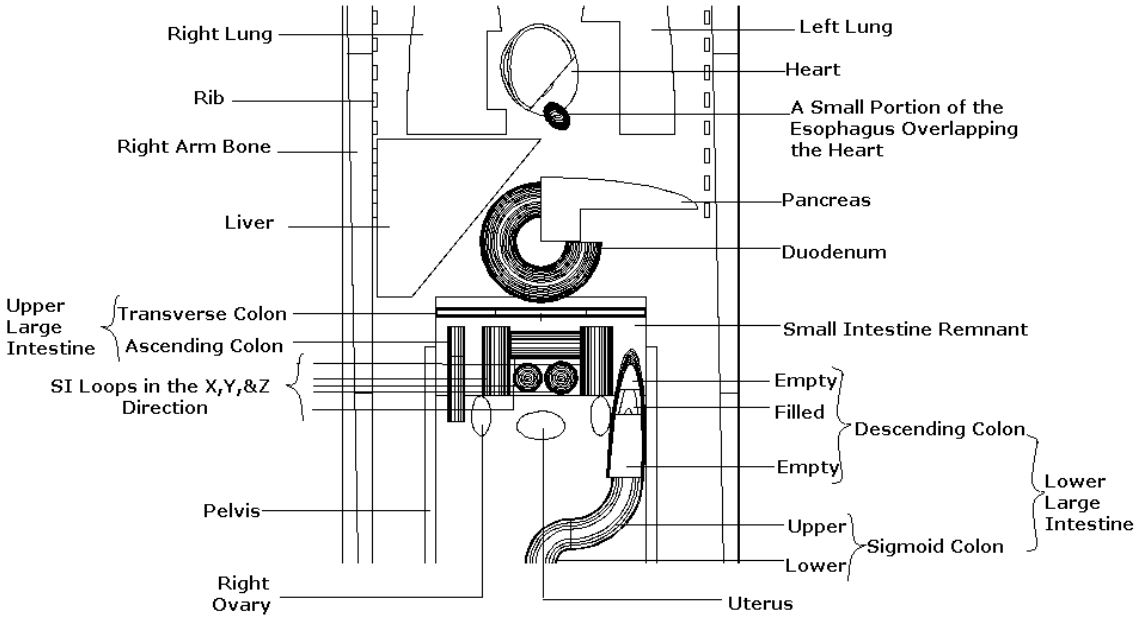

Fig. 9. Frontal view of the trunk sectioned along the coronal plane y = 0 in a reference frame centered at the base of the trunk. The y-axis directed toward the posterior of the phantom and the x-axis directed to the phantom's left.

Small intestine model. The structural and functional variations along the length of the small intestine are incorporated into the small intestine model by using three different geometries. The duodenum, which was not considered separately in the previous SI models, is part of the SI in the current model. Three-quarters of two concentric circular torii with the axis parallel to the y-axis represents the wall plus lumen of the C-shaped

duodenum (Figs. 1 and 9). Eight circular cylinders with the axes directed in x, y, and z-directions represent the jejuno-ileum folds in different orientations (Figs. 7, 9 and 10). Each cylinder, 7 cm in length, consists of two coaxial cylinders where the inner cylinder has the ends closed by two circular discs, each 0.25 cm in width, represents the lumen (6.5 cm in length) and the space between the cylinders represents the wall (7 cm in length). Of the eight cylinders, three with a total wall length of 21 (= 3 × 7) cm and 19.5 (= 3 × 6.5) cm in total lumen length represent the jejunum with filled lumen. The remaining five cylinders, with smaller radii, but each with the same 7 cm length represent the ileum with thinner walls and narrower lumen with full contents. The remnant of the jejuno-ileum region is modeled as a solid region without lumen. The "remnant" represents that part of the SI where the lumen is empty and closed. The majority of the jejuno-ileum region is empty with a closed lumen, this has been delineated in this model. The folds are not considered in the remnant as the cross-dose to the remnant without folds is not considerably different from the dose with the folds.

There is no source in the remnant. The sources are homogenously distributed in the contents of the other regions. The remnant is not directly exposed by the sources as the lumen ends are closed.

The C-shaped duodenum with the axis parallel to the y-axis is positioned around the neck of the pancreas and between the stomach and the transverse colon (Figs. 1 and 9). The antero-superior surface of the duodenum touches the postero-inferior surface of the stomach and the antero-inferior surface of the duodenum touches the posterior surface of the transverse colon. The jejuno-ileum region, bounded laterally by the

ascending and descending colons and superiorly by the transverse colon, occupies the same space defined by Snyder (1974) and later adopted by Cristy and Eckerman (1987) for the SI in their phantoms (Figs. 7, 9 and 10). The characteristic parameters for each subsection are based on anatomic data. Dose calculations are corrected for any deviation from true anatomic data.

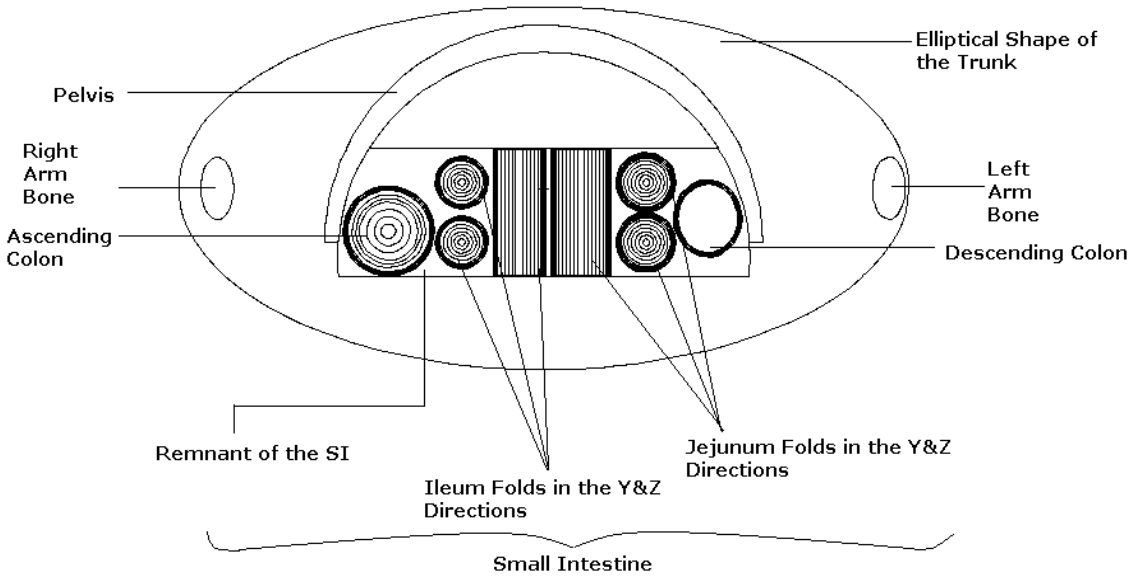

Fig. 10. Pelvis and the intestine in the lower trunk region sectioned along the transverse plane z = 18.85 cm of the phantom. Three folds in the y and z directions for each of the ileum and jejunum are shown here. Two more folds in the x-direction, located on z = 22.15 cm, for the ileum are not seen here. The ascending colon and the folds of the jejuno-ileum region are circular cylinders while the descending colon is an elliptical cylinder. Cylinders for the jejunum folds have a larger diameter than those for the ileum folds. Solid black rings in the figure represent the walls of the intestine. Indeed there are numerous closely spaced coaxial cylinders in each of these solid rings. Each wall is divided into many small tissue layers by these cylinders. The contents surrounded by the wall is also divided into many small regions so that the dose profile of the contents can be established as well. The remnant of the SI is a solid soft tissue region representing that part of the SI where the lumen is empty and closed.

The upper portion of the **duodenum wall,** which is one quarter of the space between two concentric tori, is defined by

$$\left(\sqrt{(x)^2+(z-32.6)^2}-4.3\right)^2+(y)^2 \le (1.8)^2,$$

$$\left(\sqrt{(x)^2+(z-32.6)^2}-4.3\right)^2+(y)^2 \ge (1.5)^2,$$

$$\text{and } x \le 0, \text{ and } z \ge 32.6.$$

The lower portion of the **duodenum wall,** which is one-half the space between two concentric tori, is defined by

$$\left(\sqrt{(x)^2+(z-32.6)^2}-4.3\right)^2+(y)^2 \le (1.8)^2,$$

$$\left(\sqrt{(x)^2+(z-32.6)^2}-4.3\right)^2+(y)^2 \ge (1.5)^2,$$

$$\text{and } z \le 8.72.$$

The upper portion of the **duodenum contents,** one quarter of a torus, is defined by:

$$\left(\sqrt{(x)^2+(z-32.6)^2}-4.3\right)^2+(y)^2 < (1.5)^2,$$

$$\text{and } x \le 0, \text{ and } z \ge 32.6.$$

The lower portion of the **duodenum contents,** one half of the torus, is defined by:

$$\left(\sqrt{(x)^2+(z-32.6)^2}-4.3\right)^2+(y)^2 < (1.5)^2,$$

$$\text{and } z \le 8.72.$$

Thus, the **duodenum** is 20.26 cm long, with a wall thickness of 0.3 cm and a wall mass of 64.91 g with a density of 1.03 g cm^{-3}. The lumen radius is 1.5 cm with a mass of contents of 148.96 g and a density of 1.04 g cm^{-3}.

The **jejunum wall** is defined by

$$\left.\begin{array}{l}(x-2.0333)^2+(z-18.85)^2 \le (1.65)^2,\\ (x-2.0333)^2+(z-18.85)^2 \ge (1.35)^2,\\ -4.83 \le y \le 2.17,\end{array}\right\}$$ One jejunal loop 7 cm in length in the y-direction

$$\left.\begin{array}{l}(x-5.6)^2+(y+2.98)^2 \le (1.65)^2,\\ (x-5.6)^2+(y+2.98)^2 \ge (1.35)^2,\\ (x-5.6)^2+(y-0.32)^2 \le (1.65)^2,\\ (x-5.6)^2+(y-0.32)^2 \ge (1.35)^2,\\ \text{and } 17.0 \le z \le 24.0.\end{array}\right\}$$ Two jejunal loops, each 7 cm in length, in the z-direction

The **jejunum contents** are defined by

$$\left.\begin{array}{l}(x-2.0333)^2+(z-18.85)^2 < (1.35)^2,\\ -4.58 \le y \le 1.92,\end{array}\right\}$$ One jejunal lumen 6.5 cm in length in the y-direction

$$\left.\begin{array}{l}(x-5.6)^2+(y+2.98)^2 < (1.35)^2,\\ (x-5.6)^2+(y-0.32)^2 < (1.35)^2,\\ \text{and } 17.25 \le z \le 23.75.\end{array}\right\}$$ Two jejunal lumens, each 6.5 cm in length, in the z-direction

Thus, the jejunum is 21.0 cm long, with a wall thickness of 0.3 cm and a wall mass of 61.16 g with a density of 1.03 g cm^{-3}. The lumen is 19.5 cm long, with a radius of 1.35 cm, with a mass of contents of 116.11 g and a density of 1.04 g cm^{-3}.

The **ileum wall** is defined by

$$\left.\begin{array}{l}(x+1.333)^2+(z-18.85)^2 \le (1.45)^2,\\ (x+1.333)^2+(z-18.85)^2 \ge (1.20)^2,\\ -4.83 \le y \le 2.17,\end{array}\right\}$$ One ileum loop 7 cm in length in the y-direction

$$\left.\begin{array}{l}(y+2.98)^2+(z-22.15)^2 \le (1.45)^2,\\ (y+2.98)^2+(z-22.15)^2 \ge (1.20)^2,\\ (y-0.32)^2+(z-22.15)^2 \le (1.45)^2,\\ (y-0.32)^2+(z-22.15)^2 \ge (1.20)^2,\\ \text{and } -3.05 \le x \le 3.95.\end{array}\right\}$$ Two ileum loops, each 7 cm in length, in the x-direction

$$\left.\begin{array}{l}(x+4.5)^2+(y-0.32)^2 \le (1.45)^2,\\ (x+4.5)^2+(y-0.32)^2 \ge (1.20)^2,\\ (x+4.5)^2+(y+2.98)^2 \le (1.45)^2,\\ (x+4.5)^2+(y+2.98)^2 \ge (1.20)^2,\\ \text{and } 17.0 \le z \le 24.0.\end{array}\right\}$$ Two ileum loops, each 7 cm in length, in the z-direction

The **ileum contents** is defined by

$$\left.\begin{array}{l}(x+1.333)^2+(z-18.85)^2 < (1.20)^2,\\ -4.58 \le y \le 1.92,\end{array}\right\}$$ One ileum lumen 6.5 cm in length in the y-direction

$$\left.\begin{array}{l}(y+2.98)^2+(z-22.15)^2 < (1.20)^2,\\ (y-0.32)^2+(z-22.15)^2 < (1.20)^2,\\ \text{and } -2.80 \le x \le 3.70.\end{array}\right\}$$ Two ileum loops, each 6.5 cm in length, in the x-direction

$$\left.\begin{array}{l}(x+4.5)^2+(y-0.32)^2<(1.20)^2,\\ (x+4.5)^2+(y+2.98)^2<(1.20)^2,\\ \text{and } 17.25\le z\le 23.75.\end{array}\right\}$$ Two ileum loops, each 7 cm in length, in the z-direction

Thus, the ileum is 35.0 cm long, with a wall thickness of 0.25 cm and a wall mass of 75.03 g with a density of 1.03 g cm^{-3}. The lumen is 32.5 cm long, with a radius of 1.20 cm, with a mass of contents of 152.91 g and a density of 1.04 g cm^{-3}.

The **"remnant"** of the jejuno-ileum region is represented by a section of a circular cylinder, defined by

$$(x)^2+(y+3.80)^2\le(11.30)^2,$$

$$-4.86\le y\le 2.20,$$

$$\text{and } 17.0\le z\le 27.0.$$

The jejuno-ileum region with lumen and the portion of the large intestine within this region are excluded. The volume of the remnant is 642.24 cm^3.

Large Intestine

Anatomic and histologic information. The large intestine frames the jejuno-ileum region of the small intestine superiorly and laterally and extends about 1.5 m from the ileocecal valve to the anus. It is shorter in length but larger in diameter than the small intestine. The large intestine is spatially subdivided into the upper large intestine, consisting of the cecum, ascending colon, and transverse colon, and the lower large intestine, consisting of the descending colon, sigmoid colon, and rectum. Its major function is to absorb water from undigested material, which is then eliminated from the body through the anus.

As in the small intestine, the large intestine mucosa is covered by simple columnar epithelial cells, except the anal canal which is lined with more abrasion-resistant stratified squamous epithelial cells. The surface epithelium consists of absorptive and mucus-secreting goblet cells. Epithelial invaginations form long, straight, tubular glands or crypts than contain numerous goblet cells. The crypts that extend the full thickness of the mucosa vary in length (in the range of 300-700 μm), but are longer than in the small intestine (Trier and Winter 1989; Magee 1986; Christen 1991; HAT 2001). The radiosensitive stem cells are located at the base of the crypts in the large intestine while those in the small intestine are slightly above the base of the crypts (Kaur and Potten 1986).

Unlike the small intestine, the mucosa of the colon lacks villi and circular folds (plicae circulares), thus the surface appears flat. The rectal mucosa is similar to that of the colon but its mucosa lies in circular folds, and its glands are longer and are composed almost entirely of goblet cells (ICRP 1975; Graaff and Fox 1999; HAT document 2001).

Goblet cells are abundant in the epithelium of the large intestine, in that mucus is needed to lubricate the lumenal surfaces and to protect the wall from acids and gases released by resident bacteria. The entire epithelium of the large intestine, and to a lesser extent the ileum, is covered with very thick mucus layer. The mucus thickness of proximal colon of rats was found to be 830±120 μm from *in vivo* measurements of 11 subjects (male Wister rats weighing ~200 g were fasted for 18-24 h) using a micropipette technique with intravital microscopy (Atuma et al. 2001). This mucus layer was up to 4-fold thicker compared with that in other regions of the gut (Atuma et al. 2001). Atuma et

al. (2001) noted that most of the difference in mucus thickness was due to loosely adherent mucus, which is one of the two components forming the mucus layer. The loosely adherent gel, which can be removed by suction and is rapidly replaced after removal, might have more lubricative properties *in vivo* and an underlying firmly adherent gel, which forms a thick layer over the gastric and colonic mucosal surfaces, would be expected to act as a relatively stable protective barrier (Atuma et al. 2001). The relative thickness of the two component layers of the mucus gel varies for different regions of the gut. Atuma et al. (2001) had to remove 86% of the mucus layer by suction to leave a firmly adherent gel of similar thickness to that in the stomach.

Pullan et al. (1994) measured the thickness of the adherent mucus gel on the colonic mucosa in the human. Their measured adherent mucus thicknesses were 107 μm on the surface of the "right colon" consisting of the ascending colon plus the proximal half of the transverse colon, 134 μm on the surface of the "left colon" consisting of the distal half of the transverse colon plus the descending colon, and 155 μm on the surface of the rectum. It was not mentioned in their study whether these thicknesses were for the loosely adherent or firmly adherent or the total gel layer. If these were for firmly adherent gel layers (which might be the case because the overlying sloppy mucus gel may be lost in the process of specimen preparation), the total mucus thicknesses would be, respectively, 764 μm, 957 μm, and 1107 μm, based on the assumption that loosely adherent gel constitutes the 86% of the mucus layer as shown by Atuma et al. (2001).

Christensen (1991) showed that mucus thickness on the mucosal surface of the large intestine varies between 300 and 400 μm. Stubbs et al. (1998) have arbitrarily

chosen 200 μm as the colonic mucus thickness.

In conclusion, the mucus layer is much thicker in the large intestine than any other sections of the GIT but it is hard to find a single value for the mucus thickness of the entire large intestine as the thickness widely varies along the length of the section and between two measurements that employed different techniques. However, for the sake of simplicity, we consider that the entire mucosa of the large intestine is covered by a mucus layer of uniform thickness which is taken to be 500 μm based on the data presented in the previous paragraphs.

The characteristic parameters describing the four segments of the large intestine (AC, TC, DC, RSC) in the current dosimetric model, and in various other models and references are presented in Table 7. The parameters of the current model are assessed based on previous dosimetric models, references (ICRP Reference Man, ICRP HAT model, ICRU, MIRD model, RIDC), journal articles and other sources reviewed. Table 7 shows that length, wall mass and mass of contents, each has two values in the current model. The value outside the parentheses is the actual value to be used for dosimetric calculations. This value will be called the model value. The other value within the parentheses is used for MCNP simulation. The wall is composed of ICRU recommended GIT material (ICRU 1989) with mass density, 1.03 g/cm^3, while the contents are composed of soft tissue with mass density, 1.04 g/cm^3 defined by Cristy and Eckerman (1987). The model length is based on the data given in the ICRP HAT document (2001) and the ICRP Publication 23 (1975). The masses of the walls and the contents are taken directly from the HAT model (2001). The locations, geometric shapes, and the outer

dimensions are taken directly from Cristy and Eckerman models (1987). The wall thicknesses and the lumen dimensions are derived from the other known parameters. The transit times are taken directly from the gastrointestinal model proposed by Stubbs et al. (1991, 1992). The mucus thicknesses are based on a number of different studies (Christensen 1991; Pullan et al. 1994; Atuma et al. 2001). The crypt depths are provided by Potten and Booth in a personal communication (2000).

Large intestine model. The ULI consists of the ascending colon (AC) and transverse colon (TC) (Figs. 7-9), while the LLI consists of the descending colon (DC) and recto-sigmoid colon (RSC) (Figs. 7 and 9). As indicated before, Cristy and Eckerman (1987) considered only the organ masses in their model. They ignored the other structural parameters such as length (and wall mass per unit length), wall thickness, and lumen diameter. The lumens were full in their model. The contents masses were different from the actual masses. The Monte Carlo simulation results were not corrected for these deviations. In this study, the large intestine was modeled more realistically. All characteristics parameters, except the length, were based on the anatomy and histology of the organ. The lengths used for Monte Carlo simulation were the same as those in the Cristy and Eckerman model. These lengths were much shorter than the real anatomic length (Table 7, and Figs. 7-9). But the wall mass per unit length and the source concentration closely match the anatomic data. However, appropriate factors are applied to the simulation results to correct for the deviations in the length. In the current model, the lumens, except the lumen of the RSC, are partly filled and partly empty. The RSC lumen is entirely filled in this model.

Table 7. Parameters describing the adult human large intestine in the current model, and in other models and references.

Segment[a]	Reference	Length (cm)	Wall Mass (g)[(1)]	Wall Thickness (cm)	Geometry	Lumen Radius (cm)	Contents Mass (g)[(2)]	Transit Time (h)[(2)]	Mucus Thickness (μm)[(3)]	Crypt Depth (μm)[(4)]	Stem Cell (μm)[(5)]
Cecum + AC	HAT (2001)	20	90	—	—	—	60	5	—	—	—
	ICRP 23 (1975)	7+18	90	—	—	2.5-3.5 (cecum)	—	—	—	—	—
	Cristy-Eckerman Model (1987)[(6)]	9.55	94.87	0.7085	Circular Cylinder	1.7915	100.14	—	—	—	—
	Other	—	—	—	—	—	—	8.4[(7,8)] AC: 5[(9)]	830± 120[(10)]	AC: 311±64[(9)]	—
	Current Model[(11)]	23.42 (9.55)	90 (36.70)	0.25	Circular Cylinder	2.25	60 (60.04)	8.4	500	311± 64	811±64
TC	HAT	50	120	—	—	—	90	13	—	—	—
	ICRP 23	50	120	—	—	—	—	—	—	—	—
	Cristy-Eckerman Model (1987)	21	125.58	0.527	Elliptical Cylinder	1.973, 0.973	131.72	—	—	—	—
	Other	—	—	—	—	—	—	12[(9)] 7.3[(7,8)]	—	—	—
	Current Model[(11)]	50 (21)	120 (50.42)	0.195	Elliptical Cylinder	2.305, 1.305	90 (90.02)	7.3	500	325	825
ULI: Cecum + AC + TC	HAT	70	210	—	—	—	150	18	—	—	—
	ICRP 23	75	210	—	—	—	220	13	—	—	—
	Cristy-Eckerman Model (1987)[(6)]	30.55	220.45	—	—	—	231.86	17[(9)] 15.7[(7,8)]	—	—	—
	Other	—	—	—	—	—	—	—	764[(12)]	—	—
	Current Model[(11)]	73.42 (30.55)	210 (87.12)	—	—	—	150 (150.07)	15.7	500	—	818
DC	HAT	20	90	—	—	—	25	6	—	—	—
	ICRP 23	30	90	—	—	—	—	—	—	—	—
	Cristy-Eckerman Model (1987)[(6)]	15.28	93.55	0.54	Elliptical Cylinder	1.34, 1.59	106.37	—	—	—	—
	Other	—	—	—	—	—	—	4.3[(7)]	—	—	—
	Current Model[(11)]	29.6 (15.28)	90 (46.48)	0.25	Elliptical Cylinder	1.88, 1.63	25 (25.03)	4.3	500	340	840

Table 7. Continued.

Segment[a]	Reference	Length (cm)	Wall Mass (g)[(1)]	Wall Thickness (cm)	Geometry	Lumen Radius (cm)	Contents Mass (g)[(2)]	Transit Time (h)[(2)]	Mucus Thickness (μm)[(3)]	Crypt Depth (μm)[(4)]	Stem Cell (μm)[(5)]
SC + R	HAT	60	70	—	—		70	12	—	—	—
	ICRP 23	40+15	70	—	—	R: 1.25-3.75[(13)]	—	—	—	—	—
	Cristy-Eckerman Model (1987)[(6)]	13.7	73.22	0.66	Circular Torus	0.91	37.06	—	—	—	—
	Other	—	—	—	—	—	—	11.6[(7)] 10.9± 1.6[(14)]	R: 1107[(15)]	SC: 358±84[(9)] R: 245±55[(9)]	—
	Current Model[(11)]	55.4 (13.7)	70.15 (17.34)	0.13	Circular Torus	1.44	70 (92.8)	11.5	500	327±63[(16)]	827±63
LLI: DC + SC + R	HAT	80	160	—	—	—	95	18	—	—	—
	ICRP 23	85	160	—	—	—	135	24	—	—	—
	Cristy-Eckerman Model (1987)[(6)]	28.98	166.77	—	—	—	143.43	20[(9)] 15.9[(7)]	—	—	—
	Other			—	—	—	—	—	957[(17)]	—	—
	Current Model[(11)]	85 (28.98)	160.15 (63.82)	—	—	—	95 (117.83)	15.8	500	—	830
LI: ULI + LLI	HAT	150	370	—	—	—	245	36	—	500	—
	ICRP 23	160	370	0.2-0.25[(18)] 0.1[(19)]	—	—	355	37	—	—	—
	Cristy-Eckerman Model (1987)[(6)]	59.53	387.22	—	—	—	375.29	31.6[(7)] 37.0[(9)] 39±5[(14)]	—	—	—
	Other	10[(20)]	139[(20)]	0.5[(20)] <0.30[(25)]	Circular Cylinder[(20)]	1.90[(21)] 4.0[(20)] 3.25[(26)]	523[(20)]	—	200[(20)] 300-400[(22)]	700[(20)] 500[(22)] 500[(23)] 320-345[(21)] 500[(24)]	550[(20)] 300-500[(27)]
	Current Model[(11)]	158.42 (59.53)	370.15 (150.94)	—	—	—	245 (267.9)	31.5	500	—	—

Table 7. Continued.

[(a)] In the table, AC stands for ascending colon; TC stands for transverse colon; ULI stands for upper large intestine; DC stands for descending colon; SC stands for sigmoid colon; R stands for rectum; LLI stands for lower large intestine; LI stands for large intestine.

[(1)] The reference wall masses for the LI and its segments of the adult male in the HAT model (2001) were based on data of Tipton & Cook (1969).

[(2)] Lumenal contents' masses and its transit times of the regions of the large intestine in the ICRP HAT model (2001) are presented in terms of the right colon (ascending colon plus the proximal half of the transverse colon), left colon (distal half plus the descending colon), and the rectosigmoid. The values of the HAT model (2001) presented in this table in terms of AC, TC, DC, & SC+R are estimated from those values.

The contents' masses and the transit times of the lumenal contents of the sections of the GIT in the ICRP Reference Man (1975) and in the ICRP GIT model (1979) were taken directly from Eve's review work (1966).

The reference contents' masses in the HAT model (2001) were based largely on autopsy measurements on 15 accident victims described by Eve 1966). These values were lower than that derived by Eve, who relied more on theoretical considerations than autopsy measurements and who assumed considerably longer transit times for fluids than those considered in the HAT model (HAT 2001).

The contents' masses and the transit times in the current large intestine model are taken directly from ICRP HAT model (2001) and from RIDC gastrointestinal model proposed by Stubbs et al. (1991, 1992), respectively.

[(3)] It is hard to find a single value for the mucus thickness of the entire large intestine as the thickness widely varies along the length of the section and between two measurements employed different techniques. However, for the sake of simplicity, the mucus on the mucosal surface of the large intestine is modeled in this study as a continuous sheet of uniform thickness which is taken to be 500 μm based on the data presented in the table.

[(4)] Crypt depth measures a length from the epithelial surface to the crypt's base. The crypt depths of various regions of the large intestine in the current model are set based on the measured data due to Potten and Booth (Personal communication 2000).

[(5)] The values under this column is the stem cell depth which measures the distance between contents-mucus interface to the stem cells located at the crypt's base. Thus the stem cell depth is obtained by adding the mucus thickness to the crypt depth.

[(6)] The large intestine model used by Cristy and Eckerman (1987) was the same as that of MIRD model developed by Snyder et al. (1978) with an exception in the material description. Cristy and Eckerman (1987) used the elemental composition and mass density that were slightly different from those used by Snyder et al. Later, Poston et al. (1996a) used the Cristy and Eckerman (1987) model with a modification intended both for electron and photon dosimetry. Poston et al. divided the wall into many small regions so that the radiosensitive region can be distinguished.

[(7)] Stubbs et al. (1991). [(8)] Stubbs et al. (1991, 1992); Values are also used in RIDC gastrointestinal model proposed by Stubbs et al. (1991, 1992).

[(9)] The data on half-times of retention of food (presented under the column of transit times) and crypt depths are provided by Potten and Booth in a personal communication (2000).

[(10)] This is total mean mucus thickness (firmly adherent + loosely adherent: (116 ± 51) + (714 ± 109)) of proximal colon of rat obtained from in vivo measurements of 11 subjects (male Wister rats weighing ~200 g were fasted for 18-24 h) using micropipette technique with intravital microscopy. The colonic mucus gel was found to be translucent. This mucus layer was continuous, covering the entire mucosal surface, and had a relatively even surface (Atuma et al. 2001).

[(11)] There are two values for each of the three parameters: length, wall mass and contents' mass. The upper value which is outside parentheses is the actual value used for calculations. This value is to be referred as model value. The lower value within the parentheses is used for MCNP simulation. The wall is composed of ICRU recommended GIT material (ICRU Report 44 1989) with mass density, 1.03 g/cm^3, while the contents are composed of soft tissue with mass density, 1.04 g/cm^3 defined by Cristy and Eckerman (1987). The model length is based on the data given in ICRP HAT

Table 7. Continued.

document (2001) and the ICRP 23 publication (1975). The masses of the walls and the contents are taken directly from the HAT model (2001). Geometric shapes and the outer dimensions for the current models are taken directly from Cristy & Eckerman models (1987). The wall thicknesses and the lumen dimensions are calculated from the above mentioned model values. The transit times are taken directly from RIDC gastrointestinal model proposed by Stubbs et al. (1991, 1992). The mucus thicknesses are set based on a number of different studies (Christensen 1991; Pullan et al. 1994; Atuma et al. 2000). The crypt depths are based on the data provided by Potten and Booth in a personal communication (2000).

(12) This is the total mucus thickness (loosely adherent plus firmly adherent mucus thickness) extrapolated from the measured thickness of adherent mucus gel of 107 μm on the surface of right colon (ascending colon plus proximal half of transverse colon) in surgically resected human specimens (Pullan et al. 1994). The extrapolation is based on the assumption that the measured value is the thickness of the firmly adherent gel and that the other component of the mucus which is loosely adherent gel constitutes the 86% of the total thickness as showed by Atuma et al. (2001) in a study on rat's colonic mucus.

(13) Rectum lumen radius in two extreme states: 1.25 cm at empty state and 3.75 cm at extreme distension (ICRP 23).

(14) Transit times for "right colon" (AC + proximal half of TC), "left colon" (distal half of TC + DC), "rectosigmoid colon" and total are found to be 12.9 ± 1.6, 15.2 ± 1.6, 10.9 ± 1.6, and 39 ± 5 h, respectively, from 38 human subjects with median age greater than 15 y (Arhan et al. 1981).

(15) This is the total mucus thickness (loosely adherent plus firmly adherent mucus thickness) extrapolated from the measured thickness of adherent mucus gel of 155 μm on the surface of rectum in surgically resected human specimens (Pullan et al. 1994). The extrapolation is based on the assumption that the measured value is the thickness of the firmly adherent gel and that the other component of the mucus which is loosely adherent gel constitutes the 86% of the total thickness as showed by Atuma et al. (2001) in a study on rat's colonic mucus.

(16) The mean crypt depth of rectosigmoid colon is determined by weighting the crypt depths of SC and R by their lengths. That is (358.1)(40/55) + (244.7)(15/55) = 327.17. Weighting by transit time would give better estimation if transit time of SC and R were known separately. SD = $\{(40/55)^2(84)^2 + (15/55)^2(55.5)^2\}^{1/2} = 62.94$.

(17) This is the total mucus thickness (loosely adherent plus firmly adherent mucus thickness) extrapolated from the measured thickness of adherent mucus gel of 134 μm on the surface of left colon (distal half of transverse colon plus descending colon) in surgically resected human specimens (Pullan et al. 1994). The extrapolation is based on the assumption that the measured value is the thickness of the firmly adherent gel and that the other component of the mucus which is loosely adherent gel constitutes the 86% of the total thickness as showed by Atuma et al. (2001) in a study on rat's colonic mucus. (18) Obtained from photomicrograph (ICRP 23 1975); (19) Estimated from ratio of mass to smoothed area (ICRP 23 1975)

(20) For electron dosimetry, Stubbs et al. (1998) modeled the wall plus contents of the entire large intestine as two axial circular cylinders, each 10 cm in length, where the volume within the inner cylinder with radius 4 cm represented the contents and the volume between the inner cylinder and the outer cylinder with radius 4.5 cm represented the wall. The cylinders radii were based on the ICRP reference man data (1975). The mucus thickness was arbitrarily chosen to be 200 μm. The crypt depth was taken to be 700 μm due to Trier and Winter (1989). The depth of the sensitive cells was taken to be 550 μm assuming the sensitive cells start being populated from one-half the crypt depth.

(21) The data are from cadaver measurement (Magee et. al. 1986).

(22) Christensen (1991). (23) This datum is from rat measurement (Barrett and Donowitz 2000); (24) Whitehead (1989).

(25) Wall thickness on CT for colon is less than 0.3 cm ("Normal GIT: Wall thickness on CT." Online. www.ohsu.edu/ps-DiagRadiol/kojima/gitract.htm July 20, 2002). (26) The radius of the large intestine is 3.25 cm (Solomon and Davis 1978; Graaff and Fox 1999; Vander et al. 1970).

(27) The assumed target cell layer in Poston et al. large intestine model (1996).

The **ascending colon (AC)** was modeled as two coaxial circular cylinders along the z-axis with the center at (-8.50, -2.36, 19.225). The cylinders were 9.55 cm long with radii 2.50 cm and 2.25 cm. The **AC wall** was defined by the space between the two cylinders:

$$(x+8.50)^2+(y+2.36)^2 \le (2.50)^2,$$

$$(x+8.50)^2+(y+2.36)^2 \ge (2.25)^2,$$

$$\text{and } 14.45 \le z \le 24.0.$$

The lumen was defined by the space within the inner cylinder. The lumen was only 9.30 cm long because the inferior end of the AC was closed by wall material of similar composition and thickness (0.25 cm). Thus, the **AC lumen** was given by

$$(x+8.50)^2+(y+2.36)^2 < (2.25)^2,$$

$$\text{and } 14.7 \le z \le 24.0.$$

The lumen contains 60 g of contents only in its middle part which is 3.63 cm in length. Either side was empty. Each empty side is 2.835 cm in length (Fig. 7). The **AC contents** were given by

$$(x+8.50)^2+(y+2.36)^2 < (2.25)^2,$$

$$\text{and } 17.41 \le z \le 21.04.$$

Thus, the ascending colon had a wall-thickness of 0.25 cm and the mass of the contents was 60 g.

The **transverse colon (TC)** was modeled as two coaxial elliptical cylinders along the x-axis with the center at (0, -2.36, 25.0). The elliptical cylinders were 21.0 cm in

length with the radii 2.305 cm and 1.305 cm for the inner cylinder and 2.50 cm and 1.50 cm for the outer cylinder. The **TC wall** was defined by the space between the two cylinders:

$$\left(\frac{y+2.36}{2.50}\right)^2+\left(\frac{z-25.0}{1.50}\right)^2 \le 1\ ,$$

$$\left(\frac{y+2.36}{2.305}\right)^2+\left(\frac{z-25.0}{1.305}\right)^2 \ge 1,$$

$$\text{and } -10.50 \le x \le 10.50\,.$$

The lumen was defined by the space within the inner cylinder. The lumen was only 20.61 cm long because both ends of the TC were closed by wall material of similar composition and thickness (0.195 cm). The **TC lumen** was given by

$$\left(\frac{y+2.36}{2.305}\right)^2+\left(\frac{z-25.0}{1.305}\right)^2 < 1,$$

$$\text{and } -10.305 \le x \le 10.305\,.$$

The lumen contains 90 g of contents only in its middle part which is 9.16 cm in length. Either side is empty. Each empty side is 5.725 cm in length (Figs. 7 and 8). Thus the **TC contents** are given by

$$\left(\frac{y+2.36}{2.305}\right)^2+\left(\frac{z-25.0}{1.305}\right)^2 < 1,$$

$$\text{and } -4.58 \le x \le 4.58\,.$$

Thus, the transverse colon had a wall-thickness of 0.195 cm and the mass of the contents was 90 g.

The **descending colon (DC)** was modeled as two coaxial elliptical cylinders with the axis tilted at a small angle with the z-axis of the phantom, but the ends were defined by two horizontal planes (z = 8.72 and z = 24). The wall was defined by the space between the two cylinders with semiradii 1.88 cm and 2.13 cm (outer), and 1.63 cm and 1.88 cm (inner):

$$\left(\frac{x-x_0}{1.88}\right)^2+\left(\frac{y-y_0}{2.13}\right)^2 \le 1,$$

$$\left(\frac{x-x_0}{1.63}\right)^2+\left(\frac{y-y_0}{1.88}\right)^2 \ge 1,$$

$$\text{and } 8.72 \le z \le 24,$$

where

$$x_0 = 9.25+\frac{0.78(z-24)}{15.28}$$

$$\text{and } y_0 = \frac{2.50(8.72-z)}{15.28}.$$

The **DC lumen** was defined by the space within the inner cylinder

$$\left(\frac{x-x_0}{1.63}\right)^2+\left(\frac{y-y_0}{1.88}\right)^2 < 1,$$

$$\text{and } 8.72 \le z \le 24.$$

The lumen contains 25 g of contents only in its middle part, which is about 2.50 cm in length. Either side is empty (Fig. 9). The **DC contents** were given by

$$\left(\frac{x-x_0}{1.63}\right)^2+\left(\frac{y-y_0}{1.88}\right)^2 < 1,$$

$$\text{and } 15.11 \le z \le 17.61.$$

Thus, the descending colon had a wall-thickness of 0.25 cm and the mass of the contents was 25 g.

The **recto-sigmoid colon (RSC)** consists of two regions — upper and lower (Fig. 9). The wall plus contents of each region was represented by one-quarter of two concentric circular tori. The wall was defined by the space between the tori. The contents were defined by the space within the inner torus.

Upper region

The **RSC wall** was defined by:

$$\left(\sqrt{(x-3.0)^2+(z-8.72)^2}-5.72\right)^2+(y)^2 \le (1.57)^2,$$

$$\left(\sqrt{(x-3.0)^2+(z-8.72)^2}-5.72\right)^2+(y)^2 \ge (1.44)^2,$$

$$x \ge 3.0, \text{ and } z \le 8.72.$$

The **RSC contents** were defined by:

$$\left(\sqrt{(x-3.0)^2+(z-8.72)^2}-5.72\right)^2+(y)^2 < (1.44)^2,$$

$$x \ge 3.0, \text{ and } z \le 8.72.$$

Lower region

The **RSC wall** was defined by:

$$\left(\sqrt{(x-3.0)^2+(z)^2}-3.0\right)^2+(y)^2 \le (1.57)^2,$$

$$\left(\sqrt{(x-3.0)^2+(z)^2}-3.0\right)^2+(y)^2 \geq (1.44)^2,$$

$$x \leq 3.0, \text{and } z \geq 0.$$

The **RSC contents** were defined by:

$$\left(\sqrt{(x-3.0)^2+(z)^2}-3.0\right)^2+(y)^2 < (1.44)^2,$$

$$x \leq 3.0, \text{ and } z \geq 0.$$

Thus, the recto-sigmoid colon had a wall-thickness of 0.13 cm and the mass of the contents was 92.8 g.

MONTE CARLO SIMULATION OF ELECTRON AND PHOTON TRANSPORT FOR RADIATION DOSIMETRY

INTRODUCTION

The absorbed dose due to internally deposited radionuclides is usually evaluated by Monte Carlo simulation because the complex nature of radiation transport and the complexity of the exposure geometry (e.g., human body), make analytical solution intractable. The use of Monte Carlo methods in solving dosimetric problems has dramatically increased in recent years due to a rapid increase in speed and a decrease in cost of data processing, as well as the availability of large, general-purpose software packages. MCNP is such a general-purpose Monte Carlo N-Particle code package that can be used for neutron, photon, electron, or coupled neutron/photon/electron transport (Briesmeister 2000).

The most important condition for an accurate Monte Carlo simulation is that one takes into account accurately all the relevant physical processes. As radiation passes through matter it undergoes various physical processes depending on the type of radiation (photon, neutron, or electron/positron), energy, and on the interacting medium. The fundamental quantities describing the properties of the medium in the photon and electron interactions are atomic number or "effective atomic number" (Z_{eff}) for compound media, electron concentration per unit mass, which can be represented basically by the ratio of effective atomic number to effective mass number ($(Z/A)_{eff}$), and mass-density. A multiplication of the Avogadro constant with $(Z/A)_{eff}$ gives electron

concentration per unit mass that increases with increasing the contents of low-Z, in particular hydrogen, elements in the compound. Rogers and Bielajew (1990) reviewed how the interaction cross sections vary with energy and properties of matter to show which processes are relevant in a given simulation. This review briefly describes almost all possible interaction processes of photons and electrons. Details of these interaction mechanisms are referred to the standard reference works of Heitler (1954) and Evans (1955).

A Monte Carlo simulation code has four major components: (1) the cross-section data for all the processes being considered in the simulation, (2) the algorithms that account for the processes and govern the particle transport, (3) the methods used to specify the geometry of the problem and to determine the physical quantities of interest, and (4) the analysis of the information obtained during the simulation.

The first two components affect the underlying physics of the simulation, while the last two of these components can greatly affect the running time without affecting the physics. The physics of radiation interactions is the very essence of a Monte Carlo code. Two codes are essentially different because the physics treatments in those codes are different.

This chapter provides an overview of Monte Carlo simulation of electron and photon transport, and describes the physical processes those govern the transport and the Monte Carlo simulation techniques of those processes in various codes, in particular MCNP. The salient features of two other widely used electron-photon transport codes, one is based on ETRAN (electron transport) codes originally developed at the National

Bureau of Standards by Berger and Seltzer (1973) and the other is based on the EGS (electron-*g*amma-shower) code developed by Ford and Nelson (1978) at the Stanford Linear Accelerator Center also are briefly discussed for comparison purposes.

MONTE CARLO TRANSPORT

An overview

The earliest use of a Monte Carlo simulation technique was around 1873 (Hammersley and Handscomb 1964). The real development and application of the technique, however, stemmed from the work on the atomic bomb during World War II by von Neumann, Ulam, and Fermi. von Neumann coined the term "Monte Carlo" to reflect the idea that a conceptual roulette wheel could be employed to select the random nuclear process. Today, Monte Carlo methods are used in a wide range of scientific endeavors and the term has a variety of different meanings (Shreider 1966). In the context of radiation transport, Monte Carlo methods are those which simulate the random trajectories of individual particles by using machine-generated (pseudo-)random numbers to sample from the probability distributions governing the physical processes involved. By simulating a large number of histories, information can be obtained about average values of macroscopic quantities such as energy deposition. Moreover, since one follows individual particle histories, the technique can be used to obtain information about statistical fluctuations of particular kinds of events.

Besides Monte Carlo methods, there are various analytic approaches for solving the radiation transport equation. Most analytic solutions require many simplifying assumptions, in particular for electrons because of the complex nature of electron

transport. Berger (1963) reviewed the early work in this field. Considerable progress has been made during the two decades following his review in applying the deterministic method of discrete ordinates to electron-photon transport calculations (Morel and Lorence 1986). However, since the technique solves the transport equation directly, it is not capable of answering the question about an individual particle history in as direct a manner as the Monte Carlo technique.

The transport of electrons/positrons and other charged particles is fundamentally different from that of uncharged radiations (x- or γ-rays and neutrons). The interaction of the uncharged radiations is characterized by relatively infrequent isolated collisions, with simple free flight between collisions. By contrast, a charged particle, being surrounded by its coulomb electric force field, undergoes a large number of small interactions with one or more electrons or with the nucleus of practically every atom it passes. As a result, a large number of low-energy "knock-on" electrons are set in motion and many atoms are left in excited states. Also, a large number of elastic scatterings from nuclei guide the electron in a tortuous path. This large number of interactions in various forms makes Monte Carlo simulations of electron transport intractable and unfeasible if each interaction is to be simulated individually. These problems are made tractable by using the "condensed-history" Monte Carlo technique (Berger 1963), in which the path of the electron is broken into a series of steps for which the effects of the large number of individual interactions occurring during the step are grouped together. One grouping accounts for the large number of elastic scattering using a multiple-scattering theory such as that of Molière (1948) or of Goudsmit and Saunderson (1940). The other major

grouping accounts for the large number of small energy losses through the use of a continuous-slowing-down approximation (CSDA) model. These steps are chosen to be long enough to encompass many collisions (so that multiple-scattering theories are valid) but short enough that the mean energy loss in any one step is small (so that the approximations necessary for the multiple-scattering theories are satisfied).

Berger (1963) divided charged particle (electron or positron) transport models into two broad classes distinguished by how the energy and direction of the primary charged particle are related to the individual interactions. In class I models, the energy and direction of the primary charged particle are not affected by the creation of individual secondary particles. In Class II models, individual interactions affect the energy and direction of the primary electron when they create knock-on electrons or bremsstrahlung photons above certain energy thresholds, although the effects of secondary particle production below these thresholds are still grouped together. EGS uses Class II models, whereas ETRAN-based codes that include MCNP use Class II models for bremsstarhlung production and Class I models for the production of knock-on electrons. Rogers and Bielajew (1990) discussed in detail the distinctions between these two classes with reference to EGS and ETRAN.

MCNP

Electron transport. The electron physics in MCNP is essentially that of Integrated TIGER Series (ITS) (Halbleib 1988), a system of general-purpose, application-oriented electron/photon transport codes developed and maintained by John A. Halbleib and his

collaborators at Sandia National Laboratories in Albuquerque, New Mexico. The ETRAN codes are the basis for the ITS.

In MCNP, the electron transport algorithms used to predict probability distributions for significant quantities, such as energy loss and angular deflection are based on a number of multiple-scattering theories, notably the Goudsmit-Saunderson theory for angular deflections (1940), the Landau theory of energy-loss fluctuations (Landau 1944), and the Blunck-Leisegang enhancements of the Landau theory. These theories rely on a variety of approximations that restrict their applicability, so that they cannot solve the entire transport problem. In particular, it is assumed that the energy loss is small compared to the kinetic energy of the electron. Detailed formulations of these theories are left to the detailed documentation. The salient features of the electron transport algorithms in MCNP are summarized below; more can be found in the code documentation (Briesmeister 2000).

ETRAN-based codes including MCNP chose a sequence of pathlengths of such condensed-history steps or "major steps" such that the pathlength of a major step, $s = s_n - s_{n-1}$, and the energy loss, $E = E_{n-1} - E_n$, during the step are related by (Briesmeister 2000)

$$E_{n-1} - E_n = -\int_{S_{n-1}}^{S_n} \frac{dE}{ds}\, ds \qquad (1)$$

where, s_n and E_n are the total pathlength and energy of the electron at the end of *n* steps, and *dE/ds* is the "total stopping power" (average energy loss per unit pathlength due to

both the inelastic coulomb collisions and radiative emission of bremsstrahlung). The consecutive energy values at the boundaries of the major steps are related by

$$\frac{E_n}{E_{n-1}} = k \tag{2}$$

where, k is a constant. The most commonly used value in ETRAN-based codes including MCNP code is $k = 2^{-1/8}$, which results in an average energy loss per major step of 8.3% of the initial energy of the step. Obviously, the energy-dependent pathlength of a major step, determined by Eqs. (1) and (2), is based on the CSDA that uses the total stopping-power to describe the gradual energy loss along the electron track.

Many inaccuracies associated with the inherent approximations in the theories (e.g., multiple scattering theory) underlying the electron transport algorithms can greatly be reduced if sufficiently small step sizes are employed. The ETRAN codes and MCNP break the major step into m smaller substeps, each of pathlength s/m. The number of substeps, m, is determined either from empirically-determined default values, ranging from 2 for $Z_{\text{eff}} < 6$ to 15 for $Z_{\text{eff}} > 91$, or by the user, based on geometric considerations. A user can provide the m-values to override these default values. A reasonable rule of thumb is that an electron should make roughly at least ten substeps in any material of importance to the transport problem (Briesmeister 2000). The required number of substeps, m, in any material region with dimension of t can, therefore, be determined using following inequality:

$$m(E) \geq \frac{\left(s(E) \times 10\right)}{t} \tag{3}$$

The *s*-values for different electron energies can be obtained from Table 85 in MCNP output, in which the values of the corresponding mass thickness in unit of g/cm^2 are tabulated under the column of "DRANGE" as function of energy, i.e.,

$$s(E) = \frac{DRANGE(E)}{\rho} \tag{4}$$

The number of substeps and the length of the last substep may be reduced if the electron energy falls below the energy-boundary of the current major step due to fluctuations in the energy loss-rate, and/or if the electron reaches a geometric boundary. In these circumstances, or upon the completion of *m* substeps, a new major step is begun, and the energy loss rate is resampled.

In contrast, EGS allows all physical processes as well as boundaries to affect the choice of electron step sizes. There is no substep. On average, the electron step size in EGS is much larger than that in ETRAN-based codes. Although this means that the details of the electron transport are inaccurate, it does not affect the results in this case. Larger electron step size is the only reason that EGS runs faster than ETRAN because timing is almost entirely determined by the number of electron steps taken, and this parameter is under the user's control in MCNP, as discussed before.

At the beginning of each major step, the "total collision stopping-power" is sampled using the Berger (1963) formula. The total collision stopping-power is the average energy loss per unit length in all inelastic coulomb collisions with bound atomic electrons of the medium, irrespective of the collision impact parameter, which determines the amount energy loss in the collision. The Berger formula (1963) for total collision stopping power considers the reduction in the collision stopping-power due to

the density effect* but the reduction due to shell correction** is omitted. Thus, the stopping-powers are overestimated. These overestimations are significant at very low energies.

MCNP uses the prescriptions of Sternheimer, Berger and Seltzer (1982) for calculating the density-effect correction factor in the EL03 evaluation and uses the method of Sternheimer and Peierls (1971) for the EL01 evaluation. It is worthwhile to mention here that MCNP, version 4C, has two electron interaction data libraries: 03E and 01E. Only the 01E library is available in version 4A and B. The data library 03E, utilized in the present calculations, contains more recent data evaluated from rigorous calculations. However, in the Sternheimer, Berger and Seltzer (1982) treatment, calculation of the density effect uses the conduction state of the material to determine the contribution of the outermost conduction electron to the ionization potential. The occupation numbers and atomic binding energies used in the calculation are from Carlson (1975).

---

* The density-effect correction factor, δ, is applied to the Berger formula (1963) to account for the reduction in the collision energy loss due to the polarization of the atoms near the track of the passing electron. This polarization, in turn, weakens the coulomb force field experienced by the more distant atoms so as to reduce the stopping power. This reduction is particularly strong in dense media, and is, therefore, called the density effect. The greater the electron velocity, the greater is the density effect because, by virtue of the Lorentz contraction, distant collisions become more important. In fact, at very high energies, the density-effect correction to the stopping power is significant even in gases (ICRU 1984). The results regarding the percent reduction of the electron collision stopping power due to the density effect are tabulated for a few selected media including water in ICRU Report 37 (1984).

** The "shell correction" is applied to the collision stopping-power formula to compensate for the fact that the projectile velocity is not necessarily large compared to the velocity of the target electrons. The collision stopping power equation is not well satisfied when the velocity of the passing particle ceases to be much greater than that of the atomic electrons in the stopping medium. As the particle velocity decreases toward that of the K-shell electrons ($\approx Zc/137$), those electrons gradually decrease their participation in the collision process. Thus, the stopping power becomes smaller than that obtained using the algorithm. In contrast with the density-effect correction, which becomes significant for stopping power at high energies (greater than 1 MeV), the shell correction to the stopping power is important at low energies (less than 100 keV).

As mentioned before, the collision-stopping power formula, without the shell correction term, overestimates the quantity. Now the question is how much overestimation occurs. According to ICRU Report 37 (1984), "We have attempted to make a rough estimate of the possible error in the calculated electron stopping power due to the omission of a shell correction term, assuming arbitrarily, that the error is twice as large as the reduction of the stopping power for protons with the same velocity. At an electron energy of 100 keV, the error is then estimated to be ≈0.3% for H_2O, ≈0.7% for Al, ≈1.3% for Cu, ≈2% for Ag, and ≈3% for Au. At 10 keV, the corresponding error estimates are ≈2% for H_2O, ≈4% for Al, ≈9% for Cu, ≈12% for Ag, and ≈21% for Au. The use of Eq. 2.16 (the same equation is used in MCNP for collision stopping power) is questionable at energies below 10 keV. However, for low-Z materials, such as water, air, or plastics, the evidence presented later in Section 8 suggests that the errors may be no greater than ≈3% at 5 keV, ≈7% at 2 keV, and 10 to 15% at 1 keV."

The estimations for water are equally applicable to the GIT and other soft tissue organs, the medium of interest in the present study, as the GIT or soft tissue is almost similar in Z_{eff}, $(Z/A)_{eff}$, and mass-density to that of liquid water. Above estimations illustrate that the error in the collision stopping power increases as electron slows down. In other words, the error is minimum at the beginning of an electron track and grows as the electron slows down along its track. If all these errors, from the beginning to the end of the trajectory of a primary electron, as well as the errors associated with all the

transportable knock-on electrons[§] with energies greater than the energy cut-off, produced by the primary electron and from the subsequent interactions of the energetic knock-ons, were taken into account, the "effective error" would become greater than the reported error, estimated at initial energy of the primary electron, in the ICRU Report 37 (1984).

Let us digress briefly to examine how the increment in collision stopping power might affect the average absorbed doses calculated using the MCNP code in which the shell correction has been omitted. This increment does not affect the absorbed doses to the source region except near the source boundary where charged particle equilibrium (CPE) for knock-on electrons does not exist. The source electrons and the knock-on electrons originating within the peripheral shell volume of thickness equal to the range of the source electrons carry less energy out of the source region because of the increment in collision stopping powers. Thus, average absorbed dose to the source would increase while the absorbed doses to the wall within the range of the source electrons would decrease. Beyond the source-electron range, bremsstarhlung photons are the sole contributor to the absorbed dose to the wall. Although, radiative stopping power is uncorrelated with collision stopping power, the energy depositions by the photon-

[§] The error in collision stopping power of a knock-on electrons with energy less than energy cut-off is not of concern because MCNP makes the electrons deposit all energy at the point of origin on the track of the "parent" electron. MCNP follows a particle, or a particle is transportable, only when its energy is greater than the energy cutoff. The default energy cutoff is 1 keV for both photons and electrons. User supplied cut-off of more than 1 keV can override this default value. MCNP makes a reasonable choice by setting 1 keV as the default cut-off for electrons because the stopping powers of such low-energy electrons are too large (120 MeV cm^2 g^{-1} at 1 keV in liquid water (ICRU 1984), corresponding to a CSDA range of about 0.04 μm which is far smaller than a human cell nucleus, several μm in diameter) to make any meaningful transport of their energies in separate tracks. For all dosimetry purposes, except for microdosimetry, it can be assumed with high accuracy that such low-energy electrons impart all their energy locally. This locally imparted energy loss rate is termed as "restricted stopping power." Most of the knock-on electrons have energies less than 1 keV. This fact is obvious from the ratio of restricted (at 1 keV) to total collision stopping power in liquid water reported in ICRU Report 37 (1984). This ratio is 0.8686 for 10 keV, 0.7549 for 100 keV, 0.6997 for 500 keV, 0.6780 for 1 MeV, and 0.6315 for 5 MeV.

induced-electrons are affected due to the increased collision stopping power. As a result, doses higher than the actual doses would be expected. The effect on the absorbed doses within the CSDA range might be much greater than that beyond the range. All the analyses done so far are qualitative. We do not know quantitatively how much deviation might occur in the calculated absorbed doses using an MCNP code that ignores the shell correction in the collision stopping-power formula.

Despite the fact that the collision stopping power varies (increases or decreases depending on the initial energy of the electron) as the electron slows, MCNP uses a constant collision stopping power, sampled at the beginning of a major step, for the entire length of a major step to compute the energy loss during each substep and to compute the projected energy of the primary electron at the end of the substep.

It is necessary to discuss how much variation in the collision stopping power can occur during a major step. Using Eq. 2 and data on collision stopping powers, extracted from Table 85 of MCNP output, calculations show that the percent difference between the collision stopping powers at the energy boundaries of a major step is ≈6% below 100 keV, ≈4% at 200 keV, ≈3.2% at 300 keV, ≈2.5% at 400 keV, and ≈2% at 500 keV and ≈0.5% at 1 MeV for the medium of GIT. These are the maximum possible errors in the collision stopping power at the energy end of a major step that can occur when all the substeps of the major step are completed. Obviously, the errors at the end energy are smaller than those of maximum values if the number of substeps is reduced as a result of fluctuations in the energy loss rate and/or intervention of geometric boundary. These errors in the collision stopping power should lead to the underestimations and

overestimations in the absorbed doses to low-Z media (e.g., water, soft tissue) for electron energies below 2 MeV and above 4 MeV, respectively. The errors would be negligible for the electron energies between 2 and 4 MeV because the collision stopping power is almost constant between 2 and 4 MeV for water. The underestimations for energies below 2 MeV would largely compensate the overestimations made by omission of shell correction. None of the latest three editions of MCNP manual (Briesmeister 1993, 1997, 2000) indicates that the collision stopping power, used to compute energy loss rate in a major step, is an average value or a value for the initial energy of the step. Use of an average stopping power would result in smaller error. This error might be greater if the major step is terminated before completing all the substeps in the wake of the circumstances mentioned before.

The production of secondary radiations (bremsstrahlung photons, knock-on electrons, electron-induced fluorescent x-rays and Auger electrons) and the angular deflection of the primary electron/positron are sampled at the end of each substep.

The electron energy at the end of a substep is reduced only by the energy of the sampled bremsstrahlung photon/photons, because the electron energy loss during a substep is computed by using collision stopping power, which explicitly takes into account the energy loss rate due the production of all secondaries except bremsstrahlung. Thus, the length of the substep ultimately derives from the total stopping power used in Eq. 1. The direction of the electron is unaffected by the generation of the photon, because the angular deflection of the electron caused by elastic scattering from the electron-nucleus and electron-electron interactions is controlled by the multiple-

scattering theory described later in this section. The angular deflection of the transportable bremsstrahlung photon/photons, from the direction of the primary electron is sampled from tabular data extracted from Berger and Seltzer (1970). In the EL03 evaluation, the production probability and energy spectra of bremsstrahlung photons, resulting from electron-nucleus and electron-electron inelastic radiative interactions, are sampled from the evaluations made by Seltzer and Berger (1986), and Seltzer (1988a), who applied detailed physics considerations including the screening effect to the evaluations. The "radiative stopping power", which is average energy loss per unit pathlength due to the emissions of bremsstrahlung, is also obtained from these evaluations for either EL01 or EL03.

The evaluations made by Seltzer and Berger (1986), and Seltzer (1988a) use detailed calculations of the electron-nucleus bremsstrahlung cross-section for electron energies below 2 MeV and above 50 MeV. The evaluation below 2 MeV uses the results of Tseng, Pratt, and collaborators (Tseng and Pratt 1971, 1974; Pratt et al. 1981), based on numerical phase-shift calculations. For 50 MeV and above, the analytical theory of Davies, Bethe, and Maximom (1954a, 1954b) and Olsen (1955) is used and is supplemented by the Elwert coulomb correction factor (1939) and the theory of the high-frequency limit or tip region given by Jabbur and Pratt (1963, 1964). Screening effects are accounted for by the use of Hartree-Fock atomic form factors (Hubbell et al. 1975; Hubbell and Øverbo 1979). The values between these firmly grounded theoretical limits are found by a cubic-spline interpolation as described by Seltzer and Berger (1986), and Seltzer (1988). Electron-electron bremsstrahlung is also included in the cross-section

evaluation based on the theory of Huang (1975) with screening corrections derived from Hartree-Fock incoherent scattering factors (Hubbell et al. 1975; Hubbell and Øverbo 1979). The energy spectra for the bremsstrahlung photons are provided in the evaluation. It may be noted that EGS predicts more bremsstrahlung than does ETRAN (including MCNP) and experiments for electron energies below 2 MeV (Ford and Nelson 1978; Ewart and Rogers 1982). This shortcoming of EGS is significant for problems, which isolate the bremsstrahlung from low-energy electrons, but is not important in other situations.

As electrons and positrons pass through matter, they lose energy through both radiative and collision processes. The energy loss through the later process is due to inelastic coulomb collisions with bound atomic electrons of the medium. These collisions result in atomic ionization and excitation, depending on the impact parameter of the collision. The ionization events create "knock-on" electrons with kinetic energies extending from zero to a maximum, which is one-half of or equal to the initial energy of electron or positron, respectively. In the event of ionization or excitation, or in the photon-interaction events (e.g., photoelectric, Compton, triplet production), discussed later, vacancies are produced in the electron shells of the atom, usually in the k-shell. Electrons from outer or higher-energy shells with the attendant creation of fluorescent X-rays or Auger[§§] electrons fill these vacancies. The higher shell vacancies are created

[§§] If an electron in an outer or higher-energy shell makes a transition to a vacancy in an inner or lower-energy shell, a fluorescent x-ray may be emitted with energy equal to the difference in binding energy between the two shells. Instead of emitting an x-ray, an electron in some other shell may be emitted by absorbing this "transition energy". This electron, called an Auger electron, is emitted with energy equal to the transition energy minus the binding energy of the electron. If the transition takes place between subshells of the same shell, the small difference in the binding energies may be transferred to an outer-shell electron, in this case called a Coster-Kronig electron.

and filled. A cascade of such filling events might take place to restore pre-collision status of the atom. This "relaxation process" can be very complex. However, the resultant X-rays and Auger electrons are, in general, of very low energy unless the original vacancy was in the K-shell of high-Z atoms. The "fluorescence yield", which indicates how often an X-ray be produced, instead of an Auger electron, is small for low-Z materials (0.5% for Z = 8) and over 90% in the K-shell for material with $Z \geq 60$ (Rogers and Bielajew 1990).

One major difference, important to low-energy transport, between the ETRAN-based codes including MCNP and the standard EGS code is that the EGS does not include the creation of fluorescent x-rays and Auger electrons, whereas ETRAN does. But ETRAN models for treating the fluorescent X-rays and Auger electrons are somewhat crude. ETRAN and MCNP consider only the K-shell ionization for the highest Z-component of a material. Thus, inclusion of trace high-Z impurities could mask K-shell impact ionization from other dominant components. In the EL01 evaluation, a K-shell ionization event generated a photon with the average K-shell energy. The EL03 evaluation generates photons with energies given by Everett and Cashwell (1973). The way the Auger transitions are handled is same in the EL03 and EL01 evaluations. If an atom has undergone an ionizing transition and can undergo a relaxation, and if it does not emit a photon, it will emit an Auger electron. The difference between EL01 and EL03 is the energy with which an Auger electron is emitted, given by $E_A = E_{\overline{K}}$ or $E_A = E_{\overline{K}} - 2E_{\overline{L}}$ for EL01 or EL03, respectively. The EL01 value is the

highest energy Auger electron while the EL03 value is the energy of the most probable Auger electron.

The code SANDYL (Colbert 1974) and some of the ITS codes, such as P-codes (Halbleib and Melhorn 1984), consider electron ionization of all shells, and atomic relaxation from the K, L, M, and N shells. But Halbleib and Melhorn report, "in the vast majority of problems, the P-codes give results that are virtually identical to those of the standard codes" (which use the ETRAN model).

As mentioned before, the knock-on electrons may have energies up to the half of or up to equal to the initial energy of electron or positron, respectively. The knock-on electrons with energies above the energy cut-off will only be followed separately. MCNP uses, at each electron substep, a probability function, derived from the Møller cross section for scattering of an electron by an electron, to determine randomly whether transportable knock-on electrons will be generated. If so, the energy of each knock-on electron is sampled using another probability distribution function, derived also from the Møller cross section for scattering. Once an energy has been sampled, the angle between the primary direction and the direction of the newly generated knock-on electron is determined by momentum conservation. This angular direction is used for the subsequent transport of the knock-on electron. However, the sampling of the knock-on electron, as mentioned before, alters neither the energy nor the direction of the primary particle. This is because, on the average, both the energy loss and the angular deflections of the primary electron due to elastic scattering from atomic nuclei and electrons have been taken into account by the multiple scattering theories. It may be noted that the class

II model in EGS has a slight inconsistency because the primary electron direction is altered twice for the creation of a knock-on electron with energy greater than the cut-off energy. But this effect is small (Rogers 1984a).

Because a major step represents the cumulative effect of many individual random collisions, fluctuations in the energy loss rate will occur. But Eqs. 1-2, used to predict the pathlength of a major step, are based on the CSDA in which the energy-loss fluctuations (commonly termed as "energy straggling") are disregarded, and the rate of energy loss at any point along the track is assumed to be equal to the stopping power. However, the Landau theory of energy-loss fluctuations (Landau 1944) and the Blunck-Leisegang enhancements of the Landau theory, both based on multiple-scattering theory, are applied once per major step to account for the energy straggling. In all versions prior to 1987 (e.g., EGS4), there was an error in the Landau/Blunck-Leisegang energy straggling distribution, which caused the mean energy loss to be underestimated. This error, Rogers and Bielajaw (1990) wrote, "led to about a 7% underestimate of dose near the surface for 10-20 MeV electrons on water and caused about a 4% underestimate of R_{50}, the depth at which the dose drops to 50% of its value (see Rogers and Bielajaw 1986, for details). This error was not a fundamental problem and was corrected in ETRAN in 1987 (Seltzer 1989) and in version 2.1 of the ITS system."

When the electron/positron collision impact parameter is much smaller than the atomic radius, the coulomb-force interaction takes place mainly with the nucleus. In all but 2-3% of such encounters, the electron is scattered elastically and does not emit an x-ray photon or excite nucleus (Attix 1986). It loses just the insignificant amount of kinetic

energy necessary to satisfy conservation of momentum for the collision. Hence, this is not a mechanism for the transfer of energy to the absorbing medium, but it is an important means of deflecting electrons. It is the principle reason why electrons follow very tortuous paths, especially in high-Z media, and why electron backscattering increases with Z. The differential elastic-scattering cross section per atom is proportional to Z^2 (Evans 1955). In the other 2-3% of the cases in which the electron/positron passes near the nucleus, an inelastic radiative interaction occurs in which a bremsstarhlung photon is emitted with a fraction (up to 100%) of the primary particle kinetic energy. The primary particle is deflected to conserve momentum. Change in the direction of the primary particle also occurs when a knock-on electron is produced through elastic scattering with an atomic electron.

In MCNP, the direction of the primary electron/positron is altered once at the end of each substep to account for all these scattering (i.e., angular deflection) interactions. The ETRAN codes and MCNP rely on the Goudsmit-Saunderson multiple-scattering theory (1940) for the probability distribution of angular deflections. The microscopic cross section for angular deflection is taken from numerical tabulations developed from the work of Riley (1975) for electron energies below 0.256 MeV. For higher-energy electrons, the algorithm for microscopic cross section, used in MCNP, is approximated, by Seltzer (1988b), as a combination of the Mott and Rutherford cross sections, with a screening correction. Based on the recommendation of Seltzer (1988b), a slightly modified version of the Molière (1948) formula is used for the screening factor. It may be noted that EGS uses Molière (1948) theory to account for angular deflections in

contrast to the Goudsmit-Saunderson theory (1940) used in ETRAN-based codes, as mentioned before. Berger provides a good overview and comparison of the two theories (1963) and Berger and Wang (1989) extend the comparison. One of the differences between the theories is that the Molière theory does not distinguish between electron and positron scattering whereas Goudsmit-Saunderson theory does. However, Berger (1963) has shown that, in reality, there is often little difference between the theories.

The ETRAN-based codes use identical physics for the transport of electrons and positrons but distinguishes between them for tallying purposes, and for terminal processing because each positron annihilates, creating two 511-keV photons, when its history terminates. The EGS system explicitly takes into account the differences between the electron and positron stopping powers and the Møller and Bhabha scattering cross-sections, used for electrons and positrons, respectively. Rogers (1984a, 1984b) has shown that, in some cases, these differences cannot be ignored. EGS also takes into account positron annihilation in flight but this effect is insignificant (Grosswendt and Waibel 1975).

Conclusion

In ETRAN-based codes including MCNP, major step sizes for electron transport are chosen so that, on the average, electron energy decreases by a constant fraction, usually $2^{-1/8}$ (= 0.917). For this step, the energy lost by the electron is determined by sampling from the energy-loss straggling distribution. Within this major step, a series of m substeps of equal length are taken. The value of m increases with Z_{eff}, typically being 2 for $Z_{eff} < 6$ and 15 for $Z_{eff} > 91$, since smaller steps must be taken with higher Z to

ensure that the electron transport is accurate without a pathlength correction. For each of these substeps the appropriate distributions are sampled to determine the deflection due to multiple scattering and whether a knock-on electron or bremsstrahlung photon is produced, or whether a K-shell ionization has occurred. If a secondary particle is created, the appropriate differential cross sections are sampled to determine the particle energy and direction. The point of origin is selected randomly along the substep, but the step length of the primary particle is not affected. Only the creation of a bremsstrahlung photon directly affects the energy, not the direction, of the primary particle. But the production of the other secondaries alter neither the energy nor the direction of the primary particle since the energy loss due those secondary productions has already been included in the Landau energy-loss straggling formalism. The angular deflection of the primary particle is only controlled by Goudsmit-Saunderson formalism. The number of substep and the length of the last substep may be reduced if the electron energy falls below the energy-boundary of the current major step because of fluctuations in energy loss-rate due to energy straggling and production of bremsstrahlung, and/or if the electron reaches a geometric boundary. In these circumstances, the energy loss is recomputed for the distance up to the point of "forced" termination; a new major step is begun, and the energy loss-rate is resampled. The multiple-scattering deflection in the last substep is then sampled using a Gaussian approximation since the Goudsmit-Saunderson formalism cannot be sampled for arbitrary step sizes during a simulation.

Photon transport. MCNP has two photon interaction models: simple and detailed. The simple model considers the following physical processes: photoelectric effect without fluorescence and Auger electrons, Compton (incoherent) scattering from free electrons without the use of form factors which account for electron binding effects, and pair production. The highly forward-peaked coherent scattering is ignored. The simple model is intended for high-energy photon problems or problems where electrons are free. In contrast, the detailed model considers coherent and incoherent scattering with the use of form factors, pair production, and accounts for fluorescent photons and Auger electrons after photoelectric absorption. The detailed model is the best treatment for most applications, particularly for high-Z materials or deep penetration problems. MCNP uses a detailed model by default for photon energies below 100 MeV. This detailed physics treatment was applied to the present MCNP calculations. The following discussion applies only to this model, unless otherwise specified. It may be noted that the standard EGS code uses the same model for photon transport as the MCNP simple model with the exception that EGS4 has an option to include coherent (Rayleigh) scattering without the form factor. Hence, in any situation where electron binding is comparable to the energy of the particle being transported, such as low-energy transport in high-Z material, one must exercise care with EGS code and the use of simple model of MCNP.

For energies of the order of 1 MeV, the most frequent event is a compton interaction (incoherent scattering), in which the photon scatters from an unbound electron at rest and sets it in motion. MCNP uses modified Klein-Nishina differential cross sections (Briesmeister 2000) to determine the angle and energy of the compton-

scattered photon and the recoil kinetic energy of the electron. To take into account the effects of electron binding in an atom, a modification is made in the Klein-Nishina differential cross sections (Evans 1955), derived by applying Dirac's relativistic theory of the electron to the compton effect. MCNP handles all photon-induced charged particles (electrons and positrons) including this compton electron in three distinct ways, which are the same for both the simple and detailed photon physics treatment. The kinetic energy of the photon-induced charged particle can be deposited locally irrespective of its energy, can be transported, or (default) can be treated with the thick-target bremsstrahlung (TTB) approximation. The TTB approximation assumes that the photon-induced charged particles travel in the direction of the incident photon and that they are immediately annihilated. Any bremsstarhlung photons produced by these nontransported charged particles are banked for later transport. Thus electron- or positron-induced photons are not neglected, but the time-consuming charged particle transport is omitted. However, in our calculations, the photon-induced charged particles as well as all the successive generations of these particles are transported so as to make the simulation as realistic as possible.

The Klein-Nishina differential cross section is sampled exactly by using Kahn's method (1956) below 1.5 MeV and by Koblinger's method (1975) above 1.5 MeV as analyzed and recommended by Blomquist and Gelbard (1983).

The electrons of an atom do not move independently of one another, and it is

possible for gamma-radiation scattered classically (i.e., according to Thomson theory[¶] of radiation) by one electron to interfere with that scattered by another electron. At any point in space, radiation scattered from all the electrons in the atom is received and the radiation is of the same wavelength as the primary. This type of scattering by all electrons of an atom is collectively called "coherent" (Rayleigh) scattering in contrast to the "incoherent" (Compton) scattering of a photon with an individual electron. The coherent scattering is important when the wavelength of the radiation is long compared with the electron spacing in the atom, i.e., it is important for low-energy photons and high-Z materials. The coherent scattering contributes nothing to kerma[¶¶] or absorbed dose since no energy is given to any charged particle, nor is any ionization or excitation produced. Thus, it is the only photon process that cannot produce electrons for further transport or use the TTB approximation. The algorithm used in MCNP for sampling the differential cross section for coherent scattering is obtained by multiplying the Thomson differential cross section (Attix 1986) by a factor. This factor is a decreasing function of photon energy and the cosine of the photon scattering angle (μ).This factor decreases rapidly with μ as μ varies from +1 to –1, and therefore, the coherent cross section is peaked in the forward direction. The Thomson differential cross section (Attix 1986), which accounts for the radiation scattering by a single free electron, is independent of

---

[¶] J. J. Thomson provided the earliest theoretical description of the process by which a gamma ray can be scattered by an electron (see Evans 1955). Attix (1986) wrote, "In this theory the electron was assumed to be free to oscillate under the influence of the electric vector of an incident classical electromagnetic wave, then promptly to reemit a photon of the same energy. The electron thus retains no kinetic energy as a result of this elastic scattering."

[¶¶] Kerma, which stands for Kinetic Energy Released in the Medium (the "a" has been added only for phonetic reasons), is defined by Attix (1986) as follows, "the kerma is the expectation value of the energy transferred to charged particles per unit mass at a point of interest, including radiative-loss energy but excluding energy passed from one charged particle to another."

the photon energy and Z, and is front-back symmetrical. The factor is multiplied by the Thomson differential cross section to take into account the combined scattering action of the whole atom and the binding effect of electron in the atom, and to reduce the Thomson cross section more extremely for backward scattering for high-energy and low-Z materials.

Below 1 MeV, the predominant photon interaction is the photoelectric effect, in which the atom absorbs the photon and a photoelectron is ejected, leaving a vacancy in the atom, usually in the K shell. Electrons from outer shells, with the attendant creation of fluorescent X-rays or Auger electrons[§§], fill these vacancies, as discussed before. MCNP handles these secondaries in three ways. (1) Zero photons greater than the cutoff energy are emitted. In this event, the cascade of electrons that fills up the orbital vacancy left by the photoelectron produces Auger electrons and low-energy photons. The Auger electrons with energies greater than the cut-off energy can be followed, or be treated with the TTB approximation, or be assumed to deposit energy locally. (2) One fluorescent photon with energy greater than the cutoff energy is emitted. The fluorescent photon energy E' is calculated by: $E' = E - (E - e_b) - e_b' = e_b - e_b'$, where E, $(E\text{-}e_b)$, and e_b' are the incident photon energy, kinetic energy of the photoelectron ejected from the shell with binding energy e_b, and binding energy of the upper shell that takes part in the transition process, respectively. The residual excitation energy, e_b', is ultimately dissipated by further Auger processes. This dissipation leads to additional electrons or photons of still lower energy. The photoelectron and the Auger electrons are

handled by one of the three ways, as described before. These primary transitions are taken to have the full fluorescent yield from all possible upper levels e_b', but are apportioned among the x-ray lines $K\alpha_1(L_3 \rightarrow K); K\alpha_2(L_2 \rightarrow K); K\beta_1'(M \rightarrow K);$ and $K\beta_2'(N \rightarrow K)$. (3) Two fluorescent photons can occur if the residual excitation e_b' of process (2) exceeds the cutoff energy. An electron of binding energy e_b'' can fill the orbit of binding energy e_b', emitting a second fluorescent photon with energy $E'' = e_b' - e_b''$. As before, the residual excitation e_b'' is dissipated by further Auger events. These secondary transitions come from all upper shells and go to *L* shells. Thus the primary transition must be $K\alpha_1$ or $K\alpha_2$ to leave an *L* shell vacancy.

MCNP assumes that each fluorescent photon is emitting isotropically. The emitted photon is transported, provided that $E', E'' >$ cutoff energy. The binding energies e_b, e_b', and e_b'' are very nearly the x-ray absorption edges because the x-ray absorption cross section takes an abrupt jump as it becomes energetically possible to eject (or excite) the electron of energy first $E \cong e_b''$, then e_b', then e_b, etc.

A photoelectric event is terminal for elements Z < 12 because the possible fluorescence energy is below 1 keV (minimum cutoff by default). The event is only a single fluorescence of energy above 1 keV for 31 > Z ≥ 12, but double fluorescence (each above 1 keV) is possible for Z ≥ 31. For Z ≥ 31, the primary lines $K\alpha_1, K\alpha_2,$ and $K\beta_1'$ are possible and, in addition, for Z ≥ 37, the $K\beta_2'$ line is possible.

In all photoelectric cases, where the photon track is terminated because either no fluorescence photons are emitted or the ones emitted are below the energy cutoff, the

photon is killed with probability σ_{ph}/σ_t, where σ_{ph} and σ_t are the photoelectric and total cross section, which is sum of the cross section of photoelectric effect, pair production, incoherent and coherent scatterings (i.e., $\sigma_t = \sigma_{ph} + \sigma_{pp} + \sigma_{inc} + \sigma_{coh}$).

It should be noted that the MCNP models of treating the fluorescent X-rays and Auger electrons produced from the photoelectric effect are different from those produced from electron/positron interactions. MCNP considers only K-shell ionization for the highest Z-component of the material for electron/positron interactions whereas it considers ionization of all shells, and atomic relaxation from the K, L, M, and N shells.

At photon energies above a few MeV, pair production starts dominating the photon interaction. In this interaction, the photon disappears in a coulomb force field, usually near an atomic nucleus, and gives rise to an electron and a positron. Much less frequently the photon may interact with the coulomb field of an atomic electron. This later process is usually called "triplet production", because the host electron that provides the coulomb field also acquires substantial kinetic energy in conserving momentum. Thus two electrons and a positron are ejected from the site of the interaction and a vacancy is left in the atom. The threshold energies of $2mc^2$ for the pair production and of $4mc^2$ for triplet production are required, *m* is the mass of the electron and c is the speed of light. MCNP ignores triplet production but considers pair production. MCNP handles the electrons and positrons utilizing one of the three models available for the treatment of photon-induced charged particle, as described before.

There are several other photon interactions, such as nuclear Thomson scattering, in which the photon scatters elastically from the nucleus (i.e., low-energy nuclear

Compton scattering), Delbrück scattering, in which the photon scatters elastically from the Coulomb field of the nucleus, and high-energy photonuclear interaction (exceeding a few MeV), in which the nuclear absorbs a photon and gives off a nucleon. MCNP ignores these photon interactions because these are rare events and very inefficient for energy transfer. Hence, these are rarely important in radiation dosimetry calculations.

Conclusion

MCNP has two photon interaction models: simple and detailed. The simple model considers the photoelectric effect without fluorescence and Auger electrons, considers compton (incoherent) scattering from free electrons without the use of form factors which accounts for electron binding effects, and considers pair production. The highly forward-peaked coherent scattering is ignored. In contrast, the detailed model considers both coherent and incoherent scattering with the use of form factors, pair production, and accounts for fluorescent photons and Auger electron after photoelectric absorption. But both the models ignore several other photon interactions, such as nuclear Thomson scattering, Delbrück scattering, triplet production and high-energy photonuclear interaction because these are rare events and rarely important in radiation dosimetry calculations.

This research applied the detailed physics treatment to the present MCNP calculations. In the detailed model, MCNP uses modified Klein-Nishina differential cross sections (Briesmeister 2000) to determine the angle and energy of the compton-scattered photon and the recoil kinetic energy of the electron. The modification is made to take into account the form factor. For sampling of the differential cross section for

coherent scattering, MCNP uses Thomson differential cross sections (Attix 1986) with some modification to take into account the combined scattering action of the whole atom and the binding effect of electron in the atom, and to reduce the Thomson cross section more extremely for backward scattering for high-energy and low-Z materials. MCNP handles the fluorescent X-rays or Auger electrons, resulting from the photoelectric effect, in three ways: fluorescent X-rays or Auger electrons or both types can be emitted but, (1) no fluorescence photon is emitted with energy greater than cutoff energy; (2) one fluorescent photon with energy greater than the cutoff energy is emitted; (3) two fluorescent photons with energy exceeding the cutoff energy can occur. MCNP considers all shells in the relaxation process. MCNP handles all photon-induced charged particles (electrons and positrons) in three distinct ways, which are the same for both the simple and detailed photon physics treatment. The kinetic energy of the photon-induced charged particle can be deposited locally irrespective of its energy, can be transported, or (default) can be treated with the thick-target bremsstrahlung (TTB) approximation. The charged particles are transported in the calculations described here.

RESULTS AND DISCUSSION

This section presents the results obtained from benchmark calculations and from the calculations using the revised gastrointestinal tract (GIT) model developed in this study. It also provides a discussion of the results of each task.

BENCHMARK CALCULATION

The Cristy and Eckerman adult male phantom (1987), which was a modified version of the revised MIRD 5 phantom (Snyder et al. 1978), was coded into the MCNP 4C Monte Carlo simulation package (Briesmeister 2000) for calculation of "specific absorbed fraction" (SAF) values in various organs (target organs) of the body from sources of the same 12 monoenergetic photons, 10 keV-4 MeV, distributed uniformly in the stomach (ST) contents. The SAF for a given source-target pair was defined as the fraction of the source energy absorbed per unit mass of the target organ. The SAF values obtained from the calculations were compared to the "best" estimates of Cristy and Eckerman (1987) with the ST as source organ to verify and benchmark the initial design and coding of the phantom and the Monte Carlo treatment to be employed in this study.

Cristy and Eckerman (1987) described the procedures used in choosing the "best" estimate of SAF from the estimates generated by three methods—direct Monte Carlo method, converse Monte Carlo method based on reciprocal dose principle (Loevinger 1969), and point-source kernel method (Berger 1968; Brownell et al. 1968) — for a given source-target pair. They used the ALGAM Monte Carlo computational package (Warner and Craig 1968) which lacked electron transport capability. So the photon-induced electrons (or secondary electrons) were not transported in their Monte

Carlo calculations, i.e., the electron energy was assumed to be deposited at the site of the photon interaction.

In this benchmark calculation, two sets of Monte Carlo calculations — with and without transporting the secondary electrons — were performed. The SAF values obtained from these calculations are presented in Table 8 for various target organs with the source in the stomach contents. Each cell in Table 8 contains two values. The upper and lower values were obtained with and without electron transport, respectively. The SAFs without electron transport were used for benchmark comparisons presented in Figs. 11(a-c).

Table 8 shows that the SAFs with and without electron transport are almost the same as demonstrated by Poston et al. (1996b). The small difference between the two values may be attributed to statistical fluctuations in the Monte Carlo calculation. Figs. 11(a-c) show that the SAF values for all organs, except for the whole body, obtained from benchmark calculations closely agree with those provided by Cristy and Eckerman (1987). The differences between these two calculations are relatively high at 10 and 15 keV for those organs located at relatively large distances from the stomach. This is due to the greater difference in the interaction cross-section data and in algorithms used in the ALGAM and MCNP 4C, and higher statistical fluctuations for lower energy photons.

As demonstrated in Fig 11(c), the SAF values for whole body obtained in the benchmark calculation are significantly larger than those provided by Cristy and Eckerman (1987) at photon energies ≤ 30 keV. The best estimates of SAF values made by Cristy and Eckerman (1987) are 6.8×10^{-4} kg^{-1} at 10 keV, 2.3×10^{-3} kg^{-1} at 15 keV,

Table 8. Specific absorbed fraction (SAF) of photon energy in kg^{-1} for adult male or larger-than-average-adult female developed by Cristy and Eckerman (1987) when source is stomach contents.[a]

Target	Energy (MeV)											
	0.010	0.015	0.020	0.030	0.050	0.100	0.200	0.500	1.000	1.500	2.000	4.000
Brain	0.0	0.0	0.0	0.0	3.39E-6	1.59E-5	2.75E-5	6.07E-5	1.05E-4	1.38E-4	1.77E-4	1.96E-4
	0.0	0.0	0.0	0.0	3.31E-6	1.61E-5	2.84E-5	6.12E-5	1.02E-4	1.32E-4	1.56E-4	1.90E-4
LLI Wall	0.0	3.18E-6	2.19E-4	2.27E-3	4.69E-3	4.43E-3	4.16E-3	4.05E-3	3.82E-3	3.76E-3	3.79E-3	2.99E-3
	0.0	3.75E-6	2.22E-4	2.25E-3	4.68E-3	4.50E-3	4.17E-3	4.09E-3	3.95E-3	3.76E-3	3.61E-3	3.11E-3
SI Wall	3.68E-6	2.03E-4	1.17E-3	6.19E-3	1.14E-2	1.03E-2	9.26E-3	8.66E-3	8.08E-3	7.59E-3	7.17E-3	5.91E-3
	3.78E-6	2.01E-4	1.17E-3	6.09E-3	1.14E-2	1.04E-2	9.27E-3	8.63E-3	8.01E-3	7.49E-3	7.07E-3	5.94E-3
Stomach	2.99E-1	7.02E-1	8.47E-1	6.51E-1	3.20E-1	1.87E-1	1.81E-1	1.80E-1	1.66E-1	1.49E-1	1.38E-1	1.06E-1
Wall	2.99E-1	7.01E-1	8.44E-1	6.43E-1	3.20E-1	1.88E-1	1.81E-1	1.80E-1	1.65E-1	1.50E-1	1.39E-1	1.11E-1
ULI Wall	5.57E-6	9.94E-4	5.41E-3	1.49E-2	1.76E-2	1.37E-2	1.21E-2	1.17E-2	1.01E-2	9.62E-3	8.54E-3	8.35E-3
	5.31E-6	9.83E-4	5.38E-3	1.48E-2	1.75E-2	1.36E-2	1.21E-2	1.13E-2	1.05E-2	9.70E-3	9.10E-3	7.57E-3
Kidneys	0.0	8.02E-7	4.03E-4	7.62E-3	1.58E-2	1.40E-2	1.25E-2	1.16E-2	1.06E-2	9.89E-3	9.26E-3	7.83E-3
	0.0	6.08E-7	3.91E-4	7.47E-3	1.58E-2	1.41E-2	1.25E-2	1.16E-2	1.08E-2	1.00E-2	9.42E-3	7.88E-3
Liver	0.0	9.87E-6	3.59E-4	3.57E-3	7.68E-3	7.45E-3	6.81E-3	6.57E-3	6.26E-3	5.87E-3	5.54E-3	4.75E-3
	0.0	9.92E-6	3.58E-4	3.52E-3	7.71E-3	7.52E-3	6.86E-3	6.57E-3	6.22E-3	5.87E-3	5.58E-3	4.74E-3
Lungs	1.80E-7	1.34E-4	1.20E-3	4.89E-3	6.98E-3	5.83E-3	5.27E-3	5.14E-3	4.85E-3	4.60E-3	4.48E-3	3.70E-3
	2.02E-7	1.35E-4	1.19E-3	4.83E-3	6.98E-3	5.87E-3	5.30E-3	5.12E-3	4.84E-3	4.54E-3	4.29E-3	3.62E-3
Ovaries	0.0	0.0	0.0	2.77E-4	1.75E-3	3.00E-3	2.72E-3	2.82E-3	2.94E-3	2.69E-3	2.85E-3	4.45E-3[b]
	0.0	0.0	0.0	2.68E-4	1.85E-3	2.76E-3	2.81E-3	2.88E-3	2.88E-3	2.85E-3	2.63E-3	2.40E-3
Pancreas	5.90E-5	9.26E-3	5.10E-2	1.15E-1	9.80E-2	6.36E-2	5.57E-2	5.19E-2	4.64E-2	4.33E-2	3.98E-2	3.16E-2
	6.01E-5	9.28E-3	5.06E-2	1.13E-1	9.81E-2	6.41E-2	5.59E-2	5.17E-2	4.67E-2	4.26E-2	3.95E-2	3.20E-2
Skeleton	3.87E-8	5.29E-5	5.84E-4	2.88E-3	5.25E-3	3.87E-3	2.53E-3	2.00E-3	1.85E-3	1.76E-3	1.75E-3	1.51E-3
	3.69E-8	5.24E-5	5.82E-4	2.86E-3	5.22E-3	3.86E-3	2.53E-3	1.99E-3	1.85E-3	1.77E-3	1.70E-3	1.51E-3
Testes	0.0	0.0	0.0	6.92E-6	2.63E-5	1.19E-4	2.51E-4	2.79E-4	5.87E-4[c]	4.23E-4	4.40E-4	1.50E-3[b]
	0.0	0.0	0.0	6.80E-6	2.79E-5	1.04E-4	1.54E-4	3.11E-4	3.89E-4	4.44E-4	4.66E-4	5.06E-4
Urinary	0.0	0.0	0.0	3.24E-5	4.17E-4	9.16E-4	1.02E-3	1.32E-3	1.10E-3	1.48E-3	1.20E-3	1.97E-3[b]
Bl Wall	0.0	0.0	0.0	2.82E-5	4.19E-4	8.76E-4	9.93E-4	1.17E-3	1.29E-3	1.34E-3	1.33E-3	1.27E-3
Uterus	0.0	0.0	0.0	1.99E-4	1.64E-3	2.58E-3	2.60E-3	2.71E-3	2.65E-3	2.57E-3	2.55E-3	2.32E-4[b]
	0.0	0.0	0.0	1.93E-4	1.64E-3	2.54E-3	2.58E-3	2.64E-3	2.65E-3	2.60E-3	2.53E-3	2.24E-3
Whole	1.36E-2	1.36E-2	1.35E-2	1.24E-2	9.37E-3	6.67E-3	6.13E-3	5.98E-3	5.59E-3	5.19E-3	4.85E-3	3.96E-3
Body	1.36E-2	1.36E-2	1.35E-2	1.24E-2	9.36E-3	6.68E-3	6.13E-3	6.00E-3	5.59E-3	5.18E-3	4.85E-3	3.97E-3

[a] Each cell contains two values—upper and lower, where the upper and lower are obtained from Monte Carlo calculations with and without electron transport, respectively. [b] Relative errors are 0.32 for ovaries, 0.57 for testes, 0.18 for urinary bladder wall, and 0.13 for uterus at 4 MeV. [c] Relative error is 0.40.

4.5×10^{-3} kg^{-1} at 20 keV, and 7.5×10^{-3} kg^{-1} at 30 keV for whole body with a mass of 73.7 kg without female breasts. The SAFs for the whole body were expected to be 1.35×10^{-2} kg^{-1} (≈ 1/73.7 Kg) at energies ≤ 20 keV because the photons with these energies would deposit almost all their energy within the body if they had to traverse several mean free paths (= $1/\mu_{en}$) to escape the body. In the benchmark calculations, the SAF values obtained were 1.36×10^{-2} kg^{-1}, 1.36×10^{-2} kg^{-1}, 1.35×10^{-2} kg^{-1}, and 1.24×10^{-2} kg^{-1} (see Table 8) as theoretically expected. Obviously, the Cristy and Eckerman (1987) SAFs for the whole body (≤ 30 keV) were incorrect at the low energies. For 50 keV and above, percent differences between the two SAFs were in the range of 15-20%.

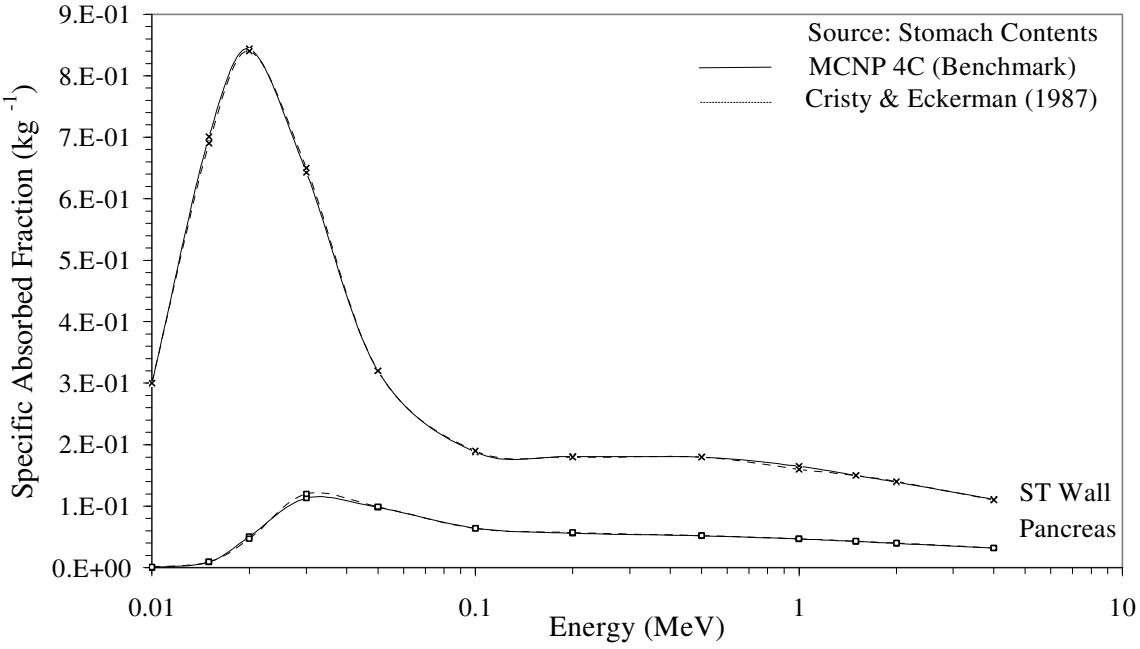

Fig. 11(a)

Fig. 11(a-c). Benchmark comparisons of specific absorbed fractions obtained with MCNP 4C in this study to the "best" estimates of Cristy and Eckerman (1987) in various organs of the body from sources of 12 monoenergetic photons, 10keV-4MeV in the stomach contents for an adult male (73.7 kg Reference Man) modeled by Cristy and Eckerman (1987).

Fig. 11. Continued.

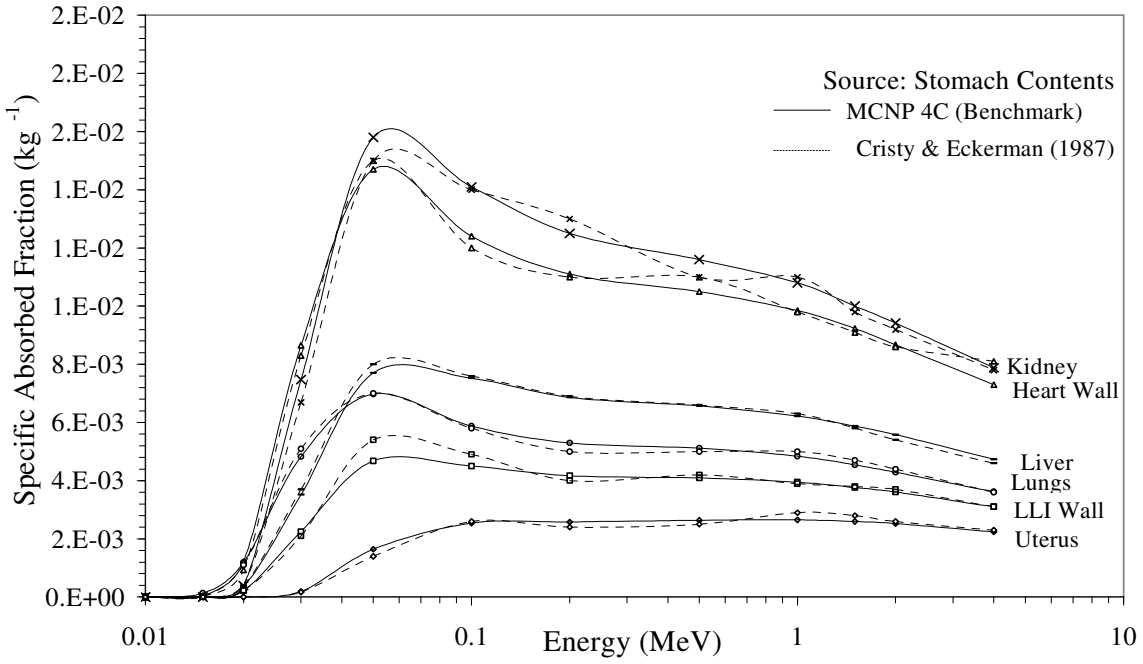

Fig. 11(b)

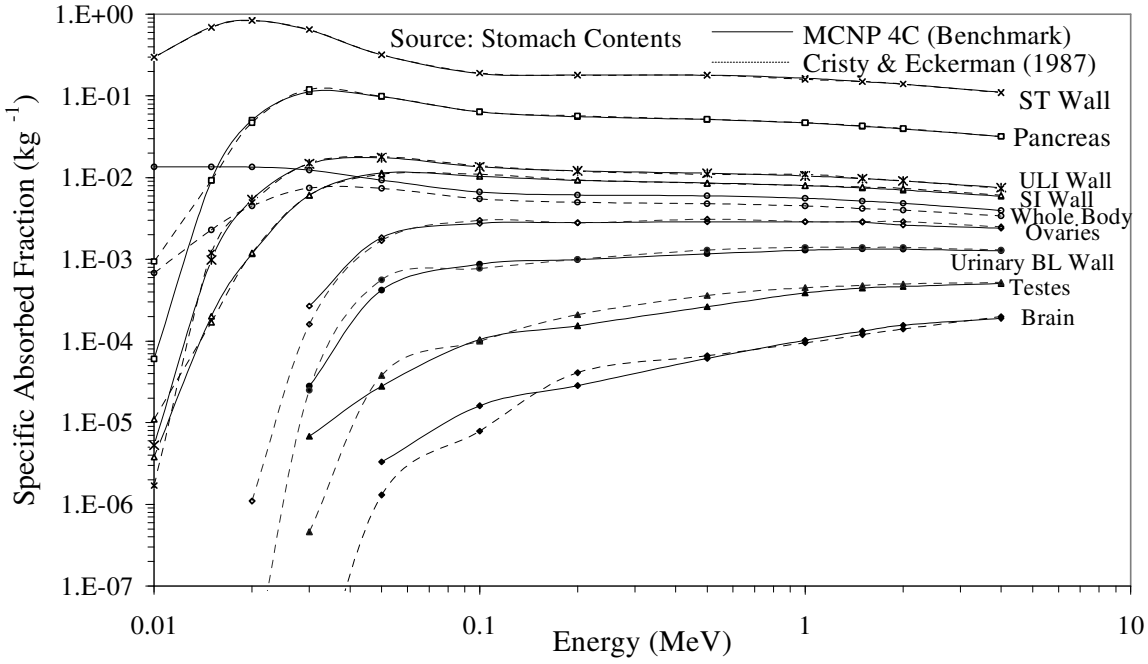

Fig. 11(c)

In the benchmark calculations, the SAFs obtained were essentially zero at low energies for small organs located at large distances from the stomach (source organ) (see Table 8). The SAFs with zero values are not shown in Fig. 11(c) as zero cannot be plotted in log chart.

The SAFs provided by Cristy and Eckerman (1987) do not follow a smooth variation with photon energy. The SAFs obtained in this benchmark calculation vary smoothly with photon energy.

The relative errors associated with the Monte Carlo calculations in the benchmark were below 0.1, but most of them were less than 0.05. These errors were not shown in the figures as they were indiscernible from the data points. The relative errors in the calculations with electron transport were relatively high because of the energy straggling. In some cases, the errors exceeded 0.1, shown in Table 8, for the organs with small masses (e.g., ovaries, testes) located at relatively large distances from the source.

In conclusion, the SAF values for all organs, except for the whole body, obtained in the benchmark calculations were in good agreement with those provided by the Cristy and Eckerman (1987). The SAFs for the whole body in the benchmark calculations were obtained as expected. So the design and the coding of the phantom and Monte Carlo treatment to be employed in this study were considered valid.

REVISED MODEL

Specific absorbed fractions (SAFs) in various organs and tissues from uniformly distributed sources of 15 monoenergetic electrons and photons, in the range of energy 10 keV-4 MeV, in the lumenal contents (source contents) of the five sections of the GIT of

an adult human male or a larger-than-average-female (72.63 kg) were calculated. These five sections of the GIT were the esophagus (ESP), stomach (ST), small intestine (SI), upper large intestine (ULI), and the lower large intestine (LLI). The SAFs[§] were calculated for 19 targets, including the walls of the five sections of the GIT, for each of the five source contents. Except for walls of the GIT, average SAFs were calculated. For the GIT, the SAFs were calculated as a function of distance or depth across the wall of the sections of the GIT. The distance was measured outward from wall-contents interface. Complete results are presented in Tables B1 and B2 in Appendix B. For an efficient discussion, only a few of the results are presented here. The following relationship can be used to convert the tabulated SAFs (in kg^{-1}) into the absorbed dose in Gy per source particle with energy E in MeV: $SAF \times E \times 1.602 \times 10^{-13}$.

The SAFs for all organs except the SI, ULI, and LLI, were calculated from the direct results of the Monte Carlo simulations performed by MCNP 4C. The simulation results for the SI, ULI, and the LLI needed to be adjusted due to the differences between the model and the actual anatomic data. The formulae used for these adjustments were derived in Appendix A.

[§]The term specific absorbed fraction (SAF) used in this context is somewhat misleading because the numerical values are, in many cases, greater than unity (not fractions of unity). This paradox is the consequence of the approach used and the adherence to standard units in this dissertation. That is, the unit for the SAF, kg^{-1}, was used in keeping with previous publications of the ICRP and others. However, in this case, the absorbed energy (i.e., absorbed fraction of energy) is calculated for a thin region of the wall of the tract. Taking the quotient of the absorbed fraction and the corresponding very small mass of the section (expressed in units of kilograms) produces an SAF value greater than unity. It is important to understand this anomaly and its impact of the SAF values. However, no attempt was made to coin a new term to represent the SAF-values obtained in this research.

The relative errors associated with the Monte Carlo calculations were below 0.1, but most of them were less than 0.05. These errors were not shown in the figures as they were indiscernible from the data points. The relative errors in the calculations with electron transport were relatively high because of the stochastic energy loss-rate of the electrons. This fluctuation of energy loss-rate is commonly termed as the energy or range straggling. The errors were the highest at the maximum penetration depth or range of the electrons. The errors also were high for organs with small masses (e.g., ovaries, testes) located at relatively large distances from the sources (e.g., esophagus, stomach). In some cases, these errors exceeded 0.1, shown in Tables B1 and B2.

The Figs. 12(a) - 12(h) show SAFs in some organs and tissues with a high risk of radiation-induced cancer as a function of energy of the source particles in the five sections of the GIT. These SAF curves have some general characteristics discussed below.

For a given source-target pair, the photon SAF rises sharply with increasing energy and reaches a maximum at around 50 keV. This is because of the strong energy dependence of mass energy-absorption coefficient (μ_{en}/ρ) below 50 keV. As the μ_{en}/ρ decreases rapidly with the increase of photon energy, the attenuation by the intervening medium between the source and the target drops sharply; conversely, a sharp rise in the energy fluence in the target region occurs. Above 60 keV, the energy fluence becomes almost constant for most of the source-target pairings because the distance between each of these source-target pairings is less than the mean free-path of a 60 keV photon which is 30 cm in water. It is noted that the μ_{en}/ρ in the human body, except the skeleton

system of the body, is almost similar to water. The μ_{en}/ρ also is almost constant over the energy range 60 keV - 4 MeV in all organs but the skeleton system for which the μ_{en}/ρ is almost constant between 150 keV – 4 MeV. A constant μ_{en}/ρ and a constant energy fluence essentially give a constant SAF, as demonstrated in Figs. 12 (a) through 12 (g), over the energy range 60 keV – 4 MeV for all the target organs but the skeleton for which the SAF curve is almost flat between 150 keV and 4 MeV.

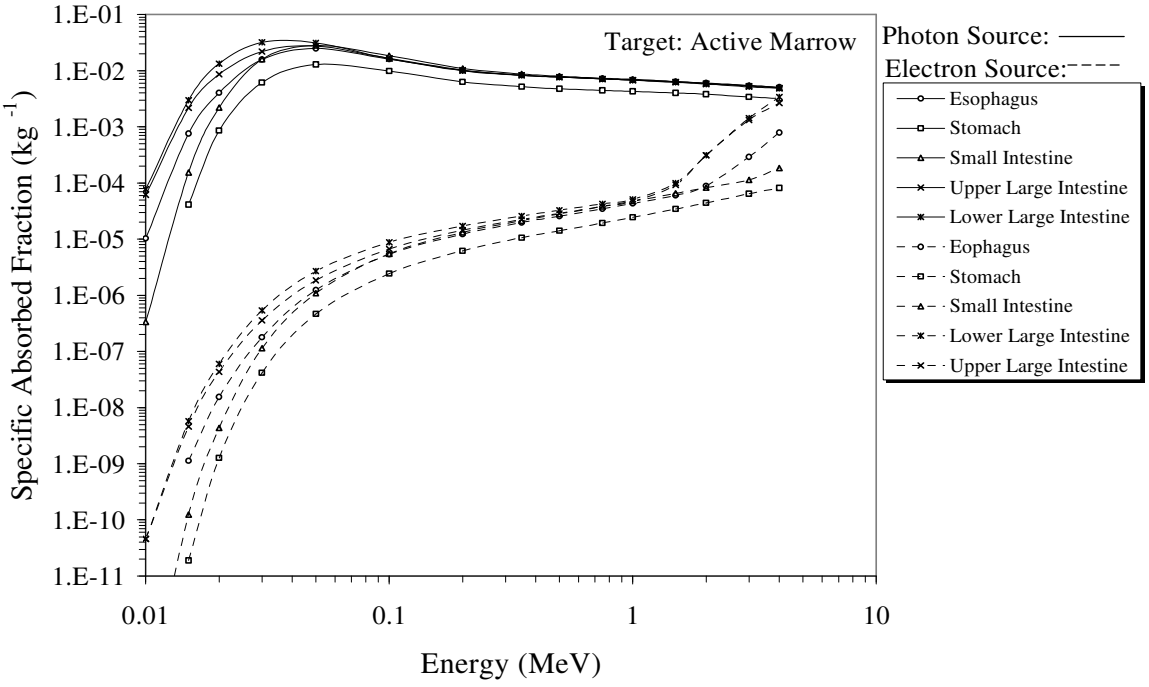

Fig. 12 (a)

Fig. 12 (a-h). Specific Absorbed Fractions (SAFs) in various organs and tissues from uniformly distributed sources of 15 monoenergetic electrons and photons in the lumenal contents of the five sections of the gastrointestinal tract of an adult human male or a larger-than-average-female (72.63 kg).

Fig. 12. Continued.

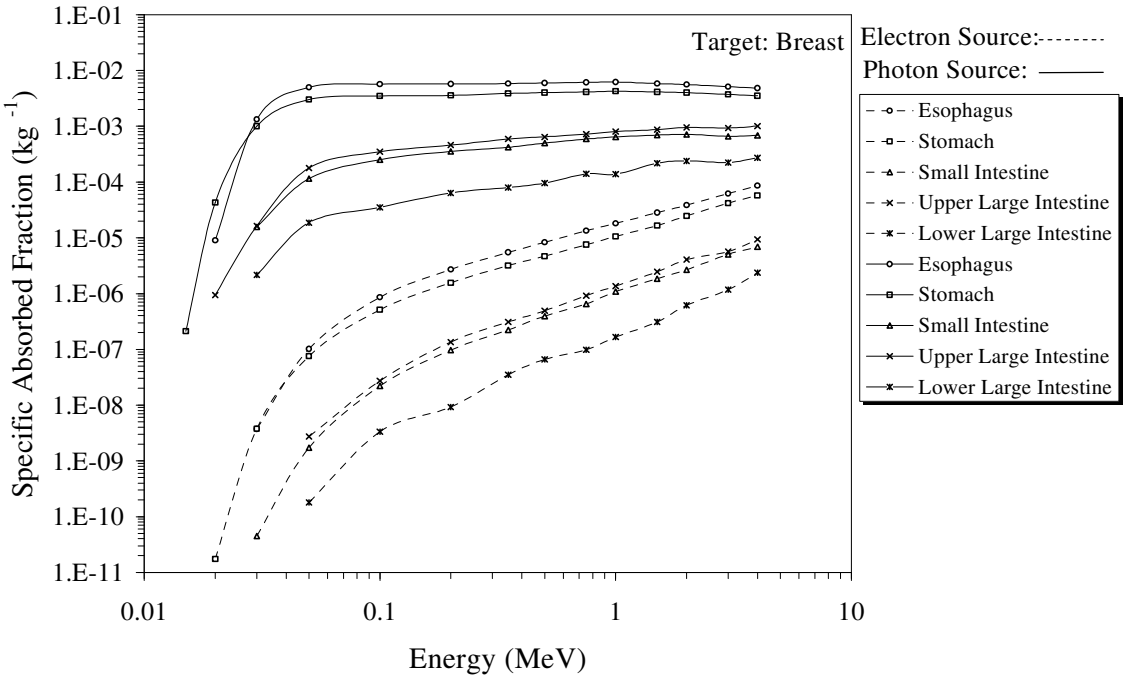

Fig. 12 (b)

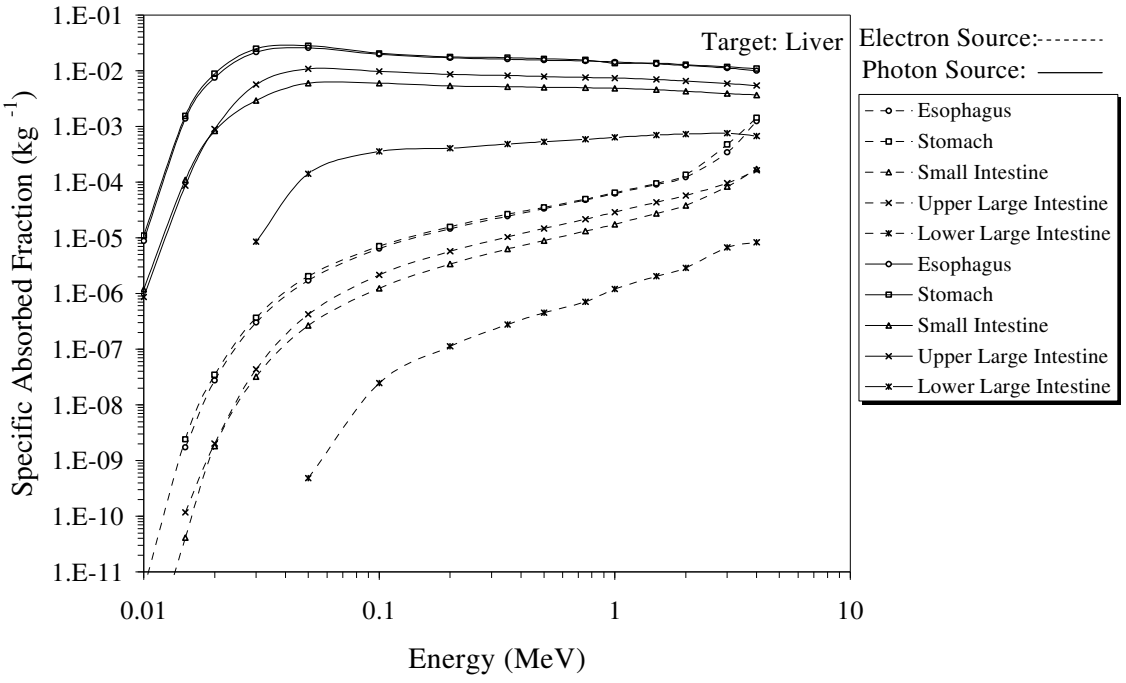

Fig. 12 (c)

Fig. 12. Continued.

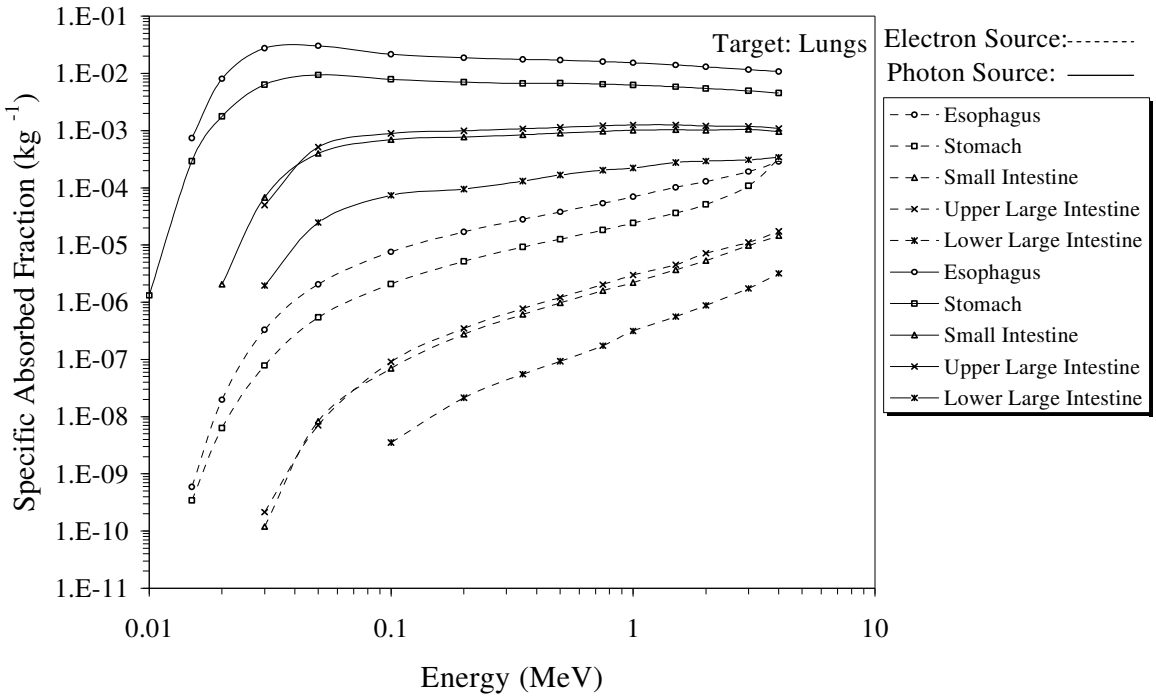

Fig. 12 (d)

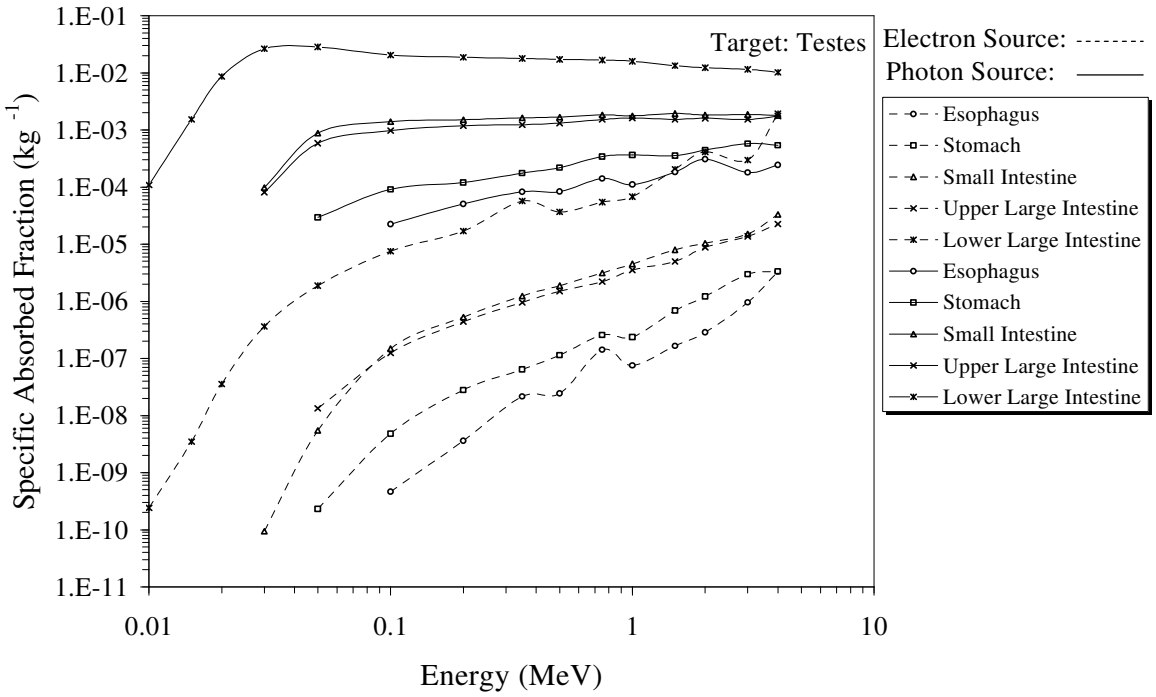

Fig. 12 (e)

Fig. 12. Continued.

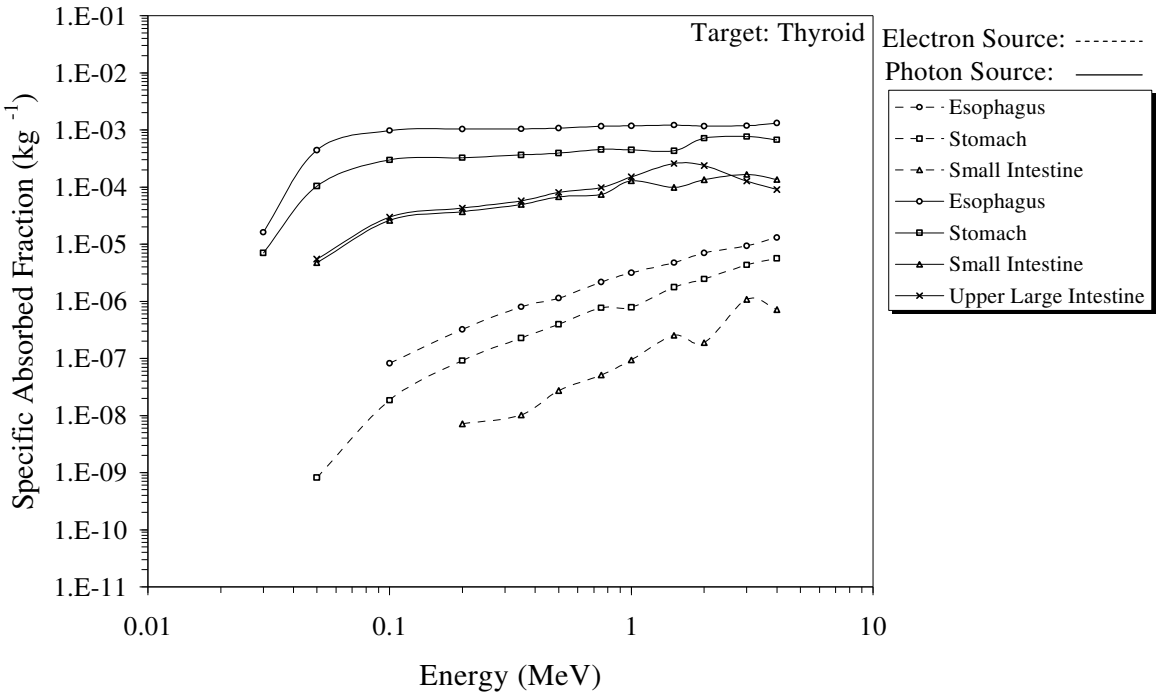

Fig. 12 (f)

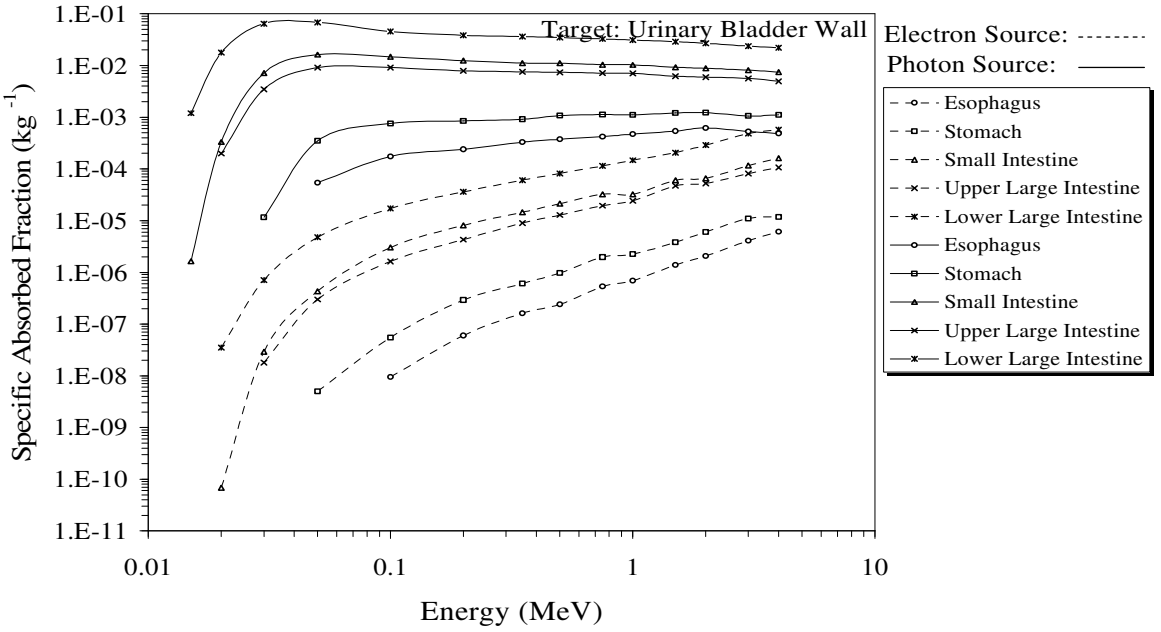

Fig. 12 (g)

Fig. 12. Continued.

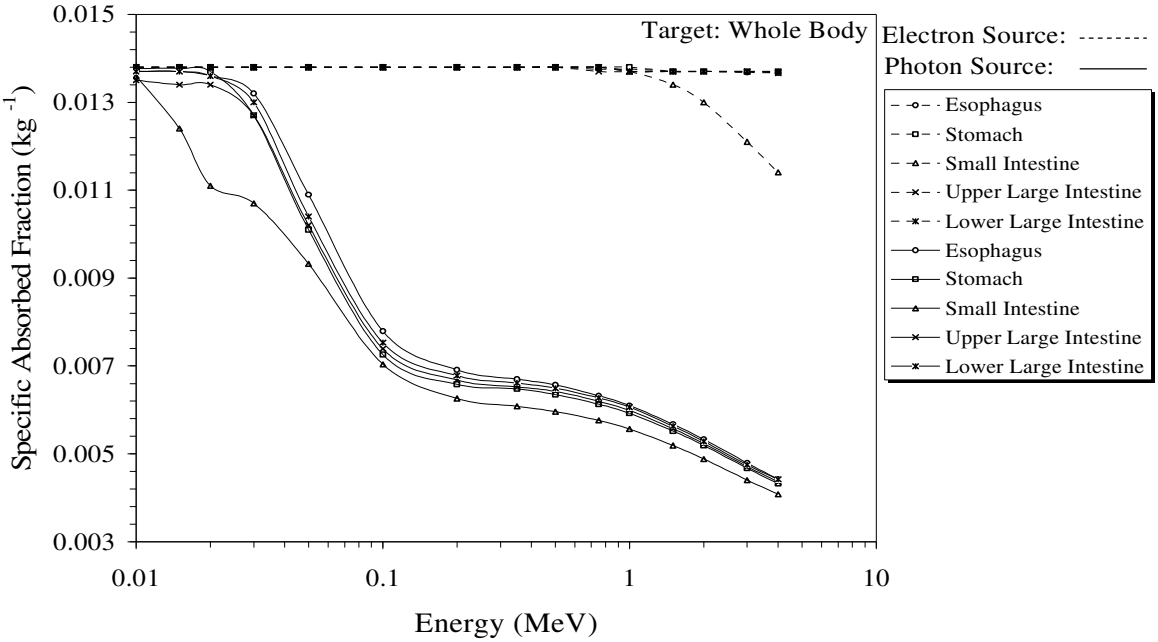

Fig. 12 (h)

The flat regions in the SAF-energy curves in these figures have small negative or positive slopes. The small negative slopes are due to the slow decrease in the μ_{en}/ρ with increasing energy. If targets are located from a source at distances greater than the mean free path of the relevant source photon, the curves have small positive slopes, i.e., the SAF slowly increases with increasing energy. This is because of the combined effects of the increase in the fluence at the target regions and the slow decrease in the μ_{en}/ρ with increasing photon energy.

For example, at least one of the three bones — the middle spine, ribs and the pelvis — containing the highest percentages of the active marrow in the body is located within the 30 cm of any of the five sections of the GIT. About 70% of the active marrow is located in these three bones. As shown in Fig. 12 (a), the photon SAF curves for the

active marrow follow the pattern having negative slope for all five sections of the GIT as source organs. A similar pattern is observed for the liver as a target when the sources are the GIT sections except the LLI (Fig. 12 (e)). The curve for the LLI as a source follows the pattern with positive slope.

Primarily, the distance between a source and a target determines the photon SAF for a given energy. The greater the distance, the smaller is the SAF value. The effects of the size and shape of the source organ on the photon SAF for other organs were not investigated. The separation between two SAF curves for the same target with two different sources is relatively small for energies above 50 keV while the separation is relatively large and increases rapidly with decreasing energy below 40 keV. This behavior reflects the same processes of photon interaction as discussed before.

The curves of photon SAFs for the whole body (Fig. 12(h)) are different in pattern than those for the other organs. The SAF is almost constant for the energies 10-20 keV for all the source organs, except the SI, because the source energy is completely absorbed within body. The complete absorption of the source energy gives a SAF-value in the body that is equal to 1.38×10^{-2} kg^{-1} (=1/72.63 kg). For the SI, a fraction of the source energy in two of the 8 loops of the SI, those directed in the y-direction, escapes from the body even for the energy as low as 15 keV. Above 20 keV, the SAF decreases for all source organs with increasing energy as the penetrability increases with the energy.

A preliminary comparison of photon SAFs obtained in this study with those obtained by Cristy and Eckerman showed that the two values differ by a factor of 1.5 to

3. Generally, the difference is the highest at low energies (<30 keV) and the lowest at the medium energies (100-500 keV). But a detailed comparative study of photon SAF values obtained in this study with those obtained in other studies was not performed.

The Figs. 12(a)-12(g) demonstrate that the electron SAF values are smaller by several orders of magnitude than the photon SAFs for the same energy in a given source-target pairing. But for the whole body, the electron SAFs are greater than the photon SAFs. For target organs other than the source organs, the electron SAFs for most targets in the body are due only to the bremsstrahlung radiation. The electron SAFs for the same target and source are discussed later. A large portion of the source electron energy is absorbed within the source organ.

A source electron contributes directly to the SAF if the target organ is located within the range of the electron. Fig. 12 (a) shows that the electron SAF for the active marrow abruptly increases with increasing energy for the energies above 1.5 MeV when the source organs are ULI, LLI, and the ESP. This is because the pelvis, which contains about 33% of the active marrow, is located within range of these electrons in the ULI and the LLI while the ribs and the middle spine, containing 19% and 17% of the active marrow, respectively, are located within the range of these electrons in the ESP. These three organs become critical for the active marrow for high energy electrons (>3 MeV). At these high energies, the electron exposure is significant for the liver and the lungs when source in the ESP and ST (Figs. 12 (c) and 12 (d)), and for the testes and the urinary bladder wall when the source in the LLI (Figs. 12 (e) and 12 (g)). These curves

indicate that the electron SAF may be greater than the photon SAF for very high energies (>4 MeV).

Fig. 12 (h) shows that the electron SAF is greater than the photon SAF in the whole body. The electron SAF is almost constant for all the source organs except the SI over the energy range investigated (10 keV – 4 MeV). For the SI, the electron SAF decreases with increasing energy for energies above 1 MeV.

Electron SAFs at different depths or positions in the walls from uniformly distributed sources of 15 monoenergetic electrons in the lumenal contents of the five sections of the GIT are shown in Figs. 13 (a) – 13 (e). The depths were measured outward from wall-contents interface. Also shown are positions of the most radiosensitive stem cells and different regions across the wall, namely mucus layer, epithelium for the ESP, gastric pit for the ST, villus and crypt for the SI, and crypt for the ULI and the LLI, for interpreting the doses at different distances from the contents.

The SAF within the penetration depth or range of the source electrons is a strong function of depth. The SAFs decrease several orders of magnitude over this short distance. The “stopping power” of source electrons determines the steepness of SAF curve. For lower energy electrons (higher stopping power), the SAF curves fall very rapidly with steep slope. The SAF at depths beyond the range becomes almost flat and decreases slowly with almost a constant logarithmic relation that depends on the energy of the source electrons. Beyond the range of the source electron, bremsstrahlung radiation and fluorescent x-rays are the only contributors to the SAF (Figs. 13(a) and 13(b)) for all organs except the ESP. For the ESP, direct electron exposure also

contributed to the SAF in the outer layers of the wall; because the outer layers of the middle ESP with closed lumen were irradiated directly by a fraction of the source electrons in the lumen of the lower ESP in which the majority of its lumen was empty. Figure 13(a) shows the bremsstrahlung and fluorescent x-ray contribution to the SAF for the depths beyond the electron range of 10 keV electrons in the ESP. The esophageal SAF curves for electron energies 10 keV-1 MeV rise at around 4250 μm**,** thus forming a hump. This is due to the direct exposure of source electron to the outer layers of the wall

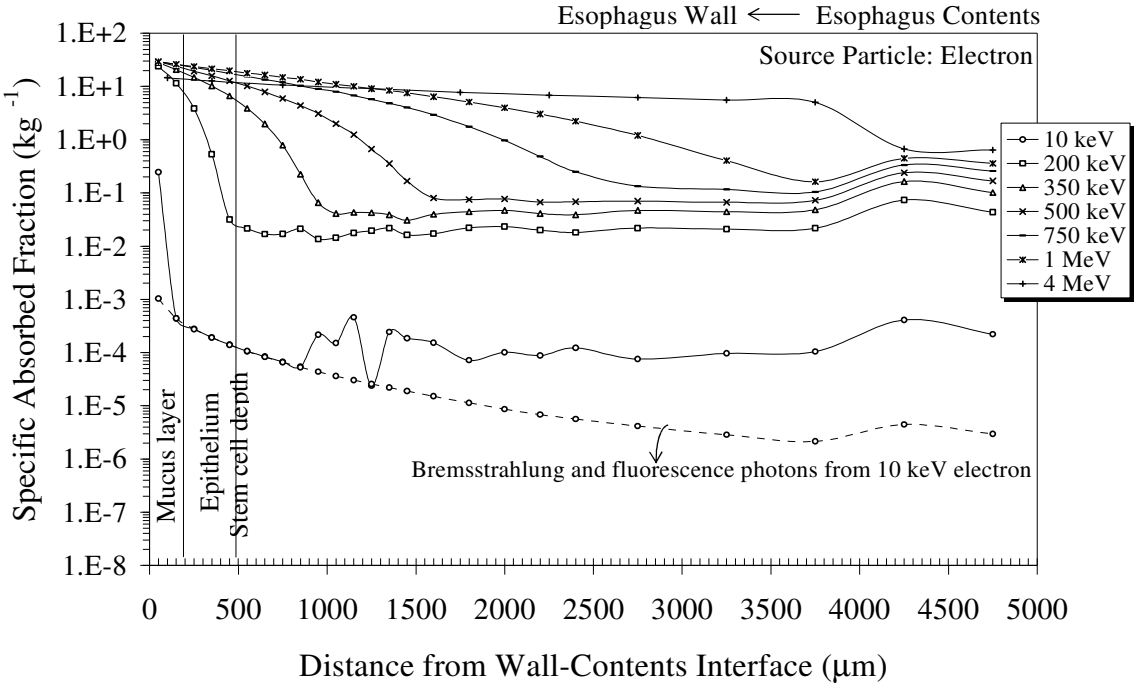

Fig. 13 (a)

Fig. 13 (a-e). Specific Absorbed Fractions (SAFs) at different depths or positions in the walls from uniformly distributed sources of 15 monoenergetic electrons in the lumenal contents of the five sections of the gastrointestinal tract of an adult human male or a larger-than-average-female (72.63 kg). The depths were measured outward from wall-contents interface. The ICRP 30 (1979) and MIRD (1975) SAF values for the stomach, small intestine, and upper large intestine are shown here for comparison. The following relationship can be used to covert the SAF to absorbed dose (Gy) per source particle: SAF (kg^{-1}) × Energy (MeV) × 1.602E-13.

Fig. 13. Continued.

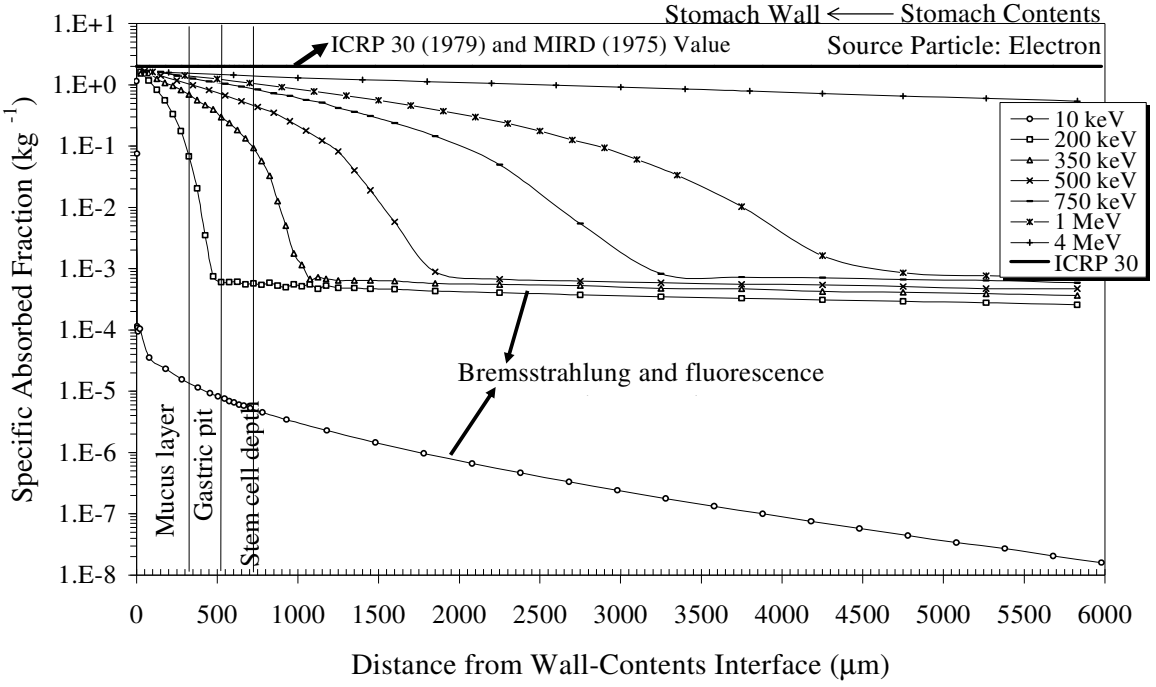

Fig. 13 (b)

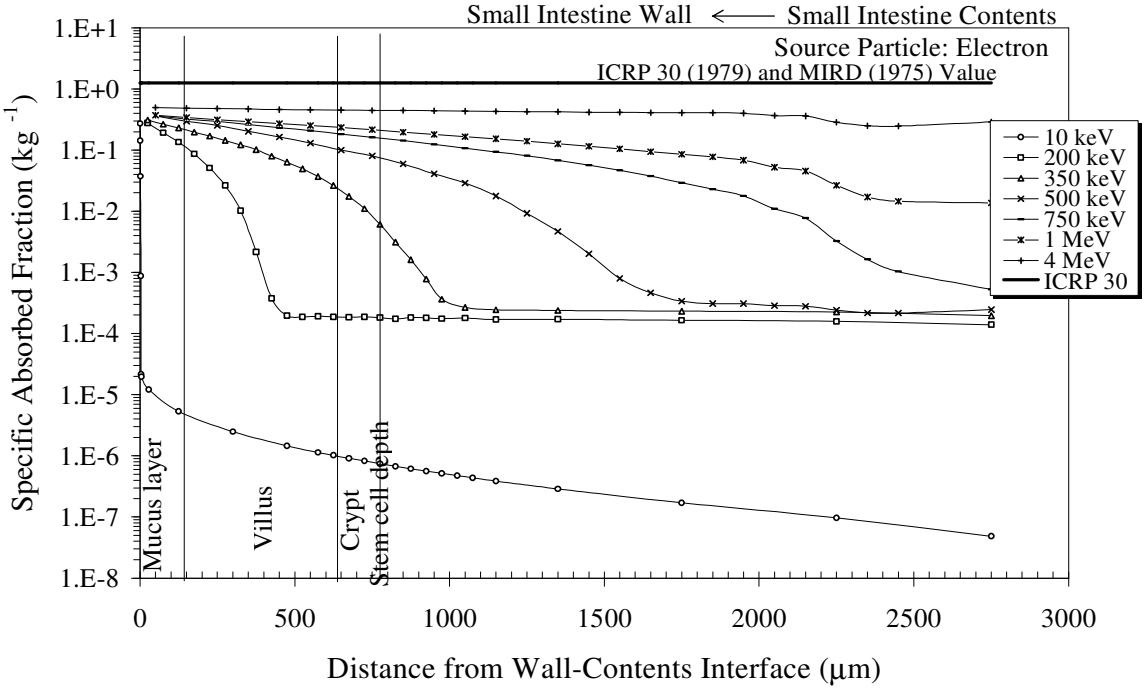

Fig. 13 (c)

Fig. 13. Continued.

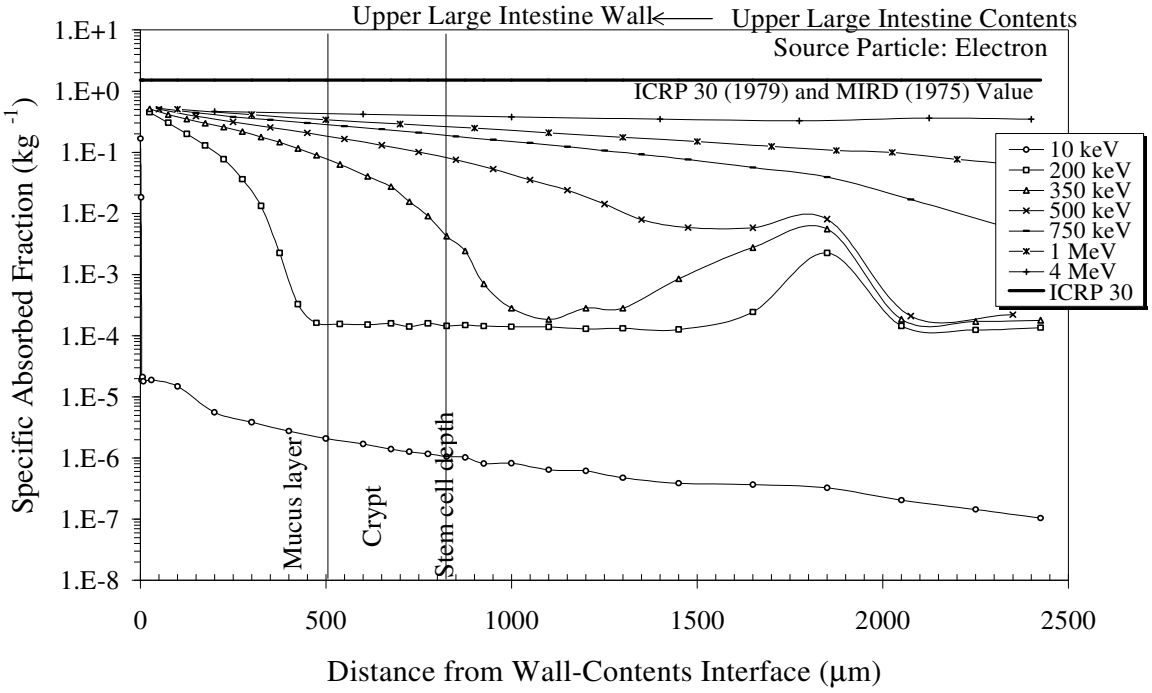

Fig. 13 (d)

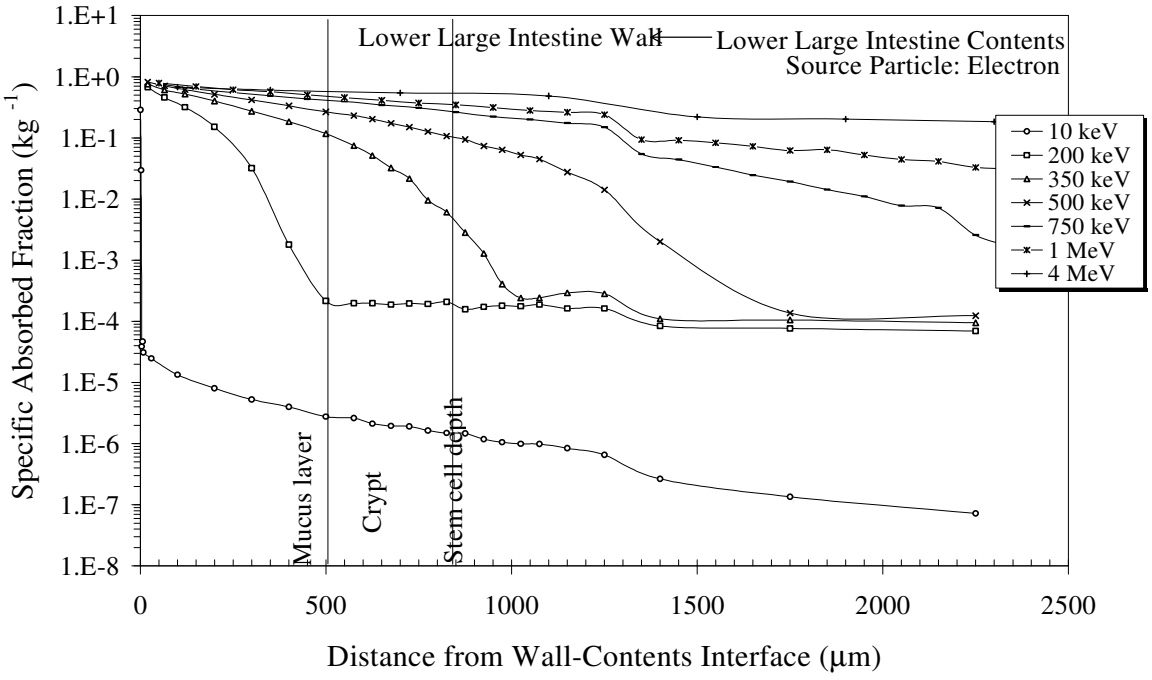

Fig. 13 (e)

of the middle ESP. Similar humps are seen in the ULI SAF curves (Fig. 13(d)) at 1850 μm. This was because of the outer layers of the wall of the transverse colon were irradiated by source electrons in the ascending colon, which is mostly empty.

As shown in the Figs**.** 13(b)-13(e) and in Table B2, the SAF curves for 10 keV electrons decrease by about 4 orders of magnitude over the distances 3-4 μm, consistent with the electron range in soft tissue**,** for all the source organs except the ESP**.** For the ESP, the SAF decrease rate is smaller. Generally, 200 keV electrons can barely penetrate a 500 μm thickness of soft tissue. Therefore, for the energies below 200 keV, the electron doses decrease sharply to negligible levels before penetrating the insensitive tissue layers overlying the stem cells (Figs**.** 13(a)-13(e)). The doses to the bottom of the esophageal epithelium, to the gastric glands in the ST, to the villi and crypts in the SI, and to the crypts in the ULI and LLI are markedly lower than the doses at the contents-mucus interface for electron energies less than 200 keV. For 350 keV electrons, the dose has fallen off by more than a factor of 1.5 before reaching the villus tip (at a depth of 210 μm)**,** more than a factor of 25 before reaching the bottom of the villi (710 μm) and more than an order of magnitude before reaching at the bottom of the crypt. The radiosensitive stem cells are located near the base of each intestinal crypt at 800-850 μm depth, which is equal to the penetration depth of 300 keV electrons in soft tissue. Thus, below 300 keV, the doses to the stem cells are due only to bremsstrahlung radiation. A 300 keV electron originating in the vicinity of the contents-mucus interface can barely reach the stem cell level and contributes only a small dose to the stem cells. For electron energies above 300 keV, the average dose to stem cells increases rapidly with energy.

This rapid increase, shown in Figs. 13(a)-13(e)**,** results from the fact that more electrons with higher average energies can now reach the stem cell depth. The SAF values are almost constant across the walls of all the sections of the GIT for 4 MeV electrons.

It is interesting to note that SAF values are 2.0 kg^{-1} for the ST, 1.25 kg^{-1} for the SI, 1.52 kg^{-1} for the ULI, and 3.7 kg^{-1} for the LLI based on both the MIRD (1975) and the ICRP (1979) dosimetric formulations for weakly-penetrating radiations in the walled organs. Regardless of the source particle energy, the SAFs are constant across these walls while Figs. 13(a)-12(e) demonstrate that the SAF has **a** strong dependence on electron energy as well as the distance of the target tissues from the wall-contents interface. For a given energy, the SAF varies by several orders of magnitude across the wall thickness.

Let us digress briefly to discuss the MIRD (1975) and the ICRP (1979) dosimetric formulations for non-penetrating radiations. The absorbed dose to hollow organs from non-penetrating radiations (alpha, beta, conversion electrons or Auger electrons, etc.) emitted in their contents was assumed to be the dose at the surface of the wall, which was approximated as one-half the equilibrium dose to the contents volume under radiation equilibrium conditions (MIRD 1975; ICRP 1979). Using this approximation, the specific absorbed fraction for the wall as the target organ and contents as the source organ, $SAF\ (Wall \leftarrow Cont)$ is

$$SAF\ (Wall \leftarrow Cont) = \frac{1}{2M_{cont}} \nu \tag{5}$$

where M_{cont} is the mass of the contents and ν is a factor between 0 and 1 representing the degree to which the radiation penetrates to the cells at risk. Regardless of the radition energies, the value of ν was set to 1.0 in both the MIRD (1975) and ICRP (1979) dosimetric formulations for weakly-penetrating radiations (beta, conversion electron or Auger electron, etc.).

The use of unity for the ν ignores radiation penetrability to the cells at risk. The dose at the interface was considered as the dose to the organ. There was enough evidence that the stem cells are the most radiosensitive and critical of the all five sections of GIT. This suggets that the absorbed dose to the stem cells should represent the dose to these sections rather than the interface dose that was routinely reported as the organ dose. If the stem cell dose represents the wall dose, then ν in Eq. (5) corresponds to the ratio of the absorbed dose to the stem cells to the absorbed dose at interface.

To prevent confusion, we have defined a parameter, called ε, that represents, for our calculations, the ratio of the absorbed dose (or SAF) to the stem cells to the absorbed dose (or SAF) at contents-mucus interface. The values of ε, listed in Table 9 for the energies 10 keV-4 MeV for the all five sections of the GIT. The table shows that the ε varies from 2.6×10^{-6} at 10 keV to 9.0×10^{-1} at 4 MeV.

Therefore, the routinely reported absorbed doses that are calculated using Eq. (5) with ν taken as 1 are severe overestimates of the actual doses to the radiosensitive target cells (stem cells) for energies below 750 keV. For electron energies above 2 MeV, the ε is close to unity. The ε-values shown in Table 9 suggests that ICRP and MIRD model is

not overly conservative for mid-energy electrons (1-4 MeV). However, more accurate dose estimates must use the appropriate ε-values for the weakly-penetrating particle-emitting radionuclides typically used in the nuclear medicine procedures, as well as for other internal dosimetery calculations.

Table 9. Ratio (ε) of electron SAF at mean depth of stem cells (radiosensitive cells) to SAF at contents-mucus interface of the five sections — esophagus (ESP), stomach (ST), small intestine (SI), upper large intestine (ULI), and lower large intestine (LLI) — of the GIT. The assumed mean depth of stem cells is 500 μm in the ESP, 730 μm in the ST, 790 μm in the SI, 818 μm in the ULI, and 830 μm in the LLI. The ε is 1 in the ICRP and MIRD formulation (Eq. 5).

Source Organ / Energy (MeV)	ε				
	ESP	**ST**	**SI**	**ULI**	**LLI**
0.01	5.00E-04	4.27E-06	2.60E-06	6.25E-06	5.192E-06
0.015	9.99E-04	1.97E-05	1.86E-05	2.76E-05	2.53E-05
0.02	1.43E-03	4.30E-05	5.88E-05	6.23E-05	5.07E-05
0.03	1.19E-03	9.48E-05	8.62E-05	1.17E-04	9.11E-05
0.05	1.08E-03	1.75E-04	2.60E-04	1.93E-04	1.65E-04
0.10	7.00E-04	2.30E-04	5.02E-04	2.14E-04	1.79E-04
0.20	1.10E-03	3.54E-04	6.45E-04	3.22E-04	3.11E-04
0.35	1.87E-01	6.03E-02	1.49E-02	8.30E-03	8.06E-03
0.50	3.93E-01	2.94E-01	1.92E-01	1.62E-01	1.30E-01
0.75	5.64E-01	5.19E-01	4.20E-01	3.58E-01	3.61E-01
1.00	6.41E-01	6.56E-01	5.55E-01	5.28E-01	4.49E-01
1.50	5.58E-01	7.34E-01	6.96E-01	6.44E-01	5.87E-01
2.00	6.26E-01	7.99E-01	7.78E-01	7.11E-01	6.64E-01
3.00	4.87E-01	8.64E-01	8.55E-01	8.19E-01	7.32E-01
4.00	5.05E-01	8.65E-01	9.00E-01	8.57E-01	7.56E-01

Two other grossly incorrect assumptions were made to formulate equation (5). It was assumed that walled organs are cylindrical in shape with the lumen full of contents. And it was assumed that the wall was irradiated in a 2π geometry by the source only in the luminal contents. Based on these assumptions, the absorbed dose at the contents-wall interface was approximated as one-half the equilibrium dose to the contents. This

approximation is known as "ICRP one-half approximation." Based on this approximation, the SAF at the interface should be 1.92 kg^{-1} for the ST, 0.1.79 kg^{-1} for the SI, 3.33 kg^{-1} for the ULI, and 5.26 kg^{-1} for the LLI if the masses of the contents of these organs modeled in this study were used. But our calculations showed that the SAFs at the interfaces were energy dependent and varied between 1.2 and 1.7 kg^{-1} for the ST, 0.3 and 0.5 kg^{-1} for the SI, 0.17-0.53 kg^{-1} for the ULI, and 0.3 and 0.8 kg^{-1} for the LLI. This is because the walled organs, except for the ST, were not full of contents and the walls were irradiated in more than 2π geometry.

Photon SAFs were also calculated at different depths in the wall of the five sections of the GIT (see Table B2). For 10 keV photons, the SAFs across the wall vary by one or two orders of magnitudes depending on the wall thickness. Above 50 keV, the SAFs are almost constant across the wall of all these organs. At a given depth, the SAF increases with increasing energy in the low-energy range while it decreases with energy for high energies. This is due to the same photon interaction processes as discussed earlier in this section. In comparison with the results of Cristy and Eckerman, the photon SAFs obtained with this revised model differ by about a factor of 2 to 3, except for the ST. For the ST, the SAFs are almost constant in the two studies. It is noted that the two models of the ST are identical in shape and size but are different in the position and orientation in the body. If we consider the SAF at the stem cell position instead of an average value for the entire wall, then the SAFs to the stem cell layer at about 730 μm differs by a factor of about 2.8 for 10 keV photons. The difference gradually diminishes as energy increases.

So far we have discussed the SAFs due to the "self absorption." That is, the target and the source are the same organ. We have also calculated both photon and electron SAFs due to "cross irradiation." Now the target is different from the source organ. Table B2 shows results on SAF distributions across the walls for 15 monoenergetic electrons and photons for all possible source-target combinations. A few points can be mentioned here. Electron SAFs from cross irradiation are not significant, except for the energies above 1 MeV for following source-target combinations: SI-ULI, SI-LLI, ULI-LLI, and vice versa. Also, cross irradiation is important when the source is the ESP and the target is the ST. But photon SAFs due to the cross irradiation are significant for all source-target combinations for all energies, except for low-energies when the target is separated by one photon free path from the source.

CONCLUSIONS

Electron transport studies using the MCNP computer code and a new model of the gastrointestinal tract (GIT) showed that the energy absorbed or SAF at the depth of the radiosensitive critical cells (stem cells) from electrons emitted in the lumenal contents is a small fraction of the dose routinely estimated at the contents-mucus interface. This fraction was obtained to increase with increasing electron energy from 2.6×10^{-6} to 9.0×10^{-1} (with some variation between two sections of the GIT) over the energy range 10 keV-4 MeV. These results clearly demonstrated that the interface dose that is routinely reported as the "wall" dose (ICRP and MIRD model) is a severe overestimation of the actual dose to the stem cells for electron energies in the range 10-500 keV. This fraction for the radionuclides emitting very low-energy electrons (<200 keV) is negligibly small, and thus the dose from these radionuclides in the GIT contents may be ignored. For electrons between 300 keV and 500 keV, the use of ICRP and MIRD model may overestimate the absorbed dose by several orders of magnitude. The ICRP and MIRD model may be conservative for electron energies up to 4 MeV. Appropriate correction factors should be applied for radionuclides emitting weakly-penetrating radiations for the energy range 10 keV – 4 MeV. The results of the calculations for 10 keV-4 MeV electrons indicate that the ICRP model may be closely fit for very energetic elelctrons (>3 MeV) penetrating right through the walls of the GIT.

This study demonstrated that the absorbed dose or SAF from electron sources in the lumenal contents of walled organs was a strong function of distance into wall. Thus,

knowing the depth of the target tissue layer, which was considered to be the stem cell in this study, is very important for electron dosimetry in walled organs.

The cross dose or the SAFs due to "cross irradiation" from electron sources are not significant, except for the energies above 1 MeV for the following source-target combinations: SI-ULI, SI-LLI, ULI-LLI, and vice versa. Also, cross irradiation is important when the source is the ESP and the target is the ST, but it is not important when the source is the ST and the target is the ESP. The results showed that the ULI and the LLI were significant sources of radiation for the active marrow and the ovaries for electron energies greater than 2 MeV. The ST as a source is important to the liver and the lungs for electrons with energies above 3 MeV. Generally, the cross dose can be ignored for electrons with energies below 2 MeV.

Photon transport studies using the present revised model showed that the photon SAFs, due to the self absorption, across the wall vary by one or two orders of magnitude depending on the wall thickness for 10 keV photons. Above 50 keV, the SAFs became almost constant across the wall of all the five sections of the GIT. At a given depth, the SAF increases with increasing energy in the low-energy range while it decreases in the high-energy range. The study also showed that the average dose or average SAF to the entire wall was significantly different from that to the radiosensitive cell layer. This study concluded that the absorbed dose to the radiosensitive cells (e.g., stem cells) should be reported as the organ dose instead of using the average dose for the energies below 50 keV.

The photon SAFs due to the cross irradiation were found to be significant for all source-target combinations except the source-target separated by a distance comparable to the mean free path of the photon under investigation.

The photon SAFs obtained using the revised model differ by a factor of 1.5 to 3 from photon SAF data obtained by Cristy and Eckerman. Generally, the difference between the two values is the highest at low-energies (<30 keV) and the lowest at medium energies (100-500 keV). This difference is mainly attributed to the difference between the two models.

These results should be used to modify currently accepted values of the annual limits on intake (ALI) for 188 radionuclides for which the GIT is significantly irradiated (ICRP 1979). New derived air concentration (DAC) should be recommended based on these calculations.

FUTURE WORK

The SAF values calculated in this study using the revised model were found to be significantly different, especially in the electron SAFs, from those commonly used values provided by the ICRP (1975) and by Cristy and Eckerman (1987). The effect of this revised model on two other important parameters, namely the annual limit on intake (ALI) and derived air concentrations (DAC) should be examined. The results obtained in this study can be used to modify currently accepted values of the ALI and DAC when sections of the GIT are the limiting organs (ICRP 1979). The recalculation of the ALI and DAC for 188 radionuclides for which the GIT is significantly irradiated (ICRP 1979) can be considered for future work in this field. These radionuclides are presented in Table C1 in Appendix C.

REFERENCES

Alberts B, Bray D, Lewis J, Raff M, Roberts K, Watson JD. Molecular biology of the cell. 2nd ed. New York: Garland Publishing, Inc.; 1989: 614.

Alpen EL. Radiation biophysics. 2nd ed. San Diego, California: Academic Press, Inc.; 1998: 247-259.

Allen A. The gastrointestinal system. In: Schultz SG, Forte JG, Rauner BB. eds. Handbook of physiology. vol. III, Section 6. Bethesda, MD: Am. Physiol. Soc.; 1989:359-382.

Atuma C, Strugala V, Allen A, Holm L. The adherent gastrointestinal mucus gel layer: thickness and physical state in vivo. Am J Physiol Gastrointest Liver Physiol 280: G922-G929; 2001.

Attix FR. Introduction to radiological physics and radiation dosimetry. New York: John Wiley & Sons; 1986: 193-197.

Balaban D, Yammamoto Y, Liu J, Pehlivanov N, Mittal RK. Identification of sustained esophageal contraction at the time of chest pain using high frequency intraluminal ultrasonography. Gastroenterology. 116:29-37; 1999.

Barrett KE, Donowitz M. Gastrointestinal transport, molecular physiology Vol 50. San Diego: Academic Press, 2000.

Berger, MJ. Energy deposition in water by photons from point isotropic sources. MIRD Pamphlet No. 2. New York: Society of Nuclear Medicine; 1968.

Berger MJ, Seltzer MS. Bremsstrahlung and photoneutrons from thick tungsten and tantalum targets. Phys Rev. C2:621-631; 1970.

Berger MJ, Seltzer SM. ETRAN, Monte Carlo code system for electron and photon transport through extended media. Oak Ridge, Tennessee: Oak Ridge Natl. Lab.; Documentation for RSIC computer code package, CCC-107; 1973.

Berger MJ, Wang R. Multiple-scattering angular deflections and energy-loss straggling in electron transport calculations. In: Nelson WR, Jenkins TM, Rindi A, Nahum AE, Rogers DWO, eds. Monte Carlo transport of electrons and photons below 50 MeV. New York: Plenum Press; 1989: 21-56.

Bickel M, Kauffman GL. Gastric gel mucus thickness: effect of distension, 16-16 dimethyl prostaglandin E_2 and carbenoxolone. Gastroenterology. 80:770-775; 1981.

Bhuiyan NU. A revised dosimetric model for calculation of electron dose in the small intestine. M.S. Thesis, College Station, Texas: Texas A&M University; 2000.

Bolch WE. The anatomical and physiological bases for internal dosimetry. In: Bolch WE. ed. Practical applications of internal dosimetry. Madison, Wisconsin: Medical Physics Publishing, Health Physics Society; 2002: 14-23.

Blomquist RN, Gelbard EM. An assessment of existing Klein-Nishina Monte Carlo sampling methods. Nucl Sci Eng 83:380; 1983.

Briesmeister JF. ed. MCNP—A general Monte Carlo N-particle transport code. Version 4A. Los Alamos, NM: Los Alamos National Laboratory; Report LA-12625-M; 1993.

Briesmeister JF. ed. MCNP—A general Monte Carlo N-particle transport code. Version 4B. Los Alamos, NM: Los Alamos National Laboratory; Report LA-12625-M; 1997.

Briesmeister JF. ed. MCNP—A general Monte Carlo N-particle transport code. Version 4C. Los Alamos, NM: Los Alamos National Laboratory; Report LA-12625-M; 2000.

Brownell GL, Ellet WH, Reddy AR. Absorbed fractions for photon dosimetry. MIRD Pamphlet No. 3. New York: Society of Nuclear Medicine; 1968.

Carlson, T. A. Photoelectron and Auger spectroscopy. New York: Plenum Press; 1975.

Cheng H, Leblond CP. Origin, differentiation and renewal of the four main epithelial cell types in the mouse small intestine. V. Unitarian theory of the origin of the four epithelial cell types. Am. J. Anat. 141:537-561; 1974.

Christensen J. The large intestine: Physiology, pathophysiology, and disease. New York: Raven Press, 1991.

Coffey JL. A revised mathematical model of the heart for use in radiation absorbed dose calculations. M. S. Thesis, Knoxville, TN: University of Tennessee; 1978.

Colbert HM. SANDYL, a computer program for calculating combined photon-electron transport in complex system. Livermore, California: Sandia Laboratories; Sandia Rep SLL-74-0012; 1974.

Cristy M. Mathematical phantoms representing children of various ages for use in estimates of internal dose. U.S. Nuclear Regulatory Commission Rep. NUREG/CR-1159 (also Oak Ridge National Laboratory Rep. ORNL/NUREG/TM-367); 1980.

Cristy M, Eckerman KF. Specific absorbed fractions of energy at various ages from internal photon sources. I. Methods. Oak Ridge, Tennessee: Oak Ridge National Laboratory; ORNL/TM-8381; 1987.

Davies H, Bethe HA, Maximom LC. Theory of bremsstrahlung and pair production. Phys Rev 93:788; 1954a.

Davies H, Bethe HA, Maximom LC. Integral cross section for pair production. Phys Rev 93; 1954b.

Ellet WH, Callahan AB, Brownell GH. Gamma-ray dosimetry of internal emitters: Monte Carlo calculations of absorbed dose from point sources. Brit. J. Radiol. 37:45-52; 1964.

Ellet WH, Callahan AB, Brownell GH. Gamma-ray dosimetry of internal emitters II: Monte Carlo calculations of absorbed dose from uniforms sources. Brit. J. Radiol. 38:541-544; 1965.

Ewart GM, Rogers DWO. Calculated thick target bremsstrahlung angular distributions and shielding calculations. Ottawa, Canada: National Research Council of Canada; Rep. PXNR-2640; 1982.

Evans RD. The atomic nucleus. New York: McGraw-Hill; 1955.

Eve, I. S. A review of the physiology of the gastrointestinal tract in relation to radiation doses from radioactive material. Health Phys. 12:131-161; 1966.

Everett CJ, Cashwell ED. MCP code fluorescence-routine revision. Los Alamos, New Mexico: Los Alamos Scientific Laboratory; LA-5240-MS; 1973.

Fawcett, D. W. A textbook of histology. 12th ed. New York: Chapman & Hall; 1994: 617-636.

Fisher HL, Snyder WS. Distribution of dose in the body from a source of gamma rays distributed uniformly in an organ. Oak Ridge, Tennessee: Oak Ridge National Laboratory; ORNL-4168/UC-41; 1967.

Fisher HL, Snyder WS. Distribution of dose in the body from a source of gamma rays distributed uniformly in an organ. In: Proc. First Internat. Congr. Radiat. Protection. Rome, Italy, September 5-10, 1966; Oxford: Pergamon Press; 1968:1473-1486.

Flemstrom G, Hallgren A, Nylander O, Engstrand L, Wilander E, Allen A. Adherent surface mucus gel restricts diffusion of macromolecules in rat duodenum in vivo. Am. J. Physiol. Gastrointest. Liver Physiol. 277:G375-G382; 1999.

Florey H. Mucin and the protection of the body. Proc. R. Soc. (Biol.) (London); 143:144-158; 1955.

Ford RL, Nelson WR. The EGS code system (version 3). Stanford, California: Stanford University; SLAC Rep 210; 1978.

Goudsmit S, Saunderson JL. Multiple scattering of electrons. Phys Rev 57:24-29; 1940.

Ganong WF. Review of medical physiology. 9th ed. Palo Alto, California: Lange Medical Publications; 1979.

Glasgow JFT, Corkey CWB, Molla A. Critical assessment of small bowel biopsy in children. Arch. Dis. Child. 54:604-608; 1979.

Golden R. Radiological examination of the small intestine. 2nd ed. Springfield, Illinois: Thomas; 1959.

Gordon JI, Hermiston ML. Differentiation and self-renewal in the mouse gastrointestinal epithelium. Curr. Opin. Cell Biol. 6:795-803; 1994.

Graaff VD, Kent M, Fox SI. Concepts of human anatomy and physiology. 5th ed. New York: McGraw-Hill; 1999.

Gray H. Gray's anatomy. Philadelphia: Running Press; 1974: 911-921.

Grosswendt B, Waibel E. Determination of detector efficiencies for gamma-ray energies up to 12 MeV. Nucl Instrum Methods 131:143-156; 1975.

Guyton AC. Text book of medical physiology. 9th ed. Philadelphia: W. B. Saunders Company; 1996.

Halbleib JA, Vandevender WH. CYLTRAN-cylindrical geometry multimaterial electron of photon Monte Carlo transport code. Oak Ridge, Tennessee: Radiation Shielding Information Center, Oak Ridge National Laboratory; ORNL Rep CCC-280; 1976.

Halbleib JA, Melhorn TA. ITS: the integrated TIGER series of coupled electron/photon Monte Carlo transport codes. Albuquerque, New Mexico: Sandia National Laboratories; Sandia Rep SAND84-0073; 1984.

Haubrich WS, Schaffner F. Bockus gastroenterology. 5th ed. Philadelphia: W. B. Saunders Company; 1995: 885-892.

Heitler W. The quantum theory of radiation. 3rd ed. Oxford: Oxford University Press; 1954.

Hendricks JS. MCNP4B, LANL memorandum. Los Alamos, New Mexico: Los Alamos National Laboratory; 1997.

Hine GJ, Brownell GL. Radiation dosimetry. New York: Academic Press Inc.; 1956: 722-730.

Hollander F. The two component mucus barrier. Its activity in protecting the gastroduodenal mucosa against peptic ulceration. Arch. Int. Med. 93:107-120; 1954.

Hubbell JH, Veigele WJ, Briggs EA, Brown RT, Cromer DT, Howerton RJ. Atomic form factors, incoherent scattering functions, and photon scattering cross sections. J Phys Chem Ref Data 4:471-538; 1975.

Hubbell JH, Øverbo I. Relativistic atomic form factors and photon coherent scattering cross sections. J Phys Chem Ref Data 8:69-105; 1979.

Hughes HG, Prael RE, Little RC. MCNPX-The LAHET/MCNP code merger. Los Alamos, New Mexico: Los Alamos National Laboratory; XTM-RN(U) 97-012; 1997.

Hwang JML, Shoup RL, Poston JW. Modifications and additions to the pediatric and adult mathematical phantoms. Oak Ridge, Tennessee: Oak Ridge National Laboratory; ORNL/TM-5454; 1976.

International Commission on Radiological Protection (ICRP). Report of Committee II on permissible dose for internal radiation. Oxford: Pergamon Press; ICRP Publication 2; 1959.

International Commission on Radiological Protection (ICRP). Report of the task group on reference man. Oxford: Pergamon Press; ICRP Publication 23; 1975.

International Commission on Radiological Protection (ICRP). Limits for intakes of radionuclides for workers. Oxford: Pergamon Press; ICRP Publication 30; 1979.

International Commission on Radiological Protection (ICRP). 1990 recommendations of the International Commission on Radiological Protection. Oxford: Pergamon Press; ICRP Publication 60; 1991.

International Commission on Radiological Protection (ICRP). Publication on the human alimentary tract (HAT). Online.

http://www.icrp.org/pdf/g_REM_Chapter_6_Alimentary_System.pdf. November 15, 2001.

International Commission on Radiation Units and Measurements. Stopping powers for electrons and positrons. Bethesda, Maryland; ICRU Report 37; 1984.

International Commission on Radiation Units and Measurements. Tissue substitutes in radiation dosimetry and measurement. Bethesda, Maryland; ICRU Publication 44; 1989.

Jabbur RJ, Pratt RH. High-frequency region of the spectrum of electron and positron bremsstrahlung. Phys Rev 129:184; 1963.

Jabbur RJ, Pratt RH. High-frequency region of the spectrum of electron and positron bremsstrahlung. Phys Rev 133:1090; 1964

Johnson LR, Christensen J, Jackson MJ, Jacobson ED, Walsh JH. Physiology of the gastrointestinal tract. 2nd ed. Vol. 2. New York: Raven Press; 1987: 975-1249.

Jönsson L, Liu X, Jönsson B, Ljungberg M, Strand SA. dosimetry model for the small intestine incorporating intestinal wall activity and cross-doses. J Nucl. Med. 43:1657-1664; 2002.

Kahn H. Applications of Monte Carlo. The Rand Corporation; AEC-3259; 1956.

Kaur P, Potten CS. Cell migration velocities in the crypts of the small intestine after cytotoxic insult are not dependent on mitotic activity. Cell Tissue Kinet. 19:601-610; 1986.

Kerss S, Allen A, Garner A. A simple method for measuring thickness of the mucus gel layer adherent to rat, frog and human gastric mucosa: influence of feeding, prostaglandin, N-acetylcysteine and other agents. Clin. Sci. 63:187-195;1982.

Koblinger L. Direct sampling from the Klein-Nishina distribution for photon energies above 1.4 MeV. Nucl Sci Eng 56:218; 1975.

Landau L. On the energy loss of fast particles by ionization. J Phys (Moscow) 8:201-205; 1944.

Lawrence JH, Tennant R. The comparative effects of neutrons and X-rays on the whole body. J. Exp. Med. 66:667; 1937.

Leeson RC, Leeson TS, Paparo AA. Textbook of histology. 5th ed. Philadelphia: W. B. Saunders Company; 1985: 343-352.

Lipkin M, Sherlock P, Bell B. Cell renewal in stomach, ileum, colon, and rectum. Gastroenterology. 45:721; 1963.

Loevinger R, Berman MA. Schema for absorbed dose calculations from biologically distributed radionuclides. MIRD Pamphlet No. 1 New York: Society of Nuclear Medicine; 1968.

Loevinger R. Distributed radionuclide sources. In: Attix FH, Tochilin E. Eds. Radiation dosimetry, 2nd ed. New York: Academic Press; 1969: 51-90.

Loevinger R, Berman MA. Revised schema for calculating the absorbed dose from biologically distributed radionuclides. MIRD Pamphlet No. 1, Revised. New York: Society of Nuclear Medicine; 1976.

Marieb EN. Human anatomy and physiology. 4th ed. Reading, Massachusetts: Addison Wesley Longman, Inc.; 1998.

Martin CL, Rogers FT. Intestinal reaction to erythema dose. Amer. J. Roentgenol. 10:11; 1923.

McClean P, Dodge JA, Nunn S, Carr KE, Sloan JM. Surface features of small-intestinal mucosa in childhood diarrheal disorders. J Ped. Gastroent. Nut. 23:538-546; 1996.

MacDonald WC, Trier JS, Everett NB. Cell proliferation and migration in the stomach, duodenum, and rectum of man: radioautographic studies. Gastroenterology. 46:405; 1964.

Magee DF, Dalley AF. Digestion and the structure and function of the gut. Farmington, Connecticut: Karger Continuing Education Series, Vol 8. 1986.

Miller LS, Liu JB, Colizzo FP, Ter H, Marzano J, Barbarevech C, Hedwig K, Leung L, Goldberg BB. Correlation of high frequency esophageal ultrasonography and manometry in the study of esophageal motility. Gastroenterology. 105:832-837; 1995.

Moe H. On goblet cells, especially of the intestine of some mammalian species. Int. Rev. Cytol. 4:299-334; 1955.

Molière GZ. Theorie der Streuung Schneller Geladener Teilchen II Mehrfach- und Vielfachstreuung. Z Naturforsch A 3A:78-79; 1948.

Morel JE, Lorene LJ. Recent developments in discrete ordinates electron transport. Trans Am Nucl Soc 52: 384-385; 1986.

Morris GP, Harding PK, Wallace JL. A functional model for extracellular gastric mucus in the rat. Virchows Arch. (Cell Pathol.). 46:239-251; 1984.

Moussa HM, Eckerman KF, Townsend LW, Pevey R. Estimation of electron absorbed fractions in the extrathoracic airways. Health Phys. 80:12-15; 2001.

National Bureau of Standards. Maximum permissible body burdens and maximum permissible concentrations of radionuclides in air and in water for occupational exposure. Recommendations of the National Committee on Radiation Protection (NCRP), Handbook 69, U. S. Department of Commerce, June 5, 1959.

National Council on Radiation Protection and Measurements. Evaluating the reliability of biokinetic and dosimetric models and parameters used to assess individual doses for risk assessment purposes. Bethesda, Maryland: National Council on Radiation Protection and Measurements; NCRP Commentary No. 15; 1998.

Nelson WR, Hirayama H, Rogers DWO. The EGS4 code system. Stanford, California: Stanford Linear Accelerator Center; Report SLAC-265-UC-32; 1985.

Nicosia MA, Brasseur JG, Liu J, Miller LS. Local longitudinal muscle shortening of the human esophagus from high-frequecny ultrasonography. Am. J Physiol Gastrointest Liver Physiol. 281:G1022-G1033; 2001.

Olsen H. Outgoing and ingoing waves in final states and bremssrtahlung. Phys Rev 99:1335; 1955.

Penna FJ, Hill ID, Kingston D, Robertson K, Slavin G, Shiner M. Jejunal mucosal morphometry in children with and without gut symptoms and normal adults. J Clin. Pathol. 34:386-392; 1981.

Pehlivanov N, Liu J, Kassab GS, Puckett JL, Mittal RK. Relationship between esophageal muscle thickness and intraluminal pressure: an ultrasonographic study. Am. J Physiol Gastrointest Liver Physiol. 280:G1093-G1098; 2001.

Poston JW, Jr., Kodimer KA, Bolch WE, Poston JW, Sr., Calculation of absorbed energy in the gastrointestinal tract. Health Phys. 71:300-306; 1996a.

Poston JW, Jr., Kodimer KA, Bolch WE, Poston JW, Sr. A revised model for the calculation of absorbed energy in the gastrointestinal tract. Health Phys. 71:307-314; 1996b.

Potten CS. Extreme sensitivity of some intestinal crypts to X and γ-irradiation. Nature 269:518-521, 1977.

Potten CS. A comprehensive study of the radiological response of the murine (BDF1) small intestine. Int. J. Radiat. Biol. 58:925-973; 1990.

Potten CS, Booth C, Pritchard DM. The intestinal epithelial stem cells: the mucosal governor. Int. J. Exp. Pathol. 78:219-243, 1997a.

Potten CS, Wilson JW, Booth C. Regulation and significance of apoptosis in the stem cells of the gastrointestinal epithelium. Stem Cells 15:82-93, 1997b.

Potten CS, Booth C. Personal communication, Paterson Institute for Cancer Research, Manchester, England; 2000.

Prael RE, Lichtenstein H. User guide to LCS: The LAHET code system. Los Alamos, New Mexico: Los Alamos National Laboratory; LA-UR-893014; 1989.

Pratt RH, Tseng HK, Lee CM, Kissel L, MacCallum C, Riley M. Brmesstrahlung energy spectra from electrons of kinetic energy 1 keV ≤ T ≤ 2000 keV incident on neutral atoms 2 < Z < 92. Atom Data and Nucl Data Tables 20:175; 1977; errata in 26:477; 1981.

Pullan RD, Thomas GA, Rhodes M, Newcombe RG, Williams GT, Allen A, Rhodes J. Thickness of adherent mucus gel on colonic mucosa in humans and its relevance to colitis. Gut. 35:353-359; 1994.

Riley ME, MacCallum CJ, Biggs F. Theoretical electron-atom elastic scattering cross sections. Selected elements, 1 keV to 256 keV. Atom Data and Nucl Data Tables 15:443; 1975.

Rogers DWO. Low energy electron transport with EGS. Nucl Instrum Methods Phys Res A227: 535-548; 1984a.

Rogers DWO. Fluence to dose equivalent conversion factors calculated with EGS3 for electron from 100 keV to 20 GeV and photons from 11 keV to 20 GeV. Health Phys 46:891-914; 1984b.

Rogers DWO, Bielajew AF. Difference in electron depth-dose curves calculated with EGS and ETRAN and improved energy range relationships. Med Phys 13: 687-694; 1986.

Rogers DWO, Bielajew AF. Monte Carlo techniques of electron and photon transport for radiation dosimetry. In: Kase KR, Bjärngard, Attix FH, eds. The dosimetry of ionizing radiation. New York: Academic Press, Inc.; 1990: 427-539.

Ross MH, Reith ED. Histology: a text and atlas. New York: Harper & Row Publishers; J. B. Lippincott Company; 1985: 426-427.

Sakata T, Engelhardt WV. Luminal mucin in the large intestine of mice, rats, and guinea pigs. Cell Tissue Res. 219:629-635; 1981.

Seltzer SM, Berger MJ. Bremsstrahlung spectra from electron interactions with screened atomic nuclei and orbital electrons. Nucl. Instr. Meth. Phys. Res. B12:95-134; 1986.

Seltzer SM. Cross sections for bremsstarhlung production and electron impact ionization. In: Jenkins TM, Nelson WR, Rindi A, eds. Monte Carlo transport of electrons and photons. New York: Plenum Press; 1988a: 81.

Seltzer SM. An overview of ETRAN Monte Carlo methods. In: Jenkins TM, Nelson WR, Rindi A, eds. Monte Carlo transport of electrons and photon. New York: Plenum Press; 1988b: 153.

Seltzer SM. An overview of ETRAN Monte Carlo methods for coupled electron/photon transport calculation. In: Nelson WR, Jenkins TM, Rindi A, Nahum AE, Rogers DWO, eds. Monte Carlo transport of electrons and photons below 50 MeV. New York: Plenum Press; 1989: 151-181.

Shreider YA. ed. The Monte Carlo method. Oxford: Pergamon Press; 1966.

Smith EM. Activities of the medical internal radiation dose committee. MIRD Supplement No. 1. New York: Society of Nuclear Medicine; 1968.

Snyder WS, Ford MR, Warner GG, Fisher HL, Jr. Estimates of absorbed fractions for monoenergetic photon sources uniformly distributed in various organs of a heterogeneous phantom. MIRD Pamphlet No. 5. New York: Society of Nuclear Medicine; 1969.

Snyder WS, Ford MR, Warner GG, Watson SB. A tabulation of dose equivalent per microcurie-day for source and target organs of an adult for various radionuclides. Oak Ridge, Tennessee: Oak Ridge National Laboratory; ORNL-5000; 1974.

Snyder WS, Ford MR, Warner GG. “S”, absorbed dose per unit cumulated activity for selected radionuclides and organs. MIRD Pamphlet No. 11. New York: Society of Nuclear Medicine; 1975.

Snyder WS, Ford MR, Warner GG. Estimates of specific absorbed fractions for photon sources uniformly distributed in various organs of a heterogeneous phantom. MIRD Pamphlet No. 5 (Revised). New York: Society of Nuclear Medicine; 1978.

Solomon EP, Davis PW. Understanding human anatomy and physiology. New York: McGraw-Hill Book Company; 1978: 316-334.

Stenling R, Fredrikzon B, Nyhlin H, Helander HF. Surface ultrastructure of the small intestine mucosa in healthy children and adults: a scanning electron microscopic study with some methodological aspects. Ultrastruct. Pathol. 6:131-140; 1984.

Sternheimer RM, Peierls RF. General expression for the density effect for the ionization loss of charged particles. Phys Rev B3:3681-3692; 1971.

Sternheimer RM, Berger MJ, Seltzer SM. Density effect of the ionization loss of charged particles in various substances. Phys Rev B26:6067; 1982.

Stubbs JB. A new mathematical model of gastrointestinal transit that incorporates age and gender-dependent physiological parameters. In: Watson EE, Schlafke-Stelson A, eds. Proceedings of the fifth international symposium on radiopharmaceutical dosimetry. National Technical Information Service, Springfield, Virginia; 1991: 229-242.

Stubbs JB. Results from a new mathematical model of gastrointestinal transit that incorporates age and gender-dependent physiological parameters. Radiat. Prot. Dosim. 41: 63-69 (1992).

Stubbs JB, Evans JF, Stabin MG. Radiation absorbed doses to the walls of hollow organs. J Nucl. Med. 39:1989-1995; 1998.

Sullivan MF, Hackett PL, George LA, Thompson RC. Irradiation of the intestine by radioisotopes. Radiat. Res. 13: 343-355; 1960.

Takeuchi K, Magee D, Critchlow J, Matthews J, Silen W. Role of pH gradient of mucus in protection of gastric mucosa. Gastoenterology. 84:331-340; 1983.

Taniguchi DK, Martin RW, Trowers EA, Dennis MB, Odegaad S, Silverstein FE. Change in esophageal wall layer during motility: measurement with a new miniature ultrasound device. Gastrointest Endosc 39:146-152; 1993.

Tipton IH, Snyder WS, Cook MJ. Elemental composition of standard man. Oak Ridge, Tennessee: Oak Ridge National Laboratory, Health Phys. Div. Annu. Prog. Rep. ORNL-4007; 1966.

Tipton IH, Cook MJ. Weight of total gastrointestinal tract and its subfractions. Oak Ridge, Tennessee: Oak Ridge National Laboratory, Health Phys. Div. Annu. Prog. Rep. ORNL-4446; 1969.

Tortora G J, Evans RL. Principles of human physiology. 2nd ed. New York: Harper & Row Publishers; 1986: 608-613.

Trier JS, Winter HS. Anatomy, embryology, and developmental abnormalities of the small intestine and colon. In: Sleisenger MH, Fordtran JS. eds. Gastrointestinal disease – pathophysiology, diagnosis, and management. 4th ed. Philadelphia: W. B. Saunders Company; 1989: 991-1021.

Tseng HK, Pratt RH. Exact screened calculations of atomic-field bremsstrahlung. Phys Rev A3:100; 1971.

Tseng HK, Pratt RH. Electron bremsstrahlung from neutral atoms. Phys Rev Lett 33:516; 1974.

Tsuzuki M. Experimental studies on the biological action of hard roentgen rays. Amer. J. Roentgenol. 16:134;1926.

Vander AJ, Sherman JH, Luciano DS. Human physiology. 2nd ed. New York: McGraw-Hill; 1970.

Warner GG, Craig AM, Jr. ALGAM, a computer program for estimating internal dose from gamma-ray sources in a man phantom. Oak Ridge, Tennessee: ORNL-TM-2250, Oak Ridge Natl. Lab.; 1968.

Warren LH. ed. Gray's anatomy of the human body. New York: Bartleby.com; Online. www.bartleby.com/107/; 2000.

Weber DA, Eckerman KF, Dillman LT, Ryman JC. MIRD: radionuclide data and decay schemes. New York: The Society of Nuclear Medicine; 1989.

Whitehead R. Gastrointestinal and oesophageal pathology. New York: Churchill Livingstone, 1989.

Yamamoto Y, Liu J, Smith TK, Mittal RK. Distension related responses in the circular and longitudinal muscles of the esophagus: an ultrasonographic study. Am. J. Physiol. Gastrointest Liver Physiol. 275:G805-G811; 1998.

APPENDIX A

DOSIMETRIC FORMULATIONS IN THE MULTI COMPARTMENTAL HOLLOW ORGAN

DOSIMETRIC FORMULATIONS IN THE MULTI COMPARTMENTAL HOLLOW ORGAN

Many factors can affect the absorbed dose to hollow organs (e.g., various sections of the GIT) from internally deposited radionuclides in their lumenal contents. The factors that significantly affect the dose relate to the structure and biokinetic of the organ of interest, namely the geometry, the degree of source dilution in the contents related to the mass of the contents, wall or target mass, and residence time of radioactive material in the organ (or transit time in general) related to the length. To facilitate Monte Carlo calculation and to avoid a "fitting" problem of an organ in the phantom, the actual anatomic data were manipulated in simulating the model with the Monte Carlo code. The simulation results should be adjusted for any change in the parameters of the actual model. In the present study with the revised GIT model, some parameters of the small and large intestines are changed in the simulated model (the model used for Monte Carlo simulation) (see Tables 6 and 7). This chapter deals with derivation of some empirical formulae to calculate the correction factors to be applied to the simulation results.

Multiple compartments are used to design each intestinal organ in the model. The sources are distributed in more than one compartment. The distribution probabilities in these compartments are calculated by weighting using the mass of the contents and the transit times. The distribution probability and the relative wall-mass of each compartment determine its contribution to the average absorbed dose per source particle to the organ as a whole or to a given segment of the wall (e.g., radiosensitive layer in the

wall). This chapter formulates necessary mathematical expressions to calculate these values.

In the following formulations, a symbol with "bar" (e.g., $\overline{D}$, $\overline{L}$, $\overline{M}$) denotes the parametric value in the simulated model and a symbol without "bar" denotes the parametric value in the actual model. For example, "$\overline{D}$" stands for average absorbed dose to the simulated model and "D" stands for average absorbed dose to the actual model.

Small intestine. As described before, the small intestine is divided into duodenum containing contents with a homogenously distributed source, a section of jejuno-ileum region containing contents with a homogenously distributed source, and the remainder of the jejuno-ileum region without a source, which is termed as remnants, representing the major part of the jejuno-ileum with closed lumen (Figs. 8-10). Table 6 lists the parametric values the simulated model and the actual model.

Actual model values of the small intestine are given below.

Total length, L = 300 cm.
Total wall mass, M_w = 650 g.
Total mass of the contents, M_c = 280 g.
Length of duodenum, L_d = 20.26 cm.
Wall mass of duodenum, $M_{d(w)}$ = 64.91 g.
Length of jejuno-ileum region, $L_{j\text{-}il}$ = (300 - 20.26) cm = 279.74 cm.
Wall mass of jejuno-ileum region with contents, $M_{j\text{-}il(w)}$ = 136.19 g.
Wall mass of remnant, $M_{r(w)}$ = (650 – (136.19 + 64.91)) g = 448.90 g

The values used in Monte Carlo simulation are given below.

Mass of the contents in duodenum, $\overline{M_{d(c)}}$ = 148.96 g.
Mass of the contents in the jejuno-ileum region, $\overline{M_{j-il(c)}}$ = 269.02 g.
Total source mass of the contents, $\overline{M_c}$ = 148.96 + 269.02 g = 417.98 g.

Total mass of remnants, $\overline{M}$ = 661.51 g.

Source is uniformly distributed in each of the two source organs but with different concentrations (number of source particles per unit mass). The distribution probabilities of the sources in the duodenum and jejuno-ileum are approximated as,

$$\left.\begin{aligned}\overline{S_d} &\approx \frac{\left(\overline{M_{d(c)}}/M_c\right)\left(T_d/T\right)}{\left(\overline{M_{j-il(c)}}/M_c\right)\left(T_{j-il}/T\right)+\left(\overline{M_{d(c)}}/M_c\right)\left(T_d/T\right)}\\ \overline{S_{j-il}} &\approx \frac{\left(\overline{M_{c(j-il)}}/M_c\right)\left(T_{j-il}/T\right)}{\left(\overline{M_{j-il(c)}}/M_c\right)\left(T_{j-il}/T\right)+\left(\overline{M_{d(c)}}/M_c\right)\left(T_d/T\right)}\end{aligned}\right\} \quad \text{(A1)}$$

where, the source probability distribution is $\overline{S_d}$ in the duodenum and is $\overline{S_{j-il}}$ in the jejuno-ileum, total transit time of the small intestine is *T*, transit time of the jejuno-ileum region is $T_{j\text{-}il}$, and transit time of duodenum is T_d. Since data of $T_{j\text{-}il}$ and T_d are not available, we can use the corresponding length as an approximation of the transit time, i.e., *L* for *T*, $L_{j\text{-}il}$ for $T_{j\text{-}il}$, and L_d for T_d.

Substituting the parameter values in the above expressions, the $\overline{S_d}$ and $\overline{S_{j-il}}$ are obtained to be 0.039 and 0.96. These are the source particle emission probabilities of the duodenum and the jejuno-ileum used in the Monte-Carlo calculations.

The average absorbed doses to the SI wall (target) are approximated as

$$D(SI \leftarrow SI) \approx \left[\left(\overline{M_{j-il(c)}}/M_c\right)\left(T_{j-il}/T\right)+\left(\overline{M_{d(c)}}/M_c\right)\left(T_d/T\right)\right]\left[\left(1/M_w\right)\left(M_{d-j-il(w)}\,\overline{D_{d-j-il}}+M_{r(w)}\,\overline{D_r}\right)\right] \quad \text{(A2)}$$

when the source is the SI contents, and

$$D(SI \leftarrow organ) \approx \left[\left(1/M_w\right)\left(M_{d-j-il(w)}\,\overline{D_{d-j-il}}+M_{r(w)}\,\overline{D_r}\right)\right] \quad \text{(A3)}$$

when the source is in any organ other than the SI.

The factor $\overline{D_{d-j-il}}$ denotes the average absorbed dose to the duodenum wall and wall of the section of the jejuno-ileum with contents, $\overline{D_r}$ denotes the average absorbed dose to the remnants (solid region of soft tissue), and $M_{d-j-il(w)}$ denotes the wall mass of the duodenum and the section of the jejuno-ileum with contents which is equal to $M_{d(w)} + M_{j-il(w)} (= 201.1g)$. Substituting the values into expressions (A2) and (A3) we obtain

$$D(SI \leftarrow SI) \approx (0.288)(\overline{D_{d-j-il}}) + (0.643)(\overline{D_r}) \tag{A4}$$

and

$$D(SI \leftarrow organ) \approx (0.309)(\overline{D_{d-j-il}}) + (0.691)(\overline{D_r}) \tag{A5}$$

When the sources are in the SI contents, $\overline{D_{d-j-il}}$ and $\overline{D_r}$ are the simulated average absorbed doses due to uniform source distributions in the duodenum contents with concentration $\overline{S_d} / \overline{M_{d(c)}}$ (= (0.039 / 148.96) source particles per gram of the mass of the contents) and in the jejuno-ileum contents with concentration $\overline{S_{j-il}} / \overline{M_{j-il(c)}}$ (= (0.96/ 269.02) source particle per gram of the mass of the contents). The actual doses were calculated using expression (A4). The expression (A4) produced approximately the same result as with a homogenously distributed source with a concentration 1/280 source particles per gram of the mass of the contents in the duodenum contents with mass 10.98 g (≈0.039×280 g) and in the jejuno-ileum contents with mass 269.02 g (=280 g-10.98 g). As discussed before, the wall was divided in many small shell volumes. The

relationships (A4) and (A5) were equally applicable to any individual shell volume (representing a tissue layer in the wall) instead of the entire wall to obtain the actual absorbed dose to that segment of the wall.

Large intestine. The large intestine was divided into two parts; the upper large intestine (ULI), consisting of ascending colon (AC) and transverse colon (TC), and the lower large intestine (LLI), consisting of descending colon (DC) and sigmoid-rectum colon (SRC). The wall plus lumen of the AC, TC, DC, and SRC were modeled as two coaxial upright circular cylinders, horizontal elliptical cylinders, oblique elliptical cylinders, and circular tori, respectively, where the contents of each colonic section except the SRC fill only a small portion of the lumenal length in the middle. More than 80% of the lumenal length in either side of the contents was empty (Fig. 7) in each of these sections except the SRC. The entire lumen of the SRC in the simulated model was full. But about 75% of the actual lumen was empty. The lengths were much shorter and the wall masses were much smaller in the simulated model (the model used for the MCNP calculation) than those in the actual model (see Table 7). So length and wall-mass adjustments were required. But the mass of the contents and the specific wall mass (mass per unit length) were almost the same in both the cases.

The empty and the filled lumen are denoted by superscript “e” and “f” in following derivations.

Upper large intestine (ULI): AC + TC.

$$\left.\begin{aligned} L_{ac}^{e} &= 19.79cm \\ L_{ac}^{f} &= 3.63cm \\ L_{ac} &= L_{ac}^{e} + L_{ac}^{f} = 23.42cm \\ M_{ac(c)} &= 60g \\ M_{ac(w)} &= 90g \\ T_{ac} &= 8.4h \end{aligned}\right\}$$ actual model values of the AC (see Table 6).

$$\left.\begin{aligned} L_{tc}^{e} &= 40.84cm \\ L_{tc}^{f} &= 9.16cm \\ L_{tc} &= L_{tc}^{e} + L_{tc}^{f} = 50cm \\ M_{tc(c)} &= 90g \\ M_{tc(w)} &= 120g \\ T_{tc} &= 7.3h \end{aligned}\right\}$$ actual model values of the TC (see Table 7).

$$\left.\begin{aligned} L_{ULI} &= L_{ac} + L_{tc} = 73.42cm \\ M_{ULI(c)} &= M_{ac(c)} + M_{tc(c)} = 150g \\ M_{ULI(w)} &= M_{ac(w)} + M_{tc(w)} = 210g \\ T_{ULI} &= T_{ac} + T_{tc} = 15.7h \end{aligned}\right\}$$ actual model values of the ULI (see Table 7).

$$\left.\begin{aligned} \overline{L_{ac}^{e}} &= 5.92cm \\ \overline{L_{ac}^{f}} &= L_{ac}^{f} = 3.63cm \\ \overline{L_{ac}} &= \overline{L_{ac}^{e}} + \overline{L_{ac}^{f}} = 9.55cm \\ \overline{M_{ac(c)}} &= M_{ac(c)} = 60g \\ \overline{M_{ac(w)}} &= 36.70g \end{aligned}\right\}$$ simulated model values of the AC (see Table 7).

$$\left.\begin{aligned}
&\overline{L_{tc}^{e}} = 11.84cm \\
&\overline{L_{tc}^{f}} = 9.16cm \\
&\overline{L_{tc}} = \overline{L_{tc}^{e} + L_{tc}^{f}} = 21cm \\
&\overline{M_{tc(c)}} = M_{tc(c)} = 90g \\
&\overline{M_{tc(w)}} = 50.42g
\end{aligned}\right\} \text{ simulated model values of the TC (see Table 7).}$$

The probability distribution of the source is given by

$$\left.\begin{aligned}
S_{ac} = \overline{S_{ac}} &\approx \frac{\left(\overline{M_{ac(c)}}/M_{ULI(c)}\right)\left(T_{ac}/T_{ULI}\right)}{\left[\left(\overline{M_{ac(c)}}/M_{ULI(c)}\right)\left(T_{ac}/T_{ULI}\right)+\left(\overline{M_{tc(c)}}/M_{ULI(c)}\right)\left(T_{tc}/T_{ULI}\right)\right]} \\
S_{tc} = \overline{S_{tc}} &\approx \frac{\left(\overline{M_{tc(c)}}/M_{ULI(c)}\right)\left(T_{tc}/T_{ULI}\right)}{\left[\left(\overline{M_{ac(c)}}/M_{ULI(c)}\right)\left(T_{ac}/T_{ULI}\right)+\left(\overline{M_{tc(c)}}/M_{ULI(c)}\right)\left(T_{tc}/T_{ULI}\right)\right]}
\end{aligned}\right\} \quad \text{(A6)}$$

Substituting the values, we obtain $S_{ac} \cong 0.434$ and $S_{tc} \cong 0.566$.

The average absorbed dose to the AC wall is approximated as

$$D_{ac} \approx \frac{1}{M_{ac}}\left\{D_{ac}^{e}\left(M_{ac}^{e}\right)+D_{ac}^{f}\left(M_{ac}^{f}\right)\right\}=\frac{1}{L_{ac}}\left\{D_{ac}^{e}\left(L_{ac}^{e}\right)+D_{ac}^{f}\left(L_{ac}^{f}\right)\right\} \quad \text{(A7)}$$

$$\overline{D_{ac}} \approx \frac{1}{\overline{L_{ac}}}\left\{\overline{D_{ac}^{e}}\left(\overline{L_{ac}^{e}}\right)+\overline{D_{ac}^{f}}\left(\overline{L_{ac}^{f}}\right)\right\} \quad \text{(A8)}$$

Since $L_{ac}^{f} = \overline{L_{ac}^{f}}$, we can assume that $D_{ac}^{f} = \overline{D_{ac}^{f}}$. We can also reasonably assume that $D_{ac}^{e} = \overline{D_{ac}^{e}}$. Using these relationships in equation (A7), we obtain

$$D_{ac} \approx \frac{1}{L_{ac}}\left\{\overline{D_{ac}^{e}}\left(L_{ac}^{e}\right)+\overline{D_{ac}^{f}}\left(L_{ac}^{f}\right)\right\} \quad \text{(A9)}$$

Applying equation (A8), equation (A9) also can be written as

$$D_{ac} \approx \frac{1}{L_{ac}}\left\{\overline{D_{ac}^{e}}\left(L_{ac}^{e}-\overline{L_{ac}^{e}}\right)+\overline{D_{ac}}\left(\overline{L_{ac}}\right)\right\} \quad \text{(A10)}$$

When the source is other than in the AC contents, we can reasonably assume that $\overline{D_{ac}^{e}} = \overline{D_{ac}}$. Under this assumption, the average absorbed dose to the AC wall, when the source is other than in the AC contents, can be estimated using equation (A10) as

$$D_{ac}^{T} \cong \overline{D_{ac}} \tag{A11}$$

Similarly, we have for the TC,

$$D_{tc} \approx \frac{1}{M_{tc}} \left\{ D_{tc}^{e}\left(M_{tc}^{e}\right) + D_{tc}^{f}\left(M_{tc}^{f}\right) \right\} = \frac{1}{L_{tc}} \left\{ D_{tc}^{e}\left(L_{tc}^{e}\right) + D_{tc}^{f}\left(L_{tc}^{f}\right) \right\} \tag{A12}$$

and

$$\overline{D_{tc}} \approx \frac{1}{\overline{L_{tc}}} \left\{ \overline{D_{tc}^{e}}\left(\overline{L_{tc}^{e}}\right) + \overline{D_{tc}^{f}}\left(\overline{L_{tc}^{f}}\right) \right\} \tag{A13}$$

Since $L_{tc}^{f} = \overline{L_{tc}^{f}}$, we can assume that $D_{tc}^{f} = \overline{D_{tc}^{f}}$. We also can reasonably assume that $D_{tc}^{e} = \overline{D_{tc}^{e}}$. Using these relationships in equation (A12), we obtain

$$D_{tc} \approx \frac{1}{L_{tc}} \left\{ \overline{D_{tc}^{e}}\left(L_{tc}^{e}\right) + \overline{D_{tc}^{f}}\left(L_{tc}^{f}\right) \right\} \tag{A14}$$

Applying equation (A13), equation (A14) also can be written as

$$D_{tc} \approx \frac{1}{L_{tc}} \left\{ \overline{D_{tc}^{e}}\left(L_{tc}^{e} - \overline{L_{tc}^{e}}\right) + \overline{D_{tc}}\left(\overline{L_{tc}}\right) \right\} \tag{A15}$$

When the source is other than the TC contents, we can reasonably assume that $\overline{D_{tc}^{e}} = \overline{D_{tc}}$. Under this assumption, the average absorbed dose to the TC wall when the source is other than the TC contents, can be estimated using equation (A15) as

$$D_{tc}^{T} \cong \overline{D_{tc}} \tag{A16}$$

Thus, the average absorbed dose to the ULI wall when the source is in the ULI contents, is approximated as

$$D_{ULI} \cong \left[\left(\overline{M_{ac(c)}}/M_{ULI(c)}\right)\left(T_{ac}/T_{ULI}\right)+\left(\overline{M_{tc(c)}}/M_{ULI(c)}\right)\left(T_{tc}/T_{ULI}\right)\right]\left[\frac{1}{M_{ULI(w)}}\left\{\left(D_{ac}M_{ac(w)}\right)+\left(D_{tc}M_{tc(w)}\right)\right\}\right] \quad \text{(A17)}$$

Substituting the parametric values, equation (A17) gives

$$\boldsymbol{D_{ULI} \cong (0.177)(D_{ac}) + (0.316)(D_{tc})} \quad \text{(A18)}$$

The average absorbed dose to the ULI wall, when the source is other than in the ULI contents, is approximated as

$$D^{T}_{ULI} \approx \left[\frac{1}{M_{ULI(w)}}\left\{\left(\overline{D_{ac}}M_{ac(w)}\right)+\left(\overline{D_{tc}}M_{tc(w)}\right)\right\}\right] \quad \text{(A19)}$$

Substituting the parametric values, equation (A19) gives

$$\boldsymbol{D^{T}_{ULI} \cong (0.36)(\overline{D_{ac}}) + (0.64)(\overline{D_{tc}})} \quad \text{(A20)}$$

<u>*Lower large intestine (LLI): DC + SRC.*</u>

$$\left.\begin{aligned} L^{e}_{dc} &= 27.1cm \\ L^{f}_{dc} &= 2.5cm \\ L_{dc} &= L^{e}_{ac} + L^{f}_{ac} = 29.6cm \\ M_{dc(c)} &= 25g \\ M_{dc(w)} &= 90g \\ T_{dc} &= 4.3h \end{aligned}\right\}$$ actual model values of the DC (see Table 7).

$$\left.\begin{aligned} L^{e}_{sc} &= 41.7cm \\ L^{f}_{dc} &= 13.7cm \\ L_{sc} &= 55.4cm \\ M_{sc(c)} &= 70g \\ M_{sc(w)} &= 70.15g \\ T_{sc} &= 11.5h \end{aligned}\right\}$$ actual model values of the SRC (see Table 7).

$$\left.\begin{aligned} L_{LLI} &= L_{dc} + L_{sc} = 85cm \\ M_{LLI(c)} &= M_{dc(c)} + M_{sc(c)} = 95g \\ M_{LLI(w)} &= M_{dc(w)} + M_{sc(w)} = 160.15g \\ T_{LLI} &= T_{dc} + T_{sc} = 15.8h \end{aligned}\right\}$$ actual model values of the LLI (see Table 7).

$$\left.\begin{aligned} \overline{L_{dc}^{e}} &= 15.28cm \\ \overline{L_{dc}^{f}} &= L_{dc}^{f} = 2.50cm \\ \overline{L_{dc}} &= \overline{L_{dc}^{e}} + \overline{L_{dc}^{f}} = 17.78cm \\ \overline{M_{dc(c)}} &= M_{dc(c)} = 25g \\ \overline{M_{dc(w)}} &= 46.48g \end{aligned}\right\}$$ simulated model values of the DC (see Table 7).

$$\left.\begin{aligned} \overline{L_{sc}} &= 13.7cm \\ \overline{M_{sc(c)}} &= 92.8g \\ \overline{M_{sc(w)}} &= 17.34g \end{aligned}\right\}$$ simulated model values of the SRC (see Table 7).

The probability distribution of the source is given by

$$\left.\begin{aligned} S_{dc} = \overline{S_{dc}} &\approx \frac{\left(\overline{M_{dc(c)}}/M_{LLI(c)}\right)\left(T_{dc}/T_{LLI}\right)}{\left[\left(\overline{M_{dc(c)}}/M_{LLI(c)}\right)\left(T_{dc}/T_{LLI}\right)+\left(\overline{M_{sc(c)}}/M_{LLI(c)}\right)\left(T_{sc}/T_{LLI}\right)\right]} \\ S_{sc} = \overline{S_{sc}} &\approx \frac{\left(\overline{M_{sc(c)}}/M_{LLL(c)}\right)\left(T_{sc}/T_{LLI}\right)}{\left[\left(\overline{M_{dc(c)}}/M_{LLI(c)}\right)\left(T_{dc}/T_{LLI}\right)+\left(\overline{M_{sc(c)}}/M_{LLI(c)}\right)\left(T_{sc}/T_{LLI}\right)\right]} \end{aligned}\right\} \quad \text{(A21)}$$

Substituting the values, we obtain $S_{ac} \cong 0.09$ and $S_{tc} \cong 0.91$.

In similar manner to the ULI, the average absorbed dose to LLI wall, when the source is in the LLI contents, is approximated as

$$D_{LLI} \approx \left[\left(\overline{M_{dc(c)}} / M_{LLI(c)} \right) \left(T_{dc} / T_{LLI} \right) + \left(\overline{M_{sc(c)}} / M_{LLI(c)} \right) \left(T_{sc} / T_{LLI} \right) \right] \left[\frac{1}{M_{LLI(w)}} \left\{ \left(D_{dc} M_{dc(w)} \right) + \left(D_{sc} M_{sc(w)} \right) \right\} \right] \quad \text{(A22)}$$

Substituting the parametric values, equation (A22) gives

$$\boldsymbol{D_{LLI} \cong (0.440)(D_{dc}) + (0.343)(D_{sc})} \quad \text{(A23)}$$

where,

$$D_{dc} \approx \frac{1}{L_{dc}} \left\{ \overline{D_{dc}^{e}} \left(L_{dc}^{e} \right) + \overline{D_{dc}^{f}} \left(L_{dc}^{f} \right) \right\} \quad \text{(A24)}$$

and

$$D_{sc} \approx \frac{1}{L_{sc}} \left\{ \overline{D_{dc}^{e}} \left(L_{sc}^{e} \right) + \overline{D_{sc}^{f}} \left(L_{sc}^{f} \right) \right\} \quad \text{(A25)}$$

In equations (A24) and (A25), we have assumed that $D_{dc}^{e} \cong \overline{D_{dc}^{e}}$, $D_{dc}^{f} \cong \overline{D_{dc}^{f}}$, $D_{sc}^{f} \cong \overline{D_{sc}^{f}}$, and $D_{sc}^{e} \cong D_{dc}^{e}$. In equation (A25), we have used $\overline{D_{dc}^{e}}$ in place of $\overline{D_{sc}^{e}}$ because both are approximately equal and because a calculated value for $\overline{D_{sc}^{e}}$ is not available as there is no empty part in the simulated SRC model.

The average absorbed dose to the LLI wall, when the source is other than the LLI contents, is approximated as

$$D_{LLI}^{T} \approx \left[\frac{1}{M_{LLI(w)}} \left\{ \left(\overline{D_{dc}} M_{dc(w)} \right) + \left(D_{sc} M_{sc(w)} \right) \right\} \right] \quad \text{(A26)}$$

where,

$$\overline{D_{dc}} \approx \frac{1}{\overline{L_{dc}}} \left\{ \overline{D_{dc}^{e}} \left(L_{dc}^{e} \right) + \overline{D_{dc}^{f}} \left(\overline{L_{dc}^{f}} \right) \right\}$$

Substituting the parametric values and using equation (A25) into the equation (A26), we obtain

$$\boldsymbol{D_{LLI}^{T} \cong (0.89)\left(\overline{D_{dc}}\right) + (0.11)\left(\overline{D_{sc}^{f}}\right)} \tag{A27}$$

provided that $D_{dc}^{e} = \overline{D_{dc}}$, which is a reasonable assumption when the source is outside the LLI.

APPENDIX B

SPECIFIC ABSORBED FRACTION (SAF) DATA

Table B1. Specific Absorbed Fractions (SAFs) in various organs and tissues from uniformly distributed sources of 15 monoenergetic electrons and photons in the lumenal contents of the five sections of the Gastrointestinal Tract (GIT) of an adult human male or a larger-than-average-female (72.63 kg). Use the following relationship to get the absorbed dose (Gy) per source particle: SAF (kg^{-1}) × Energy (MeV) × 1.602E-13.

Source Organ / Energy (MeV)	Target: Active Marrow									
	SAF (kg^{-1}) for electron					SAF (kg^{-1}) for photon				
	ESP	**ST**	**SI**	**ULI**	**LLI**	**ESP**	**ST**	**SI**	**ULI**	**LLI**
0.01	0.0	0.0	3.98E-14[e]	4.57E-11[c]	4.6E-11	1.04E-5	0.0	3.38E-7[b]	6.16E-5	7.78E-5
0.015	1.13E-9	1.90E-11[a]	1.24E-10[b]	4.60E-9	5.74E-9	7.61E-4	4.11E-5	1.55E-4[a]	2.19E-3	3.00E-3
0.02	1.55E-8	1.27E-9	4.34E-9[a]	4.35E-8	6.03E-8	4.05E-3	8.58E-4	2.21E-3	8.59E-3	1.33E-2
0.03	1.79E-7	4.18E-8	1.14E-7	3.58E-7	5.38E-7	1.58E-2	6.17E-3	1.59E-2	2.21E-2	3.22E-2
0.05	1.25E-6	4.66E-7	1.09E-6	1.86E-6	2.70E-6	2.50E-2	1.29E-2	2.81E-2	2.74E-2	3.14E-2
0.10	5.35E-6	2.44E-6	5.52E-6	6.70E-6	8.84E-6	1.61E-2	9.86E-3	1.84E-2	1.66E-2	1.63E-2
0.20	1.23E-5	6.21E-6	1.32E-5	1.44E-5	1.72E-5	1.01E-2	6.35E-3	1.10E-2	1.03E-2	9.97E-3
0.35	1.98E-5	1.06E-5	2.14E-5	2.24E-5	2.58E-5	8.34E-3	5.21E-3	8.76E-3	8.35E-3	8.27E-3
0.50	2.57E-5	1.41E-5	2.81E-5	2.89E-5	3.27E-5	7.77E-3	4.78E-3	8.01E-3	7.71E-3	7.66E-3
0.75	3.48E-5	1.94E-5	3.82E-5	3.84E-5	4.24E-5	7.24E-3	4.45E-3	7.33E-3	7.16E-3	7.14E-3
1.00	4.34E-5	2.46E-5	4.78E-5	4.72E-5	5.15E-5	6.94E-3	4.28E-3	7.01E-3	6.81E-3	6.77E-3
1.50	6.03E-5	3.46E-5	6.52E-5	9.25E-5	1.00E-4	6.43E-3	4.00E-3	6.37E-3	6.30E-3	6.22E-3
2.00	8.90E-5	4.43E-5	8.31E-5	3.14E-4	3.12E-4	6.04E-3	3.81E-3	6.00E-3	5.92E-3	5.79E-3
3.00	2.91E-4	6.43E-5	1.14E-4	1.33E-3	1.43E-3	5.44E-3	3.41E-3	5.45E-3	5.33E-3	5.18E-3
4.00	7.92E-4	8.17E-5	1.85E-4	2.66E-3	3.42E-3	5.08E-3	3.21E-3	5.00E-3	4.92E-3	4.88E-3

The source organs are esophagus (ESP), stomach (ST), small intestine (SI), upper large intestine (ULI), and lower large intestine (LLI).

The values of relative error (*R*) associated with the Monte Carlo SAF calculations were denoted by superscripts a, b, c, etc. The symbol 'a' was used for the *R*-values in the range of 0.11-0.20, 'b' was for 0.21-0.30, 'c' was for 0.31-0.40, and so on. The *R*-values less than 0.11 were not shown.

Table B1. Continued.

Source Organ / Energy (MeV)	Target: Brain									
	SAF (kg^{-1}) for electron					SAF (kg^{-1}) for photon				
	ESP	**ST**	**SI**	**ULI**	**LLI**	**ESP**	**ST**	**SI**	**ULI**	**LLI**
0.01	0.0	0.0	0.0	0.0	0.0	0.0	0.0	0.0	0.0	0.0
0.015	0.0	0.0	0.0	0.0	0.0	0.0	0.0	0.0	0.0	0.0
0.02	0.0	0.0	0.0	0.0	0.0	0.0	0.0	0.0	0.0	0.0
0.03	0.0	0.0	0.0	0.0	0.0	0.0	1.80E-7	5.88E-8	0.0	0.0
0.05	0.0	2.57E-11	8.44E-12	0.0	0.0	1.23E-5	3.60E-6	3.86E-7	1.65E-6	0.0
0.10	2.89E-9	5.79E-10	8.57E-11	0.0	0.0	5.65E-5	1.91E-5	2.15E-6	3.20E-6	1.71E-7
0.20	1.77E-8	7.09E-09	6.65E-10	3.59E-10	0.0	8.86E-5	3.41E-5	4.64E-6	7.64E-6	6.29E-7
0.35	4.27E-8	1.57E-08	2.40E-09	3.44E-09	0.0	1.32E-4	5.25E-5	1.03E-5	1.30E-5	1.34E-6
0.50	8.70E-8	3.82E-08	4.47E-09	4.87E-09	0.0	1.69E-4	7.73E-5	1.43E-5	1.72E-5	1.19E-6
0.75	1.74E-7	7.06E-08	9.55E-09	1.65E-08	0.0	2.12E-4	9.00E-5	1.91E-5	2.61E-5	7.21E-6
1.00	3.14E-7	1.05E-07	1.94E-08	3.20E-08	0.0	2.63E-4	1.15E-4	2.86E-5	3.21E-5	8.82E-6
1.50	5.92E-7	2.14E-07	3.59E-08	4.38E-08	0.0	2.77E-4	1.50E-4	4.79E-5	4.15E-5	1.70E-5
2.00	7.96E-7	3.60E-07	7.73E-08	1.07E-07	3.80E-09	3.18E-4	1.82E-4	5.18E-5	5.58E-5	2.25E-5
3.00	2.23E-6	8.59E-07	1.82E-07	2.40E-07	3.42E-08	3.36E-4	2.03E-4	6.55E-5	8.84E-5	3.12E-5
4.00	2.86E-6	1.43E-06	5.27E-07	3.33E-07	9.45E-08	3.38E-4	2.15E-4	9.08E-5	1.08E-4	2.98E-5
Target: Breasts										
0.01	0.0	0.0	0.0	0.0	0.0	0.0	0.0	0.0	0.0	0.0
0.015	0.0	0.0	0.0	0.0	0.0	0.0	2.11E-7	0.0	0.0	0.0
0.02	0.0	1.74E-11	0.0	0.0	0.0	8.97E-6	4.27E-5	0.0	9.40E-7	0.0
0.03	3.73E-9	3.77E-09	4.48E-11	0.0	0.0	1.33E-3	1.00E-3	1.57E-5	1.63E-5	2.17E-6
0.05	1.02E-7	7.54E-08	1.72E-09	2.72E-09	1.80E-10	4.98E-3	3.02E-3	1.15E-4	1.79E-4	1.87E-5
0.10	8.63E-7	5.11E-07	2.19E-08	2.72E-08	3.34E-09	5.67E-3	3.48E-3	2.52E-4	3.47E-4	3.53E-5
0.20	2.70E-6	1.56E-06	9.68E-08	1.35E-07	9.23E-09	5.74E-3	3.57E-3	3.54E-4	4.59E-4	6.36E-5
0.35	5.49E-6	3.19E-06	2.24E-07	3.10E-07	3.51E-08	5.85E-3	3.87E-3	4.18E-4	5.90E-4	7.95E-5
0.50	8.30E-6	4.66E-06	3.96E-07	4.92E-07	6.60E-08	5.97E-3	4.02E-3	5.03E-4	6.47E-4	9.57E-5
0.75	1.34E-5	7.55E-06	6.55E-07	9.18E-07	9.83E-08	6.14E-3	4.12E-3	5.90E-4	7.20E-4	1.40E-4
1.00	1.81E-5	1.06E-05	1.08E-06	1.37E-06	1.65E-07	6.20E-3	4.24E-3	6.44E-4	8.06E-4	1.38E-4
1.50	2.83E-5	1.65E-05	1.85E-06	2.46E-06	3.09E-07	5.85E-3	4.12E-3	6.92E-4	8.73E-4	2.17E-4
2.00	3.85E-5	2.46E-05	2.69E-06	4.07E-06	6.19E-07	5.58E-3	4.00E-3	7.15E-4	9.53E-4	2.40E-4
3.00	6.20E-5	4.18E-05	5.06E-06	5.65E-06	1.17E-06	5.12E-3	3.73E-3	6.63E-4	9.26E-4	2.24E-4
4.00	8.57E-5	5.71E-05	6.91E-06	9.39E-06	2.35E-06	4.85E-3	3.51E-3	6.90E-4	1.01E-3	2.70E-4

Table B1. Continued.

Source Organ / Energy (MeV)	Target: Heart Wall									
	SAF (kg^{-1}) for electron					SAF (kg^{-1}) for photon				
	ESP	**ST**	**SI**	**ULI**	**LLI**	**ESP**	**ST**	**SI**	**ULI**	**LLI**
0.01	8.38E-9	0.0	0.0	0.0	0.0	1.05E-02	6.34E-08	0.0	0.0	0.0
0.015	5.06E-7	2.52E-10	0.0	0.0	0.0	1.45E-04	4.22E-04	0.0	0.0	0.0
0.02	2.84E-6	1.01E-08	1.29E-11	0.0	0.0	2.75E-01	4.87E-03	1.52E-6	0.0	0.0
0.03	1.26E-5	2.15E-07	1.13E-09	0.0	0.0	2.93E-01	2.24E-02	1.06E-4	7.42E-5	3.16E-6
0.05	3.69E-5	1.70E-06	9.58E-09	1.16E-8	0.0	1.80E-01	3.04E-02	6.31E-4	8.03E-4	4.90E-5
0.10	8.57E-5	6.78E-06	8.26E-08	4.90E-7[a]	1.08E-8[b]	1.06E-01	2.23E-02	1.12E-3	1.42E-3	1.05E-4
0.20	1.49E-4	1.63E-05	4.47E-07	5.29E-7	4.86E-8[a]	9.59E-02	1.89E-02	1.20E-3	1.44E-3	1.66E-4
0.35	2.25E-4	2.76E-05	9.58E-07	1.26E-6	8.17E-8[a]	9.39E-02	1.81E-02	1.27E-3	1.54E-3	1.99E-4
0.50	3.36E-4	3.77E-05	1.51E-06	1.88E-6	1.34E-7[a]	9.21E-02	1.74E-02	1.29E-3	1.64E-3	2.34E-4
0.75	2.24E-4	5.36E-05	2.45E-06	2.96E-6	3.50E-7[a]	8.78E-02	1.66E-02	1.38E-3	1.67E-3	2.77E-4
1.00	1.09E-3	6.84E-05	3.38E-06	4.43E-6	3.86E-7[a]	8.45E-02	1.58E-02	1.40E-3	1.70E-3	3.07E-4
1.50	1.12E-2	1.03E-04	5.54E-06	7.40E-6	8.04E-7[a]	7.65E-02	1.46E-02	1.43E-3	1.75E-3	3.88E-4
2.00	4.96E-2	1.37E-04	7.98E-06	1.05E-5	1.30E-6[a]	7.11E-02	1.38E-02	1.34E-3	1.76E-3	4.02E-4
3.00	1.69E-1	1.96E-04	1.30E-05	1.79E-5	2.23E-6[a]	6.31E-02	1.23E-02	1.43E-3	1.63E-3	3.68E-4
4.00	2.68E-1	2.70E-04	2.04E-05	2.20E-5	5.14E-6[b]	5.84E-02	1.14E-02	1.29E-3	1.47E-3	3.68E-4
Target: Kidneys										
0.01	0.0	0.0	0.0	0.0	0.0	0.0	0.0	0.0	0.0	0.0
0.015	0.0	0.0	0.0	0.0	0.0	0.0	4.44E-07	5.46E-6	0.0	0.0
0.02	0.0	9.79E-11	5.08E-10	0.0	0.0	5.09E-05[a]	2.30E-04	3.68E-04	2.13E-4	3.94E-7
0.03	8.43E-9	2.60E-08	2.26E-08	2.13E-8	0.0	2.57E-03	6.53E-03	4.75E-03	5.23E-3	1.08E-4
0.05	1.98E-7	4.94E-07	3.59E-07	3.79E-7	7.14E-9[b]	8.43E-03	1.62E-02	1.06E-02	1.28E-2	5.79E-4
0.10	1.43E-6	2.98E-06	1.97E-06	2.32E-6	7.21E-8	9.17E-03	1.48E-02	1.04E-02	1.21E-2	9.53E-4
0.20	4.39E-6	8.26E-06	5.81E-06	6.90E-6	3.59E-7	8.36E-03	1.29E-02	9.34E-03	1.06E-2	1.05E-3
0.35	8.64E-6	1.53E-05	1.05E-05	1.20E-5	7.99E-7	8.20E-03	1.20E-02	8.96E-03	1.01E-2	1.15E-3
0.50	1.23E-5	2.16E-05	1.46E-05	1.75E-5	1.30E-6	8.04E-03	1.18E-02	8.74E-03	9.73E-3	1.21E-3
0.75	1.92E-5	3.24E-05	2.23E-05	2.55E-5	2.33E-6	7.68E-03	1.12E-02	8.41E-03	9.40E-3	1.27E-3
1.00	2.60E-5	4.19E-05	3.07E-05	3.37E-5	2.95E-6	7.47E-03	1.07E-02	8.09E-03	8.90E-3	1.34E-3
1.50	4.08E-5	6.57E-05	4.65E-05	4.16E-5[b]	5.50E-6	6.92E-03	1.00E-02	7.58E-03	8.22E-3	1.51E-3
2.00	5.22E-5	8.62E-05	6.32E-05	7.08E-5	6.67E-6	6.69E-03	9.55E-03	7.20E-03	7.86E-3	1.50E-3
3.00	8.75E-5	1.35E-04	9.64E-05	9.23E-5[a]	1.28E-5	6.16E-03	8.68E-03	6.41E-03	7.06E-3	1.37E-3
4.00	1.14E-4	1.85E-04	1.24E-04	1.47E-4	1.50E-5[c]	5.49E-03	8.08E-03	6.04E-03	6.96E-3	1.32E-3

Table B1. Continued.

Source Organ / Energy (MeV)	Target: Liver									
	SAF (kg^{-1}) for electron					SAF (kg^{-1}) for photon				
	ESP	**ST**	**SI**	**ULI**	**LLI**	**ESP**	**ST**	**SI**	**ULI**	**LLI**
0.01	0.0	4.81E-12	1.24E-13	0.0	0.0	8.76E-06	1.09E-05	1.19E-06	8.63E-07[d]	0.0
0.015	1.73E-09	2.40E-09	4.12E-11	1.18E-10[b]	0.0	1.37E-03	1.54E-03	1.10E-04	8.64E-05	0.0
0.02	2.76E-08	3.45E-08	1.81E-09	2.01E-9	0.0	7.47E-03	8.84E-03	8.27E-04	8.98E-04	0.0
0.03	3.02E-07	3.66E-07	3.20E-08	4.32E-8	0.0	2.16E-02	2.48E-02	2.93E-03	5.63E-03	8.53E-06[a]
0.05	1.72E-06	2.03E-06	2.65E-07	4.20E-7	4.80E-10[c]	2.58E-02	2.81E-02	5.98E-03	1.08E-02	1.41E-04
0.10	6.39E-06	7.03E-06	1.24E-06	2.15E-6	2.46E-8	1.97E-02	2.06E-02	5.99E-03	9.71E-03	3.55E-04
0.20	1.45E-05	1.58E-05	3.37E-06	5.69E-6	1.12E-7	1.70E-02	1.77E-02	5.33E-03	8.57E-03	4.06E-04
0.35	2.44E-05	2.64E-05	6.29E-06	1.03E-5	2.79E-7	1.61E-02	1.72E-02	5.15E-03	8.17E-03	4.81E-04
0.50	3.32E-05	3.53E-05	8.96E-06	1.46E-5	4.48E-7	1.55E-02	1.64E-02	5.03E-03	7.90E-03	5.31E-04
0.75	4.76E-05	4.95E-05	1.32E-05	2.14E-5	7.08E-7	1.49E-02	1.56E-02	4.95E-03	7.55E-03	5.83E-04
1.00	6.23E-05	6.46E-05	1.75E-05	2.89E-5	1.20E-6	1.43E-02	1.37E-02	4.84E-03	7.36E-03	6.32E-04
1.50	9.02E-05	9.45E-05	2.73E-05	4.34E-5	2.04E-6	1.32E-02	1.37E-02	4.55E-03	6.95E-03	6.97E-04
2.00	1.23E-04	1.36E-04	3.82E-05	5.75E-5	2.89E-6	1.24E-02	1.28E-02	4.29E-03	6.55E-03	7.31E-04
3.00	3.43E-04	4.72E-04	8.35E-05	9.63E-5	6.70E-6[b]	1.12E-02	1.17E-02	3.89E-03	5.88E-03	7.54E-04
4.00	1.25E-03	1.43E-03	1.72E-04	1.64E-4	8.27E-6	9.99E-03	1.09E-02	3.68E-03	5.40E-03	6.73E-04
Target: Lungs										
0.01	0.0	0.0	0.0	0.0	0.0	0.0	1.31E-06	0.0	0.0	0.0
0.015	5.92E-10[b]	3.42E-10	0.0	0.0	0.0	7.42E-04	2.91E-04	0.0	0.0	0.0
0.02	1.97E-08	6.33E-09	0.0	0.0	0.0	8.08E-03	1.76E-03	2.05E-06	0.0	0.0
0.03	3.31E-07	7.86E-08	1.20E-10	2.14E-10[e]	0.0	2.75E-02	6.38E-03	6.79E-05	5.01E-05	1.95E-06[b]
0.05	2.06E-06	5.42E-07	8.32E-09	7.07E-9[a]	0.0	3.03E-02	9.43E-03	4.00E-04	5.15E-04	2.47E-05
0.10	7.57E-06	2.09E-06	6.97E-08	9.06E-8	3.51E-9[b]	2.16E-02	7.87E-03	6.95E-04	8.90E-04	7.37E-05
0.20	1.70E-05	5.18E-06	2.76E-07	3.49E-7	2.13E-8[a]	1.87E-02	7.00E-03	7.70E-04	9.90E-04	9.46E-05
0.35	2.81E-05	9.22E-06	6.10E-07	7.74E-7	5.54E-8[a]	1.76E-02	6.69E-03	8.45E-04	1.08E-03	1.31E-04
0.50	3.79E-05	1.27E-05	9.71E-07	1.21E-6	9.30E-8	1.70E-02	6.73E-03	9.10E-04	1.14E-03	1.67E-04
0.75	5.38E-05	1.82E-05	1.59E-06	2.03E-6	1.74E-7	1.61E-02	6.49E-03	9.71E-04	1.22E-03	2.04E-04
1.00	6.95E-05	2.43E-05	2.21E-06	2.97E-6	3.15E-7[a]	1.53E-02	6.26E-03	1.02E-03	1.26E-03	2.22E-04
1.50	1.02E-04	3.65E-05	3.68E-06	4.50E-6	5.58E-7[a]	1.40E-02	5.82E-03	1.03E-03	1.26E-03	2.77E-04
2.00	1.29E-04	5.13E-05	5.36E-06	7.18E-6	8.80E-7[a]	1.30E-02	5.47E-03	1.02E-03	1.21E-03	2.93E-04
3.00	1.92E-04	1.08E-04	9.72E-06	1.11E-5	1.74E-6	1.16E-02	4.95E-03	1.05E-03	1.19E-03	3.09E-04
4.00	2.87E-04	3.23E-04	1.45E-05	1.74E-5	3.17E-6[a]	1.08E-02	4.54E-03	9.62E-04	1.09E-03	3.42E-04

Table B1. Continued.

Source Organ / Energy (MeV)	Target: Ovaries									
	SAF (kg^{-1}) for electron					SAF (kg^{-1}) for photon				
	ESP	**ST**	**SI**	**ULI**	**LLI**	**ESP**	**ST**	**SI**	**ULI**	**LLI**
0.01	0.0	0.0	0.0	0.0	0.0	0.0	0.0	8.22E-04	5.17E-04[b]	7.28E-04[a]
0.015	0.0	0.0	5.96E-08	2.08E-8[b]	4.12E-8[b]	0.0	0.0	2.49E-02	2.04E-02	2.07E-02
0.02	0.0	0.0	4.60E-07	3.47E-7[a]	3.92E-7	0.0	0.0	6.08E-02	5.78E-02	5.29E-02
0.03	0.0	0.0	2.27E-06	2.23E-6[a]	2.00E-6	0.0	1.70E-04	1.09E-01	7.76E-02	6.09E-02
0.05	0.0	2.20E-08	1.09E-05	7.94E-6	7.07E-6	1.48E-04[b]	1.56E-03	8.81E-02	5.82E-02	4.24E-02
0.10	5.58E-08[e]	2.36E-07	3.08E-05	2.08E-5	1.73E-5	5.58E-04	2.39E-03	5.72E-02	3.81E-02	2.94E-02
0.20	1.68E-07[c]	1.11E-06	5.72E-05	4.11E-5	3.12E-5	7.43E-04	2.38E-03	4.92E-02	3.29E-02	2.63E-02
0.35	4.46E-07[b]	2.08E-06	9.07E-05	6.46E-5	5.09E-5	7.45E-04	2.19E-03	4.88E-02	3.19E-02	2.51E-02
0.50	1.26E-06[b]	3.36E-06	1.13E-04	8.05E-5	6.43E-5	9.10E-04[a]	1.96E-03	4.65E-02	3.12E-02	2.46E-02
0.75	6.80E-07[c]	4.77E-06	1.59E-04	1.07E-4	8.93E-5	8.77E-04[a]	2.05E-03	4.42E-02	2.94E-02	2.19E-02
1.00	3.49E-06[c]	6.20E-06	2.11E-04	1.39E-4	1.18E-4	1.23E-03[a]	2.08E-03	3.90E-02	2.89E-02	2.07E-02
1.50	6.60E-06[c]	1.17E-05	9.49E-04	2.01E-4	1.60E-4	9.60E-04[a]	1.84E-03	3.79E-02	2.46E-02	2.02E-02
2.00	7.05E-06[c]	1.53E-05	4.94E-03	1.66E-3[d]	2.41E-3[c]	7.19E-04[b]	2.16E-03	3.55E-02	2.34E-02	1.89E-02
3.00	1.11E-05[c]	2.48E-05	1.51E-02	8.65E-3[a]	1.02E-2[a]	8.59E-04[b]	2.06E-03	3.18E-02	2.10E-02	1.70E-02
4.00	9.84E-06[b]	3.09E-05	3.05E-02	2.35E-2[a]	2.66E-2[a]	6.66E-04[d]	1.97E-03	2.88E-02	1.95E-02	1.46E-02
Target: Pancreas										
0.01	0.0	1.02E-10	8.42E-09	0.0	0.0	0.0	2.12E-04	8.95E-04	0.0	0.0
0.015	5.92E-10[b]	3.45E-08	3.15E-08	0.0	0.0	3.34E-07	2.24E-02	1.79E-03	0.0	0.0
0.02	1.32E-08[a]	4.43E-07	9.95E-08	0.0	0.0	9.56E-03	1.11E-01	3.61E-03	1.95E-04[a]	0.0
0.03	4.46E-07	4.31E-06	2.84E-07	1.79E-8[a]	0.0	4.63E-02	2.12E-01	8.44E-03	5.61E-03	1.03E-04[a]
0.05	3.17E-06	1.85E-05	9.04E-07	4.15E-7	4.81E-9[b]	5.53E-02	1.54E-01	1.19E-02	1.29E-02	6.16E-04
0.10	1.29E-05	5.27E-05	2.99E-06	2.43E-6	8.61E-8	3.95E-02	9.40E-02	9.77E-03	1.17E-02	8.75E-04
0.20	2.96E-05	1.02E-04	7.10E-06	6.52E-6	3.74E-7	3.38E-02	8.35E-02	9.07E-03	1.04E-02	9.43E-04
0.35	5.03E-05	1.58E-04	1.21E-05	1.22E-5	7.80E-7	3.19E-02	7.91E-02	9.02E-03	9.66E-03	1.05E-03
0.50	6.83E-05	2.04E-04	1.73E-05	1.72E-5	1.19E-6	3.07E-02	7.84E-02	8.52E-03	9.30E-03	1.08E-03
0.75	9.75E-05	2.84E-04	7.77E-04	2.55E-5	1.95E-6	2.89E-02	7.38E-02	8.08E-03	9.03E-03	1.16E-03
1.00	1.24E-04	3.62E-04	1.19E-03	3.33E-5	2.54E-6	2.73E-02	6.98E-02	8.11E-03	8.80E-03	1.15E-03
1.50	1.83E-04	5.17E-04	1.97E-03	5.21E-5	5.19E-6	2.48E-02	6.38E-02	7.08E-03	8.33E-03	1.36E-03
2.00	2.45E-04	7.77E-04	3.48E-03	7.09E-5	6.28E-6	2.31E-02	5.88E-02	6.66E-03	7.63E-03	1.28E-03
3.00	3.52E-04	5.25E-03	5.33E-03	1.04E-4	1.15E-5	2.13E-02	5.23E-02	6.56E-03	6.84E-03	1.21E-03
4.00	4.50E-04	2.15E-02	5.10E-03	1.33E-4	2.31E-5[c]	1.95E-02	4.76E-02	5.86E-03	6.14E-03	1.25E-03

Table B1. Continued.

Source Organ / Energy (MeV)	Target: Testes									
	SAF (kg^{-1}) for electron					SAF (kg^{-1}) for photon				
	ESP	**ST**	**SI**	**ULI**	**LLI**	**ESP**	**ST**	**SI**	**ULI**	**LLI**
0.01	0	0.0	0.0	0.0	2.42E-10[g]	0.0	0.0	0.0	0.0	1.09E-04[b]
0.015	0	0.0	0.0	0.0	3.48E-9[c]	0.0	0.0	0.0	0.0	1.53E-03
0.02	0	0.0	0.0	0.0	3.56E-8[a]	0.0	0.0	0.0	0.0	8.60E-03
0.03	0	0.0	9.39E-11[g]	0.0	3.63E-7	0.0	0.0	9.77E-05	8.04E-05[b]	2.64E-02
0.05	0	2.31E-10[g]	5.44E-09[b]	1.33E-8[d]	1.88E-6	0.0	2.94E-05	8.78E-04	5.85E-04	2.85E-02
0.10	4.64E-10[g]	4.80E-09[c]	1.48E-07	1.25E-7[a]	7.52E-6	2.23E-05[a]	9.09E-05	1.39E-03	9.75E-04	2.05E-02
0.20	3.62E-09[d]	2.79E-08[b]	5.29E-07	4.40E-7	1.69E-5	5.06E-05[a]	1.20E-04	1.51E-03	1.19E-03	1.88E-02
0.35	2.16E-08[b]	6.40E-08[b]	1.24E-06	9.60E-7	5.68E-5[e]	8.27E-05[a]	1.76E-04	1.63E-03	1.24E-03	1.79E-02
0.50	2.43E-08[b]	1.14E-07[b]	1.88E-06	1.49E-6	3.68E-5	8.35E-05[b]	2.19E-04	1.68E-03	1.32E-03	1.71E-02
0.75	1.41E-07[c]	2.56E-07[b]	3.13E-06	2.21E-6	5.48E-5	1.41E-04[b]	3.41E-04	1.84E-03	1.53E-03	1.68E-02
1.00	7.52E-08[c]	2.36E-07[b]	4.50E-06	3.53E-6[a]	6.80E-5	1.11E-04[c]	3.65E-04	1.77E-03	1.62E-03	1.59E-02
1.50	1.65E-07[b]	6.87E-07[a]	7.97E-06	4.96E-6[a]	2.05E-4[e]	1.83E-04[a]	3.57E-04	1.94E-03	1.54E-03	1.33E-02
2.00	2.84E-07[c]	1.21E-06[a]	1.04E-05	8.80E-6[a]	4.14E-4[d]	3.09E-04[b]	4.45E-04	1.82E-03	1.60E-03	1.23E-02
3.00	9.54E-07[b]	2.99E-06[a]	1.50E-05	1.37E-5[a]	2.97E-4[a]	1.80E-04[c]	5.74E-04	1.87E-03	1.53E-03	1.15E-02
4.00	3.32E-06[c]	3.34E-06[b]	3.32E-05[a]	2.25E-5[b]	1.93E-3[b]	2.44E-04[c]	5.39E-04	1.79E-03	1.75E-03[a]	1.02E-02
	Target: Thyroid									
0.01	0.0	0.0	0.0	0.0	0.0	0.0	0.0	0.0	0.0	0.0
0.015	0.0	0.0	0.0	0.0	0.0	0.0	0.0	0.0	0.0	0.0
0.02	0.0	0.0	0.0	0.0	0.0	0.0	0.0	0.0	0.0	0.0
0.03	0.0	0.0	0.0	0.0	0.0	1.62E-05[e]	7.01E-06	0.0	0.0	0.0
0.05	0.0	8.14E-10[d]	0.0	0.0	0.0	4.45E-04	1.04E-04	4.72E-06	5.48E-06[f]	6.46E-06[f]
0.10	8.23E-08[a]	1.84E-08[a]	0.0	3.27E-9	0.0	9.77E-04	2.98E-04	2.61E-05	2.96E-05[b]	0.0
0.20	3.22E-07	9.18E-08	7.12E-09[g]	1.39E-8[c]	3.63E-9[g]	1.03E-03	3.25E-04	3.71E-05	4.29E-05[a]	0.0
0.35	8.01E-07	2.28E-07[a]	1.02E-08[g]	5.26E-10[e]	0.0	1.04E-03	3.66E-04	4.95E-05	5.71E-05[a]	1.16E-05[f]
0.50	1.13E-06	3.93E-07	2.72E-08[d]	5.06E-8[b]	0.0	1.08E-03	3.93E-04	6.77E-05	8.08E-05[a]	2.71E-05[f]
0.75	2.17E-06	7.69E-07[a]	5.09E-08[d]	9.28E-8[b]	1.52E-8[f]	1.16E-03	4.54E-04	7.44E-05	9.81E-05[b]	1.93E-05[e]
1.00	3.16E-06[a]	7.89E-07[a]	9.37E-08[b]	5.83E-8[c]	2.81E-9[g]	1.18E-03[a]	4.47E-04	1.28E-04	1.51E-04[b]	6.10E-06[e]
1.50	4.72E-06[a]	1.76E-06	2.53E-07[b]	1.73E-7[c]	5.05E-8[h]	1.22E-03	4.28E-04	9.86E-05	2.57E-04[b]	1.03E-05[f]
2.00	6.98E-06[b]	2.45E-06[a]	1.88E-07[b]	2.19E-7[d]	2.70E-8[g]	1.17E-03[a]	7.14E-04	1.35E-04	2.38E-04[b]	5.81E-05[f]
3.00	9.39E-06[a]	4.34E-06[a]	1.08E-06[c]	1.56E-6[d]	0.0	1.19E-03[a]	7.66E-04	1.66E-04	1.27E-04[b]	1.06E-04[e]
4.00	1.31E-05[a]	5.64E-06[a]	7.12E-07[b]	2.68E-7[c]	2.11E-7[h]	1.32E-03[a]	6.70E-04	1.36E-04	9.01E-05[e]	1.58E-04[f]

Table B1. Continued.

Source Organ / Energy (MeV)	Target: Urinary Bladder Wall									
	SAF (kg^{-1}) for electron					SAF (kg^{-1}) for photon				
	ESP	**ST**	**SI**	**ULI**	**LLI**	**ESP**	**ST**	**SI**	**ULI**	**LLI**
0.01	0	0.0	0.0	0.0	0.0	0.0	0.0	0.0	0.0	0.0
0.015	0	0.0	0.0	0.0	0.0	0.0	0.0	1.65E-06[c]	0.0	1.20E-03
0.02	0	0.0	6.84E-11[d]	0.0	3.50E-8[a]	0.0	0.0	3.31E-04	1.99E-04[a]	1.77E-02
0.03	0	0.0	2.91E-08[a]	1.8E-8[§]	7.10E-7	0.0	1.16E-05[a]	7.16E-03	3.46E-03	6.44E-02
0.05	0	4.99E-09[a]	4.33E-07	2.99E-7	4.76E-6	5.40E-5[a]	3.48E-04	1.62E-02	9.08E-03	6.81E-02
0.10	9.50E-09[a]	5.50E-08	3.04E-06	1.62E-6	1.72E-5	1.75E-04	7.58E-04	1.47E-02	9.09E-03	4.54E-02
0.20	5.97E-08	2.91E-07	8.09E-06	4.30E-6	3.60E-5	2.40E-4	8.48E-04	1.24E-02	7.89E-03	3.85E-02
0.35	1.62E-07	6.05E-07	1.45E-05	9.01E-6	6.09E-5	3.30E-4	9.12E-04	1.12E-02	7.55E-03	3.61E-02
0.50	2.41E-07	9.74E-07	2.13E-05	1.29E-5	8.18E-5	3.74E-4	1.08E-03	1.11E-02	7.35E-03	3.47E-02
0.75	5.34E-07	1.97E-06	3.25E-05	1.95E-5	1.14E-4	4.22E-4	1.13E-03	1.04E-02	7.14E-03	3.26E-02
1.00	6.93E-07	2.25E-06	3.22E-05[b]	2.43E-5	1.47E-4	4.68E-4	1.11E-03	1.03E-02	7.02E-03	3.11E-02
1.50	1.39E-06	3.85E-06	6.00E-05	4.7E-5[a]	2.07E-4	5.38E-4	1.21E-03	9.23E-03	6.24E-03	2.89E-02
2.00	2.07E-06	6.04E-06	6.57E-05	5.25E-5	2.88E-4	6.21E-4	1.23E-03	8.84E-03	5.98E-03	2.69E-02
3.00	4.09E-06	1.10E-05	1.16E-04	8.10E-5	4.83E-4[a]	5.30E-4	1.06E-03	8.15E-03	5.65E-03	2.38E-02
4.00	6.10E-06	1.18E-05	1.62E-04	1.06E-4	5.71E-4	4.85E-4[a]	1.11E-03	7.44E-03	4.97E-03	2.21E-02
Target: Uterus										
0.01	0.0	0.0	0.0	0.0	0.0	0.0	0.0	4.10E-02	0.0	0.0
0.015	0.0	0.0	7.82E-10[b]	0.0	0.0	0.0	0.0	1.59E-03	1.29E-05[f]	4.12E-06[g]
0.02	0.0	0.0	5.09E-08[a]	0.0	1.30E-9[f]	0.0	0.0	2.58E-02	1.18E-03	6.78E-04
0.03	0.0	0.0	9.07E-07	7.51E-8	6.29E-8	1.11E-5[f]	1.13E-04	8.44E-02	1.54E-02	1.18E-02
0.05	0.0	1.81E-08	2.35E-10[b]	1.16E-6	8.28E-7	1.88E-4	1.29E-03	8.22E-02	2.87E-02	2.49E-02
0.10	4.18E-08[b]	1.96E-07	2.19E-05	5.54E-6	4.49E-6	5.28E-04	2.16E-03	5.78E-02	2.35E-02	2.16E-02
0.20	1.98E-07[a]	8.23E-07	4.69E-05	1.42E-5	1.26E-5	6.67E-4	2.15E-03	4.81E-02	2.03E-02	1.84E-02
0.35	3.87E-07[a]	1.73E-06	7.47E-05	2.59E-5	2.30E-5	7.29E-4	2.28E-03	4.47E-02	1.88E-02	1.71E-02
0.50	7.56E-07	2.70E-06	9.95E-05	3.61E-5	3.17E-5	7.87E-4	2.08E-03	4.38E-02	1.79E-02	1.59E-02
0.75	1.22E-06[a]	4.31E-06	1.44E-04	5.21E-5	4.65E-5	8.65E-4	2.13E-03	4.10E-02	1.70E-02	1.50E-02
1.00	1.76E-06[a]	5.71E-06	1.85E-04	6.83E-5	6.02E-5	9.38E-4	2.10E-03	3.91E-02	1.61E-02	1.46E-02
1.50	2.88E-06	9.81E-06	2.68E-04	1.00E-4	8.96E-5	9.75E-4	1.98E-03	3.53E-02	1.50E-02	1.37E-02
2.00	3.85E-06[a]	1.40E-05	3.62E-04	1.31E-4	1.29E-4	1.02E-3	1.90E-03	3.28E-02	1.40E-02	1.27E-02
3.00	8.23E-06[a]	2.36E-05	5.01E-04	2.09E-4	1.81E-4	9.13E-4	2.11E-03	2.96E-02	1.22E-02	1.12E-02
4.00	8.94E-06[a]	3.09E-05	6.81E-04	2.91E-4	2.69E-4	9.91E-4	2.13E-03	2.70E-02	1.11E-02	9.93E-03

Table B1. Continued.

Source Organ / Energy (MeV)	Target: Whole Body									
	SAF (kg^{-1}) for electron					SAF (kg^{-1}) for photon				
	ESP	**ST**	**SI**	**ULI**	**LLI**	**ESP**	**ST**	**SI**	**ULI**	**LLI**
0.01	1.38E-02	1.38E-02	1.38E-02	1.38E-02	1.38E-02	1.37E-02	1.38E-02	1.36E-02	1.35E-02	1.37E-02
0.015	1.38E-02	1.38E-02	1.38E-02	1.38E-02	1.38E-02	1.37E-02	1.38E-02	1.24E-02	1.34E-02	1.37E-02
0.02	1.38E-02	1.38E-02	1.38E-02	1.38E-02	1.38E-02	1.36E-02	1.37E-02	1.11E-02	1.34E-02	1.36E-02
0.03	1.38E-02	1.38E-02	1.38E-02	1.38E-02	1.38E-02	1.32E-02	1.27E-02	1.07E-02	1.27E-02	1.30E-02
0.05	1.38E-02	1.38E-02	1.38E-02	1.38E-02	1.38E-02	1.09E-02	1.01E-02	9.32E-03	1.02E-02	1.04E-02
0.10	1.38E-02	1.38E-02	1.38E-02	1.38E-02	1.38E-02	7.79E-03	7.26E-03	7.04E-03	7.39E-03	7.53E-03
0.20	1.38E-02	1.38E-02	1.38E-02	1.38E-02	1.38E-02	6.91E-03	6.58E-03	6.26E-03	6.68E-03	6.78E-03
0.35	1.38E-02	1.38E-02	1.38E-02	1.38E-02	1.38E-02	6.70E-03	6.48E-03	6.08E-03	6.52E-03	6.61E-03
0.50	1.38E-02	1.38E-02	1.38E-02	1.38E-02	1.38E-02	6.57E-03	6.35E-03	5.96E-03	6.42E-03	6.49E-03
0.75	1.38E-02	1.38E-02	1.38E-02	1.37E-02	1.38E-02	6.32E-03	6.13E-03	5.76E-03	6.19E-03	6.27E-03
1.00	1.38E-02	1.38E-02	1.37E-02	1.37E-02	1.37E-02	6.10E-03	5.92E-03	5.56E-03	5.99E-03	6.06E-03
1.50	1.37E-02	1.37E-02	1.34E-02	1.37E-02	1.37E-02	5.67E-03	5.52E-03	5.19E-03	5.57E-03	5.63E-03
2.00	1.37E-02	1.37E-02	1.30E-02	1.37E-02	1.37E-02	5.33E-03	5.19E-03	4.88E-03	5.23E-03	5.28E-03
3.00	1.37E-02	1.37E-02	1.21E-02	1.37E-02	1.37E-02	4.79E-03	4.67E-03	4.40E-03	4.71E-03	4.75E-03
4.00	1.37E-02	1.37E-02	1.14E-02	1.37E-02	1.37E-02	4.42E-03	4.32E-03	4.08E-03	4.36E-03	4.42E-03

Table B2. Specific Absorbed Fractions (SAFs) at different depths or positions in the walls from uniformly distributed sources of 15 monoenergetic electrons and photons in the lumenal contents of the five sections of the Gastrointestinal Tract of an adult human male or a larger-than-average-female (72.63 kg). The depths were measured outward from wall-contents interface. Use the following relationship to get the absorbed dose (Gy) per source particle: SAF (kg^{-1}) × Energy (MeV) × 1.602E-13.

SAF (*Esophagus Wall* ← *Esophagus Contents*) **in** kg^{-1}														
Source Particle Energy (MeV)														
0.01			**0.015**			**0.02**			**0.03**			**0.05**		
Depth (cm)	**Electron SAF**	**Photon SAF**	**Depth (cm)**	**Electron SAF**	**Photon SAF**	**Depth (cm)**	**Electron SAF**	**Photon SAF**	**Depth (cm)**	**Electron SAF**	**Photon SAF**	**Depth (cm)**	**Electron SAF**	**Photon SAF**
0.005	2.47E-01	1.03E-3	**0.005**	4.91E-01	2.21E-2	**0.005**	8.31E-1	13.25	**0.005**	1.70	5.11	**0.005**	4.05	1.65
0.015	4.42E-04	4.41E-4	**0.015**	1.15E-03	2.01E-2	**0.015**	1.85E-3	12.35	**0.015**	3.10E-3	4.83	**0.015**	5.42E-3[a]	1.57
0.025	2.81E-04	2.76E-4	**0.025**	1.09E-03[b]	1.86E-2	**0.025**	1.65E-3[a]	11.62	**0.025**	2.94E-3[a]	4.60	**0.025**	5.33E-3[a]	1.51
0.035	1.92E-04	1.91E-4	**0.035**	6.63E-04	1.73E-2	**0.035**	1.49E-3[a]	11.00	**0.035**	2.02E-3	4.40	**0.035**	4.03E-3[a]	1.45
0.045	1.41E-04	1.40E-4	**0.045**	5.30E-04	1.61E-2	**0.045**	1.32E-3[b]	10.43	**0.045**	2.25E-3[b]	4.22	**0.045**	5.17E-3[b]	1.40
0.055	1.06E-04	1.06E-4	**0.055**	4.51E-04	1.51E-2	**0.055**	1.05E-3[a]	9.93	**0.055**	1.81E-3[a]	4.05	**0.055**	3.58E-3[a]	1.35
0.065	8.45E-05	8.29E-5	**0.065**	6.26E-04[c]	1.42E-2	**0.065**	9.86E-4[b]	9.48	**0.065**	2.53E-3[b]	3.90	**0.065**	4.18E-3[b]	1.30
0.075	6.69E-05	6.59E-5	**0.075**	3.38E-04	1.34E-2	**0.075**	8.25E-4[a]	9.06	**0.075**	1.52E-3[a]	3.76	**0.075**	2.47E-3[a]	1.26
0.085	5.42E-05	5.30E-5	**0.085**	2.92E-04	1.26E-2	**0.085**	6.02E-4	8.67	**0.085**	1.38E-3[a]	3.64	**0.085**	3.14E-3[b]	1.23
0.095	2.17E-04[g]	4.36E-5	**0.095**	5.27E-04[e]	1.20E-2	**0.095**	5.64E-4	8.31	**0.095**	1.55E-3[b]	3.52	**0.095**	3.00E-3[b]	1.19
0.105	1.51E-04[g]	3.61E-5	**0.105**	7.60E-04[d]	1.13E-2	**0.105**	1.29E-3[c]	7.98	**0.105**	2.16E-3[c]	3.41	**0.105**	4.18E-3[b]	1.16
0.115	4.60E-04[f]	3.04E-5	**0.115**	7.65E-04[d]	1.07E-2	**0.115**	1.57E-3[c]	7.67	**0.115**	1.43E-3[b]	3.30	**0.115**	3.40E-3[b]	1.13
0.125	2.37E-05	2.56E-5	**0.125**	1.78E-04	1.02E-2	**0.125**	6.27E-4[b]	7.38	**0.125**	1.24E-3[b]	3.20	**0.125**	3.17E-3[b]	1.10
0.135	2.44E-04[f]	2.20E-5	**0.135**	2.95E-04[d]	9.71E-3	**0.135**	6.47E-4[d]	7.11	**0.135**	1.18E-3[b]	3.11	**0.135**	2.74E-3[b]	1.07
0.145	1.86E-04[g]	1.89E-5	**0.145**	5.62E-04[e]	9.24E-3	**0.145**	9.19E-4[c]	6.86	**0.145**	1.30E-3[b]	3.02	**0.145**	2.27E-3[a]	1.04
0.16	1.53E-04[f]	1.51E-5	**0.16**	2.50E-04[d]	8.61E-3	**0.16**	7.47E-4[b]	6.50	**0.16**	1.42E-3[b]	2.90	**0.16**	3.23E-3[b]	1.01
0.18	7.20E-05[h]	1.14E-5	**0.18**	2.16E-04[c]	7.85E-3	**0.18**	5.25E-4[c]	6.08	**0.18**	1.06E-3[b]	2.75	**0.18**	2.75E-3[b]	0.96
0.2	1.01E-04[f]	8.67E-6	**0.2**	3.27E-04[d]	7.18E-3	**0.2**	7.79E-4[b]	5.69	**0.2**	1.11E-3[b]	2.62	**0.2**	3.39E-3[a]	0.92
0.22	8.80E-05[f]	6.82E-6	**0.22**	2.98E-04[e]	6.59E-3	**0.22**	4.45E-4[c]	5.35	**0.22**	1.47E-3[b]	2.49	**0.22**	2.87E-3[a]	0.88
0.24	1.22E-04[g]	5.65E-6	**0.24**	6.61E-04[c]	6.07E-3	**0.24**	5.52E-4[c]	5.03	**0.24**	1.62E-3[b]	2.38	**0.24**	3.12E-3[a]	0.85
0.275	7.60E-05[f]	4.16E-6	**0.275**	2.45E-04[c]	5.28E-3	**0.275**	3.28E-4[b]	4.54	**0.275**	9.40E-4[a]	2.21	**0.275**	2.27E-3[a]	0.80
0.325	9.65E-05[d]	2.86E-6	**0.325**	3.84E-04[b]	4.37E-3	**0.325**	6.18E-4[a]	3.97	**0.325**	8.73E-4[a]	1.99	**0.325**	2.34E-3[a]	0.73
0.375	1.05E-04[d]	2.14E-6	**0.375**	1.84E-04[c]	3.65E-3	**0.375**	3.30E-4[b]	3.50	**0.375**	8.40E-4[a]	1.81	**0.375**	2.06E-3[a]	0.68
0.425	4.12E-04[d]	4.47E-6	**0.425**	7.53E-04[c]	6.27E-4	**0.425**	1.23E-3[b]	0.59	**0.425**	2.84E-3[b]	0.37	**0.425**	7.69E-3[a]	0.18
0.475	2.22E-04[f]	2.96E-6	**0.475**	6.07E-04[c]	5.66E-4	**0.475**	7.43E-4[c]	0.55	**0.475**	2.31E-3[b]	0.36	**0.475**	4.28E-3[a]	0.18
Wall	3.65E-03	4.28E-5	**Wall**	7.37E-03	7.13E-3	**Wall**	1.25E-2	5.42	**Wall**	2.54E-2	2.46	**Wall**	6.05E-2	0.87

The values of relative errors (*R*) associated with the Monte Carlo SAF calculations were denoted by superscripts a, b, c, etc. The symbol 'a' was used for the *R* values in the range of 0.11-0.20, 'b' was for 0.21-0.30, 'c' was for 0.31-0.40 and so on. The *R* values less than 0.11 were not shown.

Table B2. Continued.

SAF (*Esophagus Wall* ← *Esophagus Contents*) **in kg^{-1}**														
Source Particle Energy (MeV)														
0.10			**0.20**			**0.35**			**0.50**			**0.75**		
Depth (cm)	**Electron SAF**	**Photon SAF**	**Depth (cm)**	**Electron SAF**	**Photon SAF**	**Depth (cm)**	**Electron SAF**	**Photon SAF**	**Depth (cm)**	**Electron SAF**	**Photon SAF**	**Depth (cm)**	**Electron SAF**	**Photon SAF**
0.005	12.97	9.50E-1	**0.005**	24.03	1.02	**0.005**	28.07	1.08	**0.005**	29.24	1.09	**0.005**	29.34	1.06
0.015	1.54E-1	9.02E-1	**0.015**	11.48	0.97	**0.015**	20.57	1.02	**0.015**	23.89	1.03	**0.015**	25.89	1.00
0.025	9.54E-3[a]	8.62E-1	**0.025**	3.83	0.92	**0.025**	14.80	0.97	**0.025**	19.45	0.98	**0.025**	22.91	0.95
0.035	1.54E-2[a]	8.27E-1	**0.035**	5.36E-1	0.88	**0.035**	10.28	0.93	**0.035**	15.92	0.94	**0.035**	20.03	0.91
0.045	9.98E-3[a]	7.96E-1	**0.045**	3.16E-2[a]	0.85	**0.045**	6.64	0.89	**0.045**	12.82	0.90	**0.045**	17.60	0.87
0.055	8.19E-3[b]	7.68E-1	**0.055**	2.15E-2[a]	0.82	**0.055**	3.88	0.86	**0.055**	10.16	0.86	**0.055**	15.47	0.84
0.065	7.98E-3[a]	7.43E-1	**0.065**	1.68E-2[a]	0.79	**0.065**	1.98	0.83	**0.065**	7.90	0.83	**0.065**	13.44	0.81
0.075	6.44E-3[b]	7.19E-1	**0.075**	1.70E-2[a]	0.76	**0.075**	7.86E-1	0.80	**0.075**	5.92	0.80	**0.075**	11.91	0.78
0.085	7.76E-3[a]	6.97E-1	**0.085**	2.12E-2[a]	0.74	**0.085**	2.25E-1	0.77	**0.085**	4.39	0.78	**0.085**	10.32	0.75
0.095	9.28E-3[b]	6.77E-1	**0.095**	1.35E-2[a]	0.71	**0.095**	6.55E-2	0.75	**0.095**	3.10	0.75	**0.095**	8.98	0.73
0.105	9.05E-3[b]	6.57E-1	**0.105**	1.44E-2[a]	0.69	**0.105**	4.10E-2[a]	0.73	**0.105**	1.99	0.73	**0.105**	7.99	0.71
0.115	7.19E-3[b]	6.39E-1	**0.115**	1.78E-2[a]	0.67	**0.115**	4.33E-2[a]	0.70	**0.115**	1.25	0.71	**0.115**	6.78	0.68
0.125	8.21E-3[b]	6.23E-1	**0.125**	1.95E-2[a]	0.65	**0.125**	4.23E-2[a]	0.68	**0.125**	6.69E-1	0.69	**0.125**	5.72	0.66
0.135	8.31E-3[b]	6.06E-1	**0.135**	2.19E-2[a]	0.64	**0.135**	3.89E-2[a]	0.66	**0.135**	3.57E-1	0.67	**0.135**	4.81	0.65
0.145	7.01E-3[b]	5.91E-1	**0.145**	1.62E-2[a]	0.62	**0.145**	3.07E-2[a]	0.65	**0.145**	1.66E-1	0.65	**0.145**	4.03	0.63
0.16	6.94E-3[a]	5.70E-1	**0.16**	1.72E-2[a]	0.60	**0.16**	3.96E-2	0.62	**0.16**	8.03E-2	0.62	**0.16**	2.92	0.60
0.18	1.05E-2[a]	5.43E-1	**0.18**	2.21E-2[a]	0.57	**0.18**	4.45E-2	0.59	**0.18**	7.45E-2	0.59	**0.18**	1.75	0.57
0.2	8.38E-3[a]	5.20E-1	**0.2**	2.33E-2	0.54	**0.2**	4.70E-2	0.56	**0.2**	7.72E-2	0.57	**0.2**	9.70E-1	0.55
0.22	7.51E-3[a]	4.98E-1	**0.22**	2.01E-2[a]	0.52	**0.22**	4.11E-2	0.54	**0.22**	6.76E-2	0.54	**0.22**	4.81E-1	0.52
0.24	7.45E-3[a]	4.78E-1	**0.24**	1.81E-2[a]	0.50	**0.24**	3.88E-2	0.52	**0.24**	6.87E-2	0.52	**0.24**	2.48E-1	0.50
0.275	6.96E-3	4.48E-1	**0.275**	2.19E-2	0.46	**0.275**	4.70E-2	0.48	**0.275**	7.06E-2	0.48	**0.275**	1.34E-1	0.46
0.325	8.38E-3	4.11E-1	**0.325**	2.10E-2	0.42	**0.325**	4.42E-2	0.44	**0.325**	6.65E-2	0.44	**0.325**	1.17E-1	0.42
0.375	6.13E-3	3.79E-1	**0.375**	2.16E-2	0.39	**0.375**	4.82E-2	0.40	**0.375**	7.30E-2	0.40	**0.375**	1.04E-1	0.38
0.425	2.58E-2	1.11E-1	**0.425**	7.34E-2	0.11	**0.425**	1.64E-1	0.11	**0.425**	2.41E-1	0.11	**0.425**	3.36E-1	0.10
0.475	1.42E-2[a]	1.09E-1	**0.475**	4.36E-2	0.10	**0.475**	1.01E-1	0.11	**0.475**	1.68E-1	0.10	**0.475**	2.58E-1	0.10
Wall	1.95E-1	4.91E-1	**Wall**	5.98E-1	0.51	**Wall**	1.35	0.53	**Wall**	2.19	0.53	**Wall**	3.69	0.52

Table B2. Continued.

SAF (*Esophagus Wall* ← *Esophagus Contents*) **in kg^{-1}**												
Source Particle Energy (MeV)												
1.00			**1.50**			**2.00**			**3.00**			**4.00**		
Depth (cm)	**Electron SAF**	**Photon SAF**	**Depth (cm)**	**Electron SAF**	**Photon SAF**	**Depth (cm)**	**Electron SAF**	**Photon SAF**	**Depth (cm)**	**Electron SAF**	**Photon SAF**	**Depth (cm)**	**Electron SAF**	**Photon SAF**
0.005	29.30	1.02	**0.005**	27.65	0.93	**0.005**	25.32	0.86	**0.01**	18.67	0.73	**0.01**	14.55	0.67
0.015	26.15	0.96	**0.02**	24.30	0.85	**0.02**	22.82	0.79	**0.035**	16.17	0.65	**0.035**	12.65	0.59
0.025	23.77	0.91	**0.04**	21.18	0.78	**0.04**	20.27	0.72	**0.075**	13.65	0.56	**0.075**	10.67	0.51
0.035	21.59	0.87	**0.06**	18.48	0.72	**0.06**	18.17	0.67	**0.125**	11.50	0.47	**0.125**	9.09	0.43
0.045	19.78	0.84	**0.08**	16.33	0.67	**0.08**	16.64	0.62	**0.175**	9.77	0.41	**0.175**	7.81	0.38
0.055	17.81	0.81	**0.1**	14.50	0.63	**0.1**	15.04	0.58	**0.225**	8.43	0.37	**0.225**	6.88	0.33
0.065	16.46	0.78	**0.12**	12.86	0.59	**0.12**	13.56	0.55	**0.275**	7.37	0.33	**0.275**	6.18	0.30
0.075	14.85	0.75	**0.14**	11.35	0.56	**0.14**	12.39	0.51	**0.325**	6.53	0.30	**0.325**	5.55	0.27
0.085	13.66	0.72	**0.16**	10.05	0.53	**0.16**	11.27	0.49	**0.375**	5.70	0.27	**0.375**	5.05	0.25
0.095	12.16	0.70	**0.18**	8.95	0.50	**0.18**	10.31	0.46	**0.425**	7.21E-1	0.07	**0.425**	6.74E-1	0.07
0.105	11.01	0.68	**0.2**	7.99	0.48	**0.2**	9.48	0.44	**0.475**	6.76E-1	0.07	**0.475**	6.42E-1	0.06
0.115	10.07	0.66	**0.22**	6.91	0.46	**0.22**	8.65	0.42	**Wall**	8.48	0.37	**Wall**	7.11	0.33
0.125	9.09	0.64	**0.24**	6.14	0.44	**0.24**	7.79	0.40						
0.135	8.38	0.62	**0.275**	4.85	0.41	**0.275**	6.76	0.37						
0.145	7.56	0.60	**0.325**	3.34	0.37	**0.325**	5.42	0.34						
0.16	6.45	0.58	**0.375**	2.17	0.34	**0.375**	4.26	0.31						
0.18	5.13	0.55	**0.425**	5.67E-1	0.09	**0.425**	7.13E-1	0.08						
0.2	3.96	0.53	**0.475**	5.10E-1	0.09	**0.475**	6.21E-1	0.08						
0.22	3.03	0.50	**Wall**	7.74	0.45	**Wall**	8.94	0.42						
0.24	2.24	0.48												
0.275	1.20	0.45												
0.325	4.07E-1	0.40												
0.375	1.62E-1	0.37												
0.425	4.46E-1	0.10												
0.475	3.58E-1	0.09												
Wall	5.20	0.50												

Table B2. Continued.

Source Energy (MeV)	**SAF** (*Esophagus Wall* ← *Stomach Contents*) **in kg^{-1} for Electron**										
	At Mean Position (cm) in the Esophageal Wall Measured Outward from Contents-Wall Interface.										Average to the
	0.025	**0.075**	**0.125**	**0.175**	**0.225**	**0.275**	**0.325**	**0.375**	**0.425**	**0.475**	**Wall**
0.01	2.76E-11[f]	1.24E-11[g]	5.06E-11[g]	3.52E-11[h]	3.19E-11[h]	3.00E-11[g]	3.12E-11[e]	1.07E-10[g]	0.0	0.0	4.03E-11[e]
0.015	1.04E-08[d]	7.72E-09[c]	7.32E-09[c]	7.06E-09[b]	8.91E-09[c]	6.82E-09[c]	1.01E-08[c]	1.91E-08[d]	0.0	0.0	9.23E-09[b]
0.02[a]	1.25E-07	1.23E-07	1.07E-07	1.07E-07	1.05E-07	8.73E-08	8.17E-08	1.12E-07	0.0	0.0	9.47E-08
0.03	1.08E-06	9.68E-07	9.50E-07	8.73E-07	8.70E-07	8.27E-07	8.33E-07	8.08E-07	4.09E-09[a]	3.77E-09[a]	8.06E-07
0.05	4.85E-06	4.58E-06	4.26E-06	4.20E-06	4.08E-06	3.86E-06	3.71E-06	3.72E-06	1.31E-07	1.31E-07	3.73E-06
0.10	1.36E-05	1.28E-05	1.26E-05	1.21E-05	1.20E-05	1.18E-05	1.12E-05	1.08E-05	9.89E-07	9.76E-07	1.10E-05
0.20	2.98E-05	2.85E-05	2.71E-05	2.57E-05	2.52E-05	2.43E-05	2.35E-05	2.32E-05	3.33E-06	3.42E-06	2.35E-05
0.35	4.81E-05	4.51E-05	4.40E-05	4.17E-05	4.00E-05	3.96E-05	3.87E-05	3.74E-05	6.67E-06	6.64E-06	3.81E-05
0.50	6.30E-05	6.03E-05	5.79E-05	5.57E-05	5.37E-05	5.26E-05	5.39E-05	5.08E-05	9.92E-06	1.03E-05	5.12E-05
0.75	8.66E-05	7.98E-05	7.85E-05	7.72E-05	7.58E-05	7.51E-05	7.34E-05	7.18E-05	1.46E-05	1.47E-05	7.09E-05
1.00	1.11E-4	1.03E-4	1.04E-4	8.97E-5	9.48E-5	9.32E-5	9.07E-5	8.88E-5	1.68E-5	2.19E-5	9.59E-5
1.50	1.58E-4	1.41E-4	1.44E-4	1.53E-4	1.46E-4	1.67E-4	8.92E-5	1.23E-4	3.32E-5	3.59E-5	1.39E-4
2.00	4.75E-4[b]	5.46E-4[b]	5.56E-4[b]	4.06E-4[c]	4.88E-4[b]	3.58E-4[b]	3.70E-4[b]	3.49E-4[b]	4.15E-5[a]	2.97E-5[b]	4.27E-4[a]
3.00	2.64E-3[b]	2.86E-3[b]	2.79E-3[b]	3.09E-3[b]	3.13E-3[b]	2.61E-3[b]	2.67E-3[b]	2.40E-3[b]	5.29E-5[a]	4.26E-5	2.72E-3[b]
4.00	8.10E-3[a]	7.34E-3[a]	7.83E-3[a]	8.76E-3[a]	8.90E-3[a]	6.47E-3[a]	6.76E-3[a]	7.37E-3[a]	8.48E-5[a]	1.30E-4[b]	7.52E-3[a]
SAF (*Esophagus Wall* ← *Stomach Contents*) **in kg^{-1} for Photon**											
0.01	1.75E-04[f]	2.75E-04[g]	2.01E-04[g]	5.97E-04[h]	2.89E-04[f]	1.81E-04[e]	2.44E-04[e]	1.80E-04[d]	0.0	0.0	2.41E-04[c]
0.015	1.84E-03[b]	3.06E-03[d]	8.24E-03[h]	3.88E-03[c]	4.09E-03[d]	3.37E-03[c]	3.31E-03[b]	3.10E-03[b]	0.0	0.0	3.49E-03[c]
0.02	2.87E-02	2.72E-02	2.68E-02[a]	2.48E-02[a]	2.49E-02	2.51E-02	2.18E-02	2.15E-02	2.36E-05[c]	1.65E-05[d]	2.24E-02
0.03	5.28E-02	5.16E-02	4.83E-02[a]	4.61E-02	4.29E-02	3.98E-02	4.40E-02[a]	3.81E-02	1.12E-03	1.09E-03	4.06E-02
0.05	4.53E-02	4.33E-02	4.19E-02	4.14E-02	4.02E-02	3.98E-02	3.91E-02	3.68E-02	6.07E-03	5.87E-03	3.74E-02
0.10	3.11E-02	2.86E-02	2.79E-02	2.78E-02	2.69E-02	2.65E-02	2.63E-02	2.46E-02	6.90E-03	6.72E-03	2.53E-02
0.20	2.53E-02	2.42E-02	2.39E-02	2.33E-02	2.26E-02	2.27E-02	2.24E-02	2.13E-02	6.18E-03	6.13E-03	2.15E-02
0.35	2.49E-02	2.34E-02	2.27E-02	2.26E-02	2.26E-02	2.19E-02	2.13E-02	1.99E-02	5.82E-03	5.59E-03	2.07E-02
0.50	2.25E-02	2.19E-02	2.11E-02	2.10E-02	1.86E-02	2.05E-02	2.01E-02	1.90E-02	5.69E-03	5.70E-03	1.91E-02
0.75	2.23E-02	2.14E-02	2.07E-02	2.02E-02	1.78E-02	1.98E-02	1.94E-02	1.82E-02	5.07E-03	5.31E-03	1.84E-02
1.00	2.13E-02	2.01E-02	1.95E-02	2.01E-02	1.78E-02	1.97E-02	1.89E-02	1.75E-02	4.99E-03	4.82E-03	1.79E-02
1.50	1.95E-02	1.85E-02	1.79E-02	1.84E-02	1.64E-02	1.85E-02	1.72E-02	1.60E-02	5.51E-03[a]	5.27E-03[a]	1.65E-02
2.00	1.88E-02	1.79E-02	1.70E-02	1.68E-02	1.51E-02	1.68E-02	1.61E-02	1.50E-02	5.12E-03[a]	5.13E-03[a]	1.55E-02
3.00	1.66E-02	1.58E-02	1.53E-02	1.41E-02	1.39E-02	1.34E-02	1.54E-02	1.38E-02	4.69E-03[a]	4.58E-03[a]	1.37E-02
4.00	1.53E-02	1.50E-02	1.42E-02	1.31E-02	1.30E-02	1.23E-02	1.40E-02	1.28E-02	4.38E-03[a]	4.32E-03[a]	1.27E-02

Table B2. Continued.

SAF(*Esophagus Wall* ← *Small Intestine Contents*) **in kg^{-1}**														
Source Particle Energy (MeV)														
0.01			**0.015**			**0.02**			**0.03**			**0.05**		
Depth (cm)	**Electron SAF**	**Photon SAF**	**Depth (cm)**	**Electron SAF**	**Photon SAF**	**Depth (cm)**	**Electron SAF**	**Photon SAF[i]**	**Depth (cm)**	**Electron SAF[h]**	**Photon SAF**	**Depth (cm)**	**Electron SAF**	**Photon SAF**
0.005	0.0	0.0	**0.005**	0.0	0.0	**0.005**	0.0	7.02E-05	**0.005**	4.12E-09	3.07E-04[c]	**0.005**	3.09E-08	1.18E-03
0.015	0.0	0.0	**0.015**	0.0	0.0	**0.015**	0.0	6.65E-05	**0.015**	3.79E-09	2.98E-04[c]	**0.015**	3.01E-08	1.20E-03
0.025	0.0	0.0	**0.025**	0.0	0.0	**0.025**	0.0	7.07E-05	**0.025**	3.77E-09	2.92E-04[c]	**0.025**	2.93E-08	1.17E-03
0.035	0.0	0.0	**0.035**	0.0	0.0	**0.035**	0.0	6.40E-05	**0.035**	4.19E-09	2.88E-04[b]	**0.035**	2.81E-08	1.12E-03
0.045	0.0	0.0	**0.045**	0.0	0.0	**0.045**	0.0	5.99E-05	**0.045**	3.91E-09	2.83E-04[c]	**0.045**	2.72E-08	1.19E-03
0.055	0.0	0.0	**0.055**	0.0	0.0	**0.055**	0.0	5.66E-05	**0.055**	3.77E-09	2.75E-04[c]	**0.055**	2.72E-08	1.12E-03
0.065	0.0	0.0	**0.065**	0.0	0.0	**0.065**	0.0	5.38E-05	**0.065**	3.51E-09	2.64E-04[c]	**0.065**	2.65E-08	1.09E-03
0.075	0.0	0.0	**0.075**	0.0	0.0	**0.075**	0.0	5.16E-05	**0.075**	3.54E-09	2.54E-04[c]	**0.075**	2.53E-08	1.08E-03
0.085	0.0	0.0	**0.085**	0.0	0.0	**0.085**	0.0	4.98E-05	**0.085**	3.92E-09	2.40E-04[c]	**0.085**	2.58E-08	1.06E-03
0.095	0.0	0.0	**0.095**	0.0	0.0	**0.095**	0.0	4.81E-05	**0.095**	4.17E-09	2.47E-04[b]	**0.095**	2.54E-08	1.07E-03
0.105	0.0	0.0	**0.105**	0.0	0.0	**0.105**	0.0	4.67E-05	**0.105**	2.31E-08	2.36E-04[b]	**0.105**	2.38E-08	1.05E-03
0.115	0.0	0.0	**0.115**	0.0	0.0	**0.115**	0.0	4.55E-05	**0.115**	3.82E-08	2.38E-04[b]	**0.115**	2.44E-08	1.03E-03
0.125	0.0	0.0	**0.125**	0.0	0.0	**0.125**	0.0	4.45E-05	**0.125**	2.37E-08	2.34E-04[b]	**0.125**	2.52E-08	1.02E-03
0.135	0.0	0.0	**0.135**	0.0	0.0	**0.135**	0.0	4.36E-05	**0.135**	1.91E-08	2.33E-04[b]	**0.135**	2.45E-08	1.00E-03
0.145	0.0	0.0	**0.145**	0.0	0.0	**0.145**	0.0	4.24E-05	**0.145**	1.64E-08	2.50E-04[b]	**0.145**	2.65E-08	1.02E-03
0.16	0.0	0.0	**0.16**	0.0	0.0	**0.16**	0.0	4.07E-05	**0.16**	1.45E-08	2.29E-04[b]	**0.16**	2.53E-08	9.85E-04
0.18	0.0	0.0	**0.18**	0.0	0.0	**0.18**	0.0	3.85E-05	**0.18**	1.27E-08	2.30E-04[b]	**0.18**	2.35E-08	9.45E-04
0.2	0.0	0.0	**0.2**	0.0	0.0	**0.2**	0.0	3.70E-05	**0.2**	1.13E-08	2.31E-04[b]	**0.2**	2.24E-08	9.45E-04
0.22	0.0	0.0	**0.22**	0.0	0.0	**0.22**	0.0	3.68E-05	**0.22**	1.04E-08	2.34E-04[b]	**0.22**	2.47E-08	9.11E-04
0.24	0.0	0.0	**0.24**	0.0	0.0	**0.24**	0.0	3.70E-05	**0.24**	1.00E-08	2.30E-04[b]	**0.24**	2.23E-08	8.70E-04
0.275	0.0	0.0	**0.275**	0.0	0.0	**0.275**	0.0	3.49E-05	**0.275**	8.84E-09	2.13E-04[b]	**0.275**	2.14E-08	8.60E-04
0.325	0.0	0.0	**0.325**	0.0	0.0	**0.325**	0.0	3.21E-05	**0.325**	7.93E-09	2.09E-04[b]	**0.325**	2.06E-08	8.51E-04
0.375	0.0	0.0	**0.375**	0.0	0.0	**0.375**	0.0	3.02E-05	**0.375**	7.23E-09	1.95E-04[b]	**0.375**	2.12E-08	8.64E-04
Wall	0.0	0.0	**Wall**	0.0	0.0	**Wall**	0.0	3.61E-05	**Wall**	9.01E-09	2.10E-04[b]	**Wall**	2.14E-08	8.83E-04

Table B2. Continued.

SAF(*Esophagus Wall* ← *Small Intestine Contents*) **in kg^{-1}**														
Source Particle Energy (MeV)														
0.10			**0.20**			**0.35**			**0.50**			**0.75**		
Depth (cm)	**Electron SAF**	**Photon SAF**	**Depth (cm)**	**Electron SAF**	**Photon SAF**	**Depth (cm)**	**Electron SAF**	**Photon SAF**	**Depth (cm)**	**Electron SAF**	**Photon SAF**	**Depth (cm)**	**Electron SAF**	**Photon SAF**
0.005	1.67E-07	1.43E-3	**0.005**	6.45E-07	1.55E-3	**0.005**	1.23E-06	1.72E-3	**0.005**	2.07E-06	1.58E-3	**0.005**	3.27E-06	1.60E-3
0.015	1.59E-07	1.40E-3	**0.015**	6.44E-07	1.57E-3	**0.015**	1.19E-06	1.74E-3	**0.015**	2.06E-06	1.63E-3	**0.015**	3.35E-06	1.59E-3
0.025	1.61E-07	1.41E-3	**0.025**	6.34E-07	1.54E-3	**0.025**	1.20E-06	1.72E-3	**0.025**	2.02E-06	1.66E-3	**0.025**	3.36E-06	1.60E-3
0.035	1.63E-07	1.38E-3	**0.035**	6.46E-07	1.51E-3	**0.035**	1.16E-06	1.70E-3	**0.035**	2.06E-06	1.60E-3	**0.035**	3.35E-06	1.66E-3
0.045	1.59E-07	1.37E-3	**0.045**	6.04E-07	1.49E-3	**0.045**	1.18E-06	1.62E-3	**0.045**	2.04E-06	1.60E-3	**0.045**	3.30E-06	1.57E-3
0.055	1.51E-07	1.36E-3	**0.055**	5.97E-07	1.48E-3	**0.055**	1.21E-06	1.64E-3	**0.055**	1.98E-06	1.56E-3	**0.055**	3.24E-06	1.52E-3
0.065	1.49E-07	1.34E-3	**0.065**	5.92E-07	1.50E-3	**0.065**	1.16E-06	1.63E-3	**0.065**	1.91E-06	1.53E-3	**0.065**	3.26E-06	1.49E-3
0.075	1.55E-07	1.34E-3	**0.075**	5.86E-07	1.48E-3	**0.075**	1.25E-06	1.59E-3	**0.075**	1.94E-06	1.50E-3	**0.075**	3.22E-06	1.44E-3
0.085	1.71E-07	1.33E-3	**0.085**	5.81E-07	1.48E-3	**0.085**	1.19E-06	1.58E-3	**0.085**	1.93E-06	1.50E-3	**0.085**	3.24E-06	1.48E-3
0.095	1.65E-07	1.31E-3	**0.095**	5.81E-07	1.46E-3	**0.095**	1.19E-06	1.57E-3	**0.095**	1.84E-06	1.52E-3	**0.095**	3.12E-06	1.47E-3
0.105	1.69E-07	1.32E-3	**0.105**	5.81E-07	1.46E-3	**0.105**	1.16E-06	1.62E-3	**0.105**	1.85E-06	1.46E-3	**0.105**	3.13E-06	1.44E-3
0.115	1.61E-07	1.35E-3	**0.115**	5.94E-07	1.45E-3	**0.115**	1.18E-06	1.59E-3	**0.115**	1.88E-06	1.47E-3	**0.115**	3.13E-06	1.44E-3
0.125	1.82E-07	1.35E-3	**0.125**	6.05E-07	1.44E-3	**0.125**	1.19E-06	1.52E-3	**0.125**	1.93E-06	1.45E-3	**0.125**	3.17E-06	1.44E-3
0.135	1.70E-07	1.31E-3	**0.135**	6.11E-07	1.45E-3	**0.135**	1.19E-06	1.50E-3	**0.135**	1.91E-06	1.41E-3	**0.135**	3.10E-06	1.40E-3
0.145	1.64E-07	1.29E-3	**0.145**	6.02E-07	1.42E-3	**0.145**	1.15E-06	1.46E-3	**0.145**	1.89E-06	1.39E-3	**0.145**	2.96E-06	1.42E-3
0.16	1.68E-07	1.32E-3	**0.16**	5.75E-07	1.41E-3	**0.16**	1.14E-06	1.46E-3	**0.16**	1.85E-06	1.39E-3	**0.16**	3.05E-06	1.43E-3
0.18	1.58E-07	1.32E-3	**0.18**	5.57E-07	1.39E-3	**0.18**	1.08E-06	1.43E-3	**0.18**	1.82E-06	1.35E-3	**0.18**	3.03E-06	1.43E-3
0.2	1.51E-07	1.27E-3	**0.2**	5.46E-07	1.38E-3	**0.2**	1.04E-06	1.39E-3	**0.2**	1.80E-06	1.33E-3	**0.2**	2.93E-06	1.46E-3
0.22	1.58E-07	1.23E-3	**0.22**	5.47E-07	1.36E-3	**0.22**	1.01E-06	1.47E-3	**0.22**	1.71E-06	1.36E-3	**0.22**	2.87E-06	1.40E-3
0.24	1.54E-07	1.24E-3	**0.24**	5.48E-07	1.38E-3	**0.24**	1.02E-06	1.48E-3	**0.24**	1.74E-06	1.35E-3	**0.24**	2.79E-06	1.38E-3
0.275	1.53E-07	1.23E-3	**0.275**	5.61E-07	1.36E-3	**0.275**	1.05E-06	1.42E-3	**0.275**	1.68E-06	1.29E-3	**0.275**	2.85E-06	1.35E-3
0.325	1.39E-07	1.21E-3	**0.325**	5.58E-07	1.33E-3	**0.325**	1.04E-06	1.37E-3	**0.325**	1.67E-06	1.27E-3	**0.325**	2.80E-06	1.32E-3
0.375	1.43E-07	1.18E-3	**0.375**	5.57E-07	6.55E-4	**0.375**	1.01E-06	1.45E-3	**0.375**	1.73E-06	1.29E-3	**0.375**	2.83E-06	1.37E-3
Wall	1.43E-07	1.20E-3	**Wall**	5.71E-07	1.32E-3	**Wall**	3.43E-07	1.48E-3	**Wall**	1.79E-06	1.37E-3	**Wall**	2.96E-06	1.41E-3

Table B2. Continued.

SAF(*Esophagus Wall* ← *Small Intestine Contents*) **in kg^{-1}**														
Source Particle Energy (MeV)														
1.00			**1.50**			**2.00**			**3.00**			**4.00**		
Depth (cm)	**Electron SAF**	**Photon SAF**	**Depth (cm)**	**Electron SAF**	**Photon SAF**	**Depth (cm)**	**Electron SAF**	**Photon SAF**	**Depth (cm)**	**Electron SAF**	**Photon SAF**	**Depth (cm)**	**Electron SAF**	**Photon SAF**
0.005	4.36E-06	1.51E-3	**0.005**	7.17E-06	1.39E-3	**0.005**	9.56E-06	1.41E-3	**0.005**	1.71E-05	1.64E-3	**0.005**	2.54E-05	1.28E-3
0.015	4.38E-06	1.71E-3	**0.015**	7.17E-06	1.39E-3	**0.015**	9.27E-06	1.51E-3	**0.015**	1.69E-05	1.71E-3	**0.015**	2.47E-05	1.24E-3
0.025	4.42E-06	1.62E-3	**0.025**	6.92E-06	1.42E-3	**0.025**	9.19E-06	1.57E-3	**0.025**	1.71E-05	1.69E-3	**0.025**	2.51E-05	1.20E-3
0.035	4.39E-06	1.54E-3	**0.035**	6.73E-06	1.47E-3	**0.035**	9.09E-06	1.66E-3	**0.035**	1.79E-05	1.57E-3	**0.035**	2.45E-05	1.24E-3
0.045	4.20E-06	1.55E-3	**0.045**	6.78E-06	1.43E-3	**0.045**	9.31E-06	1.52E-3	**0.045**	1.70E-05	1.44E-3	**0.045**	2.37E-05	1.22E-3
0.055	4.19E-06	1.57E-3	**0.055**	6.65E-06	1.40E-3	**0.055**	9.12E-06	1.49E-3	**0.055**	1.65E-05	1.42E-3	**0.055**	2.45E-05	1.18E-3
0.065	4.22E-06	1.51E-3	**0.065**	6.65E-06	1.41E-3	**0.065**	9.16E-06	1.48E-3	**0.065**	1.62E-05	1.39E-3	**0.065**	2.34E-05	1.21E-3
0.075	4.25E-06	1.42E-3	**0.075**	6.38E-06	1.33E-3	**0.075**	9.18E-06	1.42E-3	**0.075**	1.63E-05	1.30E-3	**0.075**	2.30E-05	1.17E-3
0.085	4.16E-06	1.38E-3	**0.085**	6.38E-06	1.30E-3	**0.085**	9.03E-06	1.49E-3	**0.085**	1.61E-05	1.26E-3	**0.085**	2.30E-05	1.21E-3
0.095	4.25E-06	1.40E-3	**0.095**	6.27E-06	1.33E-3	**0.095**	8.99E-06	1.51E-3	**0.095**	1.67E-05	1.41E-3	**0.095**	2.33E-05	1.20E-3
0.105	4.20E-06	1.37E-3	**0.105**	6.31E-06	1.35E-3	**0.105**	8.93E-06	1.49E-3	**0.105**	1.59E-05	1.66E-3	**0.105**	2.21E-05	1.23E-3
0.115	4.15E-06	1.44E-3	**0.115**	6.19E-06	1.37E-3	**0.115**	9.00E-06	1.46E-3	**0.115**	1.54E-05	1.52E-3	**0.115**	2.11E-05	1.24E-3
0.125	4.17E-06	1.52E-3	**0.125**	6.12E-06	1.45E-3	**0.125**	8.91E-06	1.54E-3	**0.125**	1.54E-05	1.42E-3	**0.125**	2.28E-05	1.22E-3
0.135	4.17E-06	1.42E-3	**0.135**	6.14E-06	1.39E-3	**0.135**	8.94E-06	1.44E-3	**0.135**	1.54E-05	1.34E-3	**0.135**	2.24E-05	1.19E-3
0.145	4.16E-06	1.39E-3	**0.145**	6.31E-06	1.36E-3	**0.145**	8.96E-06	1.41E-3	**0.145**	1.50E-05	1.27E-3	**0.145**	2.42E-05	1.22E-3
0.16	4.23E-06	1.34E-3	**0.16**	6.43E-06	1.31E-3	**0.16**	8.67E-06	1.44E-3	**0.16**	1.49E-05	1.24E-3	**0.16**	2.46E-05	1.22E-3
0.18	4.21E-06	1.31E-3	**0.18**	6.26E-06	1.31E-3	**0.18**	8.53E-06	1.39E-3	**0.18**	1.62E-05	1.35E-3	**0.18**	2.32E-05	1.18E-3
0.2	4.24E-06	1.31E-3	**0.2**	6.22E-06	1.36E-3	**0.2**	8.42E-06	1.37E-3	**0.2**	1.59E-05	1.29E-3	**0.2**	2.29E-05	1.17E-3
0.22	4.03E-06	1.37E-3	**0.22**	6.20E-06	1.38E-3	**0.22**	8.51E-06	1.41E-3	**0.22**	1.51E-05	1.53E-3	**0.22**	2.18E-05	1.16E-3
0.24	4.08E-06	1.34E-3	**0.24**	6.13E-06	1.43E-3	**0.24**	8.77E-06	1.43E-3	**0.24**	1.51E-05	1.83E-3	**0.24**	2.11E-05	1.23E-3
0.275	4.01E-06	1.35E-3	**0.275**	5.94E-06	1.34E-3	**0.275**	9.00E-06	1.41E-3	**0.275**	1.51E-05	1.50E-3	**0.275**	2.20E-05	1.16E-3
0.325	3.93E-06	1.31E-3	**0.325**	6.02E-06	1.29E-3	**0.325**	8.58E-06	1.38E-3	**0.325**	1.44E-05	1.32E-3	**0.325**	2.20E-05	1.14E-3
0.375	3.82E-06	1.32E-3	**0.375**	5.88E-06	1.31E-3	**0.375**	8.35E-06	1.41E-3	**0.375**	1.50E-05	1.31E-3	**0.375**	2.13E-05	1.17E-3
Wall	3.89E-06	1.32E-3	**Wall**	5.90E-06	1.30E-3	**Wall**	8.32E-06	1.41E-3	**Wall**	1.49E-05	1.38E-3	**Wall**	2.17E-05	1.16E-3

Table B2. Continued.

Source Energy (MeV)	**SAF** (*Esophagus Wall* ← *Upper Large Intestine Contents*) **in kg^{-1} for Electron**										
	At Mean Position (cm) in the Upper Large Intestine Wall Measured Outward from Contents-Wall Interface.										Average to the
	0.025	**0.075**	**0.125**	**0.175**	**0.225**	**0.275**	**0.325**	**0.375**	**0.425**	**0.475**	**Wall**
0.01	0.0	0.0	0.0	0.0	0.0	0.0	0.0	0.0	0.0	0.0	0.0
0.015	0.0	0.0	0.0	0.0	0.0	0.0	0.0	0.0	0.0	0.0	0.0
0.02[a]	0.0	0.0	0.0	0.0	0.0	0.0	0.0	0.0	0.0	0.0	0.0
0.03	0.0	0.0	0.0	0.0	0.0	0.0	0.0	0.0	0.0	0.0	0.0
0.05	2.61E-08[b]	2.01E-08[b]	1.51E-08[b]	1.36E-08[b]	1.68E-08[b]	1.51E-08[b]	1.51E-08[b]	1.96E-08[b]	0.0	0.0	1.58E-08[a]
0.10	1.89E-07	1.87E-07	1.74E-07	1.74E-07	1.68E-07	1.66E-07	1.72E-07	1.73E-07	4.56E-08[b]	4.62E-08[b]	1.63E-07
0.20	6.80E-07	7.13E-07	6.78E-07	6.69E-07	6.33E-07	6.05E-07	6.02E-07	5.86E-07	2.52E-07	2.56E-07	6.03E-07
0.35	1.55E-06	1.49E-06	1.49E-06	1.44E-06	1.43E-06	1.43E-06	1.34E-06	1.28E-06	6.64E-07	6.63E-07	1.35E-06
0.50	2.39E-06	2.36E-06	2.22E-06	2.09E-06	2.09E-06	2.03E-06	2.04E-06	2.04E-06	9.82E-07	9.98E-07	2.03E-06
0.75	3.87E-06	3.68E-06	3.50E-06	3.40E-06	3.32E-06	3.29E-06	3.21E-06	3.21E-06	1.68E-06	1.66E-06	3.24E-06
1.00	5.63E-06	5.23E-06	5.29E-06	5.15E-06	4.85E-06	4.72E-06	4.70E-06	4.62E-06	2.31E-06	2.28E-06	4.72E-06
1.50	8.36E-06	8.35E-06	8.06E-06	7.99E-06	8.01E-06	7.85E-06	7.64E-06	7.64E-06	4.02E-06	3.84E-06	7.58E-06
2.00	1.16E-05	1.15E-05	1.08E-05	1.11E-05	1.06E-05	1.07E-05	1.09E-05	1.06E-05	5.43E-06	4.73E-06	1.04E-05
3.00	1.96E-05	1.95E-05	1.95E-05	1.82E-05	1.80E-05	1.71E-05	1.71E-05	1.81E-05	1.24E-05	1.14E-05	1.76E-05
4.00	2.51E-05	2.36E-05	2.31E-05	2.33E-05	2.31E-05	2.22E-05	2.11E-05	1.98E-05	1.20E-05	1.23E-05	2.14E-05
	SAF (*Esophagus Wall* ← *Upper Large Intestine Contents*) **in kg^{-1} for Photon**										
0.01	0.0	0.0	0.0	0.0	0.0	0.0	0.0	0.0	0.0	0.0	0.0
0.015	0.0	0.0	0.0	0.0	0.0	0.0	0.0	0.0	0.0	0.0	0.0
0.02	0.0	0.0	0.0	0.0	0.0	0.0	0.0	0.0	0.0	0.0	0.0
0.03	1.75E-04[a]	1.54E-04[a]	1.42E-04[a]	1.34E-04[a]	1.34E-04[a]	1.42E-04[a]	1.37E-04[a]	1.68E-04[a]	1.45E-05[e]	1.18E-05[e]	1.35E-04[a]
0.05	1.18E-03	1.11E-03	1.06E-03	1.04E-03	1.05E-03	1.01E-03	9.63E-04	9.82E-04	2.86E-04	2.54E-04	9.69E-04
0.10	1.81E-03	1.72E-03	1.67E-03	1.64E-03	1.64E-03	1.57E-03	1.53E-03	1.54E-03	6.99E-04	7.18E-04	1.54E-03
0.20	1.86E-03	1.73E-03	1.72E-03	1.62E-03	1.63E-03	1.60E-03	1.60E-03	1.61E-03	9.55E-04	8.58E-04	1.59E-03
0.35	1.87E-03	1.76E-03	1.70E-03	1.69E-03	1.69E-03	1.64E-03	1.61E-03	1.59E-03	8.44E-04	9.24E-04	1.61E-03
0.50	1.88E-03	1.80E-03	1.75E-03	1.68E-03	1.65E-03	1.62E-03	1.58E-03	1.56E-03	9.80E-04[a]	1.06E-03[a]	1.61E-03
0.75	1.79E-03	1.71E-03	1.75E-03	1.60E-03	1.64E-03	1.63E-03	1.62E-03	1.59E-03	1.02E-03[a]	1.08E-03[a]	1.60E-03
1.00	1.91E-03	1.80E-03	1.72E-03	1.64E-03	1.70E-03	1.66E-03	1.63E-03	1.55E-03	1.11E-03[a]	1.13E-03[a]	1.63E-03
1.50	2.10E-03	1.96E-03	1.98E-03	2.04E-03	1.97E-03	1.92E-03	1.75E-03	1.85E-03	1.49E-03[a]	1.35E-03[a]	1.88E-03
2.00	2.17E-03[a]	2.09E-03[a]	2.04E-03	1.88E-03	1.82E-03	1.79E-03	1.69E-03	1.84E-03	1.59E-03[b]	1.43E-03[a]	1.85E-03
3.00	1.83E-03	1.76E-03	1.73E-03	1.61E-03	1.58E-03	1.65E-03	1.57E-03	1.61E-03	1.47E-03[a]	1.25E-03[a]	1.62E-03
4.00	1.70E-03[a]	1.89E-03[a]	1.76E-03[a]	1.52E-03[a]	1.43E-03[a]	1.48E-03[a]	1.49E-03[a]	1.48E-03[a]	1.72E-03[d]	1.35E-03[c]	1.56E-03[a]

Table B2. Continued.

Source Energy (MeV)	**SAF** (*Esophagus Wall* ← *Lower Large Intestine Contents*) **in kg^{-1} for Electron**										
	At Mean Position (cm) in the Esophageal Wall Measured Outward from Contents-Wall Interface.										Average to the
	0.025	**0.075**	**0.125**	**0.175**	**0.225**	**0.275**	**0.325**	**0.375**	**0.425**	**0.475**	**Wall**
0.01	0.0	0.0	0.0	0.0	0.0	0.0	0.0	0.0	0.0	0.0	0.0
0.015	0.0	0.0	0.0	0.0	0.0	0.0	0.0	0.0	0.0	0.0	0.0
0.02	0.0	0.0	0.0	0.0	0.0	0.0	0.0	0.0	0.0	0.0	0.0
0.03	0.0	0.0	0.0	0.0	0.0	0.0	0.0	0.0	0.0	0.0	0.0
0.05	0.0	0.0	0.0	0.0	0.0	0.0	0.0	0.0	0.0	0.0	0.0
0.10	7.65E-09^{c}	7.60E-09^{c}	1.17E-08^{d}	8.13E-09^{c}	6.93E-09^{c}	6.65E-09^{c}	6.25E-09^{c}	4.79E-09^{c}	0.00E+00	0.0	6.74E-09^{c}
0.20	3.91E-08^{b}	3.46E-08^{b}	3.35E-08^{b}	3.15E-08^{b}	2.97E-08^{b}	3.54E-08^{b}	3.30E-08^{b}	3.25E-08^{b}	6.26E-09^{g}	8.40E-09^{e}	3.11E-08^{a}
0.35	7.40E-08^{b}	7.91E-08^{b}	8.26E-08^{a}	7.26E-08^{a}	7.44E-08^{b}	7.26E-08^{a}	7.14E-08^{a}	7.57E-08^{a}	7.82E-08^{f}	4.49E-08^{g}	7.37E-08^{a}
0.50	1.71E-07^{a}	1.75E-07^{a}	1.54E-07^{a}	1.41E-07^{a}	1.84E-07^{b}	1.56E-07^{a}	1.36E-07^{a}	1.68E-07^{a}	8.84E-08^{c}	8.01E-08^{c}	1.53E-07^{a}
0.75	4.21E-07^{a}	3.91E-07^{a}	3.89E-07^{a}	3.96E-07^{a}	3.51E-07^{a}	3.08E-07^{a}	2.97E-07^{a}	3.04E-07^{a}	1.46E-07^{d}	1.18E-07^{c}	3.29E-07^{a}
1.00	4.78E-07^{a}	4.25E-07^{a}	3.85E-07^{a}	4.22E-07^{a}	3.79E-07^{a}	4.10E-07^{a}	4.72E-07^{a}	4.49E-07^{a}	2.34E-07^{c}	2.14E-07^{c}	4.10E-07^{a}
1.50	6.75E-07^{a}	1.02E-06^{b}	8.20E-07^{a}	7.42E-07^{a}	7.46E-07^{a}	6.70E-07^{a}	6.42E-07^{a}	6.10E-07^{a}	2.46E-07^{c}	2.26E-07^{c}	6.81E-07^{a}
2.00	1.55E-06^{a}	1.38E-06^{a}	1.58E-06^{a}	1.28E-06^{a}	1.28E-06^{a}	1.50E-06^{b}	1.44E-06^{a}	1.44E-06^{a}	6.58E-07^{c}	5.82E-07^{b}	1.35E-06^{a}
3.00	2.74E-06^{b}	2.82E-06^{a}	3.16E-06^{a}	2.69E-06^{a}	2.42E-06^{a}	2.64E-06^{a}	2.49E-06^{a}	2.57E-06^{a}	1.62E-06^{c}	1.59E-06^{c}	2.57E-06^{a}
4.00	4.06E-06^{a}	4.36E-06^{a}	3.64E-06^{a}	3.47E-06^{a}	6.82E-06^{e}	4.15E-06^{b}	3.50E-06^{b}	3.25E-06^{a}	6.23E-06^{d}	3.46E-06^{b}	4.18E-06^{b}
	SAF (*Esophagus Wall* ← *Lower Large Intestine Contents*) **in kg^{-1} for Photon**										
0.01	0.0	0.0	0.0	0.0	0.0	0.0	0.0	0.0	0.0	0.0	0.0
0.015	0.0	0.0	0.0	0.0	0.0	0.0	0.0	0.0	0.0	0.0	0.0
0.02	0.0	0.0	0.0	0.0	0.0	0.0	0.0	0.0	0.0	0.0	0.0
0.03	0.0	0.0	0.0	0.0	0.0	0.0	0.0	0.0	0.0	0.0	0.0
0.05	4.03E-05^{b}	4.19E-05^{b}	4.25E-05^{b}	4.26E-05^{b}	4.89E-05^{b}	4.87E-05^{a}	4.17E-05^{a}	4.02E-05^{a}	0.0	1.74E-05^{h}	4.06E-05^{a}
0.10	1.56E-04^{a}	1.34E-04^{a}	1.16E-04^{a}	1.16E-04^{a}	1.12E-04^{a}	1.15E-04^{a}	1.18E-04^{a}	1.17E-04^{a}	4.98E-05^{b}	4.35E-05^{b}	1.14E-04
0.20	1.74E-04^{a}	1.59E-04^{a}	1.49E-04^{a}	1.68E-04^{a}	1.99E-04^{b}	1.67E-04^{a}	1.59E-04^{a}	1.54E-04^{a}	7.30E-05^{b}	6.65E-05^{b}	1.57E-04
0.35	2.08E-04^{a}	2.07E-04^{a}	1.98E-04^{a}	2.13E-04^{a}	1.93E-04^{a}	2.43E-04^{a}	2.59E-04^{a}	2.20E-04^{a}	7.51E-05^{d}	1.05E-04^{c}	2.09E-04^{a}
0.50	2.15E-04^{a}	2.02E-04^{a}	1.94E-04^{a}	1.72E-04^{a}	1.61E-04^{a}	2.07E-04^{b}	2.07E-04^{a}	1.94E-04^{a}	8.69E-05^{c}	1.18E-04^{c}	1.85E-04^{a}
0.75	3.10E-04^{a}	2.97E-04^{a}	2.81E-04^{a}	2.50E-04^{a}	2.91E-04^{a}	2.35E-04^{a}	2.60E-04^{a}	2.28E-04^{a}	1.27E-04^{c}	2.44E-04^{e}	2.57E-04^{a}
1.00	5.13E-04^{c}	3.39E-04^{b}	2.67E-04^{b}	2.88E-04^{a}	3.09E-04^{a}	2.65E-04^{a}	2.59E-04^{a}	2.88E-04^{a}	6.95E-05^{d}	2.30E-04^{g}	2.91E-04^{a}
1.50	4.01E-04^{b}	3.28E-04^{a}	2.85E-04^{a}	3.33E-04^{b}	3.03E-04^{a}	2.74E-04^{a}	2.73E-04^{a}	2.53E-04^{a}	6.98E-05^{c}	1.59E-04^{f}	2.82E-04^{a}
2.00	3.98E-04^{b}	3.24E-04^{a}	2.88E-04^{a}	2.96E-04^{a}	2.47E-04^{a}	2.45E-04^{a}	5.37E-04^{d}	4.46E-04^{d}	2.05E-05^{c}	3.23E-05^{c}	3.26E-04^{b}
3.00	4.82E-04^{b}	6.22E-04^{c}	7.41E-04^{b}	6.72E-04^{b}	5.20E-04^{b}	4.58E-04^{b}	4.24E-04^{b}	5.53E-04^{b}	3.17E-04^{c}	4.35E-04^{d}	5.35E-04^{b}
4.00	4.01E-04^{c}	7.49E-04^{d}	5.97E-04^{d}	6.67E-04^{d}	5.16E-04^{d}	4.34E-04^{c}	3.76E-04^{c}	4.54E-04^{c}	2.07E-04^{f}	4.36E-04^{g}	4.95E-04^{c}

Table B2. Continued.

Source Energy (MeV)	**SAF** $(Stomach\ Wall \leftarrow Esophagus\ Contents)$ **in kg^{-1} for Electron**															
	At Mean Position (cm) in the Stomach Wall Measured Outward from Contents-Wall Interface.														Average to	
	0.02	**0.06**	**0.1**	**0.14**	**0.18**	**0.22**	**0.26**	**0.3**	**0.34**	**0.38**	**0.425**	**0.475**	**0.5265**	**0.583**	**Wall**	**Whole**
0.01	2.29E-9	3.42E-9	4.25E-9	5.92E-9	7.66E-9	1.26E-8	1.78E-8	1.53E-8	2.94E-8	3.57E-8	5.66E-8	9.25E-8	2.23E-7	7.28E-7	1.23E-7	4.64E-8
0.015	1.26E-7	1.40E-7	1.34E-7	2.04E-7	2.58E-7	3.26E-7	2.92E-7	3.56E-7	5.02E-7	6.09E-7	7.46E-7	1.02E-6	1.56E-6	3.10E-6	8.35E-7	3.32E-7
0.02	7.54E-7	7.49E-7	8.92E-7	9.65E-7	1.03E-6	1.22E-6	1.39E-6	1.57E-6	1.69E-6	1.92E-6	2.24E-6	2.89E-6	3.84E-6	6.42E-6	2.29E-6	1.03E-6
0.03	3.57E-6	3.68E-6	3.82E-6	4.36E-6	4.38E-6	4.75E-6	5.17E-6	5.49E-6	5.88E-6	6.35E-6	7.42E-6	8.32E-6	9.90E-6	1.37E-5	6.81E-6	3.73E-6
0.05	1.26E-5	1.20E-5	1.26E-5	1.31E-5	1.29E-5	1.36E-5	1.55E-5	1.56E-5	1.65E-5	1.70E-5	1.81E-5	1.96E-5	2.22E-5	2.78E-5	1.73E-5	1.14E-5
0.10	2.96E-5	3.10E-5	3.09E-5	3.18E-5	3.24E-5	3.31E-5	3.57E-5	3.70E-5	3.70E-5	3.90E-5	4.01E-5	4.23E-5	4.55E-5	3.33E-4	6.95E-5	4.07E-5
0.20	5.46E-5	6.25E-5	5.69E-5	5.87E-5	5.93E-5	6.10E-5	6.39E-5	6.55E-5	6.60E-5	6.78E-5	6.98E-5	7.35E-5	7.72E-5	4.18E-3	5.23E-4	2.26E-4
0.35	8.54E-5	8.85E-5	9.43E-5	9.12E-5	9.33E-5	9.23E-5	9.20E-5	9.72E-5	1.00E-4	9.83E-5	1.02E-4	1.05E-4	4.36E-4	2.63E-2	3.04E-3	1.19E-3
0.50	1.16E-4	1.22E-4	1.02E-4	1.28E-4	1.15E-4	1.20E-4	1.22E-4	1.21E-4	1.25E-4	1.23E-4	1.35E-4	5.65E-4	1.12E-2	5.77E-2	7.61E-3	2.92E-3
0.75	1.61E-4	1.54E-4	1.62E-4	1.62E-4	1.93E-4	1.47E-4	1.69E-4	1.65E-4	1.82E-4	6.15E-4	6.16E-3	2.17E-2	4.93E-2	9.57E-2	1.79E-2	6.81E-3
1.00	1.5E-4[B]	2.5E-4[A]	2.0E-4	2.21E-4	1.96E-4	1.99E-4	6.4E-4[C]	2.5E-3[A]	7.8E-3[A]	1.44E-2	2.73E-2	4.86E-2	7.74E-2	1.12E-1	2.82E-2	1.07E-2
1.50	9.3E-4[B]	2.0E-3[A]	3.5E-3[A]	6.95E-3	1.06E-2	1.48E-2	2.11E-2	2.91E-2	3.67E-2	4.99E-2	6.43E-2	8.04E-2	1.01E-1	1.32E-1	4.84E-2	1.83E-2
2.00	1.30E-2	1.64E-2	2.13E-2	2.55E-2	2.99E-2	3.74E-2	4.97E-2	5.36E-2	6.14E-2	7.01E-2	8.79E-2	9.82E-2	1.14E-1	1.35E-1	6.61E-2	2.56E-2
3.00	4.44E-2	4.65E-2	5.28E-2	5.56E-2	6.80E-2	7.37E-2	7.65E-2	8.33E-2	8.87E-2	9.66E-2	1.03E-1	1.14E-1	1.27E-1	1.45E-1	9.03E-2	3.90E-2
4.00	6.61E-2	7.00E-2	7.19E-2	8.18E-2	8.59E-2	9.50E-2	9.66E-2	1.02E-1	1.05E-1	1.10E-1	1.15E-1	1.29E-1	1.35E-1	1.49E-1	1.06E-1	5.16E-2
	SAF $(Stomach\ Wall \leftarrow Esophagus\ Contents)$ **in kg^{-1} for Photon**															
0.01	2.47E-3	3.11E-3	3.99E-3	4.98E-3	6.33E-3	7.86E-3	1.00E-2	1.25E-2	1.60E-2	2.07E-2	2.78E-2	3.99E-2	5.82E-2	9.19E-2	2.73E-2	1.05E-2
0.015	3.79E-5	4.07E-5	4.36E-5	4.73E-5	5.13E-5	5.58E-5	6.02E-5	6.58E-5	7.12E-5	7.74E-5	8.62E-5	9.76E-5	1.12E-4	1.33E-4	7.61E-5	3.71E-5
0.02	7.84E-2	8.13E-2	8.39E-2	8.72E-2	9.06E-2	9.39E-2	9.69E-2	1.01E-1	1.06E-1	1.10E-1	1.15E-1	1.22E-1	1.31E-1	1.42E-1	1.07E-1	6.93E-2
0.03	1.05E-1	1.06E-1	1.07E-1	1.08E-1	1.09E-1	1.11E-1	1.12E-1	1.13E-1	1.15E-1	1.17E-1	1.19E-1	1.22E-1	1.24E-1	1.28E-1	1.15E-1	9.75E-2
0.05	8.09E-2	8.09E-2	8.10E-2	8.14E-2	8.21E-2	8.26E-2	8.27E-2	8.30E-2	8.33E-2	8.38E-2	8.45E-2	8.51E-2	8.56E-2	8.66E-2	8.35E-2	7.84E-2
0.10	5.31E-2	5.32E-2	5.33E-2	5.35E-2	5.38E-2	5.38E-2	5.39E-2	5.42E-2	5.45E-2	5.48E-2	5.52E-2	5.56E-2	5.61E-2	5.08E-2	5.44E-2	5.21E-2
0.20	4.69E-2	4.70E-2	4.71E-2	4.74E-2	4.76E-2	4.78E-2	4.79E-2	4.83E-2	4.85E-2	4.87E-2	4.90E-2	4.94E-2	4.99E-2	5.05E-2	4.85E-2	4.61E-2
0.35	4.56E-2	4.60E-2	4.61E-2	4.63E-2	4.67E-2	4.65E-2	4.66E-2	4.68E-2	4.73E-2	4.77E-2	4.80E-2	4.86E-2	4.90E-2	4.97E-2	4.75E-2	4.47E-2
0.50	4.46E-2	4.49E-2	4.47E-2	4.52E-2	4.54E-2	4.54E-2	4.52E-2	4.58E-2	4.61E-2	4.67E-2	4.71E-2	4.76E-2	4.81E-2	4.87E-2	4.64E-2	4.36E-2
0.75	4.26E-2	4.27E-2	4.25E-2	4.31E-2	4.35E-2	4.32E-2	4.34E-2	4.42E-2	4.45E-2	4.48E-2	4.50E-2	4.56E-2	4.61E-2	4.68E-2	4.44E-2	4.15E-2
1.00	4.03E-2	4.03E-2	4.01E-2	4.06E-2	4.08E-2	4.07E-2	4.10E-2	4.16E-2	4.19E-2	4.25E-2	4.28E-2	4.35E-2	4.38E-2	4.44E-2	4.20E-2	3.95E-2
1.50	3.72E-2	3.73E-2	3.71E-2	3.77E-2	3.82E-2	3.80E-2	3.82E-2	3.86E-2	3.87E-2	3.91E-2	3.94E-2	3.99E-2	4.05E-2	4.09E-2	3.89E-2	3.63E-2
2.00	3.43E-2	3.44E-2	3.41E-2	3.44E-2	3.49E-2	3.50E-2	3.50E-2	3.52E-2	3.55E-2	3.59E-2	3.63E-2	3.68E-2	3.73E-2	3.77E-2	3.57E-2	3.35E-2
3.00	3.02E-2	3.02E-2	3.03E-2	3.04E-2	3.08E-2	3.07E-2	3.08E-2	3.14E-2	3.13E-2	3.16E-2	3.18E-2	3.23E-2	3.31E-2	3.34E-2	3.15E-2	2.98E-2
4.00	2.75E-2	2.73E-2	2.76E-2	2.78E-2	2.76E-2	2.80E-2	2.78E-2	2.93E-2	2.87E-2	2.90E-2	2.90E-2	2.96E-2	3.04E-2	3.05E-2	2.88E-2	2.70E-2

Table B2. Continued.

SAF (*Stomach Wall* ← *Stomach Contents*) **in kg^{-1}**															
Source Particle Energy (MeV)															
0.01			**0.015**			**0.02**			**0.03**			**0.05**			
Depth (cm)	**Electron SAF**	**Photon SAF**	**Depth (cm)**	**Electron SAF[d]**	**Photon SAF**	**Depth (cm)**	**Electron SAF**	**Photon SAF**	**Depth (cm)**	**Electron SAF**	**Photon SAF**	**Depth (cm)**	**Electron SAF**	**Photon SAF**	
0.00005	1.15[a]	2.02	**0.00005**	1.24[a]	1.73	**0.0001**	1.23[a]	1.47	**0.0001**	1.24[a]	9.15E-01	**0.0005**	1.30[a]	4.18E-01	
0.00020	7.54E-2[d]	1.97	**0.00020**	5.19E-1[b]	1.71	**0.00035**	6.04E-1[a]	1.56	**0.00035**	9.49E-1[a]	9.62E-01	**0.0015**	5.89E-1[a]	4.14E-01	
0.00040	1.15E-4	1.96	**0.00040**	5.98E-2[d]	1.71	**0.00075**	5.03E-2[a]	1.47	**0.00075**	4.95E-1[a]	9.08E-01	**0.003**	1.57E-1[b]	4.14E-01	
0.00060	1.09E-4	1.94	**0.00060**	5.98E-4[g]	1.70	**0.0015**	2.12E-4	1.49	**0.0015**	6.32E-2[a]	9.21E-01	**0.005**	2.42E-3[d]	4.14E-01	
0.00085	9.47E-5	1.89	**0.00085**	1.69E-4	1.67	**0.0025**	3.67E-4	2.99	**0.0025**	6.21E-4	1.85	**0.007**	4.01E-4	4.12E-01	
0.00200	1.05E-4	2.77	**0.00200**	1.96E-4	2.52	**0.0055**	1.25E-4	1.18	**0.0055**	2.06E-4	7.35E-01	**0.009**	3.83E-4	4.11E-01	
0.00800	3.56E-5	1.49	**0.00800**	7.95E-5	1.45	**0.0105**	1.30E-4	1.45	**0.0105**	2.25E-4	9.06E-01	**0.0115**	3.62E-4	4.10E-01	
0.01800	2.33E-5	1.45	**0.01800**	6.28E-5	1.54	**0.018**	1.08E-4	1.43	**0.018**	1.96E-4	9.00E-01	**0.018**	3.36E-4	4.07E-01	
0.02800	1.57E-5	1.29	**0.02800**	4.92E-5	1.47	**0.028**	8.93E-5	1.39	**0.028**	1.73E-4	8.85E-01	**0.028**	3.01E-4	4.03E-01	
0.03800	1.15E-5	1.16	**0.03800**	4.04E-5	1.41	**0.038**	7.74E-5	1.35	**0.038**	1.56E-4	8.72E-01	**0.038**	2.77E-4	3.99E-01	
0.04550	9.31E-6	1.07	**0.04550**	3.57E-5	1.36	**0.0455**	7.03E-5	1.33	**0.0455**	1.45E-4	8.63E-01	**0.0455**	2.61E-4	3.96E-01	
0.05050	8.22E-6	1.02	**0.05050**	3.31E-5	1.34	**0.0505**	6.59E-5	1.31	**0.0505**	1.39E-4	8.56E-01	**0.0505**	2.53E-4	3.94E-01	
0.05450	7.57E-6	9.88E-01	**0.05450**	3.15E-5	1.33	**0.0545**	6.43E-5	1.31	**0.0545**	1.36E-4	8.58E-01	**0.0545**	2.55E-4	3.95E-01	
0.05750	6.90E-6	9.50E-01	**0.05750**	2.99E-5	1.30	**0.0575**	6.07E-5	1.29	**0.0575**	1.32E-4	8.46E-01	**0.0575**	2.44E-4	3.90E-01	
0.06050	6.57E-6	9.34E-01	**0.06050**	2.90E-5	1.30	**0.0605**	6.07E-5	1.29	**0.0605**	1.27E-4	8.50E-01	**0.0605**	2.42E-4	3.93E-01	
0.06350	6.02E-6	8.98E-01	**0.06350**	2.75E-5	1.27	**0.0635**	5.77E-5	1.27	**0.0635**	1.29E-4	8.39E-01	**0.0635**	2.33E-4	3.88E-01	
0.06650	5.80E-6	8.87E-01	**0.06650**	2.69E-5	1.27	**0.0665**	5.69E-5	1.28	**0.0665**	1.27E-4	8.46E-01	**0.0665**	2.26E-4	3.92E-01	
0.07050	5.28E-6	8.48E-01	**0.07050**	2.55E-5	1.24	**0.0705**	5.47E-5	1.26	**0.0705**	1.19E-4	8.35E-01	**0.0705**	2.35E-4	3.87E-01	
0.07800	4.54E-6	7.95E-01	**0.07800**	2.33E-5	1.21	**0.078**	5.10E-5	1.24	**0.078**	1.16E-4	8.29E-01	**0.078**	2.19E-4	3.86E-01	
0.09300	3.46E-6	7.01E-01	**0.09300**	2.00E-5	1.15	**0.093**	4.54E-5	1.20	**0.093**	1.07E-4	8.14E-01	**0.093**	2.07E-4	3.81E-01	
0.11800	2.29E-6	5.72E-01	**0.11800**	1.57E-5	1.06	**0.118**	3.82E-5	1.15	**0.118**	9.39E-5	7.91E-01	**0.118**	1.89E-4	3.74E-01	
0.14800	1.45E-6	4.53E-01	**0.14800**	1.22E-5	9.66E-01	**0.148**	3.17E-5	1.08	**0.148**	8.23E-5	7.66E-01	**0.148**	1.70E-4	3.65E-01	
0.17800	9.65E-7	3.62E-01	**0.17800**	9.71E-6	8.83E-01	**0.178**	2.69E-5	1.03	**0.178**	7.34E-5	7.42E-01	**0.178**	1.57E-4	3.57E-01	
0.20800	6.63E-7	2.92E-01	**0.20800**	7.91E-6	8.10E-01	**0.208**	2.33E-5	9.78E-01	**0.208**	6.64E-5	7.20E-01	**0.208**	1.44E-4	3.50E-01	
0.23800	4.67E-7	2.37E-01	**0.23800**	6.52E-6	7.46E-01	**0.238**	2.04E-5	9.32E-01	**0.238**	6.03E-5	7.00E-01	**0.238**	1.34E-4	3.44E-01	
0.26800	3.32E-7	1.93E-01	**0.26800**	5.44E-6	6.87E-01	**0.268**	1.78E-5	8.87E-01	**0.268**	5.48E-5	6.80E-01	**0.268**	1.26E-4	3.37E-01	
0.29800	2.42E-7	1.58E-01	**0.29800**	4.59E-6	6.34E-01	**0.298**	1.58E-5	8.46E-01	**0.298**	5.08E-5	6.61E-01	**0.298**	1.18E-4	3.30E-01	
0.32800	1.78E-7	1.30E-01	**0.32800**	3.89E-6	5.85E-01	**0.328**	1.42E-5	8.07E-01	**0.328**	4.64E-5	6.43E-01	**0.328**	1.11E-4	3.23E-01	
0.35800	1.33E-7	1.07E-01	**0.35800**	3.35E-6	5.43E-01	**0.358**	1.27E-5	7.73E-01	**0.358**	4.35E-5	6.27E-01	**0.358**	1.06E-4	3.18E-01	
0.38800	1.00E-7	8.82E-02	**0.38800**	2.87E-6	5.02E-01	**0.388**	1.15E-5	7.37E-01	**0.388**	4.03E-5	6.10E-01	**0.388**	9.96E-5	3.12E-01	
0.41800	7.56E-8	7.31E-02	**0.41800**	2.50E-6	4.67E-01	**0.418**	1.03E-5	7.06E-01	**0.418**	3.77E-5	5.95E-01	**0.418**	9.40E-5	3.07E-01	
0.44800	5.73E-8	6.07E-02	**0.44800**	2.17E-6	4.34E-01	**0.448**	9.48E-6	6.77E-01	**0.448**	3.52E-5	5.80E-01	**0.448**	8.95E-5	3.01E-01	
0.47800	4.41E-8	5.04E-02	**0.47800**	1.89E-6	4.03E-01	**0.478**	8.60E-6	6.48E-01	**0.478**	3.29E-5	5.65E-01	**0.478**	8.52E-5	2.96E-01	
0.50800	3.37E-8	4.20E-02	**0.50800**	1.66E-6	3.75E-01	**0.508**	7.87E-6	6.22E-01	**0.508**	3.09E-5	5.52E-01	**0.508**	8.11E-5	2.91E-01	
0.53800	2.71E-8	3.51E-02	**0.53800**	1.46E-6	3.50E-01	**0.538**	7.17E-6	5.96E-01	**0.538**	2.92E-5	5.39E-01	**0.538**	7.72E-5	2.86E-01	
0.56800	2.06E-8	2.93E-02	**0.56800**	1.29E-6	3.26E-01	**0.568**	6.61E-6	5.72E-01	**0.568**	2.74E-5	5.26E-01	**0.568**	7.46E-5	2.82E-01	
0.59800	1.60E-8	2.45E-02	**0.59800**	1.14E-6	3.04E-01	**0.598**	6.09E-6	5.50E-01	**0.598**	2.61E-5	5.14E-01	**0.598**	7.15E-5	2.77E-01	
Wall	1.11E-4[a]	2.97E-01	**Wall**	3.45E-4	6.92E-01	**Wall**	6.58E-4[a]	8.66E-01	**Wall**	1.24E-3	6.64E-01	**Wall**	3.22E-3[a]	3.30E-01	

Table B2. Continued.

SAF $(Stomach\ Wall \leftarrow Stomach\ Contents)$ **in kg^{-1}**															
Source Particle Energy (MeV)															
0.10			**0.20**			**0.35**			**0.50**			**0.75**			
Depth (cm)	**Electron SAF**	**Photon SAF**	**Depth (cm)**	**Electron SAF**	**Photon SAF**	**Depth (cm)**	**Electron SAF**	**Photon SAF**	**Depth (cm)**	**Electron SAF**	**Photon SAF**	**Depth (cm)**	**Electron SAF**	**Photon SAF**	
0.0005	1.71	2.42E-01	**0.0025**	1.62	2.37E-01	**0.0025**	1.54	2.39E-01	**0.005**	1.66	2.36E-01	**0.005**	1.71	2.26E-01	
0.0015	1.42	2.39E-01	**0.0075**	1.17	2.35E-01	**0.0075**	1.56	2.37E-01	**0.015**	1.41	2.32E-01	**0.015**	1.62	2.23E-01	
0.003	1.03	2.40E-01	**0.0125**	8.26E-1	2.33E-01	**0.0125**	1.26	2.36E-01	**0.025**	1.17	2.29E-01	**0.025**	1.41	2.20E-01	
0.005	7.10E-1	2.39E-01	**0.0175**	5.59E-1	2.32E-01	**0.0175**	1.08	2.34E-01	**0.035**	9.88E-1	2.26E-01	**0.035**	1.27	2.17E-01	
0.007	4.07E-1[a]	2.39E-01	**0.0225**	3.32E-1	2.30E-01	**0.0225**	9.62E-1	2.32E-01	**0.045**	8.21E-1	2.23E-01	**0.045**	1.14	2.15E-01	
0.009	1.85E-1[a]	2.38E-01	**0.0275**	1.76E-1[a]	2.29E-01	**0.0275**	8.25E-1	2.31E-01	**0.055**	6.69E-1	2.21E-01	**0.055**	1.04	2.12E-01	
0.0115	4.57E-2[a]	2.37E-01	**0.0325**	6.83E-2[a]	2.28E-01	**0.0325**	6.94E-1	2.30E-01	**0.065**	5.38E-1	2.19E-01	**0.065**	9.37E-1	2.10E-01	
0.018	1.06E-3[a]	2.36E-01	**0.0375**	2.05E-2[b]	2.26E-01	**0.0375**	5.65E-1	2.28E-01	**0.075**	4.37E-1	2.16E-01	**0.075**	8.38E-1	2.08E-01	
0.028	4.87E-4	2.33E-01	**0.0425**	3.50E-3	2.25E-01	**0.0425**	4.66E-1	2.27E-01	**0.085**	3.50E-1	2.14E-01	**0.085**	7.22E-1	2.06E-01	
0.038	4.60E-4	2.31E-01	**0.0475**	7.51E-4	2.24E-01	**0.0475**	3.97E-1	2.26E-01	**0.095**	2.55E-1	2.12E-01	**0.095**	6.59E-1	2.04E-01	
0.0455	4.36E-4	2.29E-01	**0.0525**	6.03E-4	2.23E-01	**0.0525**	2.98E-1	2.24E-01	**0.105**	1.79E-1	2.10E-01	**0.105**	5.67E-1	2.02E-01	
0.0505	4.21E-4	2.28E-01	**0.0575**	6.04E-4	2.22E-01	**0.0575**	2.37E-1	2.23E-01	**0.115**	1.23E-1	2.08E-01	**0.115**	5.09E-1	2.00E-01	
0.0545	4.02E-4	2.28E-01	**0.0625**	6.10E-4	2.21E-01	**0.0625**	1.82E-1	2.22E-01	**0.125**	8.17E-2	2.06E-01	**0.125**	4.21E-1	1.98E-01	
0.0575	4.02E-4	2.25E-01	**0.0675**	5.53E-4	2.19E-01	**0.0675**	1.34E-1[a]	2.21E-01	**0.135**	4.02E-2[a]	2.04E-01	**0.135**	3.62E-1	1.96E-01	
0.0605	4.14E-4	2.27E-01	**0.0725**	5.73E-4	2.18E-01	**0.0725**	9.29E-2[a]	2.20E-01	**0.145**	1.90E-2[a]	2.02E-01	**0.145**	3.10E-1	1.94E-01	
0.0635	4.19E-4	2.24E-01	**0.0775**	5.44E-4	2.17E-01	**0.0775**	5.75E-2[a]	2.19E-01	**0.16**	5.77E-3[a]	2.00E-01	**0.16**	2.38E-1	1.92E-01	
0.0665	3.75E-4	2.27E-01	**0.0825**	5.88E-4	2.16E-01	**0.0825**	3.28E-2[a]	2.18E-01	**0.185**	8.91E-4	1.96E-01	**0.185**	1.45E-1	1.88E-01	
0.0705	4.08E-4	2.24E-01	**0.0875**	5.29E-4	2.15E-01	**0.0875**	1.27E-2[b]	2.17E-01	**0.225**	6.75E-4	1.90E-01	**0.225**	4.98E-2	1.82E-01	
0.078	3.78E-4	2.23E-01	**0.0925**	4.98E-4	2.14E-01	**0.0925**	5.03E-3[b]	2.16E-01	**0.275**	6.32E-4	1.82E-01	**0.275**	5.46E-3	1.75E-01	
0.093	3.62E-4	2.20E-01	**0.0975**	5.54E-4	2.13E-01	**0.0975**	1.77E-3[c]	2.15E-01	**0.325**	5.90E-4	1.76E-01	**0.325**	8.25E-4	1.68E-01	
0.118	3.33E-4	2.16E-01	**0.1025**	5.16E-4	2.12E-01	**0.1025**	1.15E-3[b]	2.14E-01	**0.375**	5.57E-4	1.70E-01	**0.375**	7.29E-4	1.62E-01	
0.148	3.10E-4	2.11E-01	**0.1075**	5.53E-4	2.12E-01	**0.1075**	6.81E-4	2.13E-01	**0.425**	5.44E-4	1.64E-01	**0.425**	7.12E-4	1.57E-01	
0.178	2.90E-4	2.06E-01	**0.1125**	4.67E-4	2.11E-01	**0.1125**	7.25E-4	2.12E-01	**0.475**	5.12E-4	1.59E-01	**0.475**	6.65E-4	1.52E-01	
0.208	2.73E-4	2.02E-01	**0.1175**	5.30E-4	2.10E-01	**0.1175**	6.82E-4	2.11E-01	**0.5265**	4.73E-4	1.53E-01	**0.5265**	6.44E-4	1.47E-01	
0.238	2.56E-4	1.99E-01	**0.125**	4.88E-4	2.08E-01	**0.125**	6.45E-4	2.10E-01	**0.583**	4.74E-4	1.48E-01	**0.583**	5.87E-4	1.42E-01	
0.268	2.44E-4	1.94E-01	**0.135**	4.83E-4	2.07E-01	**0.135**	6.43E-4	2.08E-01	**Wall**	1.25E-1	1.80E-01	**Wall**	2.13E-1	1.72E-01	
0.298	2.32E-4	1.91E-01	**0.145**	4.67E-4	2.05E-01	**0.145**	6.43E-4	2.06E-01							
0.328	2.20E-4	1.87E-01	**0.16**	4.60E-4	2.02E-01	**0.16**	6.31E-4	2.03E-01							
0.358	2.10E-4	1.84E-01	**0.185**	4.32E-4	1.99E-01	**0.185**	5.77E-4	1.99E-01							
0.388	2.02E-4	1.81E-01	**0.225**	4.06E-4	1.92E-01	**0.225**	5.52E-4	1.93E-01							
0.418	1.93E-4	1.78E-01	**0.275**	3.73E-4	1.86E-01	**0.275**	5.29E-4	1.86E-01							
0.448	1.86E-4	1.75E-01	**0.325**	3.49E-4	1.79E-01	**0.325**	4.75E-4	1.79E-01							
0.478	1.78E-4	1.72E-01	**0.375**	3.29E-4	1.73E-01	**0.375**	4.69E-4	1.73E-01							
0.508	1.72E-4	1.69E-01	**0.425**	3.10E-4	1.68E-01	**0.425**	4.24E-4	1.67E-01							
0.538	1.65E-4	1.66E-01	**0.475**	2.93E-4	1.62E-01	**0.475**	4.11E-4	1.62E-01							
0.568	1.59E-4	1.63E-01	**0.5265**	2.78E-4	1.58E-01	**0.5265**	3.92E-4	1.57E-01							
0.598	1.55E-4	1.61E-01	**0.583**	2.58E-4	1.52E-01	**0.583**	3.65E-4	1.51E-01							
Wall	1.14E-2	1.91E-01	**Wall**	3.40E-2	1.83E-01	**Wall**	7.40E-2	1.83E-01							

Table B2. Continued.

SAF (*Stomach Wall* ← *Stomach Contents*) **in kg^{-1}**													
Source Particle Energy (MeV)													
1.00			**1.50**			**2.00**			**3.00**			**4.00**		
Depth (cm)	**Electron SAF**	**Photon SAF**	**Depth (cm)**	**Electron SAF**	**Photon SAF**	**Depth (cm)**	**Electron SAF**	**Photon SAF**	**Depth (cm)**	**Electron SAF**	**Photon SAF**	**Depth (cm)**	**Electron SAF**	**Photon SAF**
0.01	1.63	2.15E-01	**0.01**	1.69	1.96E-01	**0.015**	1.64	1.80E-01	**0.02**	1.54	1.58E-01	**0.02**	1.59	1.44E-01
0.03	1.42	2.09E-01	**0.03**	1.51	1.91E-01	**0.045**	1.46	1.73E-01	**0.06**	1.39	1.50E-01	**0.06**	1.45	1.37E-01
0.05	1.25	2.04E-01	**0.05**	1.36	1.86E-01	**0.075**	1.31	1.67E-01	**0.1**	1.27	1.44E-01	**0.1**	1.30	1.31E-01
0.07	1.07	2.00E-01	**0.07**	1.24	1.82E-01	**0.105**	1.18	1.62E-01	**0.14**	1.16	1.39E-01	**0.14**	1.21	1.26E-01
0.09	9.16E-1	1.95E-01	**0.09**	1.13	1.79E-01	**0.135**	1.06	1.58E-01	**0.18**	1.06	1.34E-01	**0.18**	1.13	1.22E-01
0.11	7.83E-1	1.92E-01	**0.11**	1.04	1.75E-01	**0.165**	9.59E-1	1.54E-01	**0.22**	9.64E-1	1.30E-01	**0.22**	1.06	1.18E-01
0.13	6.65E-1	1.88E-01	**0.13**	9.47E-1	1.72E-01	**0.195**	8.63E-1	1.50E-01	**0.26**	8.82E-1	1.26E-01	**0.26**	9.83E-1	1.14E-01
0.15	5.58E-1	1.85E-01	**0.15**	8.54E-1	1.69E-01	**0.23**	7.59E-1	1.46E-01	**0.3**	8.14E-1	1.22E-01	**0.3**	9.18E-1	1.11E-01
0.17	4.60E-1	1.82E-01	**0.17**	7.77E-1	1.66E-01	**0.275**	6.39E-1	1.41E-01	**0.34**	7.39E-1	1.18E-01	**0.34**	8.52E-1	1.08E-01
0.19	3.72E-1	1.79E-01	**0.19**	7.06E-1	1.63E-01	**0.325**	5.30E-1	1.35E-01	**0.38**	6.70E-1	1.15E-01	**0.38**	7.93E-1	1.05E-01
0.21	2.99E-1	1.76E-01	**0.21**	6.30E-1	1.61E-01	**0.375**	4.29E-1	1.31E-01	**0.425**	5.99E-1	1.11E-01	**0.425**	7.22E-1	1.01E-01
0.23	2.34E-1	1.73E-01	**0.23**	5.72E-1	1.58E-01	**0.425**	3.41E-1	1.26E-01	**0.475**	5.26E-1	1.08E-01	**0.475**	6.55E-1	9.81E-02
0.25	1.77E-1	1.70E-01	**0.25**	5.12E-1	1.55E-01	**0.475**	2.66E-1	1.22E-01	**0.5265**	4.61E-1	1.04E-01	**0.5265**	6.03E-1	9.49E-02
0.27	1.26E-1	1.68E-01	**0.27**	4.57E-1	1.53E-01	**0.5265**	1.99E-1	1.18E-01	**0.583**	3.92E-1	1.00E-01	**0.583**	5.43E-1	9.15E-02
0.29	9.40E-2	1.65E-01	**0.29**	4.04E-1	1.51E-01	**0.583**	1.37E-1	1.14E-01	**Wall**	8.25E-1	1.22E-01	**Wall**	9.28E-1	1.11E-01
0.31	6.02E-2	1.63E-01	**0.31**	3.51E-1	1.48E-01	**Wall**	6.39E-1	1.39E-01						
0.335	3.36E-2	1.60E-01	**0.335**	2.99E-1	1.46E-01									
0.375	1.03E-2	1.55E-01	**0.375**	2.19E-1	1.42E-01									
0.425	1.64E-3	1.50E-01	**0.425**	1.39E-1	1.37E-01									
0.475	8.59E-4	1.45E-01	**0.475**	7.91E-2	1.32E-01									
0.5265	7.65E-4	1.40E-01	**0.5265**	3.81E-2	1.28E-01									
0.583	7.76E-4	1.35E-01	**0.583**	1.38E-2	1.23E-01									
Wall	2.99E-1	1.65E-01	**Wall**	4.79E-1	1.50E-01									

Table B2. Continued.

SAF $(Stomach\ Wall \leftarrow Small\ Intestine\ Contents)$ **in kg^{-1}**													
Source Particle Energy (MeV)													
0.01			**0.015**			**0.02**			**0.03**			**0.05**		
Depth (cm)	**Electron SAF**	**Photon SAF**	**Depth (cm)**	**Electron SAF[d]**	**Photon SAF[c]**	**Depth (cm)**	**Electron SAF**	**Photon SAF[b]**	**Depth (cm)**	**Electron SAF**	**Photon SAF**	**Depth (cm)**	**Electron SAF[a]**	**Photon SAF**
0.0025	0.0	0.0	**0.0025**	5.08E-10	2.07E-04	**0.0025**	2.49E-09[d]	1.25E-03	**0.0025**	3.72E-08[b]	5.26E-03	**0.0025**	4.16E-07	9.37E-03
0.0075	0.0	0.0	**0.0075**	5.09E-10	2.06E-04	**0.0075**	2.53E-09[d]	1.24E-03	**0.0075**	3.71E-08[b]	5.24E-03	**0.0075**	3.85E-07	9.46E-03
0.0125	0.0	0.0	**0.0125**	5.11E-10	2.06E-04	**0.0125**	2.63E-09[d]	1.23E-03	**0.0125**	3.73E-08[c]	5.32E-03	**0.0125**	3.66E-07	9.36E-03
0.0175	0.0	0.0	**0.0175**	5.14E-10	2.05E-04	**0.0175**	2.65E-09[d]	1.23E-03	**0.0175**	3.75E-08[c]	5.42E-03	**0.0175**	3.56E-07	9.37E-03
0.0225	0.0	0.0	**0.0225**	5.34E-10	2.05E-04	**0.0225**	2.62E-09[d]	1.21E-03	**0.0225**	3.69E-08[c]	5.27E-03	**0.0225**	3.52E-07	9.46E-03
0.0275	0.0	0.0	**0.0275**	5.38E-10	2.11E-04	**0.0275**	2.68E-09[d]	1.21E-03	**0.0275**	3.72E-08[c]	5.27E-03	**0.0275**	5.25E-07	9.40E-03
0.0325	0.0	0.0	**0.0325**	5.41E-10	2.11E-04	**0.0325**	2.67E-09[d]	1.23E-03	**0.0325**	3.72E-08[c]	5.25E-03	**0.0325**	4.20E-07	9.44E-03
0.0375	0.0	0.0	**0.0375**	5.45E-10	2.10E-04	**0.0375**	2.64E-09[d]	1.21E-03	**0.0375**	3.75E-08[b]	5.21E-03	**0.0375**	4.05E-07	9.41E-03
0.0425	0.0	0.0	**0.0425**	5.45E-10	2.16E-04	**0.0425**	2.68E-09[d]	1.20E-03	**0.0425**	3.74E-08[b]	5.26E-03	**0.0425**	4.01E-07	9.48E-03
0.0475	0.0	0.0	**0.0475**	5.46E-10	2.16E-04	**0.0475**	2.77E-09[d]	1.21E-03	**0.0475**	3.78E-08[c]	5.20E-03	**0.0475**	3.99E-07	9.36E-03
0.0525	0.0	0.0	**0.0525**	5.47E-10	2.15E-04	**0.0525**	2.69E-09[d]	1.20E-03	**0.0525**	3.77E-08[c]	5.15E-03	**0.0525**	3.88E-07	9.36E-03
0.0575	0.0	0.0	**0.0575**	5.52E-10	2.17E-04	**0.0575**	2.66E-09[d]	1.22E-03	**0.0575**	3.83E-08[b]	5.37E-03	**0.0575**	3.90E-07	9.49E-03
0.0625	0.0	0.0	**0.0625**	5.65E-10	2.19E-04	**0.0625**	2.66E-09[d]	1.20E-03	**0.0625**	3.76E-08[b]	5.59E-03	**0.0625**	3.77E-07	9.53E-03
0.0675	0.0	0.0	**0.0675**	5.69E-10	2.25E-04	**0.0675**	2.73E-09[d]	1.20E-03	**0.0675**	3.80E-08[b]	5.45E-03	**0.0675**	3.70E-07	9.47E-03
0.0725	0.0	0.0	**0.0725**	5.75E-10	2.24E-04	**0.0725**	2.72E-09[d]	1.20E-03	**0.0725**	3.85E-08[b]	5.39E-03	**0.0725**	3.64E-07	9.35E-03
0.0775	0.0	0.0	**0.0775**	5.82E-10	2.22E-04	**0.0775**	2.71E-09[d]	1.20E-03	**0.0775**	3.80E-08[b]	5.35E-03	**0.0775**	3.62E-07	9.34E-03
0.0825	0.0	0.0	**0.0825**	5.92E-10	2.24E-04	**0.0825**	2.85E-09[d]	1.22E-03	**0.0825**	3.73E-08[b]	5.39E-03	**0.0825**	3.61E-07	9.43E-03
0.0875	0.0	0.0	**0.0875**	5.97E-10	2.24E-04	**0.0875**	2.77E-09[d]	1.22E-03	**0.0875**	3.74E-08[b]	5.40E-03	**0.0875**	3.57E-07	9.41E-03
0.0925	0.0	0.0	**0.0925**	6.09E-10	2.24E-04	**0.0925**	2.71E-09[d]	1.21E-03	**0.0925**	3.83E-08[b]	5.31E-03	**0.0925**	3.57E-07	9.43E-03
0.0975	0.0	0.0	**0.0975**	6.48E-10	2.24E-04	**0.0975**	2.70E-09[d]	1.22E-03	**0.0975**	3.85E-08[b]	5.30E-03	**0.0975**	3.56E-07	9.45E-03
0.1025	0.0	0.0	**0.1025**	6.89E-10	2.27E-04	**0.1025**	2.70E-09[d]	1.20E-03	**0.1025**	3.87E-08[b]	5.29E-03	**0.1025**	3.58E-07	9.38E-03
0.1075	0.0	0.0	**0.1075**	6.79E-10	2.25E-04	**0.1075**	2.70E-09[d]	1.20E-03	**0.1075**	3.81E-08[b]	5.41E-03	**0.1075**	3.54E-07	9.67E-03
0.1125	0.0	0.0	**0.1125**	6.70E-10	2.25E-04	**0.1125**	2.77E-09[d]	1.21E-03	**0.1125**	3.81E-08[b]	5.32E-03	**0.1125**	3.50E-07	9.59E-03
0.1175	0.0	0.0	**0.1175**	6.70E-10	2.25E-04	**0.1175**	2.74E-09[d]	1.20E-03	**0.1175**	3.80E-08[b]	5.27E-03	**0.1175**	3.50E-07	9.52E-03
0.125	0.0	0.0	**0.125**	6.76E-10	2.32E-04	**0.125**	2.79E-09[d]	1.19E-03	**0.125**	3.77E-08[b]	5.27E-03	**0.125**	3.49E-07	9.50E-03
0.135	0.0	0.0	**0.135**	6.96E-10	2.34E-04	**0.135**	2.79E-09[d]	1.20E-03	**0.135**	3.79E-08[b]	5.26E-03	**0.135**	3.46E-07	9.52E-03
0.145	0.0	0.0	**0.145**	7.34E-10	2.39E-04	**0.145**	2.82E-09[d]	1.20E-03	**0.145**	3.79E-08[b]	5.20E-03	**0.145**	3.44E-07	9.43E-03
0.16	0.0	0.0	**0.16**	7.39E-10	2.44E-04	**0.16**	2.82E-09[d]	1.20E-03	**0.16**	3.87E-08[b]	5.34E-03	**0.16**	3.48E-07	9.47E-03
0.185	0.0	0.0	**0.185**	7.71E-10	2.47E-04	**0.185**	2.87E-09[d]	1.22E-03	**0.185**	3.90E-08[b]	5.44E-03	**0.185**	3.71E-07	9.51E-03
0.225	0.0	0.0	**0.225**	8.37E-10	2.57E-04	**0.225**	3.18E-09[d]	1.22E-03	**0.225**	3.99E-08[b]	5.37E-03	**0.225**	3.66E-07	9.45E-03
0.275	0.0	0.0	**0.275**	9.63E-10	2.70E-04	**0.275**	3.57E-09[d]	1.24E-03	**0.275**	4.08E-08[b]	5.37E-03	**0.275**	3.60E-07	9.45E-03
0.325	0.0	0.0	**0.325**	1.07E-09	2.88E-04	**0.325**	3.63E-09[d]	1.26E-03	**0.325**	4.12E-08[b]	5.36E-03	**0.325**	3.56E-07	9.45E-03
0.375	0.0	0.0	**0.375**	1.19E-09	3.08E-04	**0.375**	3.81E-09[d]	1.42E-03	**0.375**	4.24E-08[b]	5.50E-03	**0.375**	3.55E-07	9.49E-03
0.425	0.0	0.0	**0.425**	1.36E-09	3.27E-04	**0.425**	4.00E-09[c]	1.75E-03	**0.425**	4.32E-08[b]	5.79E-03	**0.425**	3.58E-07	9.67E-03
0.475	0.0	0.0	**0.475**	1.58E-09	3.53E-04	**0.475**	4.34E-09[c]	1.83E-03	**0.475**	4.35E-08[b]	5.97E-03	**0.475**	3.61E-07	9.75E-03
0.5265	0.0	0.0	**0.5265**	1.81E-09	3.82E-04	**0.5265**	4.54E-09[c]	1.70E-03	**0.5265**	4.51E-08[b]	5.87E-03	**0.5265**	4.09E-07	9.73E-03
0.583	0.0	0.0	**0.583**	2.09E-09	4.27E-04	**0.583**	4.78E-09[c]	2.11E-03	**0.583**	6.12E-08[b]	6.37E-03	**0.583**	3.89E-07	1.00E-02
Wall	0.0	0.0	**Wall**	1.18E-09	3.01E-04	**Wall**	3.65E-09[c]	1.48E-03	**Wall**	4.32E-08[b]	5.62E-03	**Wall**	3.71E-07	9.59E-03

Table B2. Continued.

SAF $(Stomach\ Wall \leftarrow Small\ Intestine\ Contents)$ **in kg^{-1}**														
Source Particle Energy (MeV)														
0.10			**0.20**			**0.35**			**0.50**			**0.75**		
Depth (cm)	**Electron SAF**	**Photon SAF**	**Depth (cm)**	**Electron SAF**	**Photon SAF**	**Depth (cm)**	**Electron SAF**	**Photon SAF**	**Depth (cm)**	**Electron SAF**	**Photon SAF**	**Depth (cm)**	**Electron SAF**	**Photon SAF**
0.0025	1.89E-06	9.10E-03	**0.0025**	5.31E-06	8.04E-03	**0.0025**	9.01E-06	7.58E-03	**0.0025**	1.36E-05	7.54E-03	**0.0025**	2.05E-05	7.31E-03
0.0075	1.88E-06	9.20E-03	**0.0075**	5.25E-06	8.08E-03	**0.0075**	9.01E-06	7.68E-03	**0.0075**	1.35E-05	7.66E-03	**0.0075**	2.03E-05	7.39E-03
0.0125	1.91E-06	9.21E-03	**0.0125**	5.26E-06	8.04E-03	**0.0125**	9.09E-06	7.66E-03	**0.0125**	1.35E-05	7.57E-03	**0.0125**	2.02E-05	7.36E-03
0.0175	1.88E-06	9.25E-03	**0.0175**	5.30E-06	8.09E-03	**0.0175**	9.08E-06	7.72E-03	**0.0175**	1.37E-05	7.57E-03	**0.0175**	2.02E-05	7.50E-03
0.0225	1.90E-06	9.19E-03	**0.0225**	5.36E-06	8.08E-03	**0.0225**	9.06E-06	7.73E-03	**0.0225**	1.35E-05	7.53E-03	**0.0225**	2.01E-05	7.26E-03
0.0275	1.87E-06	9.12E-03	**0.0275**	5.31E-06	8.05E-03	**0.0275**	9.05E-06	7.67E-03	**0.0275**	1.36E-05	7.45E-03	**0.0275**	2.01E-05	7.32E-03
0.0325	1.86E-06	9.12E-03	**0.0325**	5.25E-06	7.99E-03	**0.0325**	9.04E-06	7.63E-03	**0.0325**	1.35E-05	7.46E-03	**0.0325**	2.03E-05	7.29E-03
0.0375	1.86E-06	9.06E-03	**0.0375**	5.29E-06	8.03E-03	**0.0375**	8.99E-06	7.64E-03	**0.0375**	1.35E-05	7.35E-03	**0.0375**	2.03E-05	7.26E-03
0.0425	1.88E-06	9.17E-03	**0.0425**	5.27E-06	8.00E-03	**0.0425**	9.09E-06	7.75E-03	**0.0425**	1.36E-05	7.36E-03	**0.0425**	2.03E-05	7.23E-03
0.0475	1.87E-06	9.16E-03	**0.0475**	5.23E-06	7.99E-03	**0.0475**	9.16E-06	7.66E-03	**0.0475**	1.35E-05	7.41E-03	**0.0475**	2.04E-05	7.21E-03
0.0525	1.87E-06	9.07E-03	**0.0525**	5.29E-06	8.00E-03	**0.0525**	9.16E-06	7.53E-03	**0.0525**	1.35E-05	7.27E-03	**0.0525**	2.05E-05	7.46E-03
0.0575	1.87E-06	9.20E-03	**0.0575**	5.28E-06	8.06E-03	**0.0575**	9.08E-06	7.73E-03	**0.0575**	1.35E-05	7.46E-03	**0.0575**	2.05E-05	7.49E-03
0.0625	1.87E-06	9.27E-03	**0.0625**	5.26E-06	8.10E-03	**0.0625**	9.07E-06	7.69E-03	**0.0625**	1.35E-05	7.38E-03	**0.0625**	2.03E-05	7.39E-03
0.0675	1.90E-06	9.20E-03	**0.0675**	5.25E-06	8.07E-03	**0.0675**	9.08E-06	7.74E-03	**0.0675**	1.34E-05	7.33E-03	**0.0675**	2.06E-05	7.29E-03
0.0725	1.88E-06	9.15E-03	**0.0725**	5.26E-06	8.06E-03	**0.0725**	9.30E-06	7.67E-03	**0.0725**	1.34E-05	7.46E-03	**0.0725**	2.06E-05	7.29E-03
0.0775	1.88E-06	9.11E-03	**0.0775**	5.20E-06	8.05E-03	**0.0775**	9.27E-06	7.68E-03	**0.0775**	1.34E-05	7.40E-03	**0.0775**	2.04E-05	7.30E-03
0.0825	1.87E-06	9.10E-03	**0.0825**	5.24E-06	8.03E-03	**0.0825**	9.14E-06	7.72E-03	**0.0825**	1.34E-05	7.50E-03	**0.0825**	2.06E-05	7.31E-03
0.0875	1.86E-06	9.11E-03	**0.0875**	5.31E-06	8.08E-03	**0.0875**	9.17E-06	7.76E-03	**0.0875**	1.34E-05	7.50E-03	**0.0875**	2.06E-05	7.41E-03
0.0925	1.86E-06	9.07E-03	**0.0925**	5.28E-06	8.08E-03	**0.0925**	9.23E-06	7.68E-03	**0.0925**	1.35E-05	7.56E-03	**0.0925**	2.06E-05	7.53E-03
0.0975	1.89E-06	9.10E-03	**0.0975**	5.31E-06	8.16E-03	**0.0975**	9.18E-06	7.67E-03	**0.0975**	1.35E-05	7.54E-03	**0.0975**	2.08E-05	7.47E-03
0.1025	1.90E-06	9.05E-03	**0.1025**	5.32E-06	8.06E-03	**0.1025**	9.26E-06	7.55E-03	**0.1025**	1.34E-05	7.48E-03	**0.1025**	2.06E-05	7.34E-03
0.1075	1.90E-06	9.11E-03	**0.1075**	5.28E-06	8.03E-03	**0.1075**	9.31E-06	7.60E-03	**0.1075**	1.35E-05	7.45E-03	**0.1075**	2.04E-05	7.34E-03
0.1125	1.90E-06	9.11E-03	**0.1125**	5.29E-06	8.12E-03	**0.1125**	9.33E-06	7.87E-03	**0.1125**	1.35E-05	7.66E-03	**0.1125**	2.06E-05	7.58E-03
0.1175	1.88E-06	9.11E-03	**0.1175**	5.26E-06	8.07E-03	**0.1175**	9.24E-06	7.67E-03	**0.1175**	1.37E-05	7.63E-03	**0.1175**	2.06E-05	7.43E-03
0.125	1.87E-06	9.17E-03	**0.125**	5.31E-06	8.04E-03	**0.125**	9.15E-06	7.65E-03	**0.125**	1.38E-05	7.66E-03	**0.125**	2.08E-05	7.41E-03
0.135	1.87E-06	9.13E-03	**0.135**	5.38E-06	8.05E-03	**0.135**	9.25E-06	7.73E-03	**0.135**	1.38E-05	7.47E-03	**0.135**	2.07E-05	7.37E-03
0.145	1.88E-06	9.07E-03	**0.145**	5.40E-06	8.06E-03	**0.145**	9.21E-06	7.62E-03	**0.145**	1.36E-05	7.44E-03	**0.145**	2.06E-05	7.27E-03
0.16	1.91E-06	9.05E-03	**0.16**	5.39E-06	8.13E-03	**0.16**	9.20E-06	7.66E-03	**0.16**	1.36E-05	7.51E-03	**0.16**	2.06E-05	7.35E-03
0.185	1.90E-06	9.20E-03	**0.185**	5.34E-06	8.15E-03	**0.185**	9.16E-06	7.73E-03	**0.185**	1.36E-05	7.59E-03	**0.185**	2.06E-05	7.30E-03
0.225	1.96E-06	9.10E-03	**0.225**	5.29E-06	8.09E-03	**0.225**	9.32E-06	7.63E-03	**0.225**	1.36E-05	7.51E-03	**0.225**	2.07E-05	7.32E-03
0.275	1.98E-06	9.04E-03	**0.275**	5.27E-06	8.19E-03	**0.275**	9.37E-06	7.67E-03	**0.275**	1.38E-05	7.49E-03	**0.275**	2.09E-05	7.37E-03
0.325	1.99E-06	9.12E-03	**0.325**	5.36E-06	8.20E-03	**0.325**	9.43E-06	7.62E-03	**0.325**	1.39E-05	7.45E-03	**0.325**	2.07E-05	7.25E-03
0.375	1.98E-06	9.15E-03	**0.375**	5.37E-06	8.18E-03	**0.375**	9.45E-06	7.51E-03	**0.375**	1.38E-05	7.51E-03	**0.375**	2.07E-05	7.29E-03
0.425	2.01E-06	9.09E-03	**0.425**	5.36E-06	8.15E-03	**0.425**	9.48E-06	7.48E-03	**0.425**	1.37E-05	7.55E-03	**0.425**	2.08E-05	7.29E-03
0.475	2.06E-06	9.18E-03	**0.475**	5.40E-06	8.16E-03	**0.475**	9.46E-06	7.70E-03	**0.475**	1.39E-05	7.55E-03	**0.475**	2.08E-05	7.32E-03
0.5265	2.06E-06	9.04E-03	**0.5265**	5.43E-06	8.20E-03	**0.5265**	9.47E-06	7.54E-03	**0.5265**	1.41E-05	7.59E-03	**0.5265**	2.09E-05	7.38E-03
0.583	2.06E-06	9.11E-03	**0.583**	5.43E-06	8.20E-03	**0.583**	9.47E-06	7.73E-03	**0.583**	1.41E-05	7.49E-03	**0.583**	2.11E-05	7.36E-03
Wall	1.98E-06	9.11E-03	**Wall**	5.35E-06	8.15E-03	**Wall**	9.35E-06	7.63E-03	**Wall**	1.38E-05	7.52E-03	**Wall**	2.08E-05	7.33E-03

Table B2. Continued.

SAF $(Stomach\ Wall \leftarrow Small\ Intestine\ Contents)$ **in kg^{-1}**														
Source Particle Energy (MeV)														
1.00			**1.50**			**2.00**			**3.00**			**4.00**		
Depth (cm)	**Electron SAF**	**Photon SAF**	**Depth (cm)**	**Electron SAF**	**Photon SAF**	**Depth (cm)**	**Electron SAF**	**Photon SAF**	**Depth (cm)**	**Electron SAF**	**Photon SAF**	**Depth (cm)**	**Electron SAF**	**Photon SAF**
0.0025	2.65E-05	6.56E-03	**0.0025**	4.02E-05	6.58E-03	**0.0025**	5.27E-05	6.33E-03	**0.0025**	8.40E-05	5.74E-03	**0.0025**	2.23E-04	5.18E-03
0.0075	2.64E-05	6.81E-03	**0.0075**	4.04E-05	6.70E-03	**0.0075**	5.25E-05	6.53E-03	**0.0075**	8.39E-05	5.99E-03	**0.0075**	2.23E-04	5.28E-03
0.0125	2.63E-05	6.65E-03	**0.0125**	4.05E-05	6.63E-03	**0.0125**	5.25E-05	6.29E-03	**0.0125**	8.53E-05	6.04E-03	**0.0125**	2.23E-04	5.28E-03
0.0175	2.65E-05	6.77E-03	**0.0175**	4.01E-05	6.64E-03	**0.0175**	5.35E-05	6.42E-03	**0.0175**	8.40E-05	6.07E-03	**0.0175**	2.23E-04	5.33E-03
0.0225	2.65E-05	6.76E-03	**0.0225**	3.99E-05	6.50E-03	**0.0225**	5.28E-05	6.27E-03	**0.0225**	8.40E-05	5.92E-03	**0.0225**	2.23E-04	5.26E-03
0.0275	2.66E-05	6.74E-03	**0.0275**	4.00E-05	6.48E-03	**0.0275**	5.28E-05	6.24E-03	**0.0275**	8.40E-05	6.21E-03	**0.0275**	2.23E-04	5.36E-03
0.0325	2.67E-05	6.54E-03	**0.0325**	4.02E-05	6.55E-03	**0.0325**	5.27E-05	6.38E-03	**0.0325**	8.41E-05	6.11E-03	**0.0325**	2.23E-04	5.37E-03
0.0375	2.66E-05	6.45E-03	**0.0375**	4.03E-05	6.60E-03	**0.0375**	5.27E-05	6.35E-03	**0.0375**	8.37E-05	5.93E-03	**0.0375**	2.23E-04	5.40E-03
0.0425	2.67E-05	6.54E-03	**0.0425**	4.00E-05	6.62E-03	**0.0425**	5.27E-05	6.27E-03	**0.0425**	8.35E-05	6.03E-03	**0.0425**	2.23E-04	5.33E-03
0.0475	2.68E-05	6.70E-03	**0.0475**	3.98E-05	6.77E-03	**0.0475**	5.25E-05	6.28E-03	**0.0475**	8.44E-05	5.86E-03	**0.0475**	2.23E-04	5.32E-03
0.0525	2.65E-05	6.56E-03	**0.0525**	4.00E-05	6.80E-03	**0.0525**	5.31E-05	6.27E-03	**0.0525**	8.47E-05	5.75E-03	**0.0525**	2.23E-04	5.34E-03
0.0575	2.66E-05	6.86E-03	**0.0575**	4.00E-05	6.84E-03	**0.0575**	5.25E-05	6.39E-03	**0.0575**	8.43E-05	5.92E-03	**0.0575**	2.23E-04	5.37E-03
0.0625	2.66E-05	6.79E-03	**0.0625**	4.01E-05	6.70E-03	**0.0625**	5.31E-05	6.29E-03	**0.0625**	8.47E-05	5.80E-03	**0.0625**	2.23E-04	5.26E-03
0.0675	2.68E-05	6.87E-03	**0.0675**	4.00E-05	6.68E-03	**0.0675**	5.35E-05	6.39E-03	**0.0675**	8.50E-05	5.98E-03	**0.0675**	2.23E-04	5.23E-03
0.0725	2.66E-05	7.07E-03	**0.0725**	3.99E-05	6.78E-03	**0.0725**	5.29E-05	6.40E-03	**0.0725**	8.43E-05	5.77E-03	**0.0725**	2.23E-04	5.27E-03
0.0775	2.69E-05	6.84E-03	**0.0775**	4.03E-05	6.69E-03	**0.0775**	5.34E-05	6.35E-03	**0.0775**	8.42E-05	5.72E-03	**0.0775**	2.23E-04	5.26E-03
0.0825	2.71E-05	6.91E-03	**0.0825**	4.02E-05	6.73E-03	**0.0825**	5.33E-05	6.46E-03	**0.0825**	8.60E-05	5.76E-03	**0.0825**	3.61E-04	5.28E-03
0.0875	2.70E-05	6.81E-03	**0.0875**	4.03E-05	7.00E-03	**0.0875**	5.37E-05	6.47E-03	**0.0875**	8.57E-05	6.04E-03	**0.0875**	3.61E-04	5.24E-03
0.0925	2.72E-05	6.82E-03	**0.0925**	4.04E-05	6.86E-03	**0.0925**	5.33E-05	6.50E-03	**0.0925**	8.63E-05	6.05E-03	**0.0925**	3.61E-04	5.21E-03
0.0975	2.70E-05	6.72E-03	**0.0975**	4.03E-05	6.84E-03	**0.0975**	5.34E-05	6.42E-03	**0.0975**	8.69E-05	6.03E-03	**0.0975**	3.61E-04	5.24E-03
0.1025	2.69E-05	6.70E-03	**0.1025**	4.06E-05	6.81E-03	**0.1025**	5.34E-05	6.28E-03	**0.1025**	8.64E-05	5.91E-03	**0.1025**	3.61E-04	5.29E-03
0.1075	2.68E-05	6.73E-03	**0.1075**	4.04E-05	6.68E-03	**0.1075**	5.34E-05	6.18E-03	**0.1075**	8.63E-05	5.95E-03	**0.1075**	3.61E-04	5.19E-03
0.1125	2.68E-05	7.10E-03	**0.1125**	4.01E-05	6.88E-03	**0.1125**	5.31E-05	6.47E-03	**0.1125**	8.59E-05	6.58E-03	**0.1125**	3.61E-04	5.32E-03
0.1175	2.68E-05	6.80E-03	**0.1175**	4.04E-05	6.78E-03	**0.1175**	5.30E-05	6.44E-03	**0.1175**	8.58E-05	6.21E-03	**0.1175**	3.61E-04	5.34E-03
0.125	2.68E-05	6.88E-03	**0.125**	4.06E-05	6.79E-03	**0.125**	5.30E-05	6.37E-03	**0.125**	8.55E-05	5.98E-03	**0.125**	3.61E-04	5.27E-03
0.135	2.71E-05	6.85E-03	**0.135**	4.04E-05	6.66E-03	**0.135**	5.33E-05	6.24E-03	**0.135**	8.59E-05	5.85E-03	**0.135**	3.61E-04	5.17E-03
0.145	2.68E-05	6.75E-03	**0.145**	4.06E-05	6.59E-03	**0.145**	5.31E-05	6.23E-03	**0.145**	8.62E-05	5.82E-03	**0.145**	3.61E-04	5.15E-03
0.16	2.69E-05	6.80E-03	**0.16**	4.06E-05	6.72E-03	**0.16**	5.32E-05	6.39E-03	**0.16**	8.60E-05	5.85E-03	**0.16**	3.61E-04	5.16E-03
0.185	2.71E-05	6.87E-03	**0.185**	4.10E-05	6.73E-03	**0.185**	5.33E-05	6.40E-03	**0.185**	8.62E-05	6.05E-03	**0.185**	3.61E-04	5.15E-03
0.225	2.72E-05	6.73E-03	**0.225**	4.09E-05	6.73E-03	**0.225**	5.34E-05	6.27E-03	**0.225**	8.59E-05	5.67E-03	**0.225**	4.65E-04	5.14E-03
0.275	2.73E-05	6.62E-03	**0.275**	4.10E-05	6.84E-03	**0.275**	5.39E-05	6.28E-03	**0.275**	8.43E-05	5.73E-03	**0.275**	4.65E-04	5.20E-03
0.325	2.72E-05	6.64E-03	**0.325**	4.15E-05	6.66E-03	**0.325**	5.41E-05	6.33E-03	**0.325**	8.42E-05	5.75E-03	**0.325**	4.65E-04	5.23E-03
0.375	2.74E-05	6.83E-03	**0.375**	4.19E-05	6.72E-03	**0.375**	5.42E-05	6.32E-03	**0.375**	8.38E-05	5.86E-03	**0.375**	4.65E-04	5.27E-03
0.425	2.75E-05	6.94E-03	**0.425**	4.16E-05	6.71E-03	**0.425**	5.48E-05	6.37E-03	**0.425**	8.42E-05	5.65E-03	**0.425**	4.65E-04	5.28E-03
0.475	2.74E-05	6.98E-03	**0.475**	4.17E-05	6.71E-03	**0.475**	5.46E-05	6.31E-03	**0.475**	8.50E-05	5.71E-03	**0.475**	4.65E-04	5.36E-03
0.5265	2.76E-05	6.83E-03	**0.5265**	4.19E-05	6.75E-03	**0.5265**	5.45E-05	6.21E-03	**0.5265**	8.48E-05	5.60E-03	**0.5265**	5.34E-04	5.28E-03
0.583	2.78E-05	6.98E-03	**0.583**	4.18E-05	6.71E-03	**0.583**	5.53E-05	6.08E-03	**0.583**	8.51E-05	5.93E-03	**0.583**	5.66E-04	5.28E-03
Wall	2.73E-05	6.82E-03	**Wall**	4.365E-05	6.72E-03	**Wall**	5.80E-05	6.29E-03	**Wall**	8.49E-05	5.81E-03	**Wall**	3.50E-04	5.25E-03

Table B2. Continued.

Source Energy (MeV)	**SAF** (*Stomach Wall* ← *Upper Large Intestine Contents*) **in kg^{-1} for Electron**															
	At Mean Position (cm) in the Stomach Wall Measured Outward from Contents-Wall Interface.														Average to	
	0.02	**0.06**	**0.1**	**0.14**	**0.18**	**0.22**	**0.26**	**0.3**	**0.34**	**0.38**	**0.425**	**0.475**	**0.5265**	**0.583**	**Wall**	**Whole**
0.01	0.0	0.0	0.0	0.0	0.0	0.0	0.0	0.0	0.0	0.0	0.0	0.0	0.0	0.0	0.0	0.0
0.015	0.0	0.0	0.0	0.0	0.0	0.0	0.0	0.0	0.0	0.0	0.0	0.0	0.0	0.0	0.0	0.0
0.02[d,e]	5.0E-10	4.8E-10	4.7E-10	4.5E-10	4.4E-10	6.7E-10	8.0E-10	7.8E-10	7.6E-10	7.4E-10	7.2E-10	7.9E-10	1.80E-9	1.40E-9	8.4E-10	5.5E-10
0.03	6.03E-8	5.73E-8	6.20E-8	6.28E-8	6.38E-8	6.46E-8	6.48E-8	7.00E-8	7.19E-8	7.18E-8	7.18E-8	7.84E-8	7.21E-8	7.13E-8	6.83E-8	5.29E-8
0.05	6.12E-7	6.20E-7	6.40E-7	6.40E-7	6.33E-7	6.67E-7	6.63E-7	6.67E-7	6.67E-7	6.80E-7	6.96E-7	7.23E-7	7.39E-7	7.35E-7	6.78E-7	5.72E-7
0.10	3.7E-6[a]	3.7E-6[a]	3.7E-6[a]	3.7E-6[a]	3.7E-6[a]	3.7E-6[a]	3.71E-6	3.68E-6	3.72E-6	3.72E-6	3.74E-6	3.75E-6	3.81E-6	3.79E-6	3.73E-6	3.4E-6[a]
0.20	8.14E-6	8.15E-6	8.18E-6	8.18E-6	8.25E-6	8.23E-6	8.27E-6	8.38E-6	8.39E-6	8.41E-6	8.52E-6	8.59E-6	8.61E-6	8.66E-6	8.39E-6	7.72E-6
0.35	1.45E-5	1.46E-5	1.47E-5	1.47E-5	1.48E-5	1.48E-5	1.49E-5	1.51E-5	1.51E-5	1.51E-5	1.52E-5	1.54E-5	1.54E-5	1.54E-5	1.50E-5	1.39E-5
0.50	2.05E-5	2.05E-5	2.06E-5	2.06E-5	2.07E-5	2.08E-5	2.08E-5	2.09E-5	2.09E-5	2.11E-5	2.11E-5	2.11E-5	2.11E-5	2.13E-5	2.09E-5	1.95E-5
0.75	2.98E-5	3.00E-5	3.07E-5	3.03E-5	3.02E-5	3.04E-5	3.05E-5	3.06E-5	3.07E-5	3.06E-5	3.07E-5	3.08E-5	3.11E-5	3.13E-5	3.06E-5	2.87E-5
1.00	4.32E-5	3.68E-5	4.23E-5	3.72E-5	4.27E-5	3.57E-5	3.82E-5	4.07E-5	4.06E-5	4.74E-5	3.84E-5	3.79E-5	4.28E-5	4.14E-5	4.04E-5	3.74E-5
1.50	5.94E-5	5.94E-5	5.93E-5	6.03E-5	5.99E-5	6.02E-5	6.13E-5	6.15E-5	6.10E-5	6.14E-5	6.17E-5	6.23E-5	6.17E-5	6.17E-5	6.10E-5	5.77E-5
2.00	7.85E-5	7.89E-5	7.74E-5	7.87E-5	7.92E-5	7.98E-5	7.96E-5	8.09E-5	8.17E-5	8.07E-5	8.07E-5	7.99E-5	8.13E-5	8.23E-5	8.02E-5	7.58E-5
3.00	1.16E-4	1.14E-4	1.17E-4	1.20E-4	1.17E-4	1.17E-4	1.18E-4	1.19E-4	1.19E-4	1.19E-4	1.21E-4	1.22E-4	1.22E-4	1.22E-4	1.19E-4	1.13E-4
4.00	1.68E-4	1.66E-4	1.67E-4	1.68E-4	1.66E-4	1.69E-4	1.66E-4	1.65E-4	1.68E-4	1.67E-4	1.67E-4	1.69E-4	1.79E-4	1.77E-4	1.69E-4	1.59E-4
	SAF (*Stomach Wall* ← *Upper Large Intestine Contents*) **in kg^{-1} for Photon**															
0.01	0.0	0.0	0.0	0.0	0.0	0.0	0.0	0.0	0.0	0.0	0.0	0.0	0.0	0.0	0.0	0.0
0.015	1.17E-5	1.39E-5	1.40E-5	1.54E-5	3.64E-5	2.79E-5	2.61E-5	3.19E-5	3.13E-5	3.20E-5	3.13E-5	3.04E-5	4.61E-5	3.37E-5	2.87E-5	1.62E-5
0.02	1.04E-3	1.11E-3	1.08E-3	1.08E-3	1.12E-3	1.16E-3	1.16E-3	1.24E-3	1.27E-3	1.33E-3	1.33E-3	1.41E-3	1.44E-3	1.40E-3	1.25E-3	8.64E-4
0.03	9.16E-3	9.34E-3	9.30E-3	9.41E-3	9.58E-3	9.55E-3	9.66E-3	9.73E-3	9.93E-3	1.02E-2	1.03E-2	1.03E-2	1.05E-2	1.07E-2	9.93E-3	8.36E-3
0.05	1.57E-2	1.57E-2	1.58E-2	1.59E-2	1.60E-2	1.60E-2	1.60E-2	1.61E-2	1.61E-2	1.62E-2	1.61E-2	1.63E-2	1.63E-2	1.65E-2	1.61E-2	1.48E-2
0.10	1.31E-2	1.31E-2	1.32E-2	1.32E-2	1.32E-2	1.32E-2	1.32E-2	1.33E-2	1.33E-2	1.34E-2	1.33E-2	1.34E-2	1.35E-2	1.35E-2	1.33E-2	1.27E-2
0.20	1.16E-2	1.15E-2	1.16E-2	1.17E-2	1.16E-2	1.17E-2	1.17E-2	1.17E-2	1.17E-2	1.18E-2	1.18E-2	1.17E-2	1.18E-2	1.19E-2	1.17E-2	1.11E-2
0.35	1.10E-2	1.11E-2	1.10E-2	1.10E-2	1.10E-2	1.10E-2	1.10E-2	1.11E-2	1.11E-2	1.12E-2	1.12E-2	1.12E-2	1.12E-2	1.12E-2	1.11E-2	1.06E-2
0.50	1.05E-2	1.07E-2	1.06E-2	1.07E-2	1.08E-2	1.07E-2	1.09E-2	1.10E-2	1.09E-2	1.10E-2	1.09E-2	1.08E-2	1.09E-2	1.09E-2	1.08E-2	1.04E-2
0.75	1.00E-2	1.01E-2	1.01E-2	1.01E-2	1.02E-2	1.02E-2	1.05E-2	1.04E-2	1.04E-2	1.06E-2	1.05E-2	1.04E-2	1.04E-2	1.03E-2	1.03E-2	9.96E-3
1.00	9.91E-3	9.89E-3	9.84E-3	1.00E-2	1.02E-2	1.01E-2	1.03E-2	1.02E-2	1.02E-2	1.03E-2	1.03E-2	1.02E-2	1.03E-2	1.02E-2	1.01E-2	9.71E-3
1.50	9.13E-3	9.39E-3	9.20E-3	9.34E-3	9.56E-3	9.23E-3	9.21E-3	9.10E-3	9.13E-3	9.27E-3	9.34E-3	9.37E-3	9.49E-3	9.17E-3	9.28E-3	8.97E-3
2.00	8.47E-3	8.58E-3	8.58E-3	8.49E-3	8.68E-3	8.35E-3	8.43E-3	8.34E-3	8.30E-3	8.48E-3	8.64E-3	8.65E-3	8.89E-3	8.66E-3	8.56E-3	8.24E-3
3.00	7.76E-3	7.93E-3	7.98E-3	7.95E-3	7.99E-3	7.73E-3	7.70E-3	7.67E-3	7.79E-3	8.18E-3	8.02E-3	7.85E-3	7.99E-3	7.82E-3	7.89E-3	7.61E-3
4.00	7.12E-3	7.10E-3	7.24E-3	6.99E-3	6.88E-3	6.67E-3	6.69E-3	6.83E-3	6.92E-3	7.35E-3	7.41E-3	7.10E-3	7.06E-3	7.12E-3	7.05E-3	6.95E-3

Table B2. Continued.

Source Energy (MeV)	**SAF** (*Stomach Wall* ← *Lower Large Intestine Contents*) **in kg^{-1} for Electron**															
	At Mean Position (cm) in the Stomach Wall Measured Outward from Contents-Wall Interface.														Average to	
	0.02	**0.06**	**0.1**	**0.14**	**0.18**	**0.22**	**0.26**	**0.3**	**0.34**	**0.38**	**0.425**	**0.475**	**0.5265**	**0.583**	**Wall**	**Whole**
0.01	0.0	0.0	0.0	0.0	0.0	0.0	0.0	0.0	0.0	0.0	0.0	0.0	0.0	0.0	0.0	0.0
0.015	0.0	0.0	0.0	0.0	0.0	0.0	0.0	0.0	0.0	0.0	0.0	0.0	0.0	0.0	0.0	0.0
0.02	0.0	0.0	0.0	0.0	0.0	0.0	0.0	0.0	0.0	0.0	0.0	0.0	0.0	0.0	0.0	0.0
0.03	0.0	0.0	0.0	0.0	0.0	0.0	0.0	0.0	0.0	0.0	0.0	0.0	0.0	0.0	0.0	0.0
0.05	1.4E-8[c]	9.3E-9[b]	9.6E-9[b]	8.3E-9[a]	7.7E-9[a]	7.1E-9[a]	7.6E-9[a]	7.1E-9[a]	6.5E-9[a]	7.8E-9[a]	9.8E-9[b]	7.7E-9[a]	8.3E-9[a]	7.3E-9[a]	8.1E-9[a]	7.5E-9[a]
0.10	9.56E-8	9.90E-8	9.86E-8	1.07E-7	1.07E-7	1.03E-7	1.02E-7	9.55E-8	9.34E-8	1.02E-7	9.42E-8	9.08E-8	1.01E-7	9.68E-8	9.86E-8	9.14E-8
0.20	3.54E-7	3.45E-7	3.67E-7	3.53E-7	3.67E-7	3.70E-7	3.60E-7	3.74E-7	3.51E-7	3.44E-7	3.33E-7	3.34E-7	3.35E-7	3.41E-7	3.50E-7	3.34E-7
0.35	7.45E-7	7.20E-7	7.04E-7	7.10E-7	7.38E-7	7.52E-7	7.35E-7	7.37E-7	7.29E-7	7.55E-7	7.31E-7	7.57E-7	7.38E-7	7.32E-7	7.35E-7	7.25E-7
0.50	1.16E-6	1.17E-6	1.19E-6	1.18E-6	1.23E-6	1.16E-6	1.16E-6	1.17E-6	1.16E-6	1.15E-6	1.20E-6	1.21E-6	1.21E-6	1.23E-6	1.19E-6	1.16E-6
0.75	2.04E-6	1.97E-6	1.94E-6	1.93E-6	1.95E-6	1.91E-6	1.94E-6	2.00E-6	1.90E-6	1.97E-6	1.94E-6	1.97E-6	1.89E-6	1.91E-6	1.94E-6	1.88E-6
1.00	2.68E-6	2.72E-6	2.73E-6	2.84E-6	2.82E-6	2.82E-6	2.78E-6	2.74E-6	2.63E-6	2.71E-6	2.82E-6	2.73E-6	2.79E-6	2.78E-6	2.76E-6	2.72E-6
1.50	4.15E-6	4.29E-6	4.42E-6	4.43E-6	4.29E-6	4.35E-6	4.41E-6	4.42E-6	4.26E-6	4.37E-6	4.28E-6	4.25E-6	4.37E-6	4.32E-6	4.33E-6	4.29E-6
2.00	1.04E-5	1.06E-5	1.10E-5	1.05E-5	1.07E-5	1.14E-5	1.09E-5	1.12E-5	1.10E-5	1.12E-5	1.13E-5	1.10E-5	1.11E-5	1.13E-5	1.10E-5	1.10E-5
3.00	1.04E-5	1.06E-5	1.10E-5	1.05E-5	1.07E-5	1.14E-5	1.09E-5	1.12E-5	1.10E-5	1.12E-5	1.13E-5	1.10E-5	1.11E-5	1.13E-5	1.10E-5	1.10E-5
4.00	1.58E-5	1.72E-5	1.65E-5	1.66E-5	1.70E-5	1.59E-5	1.64E-5	1.75E-5	1.99E-5	1.80E-5	1.72E-5	1.63E-5	1.64E-5	1.67E-5	1.69E-5	1.61E-5
SAF (*Stomach Wall* ← *Lower Large Intestine Contents*) **in kg^{-1} for Photon**																
0.01	0.0	0.0	0.0	0.0	0.0	0.0	0.0	0.0	0.0	0.0	0.0	0.0	0.0	0.0	0.0	0.0
0.015	0.0	0.0	0.0	0.0	0.0	0.0	0.0	0.0	0.0	0.0	0.0	0.0	0.0	0.0	0.0	0.0
0.02[f]	3.05E-6	2.95E-6	2.86E-6	2.77E-6	2.69E-6	2.62E-6	2.55E-6	2.48E-6	2.42E-6	2.36E-6	2.29E-6	2.22E-6	2.16E-6	2.74E-6	2.55E-6	2.78E-6
0.03	1.31E-4	1.33E-4	1.36E-4	1.44E-4	1.46E-4	1.65E-4	1.56E-4	1.52E-4	1.63E-4	1.57E-4	1.57E-4	1.66E-4	1.59E-4	1.68E-4	1.54E-4	1.40E-4
0.05	5.45E-4	5.68E-4	5.60E-4	5.45E-4	5.52E-4	5.53E-4	5.75E-4	5.78E-4	5.77E-4	5.77E-4	5.82E-4	5.77E-4	5.73E-4	5.60E-4	5.67E-4	5.47E-4
0.10	8.47E-4	8.71E-4	8.53E-4	8.22E-4	8.29E-4	8.44E-4	8.34E-4	8.46E-4	8.57E-4	8.51E-4	8.35E-4	8.40E-4	8.64E-4	8.46E-4	8.46E-4	8.35E-4
0.20	8.71E-4	8.89E-4	8.80E-4	8.70E-4	8.59E-4	8.74E-4	8.82E-4	8.76E-4	8.88E-4	9.06E-4	9.10E-4	9.36E-4	9.26E-4	9.24E-4	8.97E-4	8.93E-4
0.35	1.04E-3	1.07E-3	1.06E-3	1.05E-3	1.08E-3	1.04E-3	1.02E-3	1.05E-3	1.06E-3	1.08E-3	1.08E-3	1.10E-3	1.03E-3	1.05E-3	1.06E-3	1.02E-3
0.50	1.02E-3	1.04E-3	1.00E-3	1.02E-3	1.08E-3	1.06E-3	1.05E-3	1.05E-3	1.09E-3	1.11E-3	1.13E-3	1.12E-3	1.07E-3	1.02E-3	1.06E-3	1.02E-3
0.75	1.11E-3	1.11E-3	1.10E-3	1.11E-3	1.10E-3	1.10E-3	1.04E-3	1.05E-3	1.05E-3	1.05E-3	1.11E-3	1.09E-3	1.06E-3	1.03E-3	1.08E-3	1.08E-3
1.00	9.73E-4	9.90E-4	1.01E-3	1.07E-3	1.03E-3	1.09E-3	1.04E-3	1.03E-3	1.08E-3	1.10E-3	1.11E-3	1.09E-3	1.07E-3	1.04E-3	1.05E-3	1.07E-3
1.50	1.03E-3	1.07E-3	1.07E-3	1.12E-3	1.03E-3	1.07E-3	1.06E-3	1.10E-3	1.09E-3	1.09E-3	1.14E-3	1.16E-3	1.19E-3	1.14E-3	1.10E-3	1.12E-3
2.00	1.05E-3	1.13E-3	1.10E-3	1.06E-3	1.08E-3	1.19E-3	1.19E-3	1.24E-3	1.16E-3	1.20E-3	1.24E-3	1.22E-3	1.24E-3	1.17E-3	1.17E-3	1.16E-3
3.00	1.02E-3	1.01E-3	1.00E-3	9.79E-4	9.49E-4	1.05E-3	1.01E-3	9.82E-4	1.00E-3	9.89E-4	9.95E-4	9.68E-4	1.00E-3	1.03E-3	1.00E-3	1.06E-3
4.00	1.01E-3	1.15E-3	1.18E-3	1.00E-3	9.71E-4	1.08E-3	9.60E-4	1.02E-3	9.95E-4	1.01E-3	1.03E-3	1.06E-3	1.03E-3	1.05E-3	1.04E-3	9.84E-4

Table B2. Continued.

Source Energy (MeV)	**SAF** (*Small Intestine Wall* ← *Esophagus Contents*) **in kg^{-1} for Electron**												
	At Mean Position (cm) in the Small Intestine Wall Measured Outward from Contents-Wall Interface.										Average to the		
	0.025	**0.0625**	**0.085**	**0.1125**	**0.1475**	**0.1825**	**0.2125**	**0.2375**	**0.2625**	**0.2875**	**Wall**	**Contents**	**Wall+Contents**
0.01	0.0	0.0	0.0	0.0	0.0	0.0	0.0	0.0	0.0	0.0	0.0	0.0	0.0
0.015	0.0	0.0	0.0	0.0	0.0	0.0	0.0	0.0	0.0	0.0	0.0	0.0	0.0
0.02[f]	3.2E-11	3.1E-11	3.0E-11	3.0E-11	1.8E-10	9.4E-11	7.5E-11	6.3E-11	8.5E-11	7.9E-11	7.1E-11	6.1E-11	6.4E-11
0.03	3.82E-9	4.20E-9[a]	3.93E-9[a]	3.54E-9	3.99E-9[a]	4.22E-9	4.81E-9[a]	4.86E-9	9.14E-9[a]	8.18E-9	4.64E-9	4.00E-9	4.20E-9
0.05	7.49E-8	7.44E-8	7.31E-8	7.44E-8	7.52E-8	7.49E-8	7.46E-8	7.38E-8	1.17E-7	1.18E-7	7.94E-8	8.03E-8	8.00E-8
0.10	5.11E-7	5.07E-7	5.07E-7	5.06E-7	5.05E-7	5.01E-7	5.07E-7	5.07E-7	7.28E-7	7.25E-7	5.31E-7	5.33E-7	5.33E-7
0.20	1.62E-6	1.62E-6	1.62E-6	1.63E-6	1.62E-6	1.63E-6	1.63E-6	1.62E-6	2.17E-6	2.19E-6	1.69E-6	1.70E-6	1.69E-6
0.35	3.22E-6	3.21E-6	3.22E-6	3.21E-6	3.22E-6	3.22E-6	3.23E-6	3.21E-6	4.23E-6	4.21E-6	3.33E-6	3.36E-6	3.35E-6
0.50	4.80E-6	4.80E-6	4.79E-6	4.77E-6	4.73E-6	4.75E-6	4.76E-6	4.75E-6	6.12E-6	6.11E-6	4.92E-6	5.01E-6	4.99E-6
0.75	7.41E-6	7.37E-6	7.37E-6	7.40E-6	7.41E-6	7.36E-6	7.34E-6	7.38E-6	9.40E-6	9.45E-6	7.61E-6	7.70E-6	7.67E-6
1.00	9.79E-6	9.96E-6	9.06E-6	9.85E-6	1.00E-5	9.47E-6	9.53E-6	9.76E-6	1.26E-5	1.19E-5	1.00E-5	1.03E-5	1.02E-5
1.50	1.53E-5	1.63E-5	1.50E-5	1.57E-5	1.56E-5	1.48E-5	1.57E-5	1.56E-5	1.95E-5	1.94E-5	1.60E-5	1.60E-5	1.60E-5
2.00	2.25E-5	2.25E-5	2.24E-5	2.26E-5	2.26E-5	2.26E-5	2.27E-5	2.27E-5	2.79E-5	2.86E-5	2.32E-5	2.30E-5	2.31E-5
3.00	3.62E-5	3.40E-5	3.33E-5	3.71E-5	3.31E-5	3.45E-5	3.56E-5	3.27E-5	4.26E-5	4.53E-5	3.58E-5	3.61E-5	3.60E-5
4.00	4.66E-5	4.65E-5	4.63E-5	4.64E-5	4.65E-5	4.68E-5	4.69E-5	4.67E-5	5.73E-5	5.68E-5	4.78E-5	4.85E-5	4.83E-5
	SAF (*Small Intestine Wall* ← *Esophagus Contents*) **in kg^{-1} for Photon**												
0.01	0.0	0.0	0.0	0.0	0.0	0.0	0.0	0.0	0.0	0.0	0.0	0.0	0.0
0.015	0.00E+0	0.00E+0	0.00E+0	5.5E-7[f]	1.5E-6[d]	1.7E-6[d]	1.6E-6[d]	1.5E-6[d]	3.3E-6	3.4E-6[d]	1.3E-6[d]	3.1E-7[f]	6.1E-7[d]
0.02	7.58E-5	7.85E-5	8.54E-5	7.86E-5	7.76E-5	8.06E-5	8.22E-5	8.26E-5	1.39E-4	1.37E-4	8.62E-5	7.35E-5	7.75E-5
0.03	9.85E-4	9.94E-4	9.90E-4	9.72E-4	9.75E-4	9.84E-4	9.65E-4	9.77E-4	1.60E-3	1.58E-3	1.05E-3	1.03E-3	1.04E-3
0.05	2.83E-3	2.85E-3	2.85E-3	2.85E-3	2.84E-3	2.84E-3	2.83E-3	2.84E-3	3.95E-3	3.94E-3	2.97E-3	2.99E-3	2.98E-3
0.10	3.40E-3	3.39E-3	3.38E-3	3.38E-3	3.38E-3	3.39E-3	3.38E-3	3.38E-3	4.31E-3	4.30E-3	3.49E-3	3.54E-3	3.53E-3
0.20	3.27E-3	3.27E-3	3.26E-3	3.25E-3	3.25E-3	3.25E-3	3.25E-3	3.24E-3	4.02E-3	4.01E-3	3.34E-3	3.40E-3	3.38E-3
0.35	3.24E-3	3.26E-3	3.26E-3	3.25E-3	3.25E-3	3.24E-3	3.26E-3	3.25E-3	3.97E-3	3.99E-3	3.33E-3	3.39E-3	3.37E-3
0.50	3.16E-3	3.17E-3	3.19E-3	3.18E-3	3.20E-3	3.20E-3	3.19E-3	3.16E-3	3.86E-3	3.86E-3	3.26E-3	3.29E-3	3.28E-3
0.75	3.15E-3	3.12E-3	3.14E-3	3.15E-3	3.16E-3	3.17E-3	3.14E-3	3.13E-3	3.74E-3	3.73E-3	3.21E-3	3.25E-3	3.24E-3
1.00	3.10E-3	3.09E-3	3.15E-3	3.13E-3	3.16E-3	3.15E-3	3.13E-3	3.12E-3	3.71E-3	3.71E-3	3.20E-3	3.23E-3	3.22E-3
1.50	3.03E-3	3.00E-3	3.02E-3	3.03E-3	3.05E-3	3.00E-3	3.00E-3	3.00E-3	3.57E-3	3.55E-3	3.08E-3	3.09E-3	3.09E-3
2.00	2.90E-3	2.87E-3	2.90E-3	2.91E-3	2.93E-3	2.89E-3	2.87E-3	2.84E-3	3.39E-3	3.35E-3	2.94E-3	2.94E-3	2.94E-3
3.00	2.69E-3	2.67E-3	2.69E-3	2.69E-3	2.69E-3	2.68E-3	2.65E-3	2.63E-3	3.06E-3	3.13E-3	2.72E-3	2.77E-3	2.75E-3
4.00	2.68E-3	2.66E-3	2.70E-3	2.71E-3	2.63E-3	2.64E-3	2.60E-3	2.56E-3	2.95E-3	3.01E-3	2.69E-3	2.74E-3	2.72E-3

Table B2. Continued.

Source Energy (MeV)	SAF (*Small Intestine Wall* ← *Stomach Contents*) in kg^{-1} for Electron												
	At Mean Position (cm) in the Small Intestine Wall Measured Outward from Contents-Wall Interface.										Average to the		
	0.025	**0.0625**	**0.085**	**0.1125**	**0.1475**	**0.1825**	**0.2125**	**0.2375**	**0.2625**	**0.2875**	**Wall**	**Contents**	**Wall+Contents**
0.01	3.12E-13[f]	5.11E-13[g]	4.83E-13[f]	1.83E-13[i]	1.87E-13[i]	3.04E-13[h]	3.76E-13[f]	4.53E-13[g]	1.13E-12[g]	1.49E-12[h]	4.40E-13[f]	1.36E-15[g]	1.39E-13[f]
0.015[b]	2.55E-10	2.63E-10	2.65E-10	2.71E-10	3.30E-10	3.26E-10	3.35E-10	3.47E-10	6.36E-10	7.01E-10	3.40E-10	1.15E-10	1.86E-10
0.02	5.88E-9	6.20E-9	6.12E-9	6.30E-9	6.83E-9	6.70E-9	6.59E-9	6.92E-9	1.18E-8	1.35E-8	7.13E-9	4.50E-9	5.33E-9
0.03	8.97E-8	8.80E-8	9.08E-8	9.08E-8	8.91E-8	9.30E-8	8.73E-8	9.89E-8	1.51E-7	1.58E-7	9.81E-8	8.91E-8	9.19E-8
0.05	6.74E-7	6.63E-7	6.96E-7	6.74E-7	6.69E-7	6.89E-7	6.75E-7	6.79E-7	9.79E-7	1.04E-6	7.14E-7	7.05E-7	7.08E-7
0.10	2.88E-6	2.91E-6	2.86E-6	2.90E-6	2.88E-6	2.98E-6	2.77E-6	2.81E-6	4.04E-6	3.97E-6	3.01E-6	3.00E-6	3.01E-6
0.20	7.57E-6	7.58E-6	7.40E-6	7.48E-6	7.33E-6	7.42E-6	7.55E-6	7.26E-6	9.78E-6	9.42E-6	7.70E-6	7.72E-6	7.72E-6
0.35	6.47E-6	6.46E-6	6.45E-6	6.44E-6	6.44E-6	6.45E-6	6.43E-6	6.44E-6	7.62E-6	7.62E-6	6.58E-6	6.61E-6	6.60E-6
0.50	1.81E-5	1.86E-5	1.82E-5	1.85E-5	1.77E-5	1.78E-5	1.84E-5	1.86E-5	2.25E-5	2.35E-5	1.88E-5	1.92E-5	1.91E-5
0.75	1.31E-5	1.31E-5	1.31E-5	1.30E-5	1.30E-5	1.30E-5	1.31E-5	1.30E-5	1.52E-5	1.52E-5	1.33E-5	1.35E-5	1.34E-5
1.00	3.53E-5	3.58E-5	3.76E-5	3.44E-5	3.44E-5	3.46E-5	3.49E-5	3.36E-5	4.22E-5	4.53E-5	3.60E-5	3.64E-5	3.62E-5
1.50	5.48E-5	5.04E-5	4.75E-5	5.36E-5	5.30E-5	5.29E-5	4.77E-5	5.19E-5	6.22E-5	6.91E-5	5.36E-5	5.46E-5	5.43E-5
2.00	6.99E-5	6.72E-5	7.08E-5	7.29E-5	7.64E-5	6.44E-5	7.09E-5	7.24E-5	8.82E-5	9.31E-5	7.29E-5	7.44E-5	7.39E-5
3.00	1.25E-4	1.09E-4	1.26E-4	1.30E-4	1.39E-4	1.42E-4	1.50E-4	1.42E-4	1.65E-4	2.34E-4	1.41E-4	1.11E-4	1.20E-4
4.00	2.28E-4	2.14E-4	1.69E-4	2.23E-4	2.62E-4	2.79E-4	2.68E-4	2.97E-4	5.40E-4	5.57E-4	2.79E-4	1.76E-4	2.08E-4
	SAF (*Small Intestine Wall* ← *Stomach Contents*) **in kg^{-1} for Photon**												
0.01	1.19E-6[e]	1.56E-6[e]	1.35E-6[e]	1.17E-6[g]	1.32E-6[g]	1.58E-6[g]	1.94E-6[g]	2.16E-6[g]	4.17E-6[g]	4.79E-6[g]	1.83E-6[f]	5.78E-7[c]	9.72E-7[d]
0.015[a]	2.38E-4	2.25E-4	2.17E-4	2.17E-4	2.16E-4	2.19E-4	2.50E-4	2.52E-4	4.56E-4	4.72E-4	2.56E-4	1.44E-4	1.79E-4
0.02	2.10E-3	2.11E-3	2.11E-3	2.16E-3	2.14E-3	2.23E-3	2.26E-3	2.21E-3	3.74E-3	3.81E-3	2.35E-3	2.04E-3	2.14E-3
0.03	8.45E-3	8.59E-3	8.33E-3	8.40E-3	8.35E-3	8.46E-3	8.54E-3	8.42E-3	1.28E-2	1.25E-2	8.92E-3	8.87E-3	8.88E-3
0.05	1.37E-2	1.38E-2	1.38E-2	1.38E-2	1.37E-2	1.37E-2	1.37E-2	1.36E-2	1.76E-2	1.76E-2	1.42E-2	1.43E-2	1.43E-2
0.10	1.20E-2	1.21E-2	1.20E-2	1.20E-2	1.20E-2	1.19E-2	1.20E-2	1.19E-2	1.45E-2	1.44E-2	1.23E-2	1.25E-2	1.24E-2
0.20	1.05E-2	1.05E-2	1.05E-2	1.05E-2	1.04E-2	1.05E-2	1.05E-2	1.04E-2	1.26E-2	1.26E-2	1.07E-2	1.09E-2	1.08E-2
0.35	1.02E-2	1.03E-2	1.03E-2	1.03E-2	1.02E-2	1.02E-2	1.02E-2	1.02E-2	1.23E-2	1.22E-2	1.05E-2	1.07E-2	1.06E-2
0.50	9.71E-3	9.67E-3	9.57E-3	9.60E-3	9.57E-3	9.62E-3	9.57E-3	9.56E-3	1.14E-2	1.15E-2	9.83E-3	1.01E-2	1.00E-2
0.75	9.37E-3	9.30E-3	9.23E-3	9.20E-3	9.16E-3	9.22E-3	9.16E-3	9.12E-3	1.09E-2	1.11E-2	9.43E-3	9.69E-3	9.61E-3
1.00	8.97E-3	8.90E-3	8.78E-3	8.78E-3	8.77E-3	8.80E-3	8.78E-3	8.70E-3	1.03E-2	1.06E-2	9.00E-3	9.29E-3	9.20E-3
1.50	8.30E-3	8.26E-3	8.16E-3	8.16E-3	8.12E-3	8.18E-3	8.15E-3	8.09E-3	9.52E-3	9.69E-3	8.34E-3	8.59E-3	8.51E-3
2.00	7.77E-3	7.72E-3	7.65E-3	7.66E-3	7.66E-3	7.69E-3	7.66E-3	7.59E-3	8.93E-3	9.12E-3	7.83E-3	8.06E-3	7.99E-3
3.00	6.88E-3	6.86E-3	6.84E-3	6.84E-3	6.87E-3	6.85E-3	6.82E-3	6.80E-3	8.14E-3	8.14E-3	6.99E-3	7.22E-3	7.15E-3
4.00	6.35E-3	6.35E-3	6.32E-3	6.32E-3	6.38E-3	6.35E-3	6.30E-3	6.28E-3	7.50E-3	7.50E-3	6.47E-3	6.69E-3	6.62E-3

Table B2. Continued.

SAF SAF (*Small Intestine Wall ← Small Intestine Contents*) **in kg^{-1}**															
Source Particle Energy (MeV)															
0.01			**0.015**			**0.02**			**0.03**			**0.05**			
Depth (cm)	**Electron SAF**	**Photon SAF**	**Depth (cm)**	**Electron SAF**	**Photon SAF**	**Depth (cm)**	**Electron SAF**	**Photon SAF**	**Depth (cm)**	**Electron SAF**	**Photon SAF**	**Depth (cm)**	**Electron SAF**	**Photon SAF**
2.5E-5	2.73E-1	3.33E-1	**5.0E-5**	2.30E-1[a]	3.81E-1	**1.0E-4**	1.82E-1[b]	3.90E-1	**1.0E-4**	3.15E-1[b]	3.02E-1	**0.0005**	2.30E-1[b]	1.60E-1
7.5E-5	1.43E-1[a]	3.32E-1	**1.5E-4**	1.12E-1[a]	3.79E-1	**3.5E-4**	7.81E-2[b]	3.91E-1	**3.5E-4**	1.57E-1[b]	3.01E-1	**0.0015**	8.85E-2[c]	1.60E-1
1.5E-4	3.72E-2[a]	3.31E-1	**2.5E-4**	4.59E-2[b]	3.78E-1	**7.5E-4**	6.00E-3[d]	3.90E-1	**7.5E-4**	5.45E-2[c]	3.01E-1	**0.0030**	1.74E-2[d]	1.60E-1
2.5E-4	8.77E-4[c]	3.30E-1	**3.5E-4**	1.23E-2[c]	3.78E-1	**1.5E-3**	4.04E-5	3.90E-1	**1.5E-3**	1.35E-3[g]	3.00E-1	**0.0050**	1.99E-4[e]	1.60E-1
3.5E-4	2.16E-5	3.30E-1	**5.0E-4**	1.02E-3[d]	3.77E-1	**3.0E-3**	3.45E-5	3.88E-1	**3.0E-3**	5.62E-5	3.00E-1	**0.0075**	8.76E-5	1.59E-1
5.0E-4	1.97E-5	3.28E-1	**7.0E-4**	2.98E-5	3.77E-1	**6.0E-3**	2.93E-5	3.86E-1	**6.0E-3**	5.14E-5	2.99E-1	**0.0105**	8.60E-5	1.59E-1
2.8E-3	1.21E-5	3.13E-1	**2.9E-3**	2.30E-5	3.73E-1	**0.0115**	2.44E-5	3.82E-1	**0.0115**	4.56E-5	2.98E-1	**0.0135**	8.29E-5	1.59E-1
0.0125	5.36E-6	2.71E-1	**0.0125**	1.39E-5	3.56E-1	**0.0200**	2.02E-5	3.77E-1	**0.0200**	4.04E-5	2.96E-1	**0.0200**	7.75E-5	1.59E-1
0.0300	2.48E-6	2.20E-1	**0.0300**	8.67E-6	3.34E-1	**0.0325**	1.66E-5	3.69E-1	**0.0325**	3.57E-5	2.93E-1	**0.0325**	7.07E-5	1.58E-1
0.0475	1.46E-6	1.84E-1	**0.0475**	6.38E-6	3.17E-1	**0.0475**	1.40E-5	3.62E-1	**0.0475**	3.21E-5	2.91E-1	**0.0475**	6.63E-5	1.57E-1
0.0575	1.14E-6	1.68E-1	**0.0575**	5.53E-6	3.08E-1	**0.0575**	1.27E-5	3.58E-1	**0.0575**	3.01E-5	2.89E-1	**0.0575**	6.36E-5	1.57E-1
0.0625	1.02E-6	1.60E-1	**0.0625**	5.20E-6	3.04E-1	**0.0625**	1.22E-5	3.57E-1	**0.0625**	2.95E-5	2.89E-1	**0.0625**	6.15E-5	1.57E-1
0.0675	9.12E-7	1.53E-1	**0.0675**	4.92E-6	3.00E-1	**0.0675**	1.17E-5	3.54E-1	**0.0675**	2.87E-5	2.89E-1	**0.0675**	6.20E-5	1.57E-1
0.0725	8.24E-7	1.47E-1	**0.0725**	4.65E-6	2.97E-1	**0.0725**	1.13E-5	3.52E-1	**0.0725**	2.80E-5	2.88E-1	**0.0725**	5.99E-5	1.56E-1
0.0775	7.43E-7	1.41E-1	**0.0775**	4.39E-6	2.93E-1	**0.0775**	1.09E-5	3.50E-1	**0.0775**	2.77E-5	2.88E-1	**0.0775**	6.04E-5	1.56E-1
0.0825	6.75E-7	1.35E-1	**0.0825**	4.18E-6	2.90E-1	**0.0825**	1.05E-5	3.49E-1	**0.0825**	2.66E-5	2.87E-1	**0.0825**	5.94E-5	1.56E-1
0.0875	6.16E-7	1.30E-1	**0.0875**	3.96E-6	2.86E-1	**0.0875**	1.02E-5	3.48E-1	**0.0875**	2.65E-5	2.87E-1	**0.0875**	5.80E-5	1.56E-1
0.0925	5.63E-7	1.25E-1	**0.0925**	3.80E-6	2.83E-1	**0.0925**	9.84E-6	3.46E-1	**0.0925**	2.60E-5	2.86E-1	**0.0925**	5.73E-5	1.56E-1
0.0975	5.16E-7	1.20E-1	**0.0975**	3.63E-6	2.80E-1	**0.0975**	9.56E-6	3.44E-1	**0.0975**	2.55E-5	2.86E-1	**0.0975**	5.68E-5	1.56E-1
0.1025	4.74E-7	1.15E-1	**0.1025**	3.47E-6	2.77E-1	**0.1025**	9.34E-6	3.42E-1	**0.1025**	2.50E-5	2.85E-1	**0.1025**	5.62E-5	1.55E-1
0.1075	4.36E-7	1.11E-1	**0.1075**	3.32E-6	2.74E-1	**0.1075**	9.07E-6	3.41E-1	**0.1075**	2.46E-5	2.84E-1	**0.1075**	5.52E-5	1.55E-1
0.1150	3.87E-7	1.05E-1	**0.1150**	3.12E-6	2.70E-1	**0.1150**	8.72E-6	3.38E-1	**0.1150**	2.41E-5	2.83E-1	**0.1150**	5.48E-5	1.55E-1
0.1350	2.88E-7	9.12E-2	**0.1350**	2.70E-6	2.59E-1	**0.1350**	7.95E-6	3.32E-1	**0.1350**	2.28E-5	2.81E-1	**0.1350**	5.28E-5	1.54E-1
0.1750	1.70E-7	7.04E-2	**0.1750**	2.10E-6	2.42E-1	**0.1750**	6.83E-6	3.22E-1	**0.1750**	2.08E-5	2.77E-1	**0.1750**	4.95E-5	1.53E-1
0.2250	9.69E-8	5.27E-2	**0.2250**	1.64E-6	2.24E-1	**0.2250**	5.88E-6	3.11E-1	**0.2250**	1.91E-5	2.73E-1	**0.2250**	4.68E-5	1.52E-1
0.2750	4.84E-8	3.35E-2	**0.2750**	1.11E-6	1.79E-1	**0.2750**	4.37E-6	2.66E-1	**0.2750**	1.52E-5	2.40E-1	**0.2750**	3.86E-5	1.37E-1
Wall	8.07E-5	1.08E-1	**Wall**	1.34E-4	2.61E-1	**Wall**	2.14E-4	3.30E-1	**Wall**	4.74E-4	2.78E-1	**Wall**	1.20E-3	1.53E-1

Table B2. Continued.

SAF (*Small Intestine Wall* ← *Small Intestine Contents*) **in kg^{-1}**														
Source Particle Energy (MeV)														
0.10			**0.20**			**0.35**			**0.50**			**0.75**		
Depth (cm)	**Electron SAF**	**Photon SAF**	**Depth (cm)**	**Electron SAF**	**Photon SAF**	**Depth (cm)**	**Electron SAF**	**Photon SAF**	**Depth (cm)**	**Electron SAF**	**Photon SAF**	**Depth (cm)**	**Electron SAF**	**Photon SAF**
0.0005	2.30E-1[a]	9.76E-2	**0.0025**	2.76E-1	9.12E-2	**0.0025**	3.10E-1	9.03E-2	**0.0050**	3.63E-1	8.89E-2	**0.005**	3.63E-1	8.52E-2
0.0015	1.88E-1[a]	9.77E-2	**0.0075**	1.92E-1	9.09E-2	**0.0075**	2.64E-1	9.01E-2	**0.0150**	2.95E-1	8.85E-2	**0.015**	3.22E-1	8.47E-2
0.0030	1.31E-1[a]	9.76E-2	**0.0125**	1.36E-1	9.07E-2	**0.0125**	2.30E-1	8.99E-2	**0.0250**	2.53E-1	8.80E-2	**0.025**	2.93E-1	8.43E-2
0.0050	8.09E-2[a]	9.74E-2	**0.0175**	8.69E-2	9.05E-2	**0.0175**	1.97E-1	8.96E-2	**0.0350**	2.03E-1	8.77E-2	**0.035**	2.62E-1	8.39E-2
0.0075	3.71E-2[a]	9.73E-2	**0.0225**	5.10E-2	9.03E-2	**0.0225**	1.70E-1	8.93E-2	**0.0450**	1.64E-1	8.73E-2	**0.045**	2.33E-1	8.36E-2
0.0105	7.45E-3[b]	9.73E-2	**0.0275**	2.64E-2	9.01E-2	**0.0275**	1.44E-1	8.90E-2	**0.0550**	1.31E-1	8.70E-2	**0.055**	2.08E-1	8.33E-2
0.0135	5.49E-4[c]	9.71E-2	**0.0325**	1.02E-2	9.00E-2	**0.0325**	1.22E-1	8.89E-2	**0.0650**	1.00E-1	8.68E-2	**0.065**	1.82E-1	8.31E-2
0.0200	1.41E-4	9.68E-2	**0.0375**	2.16E-3	8.98E-2	**0.0375**	1.02E-1	8.87E-2	**0.0750**	8.02E-2	8.66E-2	**0.075**	1.62E-1	8.29E-2
0.0325	1.31E-4	9.65E-2	**0.0425**	3.77E-4	8.97E-2	**0.0425**	7.99E-2	8.86E-2	**0.0850**	5.94E-2	8.62E-2	**0.085**	1.43E-1	8.25E-2
0.0475	1.25E-4	9.60E-2	**0.0475**	1.96E-4	8.95E-2	**0.0475**	6.33E-2	8.84E-2	**0.0950**	4.09E-2	8.60E-2	**0.095**	1.24E-1	8.22E-2
0.0575	1.21E-4	9.58E-2	**0.0525**	1.87E-4	8.93E-2	**0.0525**	4.96E-2	8.84E-2	**0.1050**	2.89E-2	8.57E-2	**0.105**	1.07E-1	8.20E-2
0.0625	1.22E-4	9.59E-2	**0.0575**	1.92E-4	8.92E-2	**0.0575**	3.71E-2	8.82E-2	**0.1150**	1.78E-2	8.55E-2	**0.115**	9.38E-2	8.18E-2
0.0675	1.19E-4	9.58E-2	**0.0625**	1.87E-4	8.91E-2	**0.0625**	2.63E-2	8.82E-2	**0.1250**	9.24E-3	8.53E-2	**0.125**	8.08E-2	8.16E-2
0.0725	1.16E-4	9.56E-2	**0.0675**	1.85E-4	8.90E-2	**0.0675**	1.75E-2	8.81E-2	**0.1350**	4.67E-3	8.51E-2	**0.135**	6.81E-2	8.13E-2
0.0775	1.15E-4	9.54E-2	**0.0725**	1.87E-4	8.89E-2	**0.0725**	1.10E-2	8.80E-2	**0.1450**	2.02E-3	8.50E-2	**0.145**	5.66E-2	8.12E-2
0.0825	1.16E-4	9.54E-2	**0.0775**	1.82E-4	8.87E-2	**0.0775**	6.09E-3	8.78E-2	**0.1550**	7.95E-4	8.46E-2	**0.155**	4.66E-2	8.09E-2
0.0875	1.15E-4	9.54E-2	**0.0825**	1.74E-4	8.85E-2	**0.0825**	3.13E-3	8.75E-2	**0.1650**	4.61E-4	8.45E-2	**0.165**	3.75E-2	8.07E-2
0.0925	1.11E-4	9.53E-2	**0.0875**	1.83E-4	8.85E-2	**0.0875**	1.61E-3	8.74E-2	**0.1750**	3.38E-4	8.42E-2	**0.175**	2.90E-2	8.05E-2
0.0975	1.13E-4	9.53E-2	**0.0925**	1.80E-4	8.84E-2	**0.0925**	7.82E-4	8.73E-2	**0.1850**	3.10E-4	8.41E-2	**0.185**	2.29E-2	8.03E-2
0.1025	1.11E-4	9.50E-2	**0.0975**	1.75E-4	8.83E-2	**0.0975**	3.64E-4	8.71E-2	**0.1950**	3.08E-4	8.40E-2	**0.195**	1.78E-2	8.02E-2
0.1075	1.11E-4	9.50E-2	**0.105**	1.79E-4	8.81E-2	**0.105**	2.67E-4	8.71E-2	**0.2050**	2.87E-4	8.37E-2	**0.205**	1.10E-2	8.01E-2
0.1150	1.10E-4	9.47E-2	**0.115**	1.70E-4	8.79E-2	**0.115**	2.44E-4	8.69E-2	**0.2150**	2.80E-4	8.36E-2	**0.215**	7.73E-3	7.99E-2
0.1350	1.07E-4	9.42E-2	**0.135**	1.71E-4	8.76E-2	**0.135**	2.38E-4	8.64E-2	**0.2250**	2.42E-4	8.34E-2	**0.225**	3.25E-3	7.98E-2
0.1750	1.03E-4	9.36E-2	**0.175**	1.65E-4	8.68E-2	**0.175**	2.32E-4	8.57E-2	**0.2350**	2.16E-4	8.33E-2	**0.235**	1.63E-3	7.96E-2
0.2250	9.82E-5	9.30E-2	**0.225**	1.59E-4	8.60E-2	**0.225**	2.25E-4	8.49E-2	**0.2450**	2.16E-4	8.31E-2	**0.245**	1.03E-3	7.94E-2
0.2750	8.35E-5	8.40E-2	**0.275**	1.39E-4	7.75E-2	**0.275**	1.96E-4	7.61E-2	**0.2750**	2.46E-4	7.48E-2	**0.275**	5.25E-4	7.16E-2
Wall	3.27E-3	9.34E-2	**Wall**	1.29E-2	8.67E-2	**Wall**	3.04E-2	8.56E-2	**Wall**	4.96E-2	8.42E-2	**Wall**	8.30E-2	8.06E-2

Table B2. Continued.

SAF SAF (*Small Intestine Wall* ← *Small Intestine Contents*) **in kg^{-1}**														
Source Particle Energy (MeV)														
1.00			**1.50**			**2.00**			**3.00**			**4.00**		
Depth (cm)	**Electron SAF**	**Photon SAF**	**Depth (cm)**	**Electron SAF**	**Photon SAF**	**Depth (cm)**	**Electron SAF**	**Photon SAF**	**Depth (cm)**	**Electron SAF**	**Photon SAF**	**Depth (cm)**	**Electron SAF**	**Photon SAF**
0.005	3.71E-1	8.10E-2	**0.005**	3.90E-1	7.43E-2	**0.005**	4.13E-1	6.86E-2	**0.005**	4.61E-1	6.03E-2	**0.005**	4.95E-1	5.52E-2
0.015	3.42E-1	8.06E-2	**0.015**	3.65E-1	7.39E-2	**0.015**	3.96E-1	6.82E-2	**0.015**	4.49E-1	6.01E-2	**0.015**	4.85E-1	5.49E-2
0.025	3.14E-1	8.02E-2	**0.025**	3.50E-1	7.35E-2	**0.025**	3.84E-1	6.79E-2	**0.025**	4.35E-1	5.97E-2	**0.025**	4.78E-1	5.46E-2
0.035	2.92E-1	7.99E-2	**0.035**	3.33E-1	7.31E-2	**0.035**	3.70E-1	6.76E-2	**0.035**	4.27E-1	5.94E-2	**0.035**	4.72E-1	5.43E-2
0.045	2.72E-1	7.96E-2	**0.045**	3.17E-1	7.28E-2	**0.045**	3.60E-1	6.73E-2	**0.045**	4.18E-1	5.92E-2	**0.045**	4.60E-1	5.41E-2
0.055	2.52E-1	7.93E-2	**0.055**	3.00E-1	7.26E-2	**0.055**	3.49E-1	6.70E-2	**0.055**	4.09E-1	5.90E-2	**0.055**	4.58E-1	5.39E-2
0.065	2.36E-1	7.91E-2	**0.065**	2.88E-1	7.24E-2	**0.065**	3.37E-1	6.69E-2	**0.065**	4.03E-1	5.90E-2	**0.065**	4.54E-1	5.37E-2
0.075	2.15E-1	7.88E-2	**0.075**	2.77E-1	7.22E-2	**0.075**	3.26E-1	6.67E-2	**0.075**	3.96E-1	5.88E-2	**0.075**	4.46E-1	5.36E-2
0.085	1.97E-1	7.85E-2	**0.085**	2.66E-1	7.19E-2	**0.085**	3.17E-1	6.64E-2	**0.085**	3.92E-1	5.85E-2	**0.085**	4.45E-1	5.34E-2
0.095	1.81E-1	7.83E-2	**0.095**	2.54E-1	7.17E-2	**0.095**	3.09E-1	6.62E-2	**0.095**	3.84E-1	5.84E-2	**0.095**	4.40E-1	5.32E-2
0.105	1.66E-1	7.81E-2	**0.105**	2.44E-1	7.14E-2	**0.105**	3.00E-1	6.60E-2	**0.105**	3.75E-1	5.81E-2	**0.105**	4.32E-1	5.31E-2
0.115	1.53E-1	7.79E-2	**0.115**	2.31E-1	7.12E-2	**0.115**	2.90E-1	6.59E-2	**0.115**	3.70E-1	5.80E-2	**0.115**	4.28E-1	5.29E-2
0.125	1.40E-1	7.77E-2	**0.125**	2.20E-1	7.11E-2	**0.125**	2.81E-1	6.58E-2	**0.125**	3.66E-1	5.78E-2	**0.125**	4.25E-1	5.29E-2
0.135	1.27E-1	7.75E-2	**0.135**	2.08E-1	7.09E-2	**0.135**	2.72E-1	6.56E-2	**0.135**	3.61E-1	5.76E-2	**0.135**	4.22E-1	5.27E-2
0.145	1.16E-1	7.73E-2	**0.145**	2.00E-1	7.08E-2	**0.145**	2.65E-1	6.54E-2	**0.145**	3.57E-1	5.76E-2	**0.145**	4.18E-1	5.26E-2
0.155	1.05E-1	7.71E-2	**0.155**	1.89E-1	7.05E-2	**0.155**	2.59E-1	6.52E-2	**0.155**	3.48E-1	5.74E-2	**0.155**	4.17E-1	5.24E-2
0.165	9.45E-2	7.69E-2	**0.165**	1.80E-1	7.04E-2	**0.165**	2.51E-1	6.50E-2	**0.165**	3.46E-1	5.72E-2	**0.165**	4.11E-1	5.23E-2
0.175	8.53E-2	7.67E-2	**0.175**	1.70E-1	7.02E-2	**0.175**	2.44E-1	6.49E-2	**0.175**	3.39E-1	5.71E-2	**0.175**	4.07E-1	5.22E-2
0.185	7.71E-2	7.66E-2	**0.185**	1.63E-1	7.01E-2	**0.185**	2.37E-1	6.48E-2	**0.185**	3.36E-1	5.69E-2	**0.185**	4.07E-1	5.21E-2
0.195	6.85E-2	7.64E-2	**0.195**	1.57E-1	7.00E-2	**0.195**	2.31E-1	6.47E-2	**0.195**	3.31E-1	5.69E-2	**0.195**	4.02E-1	5.21E-2
0.205	5.24E-2	7.63E-2	**0.205**	1.32E-1	6.98E-2	**0.205**	1.98E-1	6.45E-2	**0.205**	2.97E-1	5.68E-2	**0.205**	3.66E-1	5.20E-2
0.215	4.55E-2	7.61E-2	**0.215**	1.26E-1	6.97E-2	**0.215**	1.96E-1	6.44E-2	**0.215**	2.89E-1	5.67E-2	**0.215**	3.60E-1	5.19E-2
0.225	2.65E-2	7.59E-2	**0.225**	8.43E-2	6.95E-2	**0.225**	1.40E-1	6.43E-2	**0.225**	2.25E-1	5.65E-2	**0.225**	2.86E-1	5.18E-2
0.235	1.71E-2	7.58E-2	**0.235**	6.40E-2	6.94E-2	**0.235**	1.13E-1	6.42E-2	**0.235**	1.92E-1	5.64E-2	**0.235**	2.50E-1	5.17E-2
0.245	1.46E-2	7.57E-2	**0.245**	6.11E-2	6.93E-2	**0.245**	1.10E-1	6.40E-2	**0.245**	1.89E-1	5.63E-2	**0.245**	2.47E-1	5.15E-2
0.275	1.37E-2	6.81E-2	**0.275**	7.28E-2	6.24E-2	**0.275**	1.34E-1	5.76E-2	**0.275**	2.24E-1	5.06E-2	**0.275**	2.90E-1	4.65E-2
Wall	1.20E-1	7.67E-2	**Wall**	1.82E-1	7.02E-2	**0.005**	2.38E-1	6.49E-2	**Wall**	3.18E-1	5.71E-2	**Wall**	0.00E+0	5.22E-2

Table B2. Continued.

Source Energy (MeV)	**SAF** (*Small Intestine Wall* ← *Upper Large Intestine Contents*) **in kg^{-1} for Electron**												
	At Mean Position (cm) in the Small Intestine Wall Measured Outward from Contents-Wall Interface.										Average to the		
	0.025	**0.0625**	**0.085**	**0.1125**	**0.1475**	**0.1825**	**0.2125**	**0.2375**	**0.2625**	**0.2875**	**Wall**	**Contents**	**Wall+Contents**
0.01	2.73E-8	2.72E-8	2.72E-8	2.75E-8	2.76E-8	2.78E-8	2.79E-8	2.82E-8	2.82E-8	2.82E-8	2.76E-8	2.73E-8	2.74E-8
0.015	4.61E-7	4.62E-7	4.64E-7	4.67E-7	4.69E-7	4.73E-7	4.75E-7	4.80E-7	4.71E-7	4.74E-7	4.69E-7	4.52E-7	4.57E-7
0.02	2.01E-6	2.01E-6	2.02E-6	2.03E-6	2.04E-6	2.05E-6	2.06E-6	2.07E-6	1.98E-6	1.99E-6	2.03E-6	1.94E-6	1.97E-6
0.03	8.16E-6	8.20E-6	8.21E-6	8.24E-6	8.27E-6	8.32E-6	8.34E-6	8.37E-6	7.83E-6	7.86E-6	8.21E-6	7.88E-6	7.99E-6
0.05	2.35E-5	2.36E-5	2.36E-5	2.37E-5	2.37E-5	2.38E-5	2.39E-5	2.39E-5	2.21E-5	2.22E-5	2.35E-5	2.28E-5	2.30E-5
0.10	5.50E-5	5.51E-5	5.51E-5	5.52E-5	5.53E-5	5.55E-5	5.56E-5	5.57E-5	5.11E-5	5.12E-5	5.48E-5	5.34E-5	5.39E-5
0.20	9.68E-5	9.69E-5	9.70E-5	9.72E-5	9.74E-5	9.76E-5	9.77E-5	9.79E-5	8.98E-5	8.99E-5	9.65E-5	9.44E-5	9.50E-5
0.35	1.43E-4	1.43E-4	1.43E-4	1.43E-4	1.44E-4	1.44E-4	1.44E-4	1.44E-4	1.32E-4	1.32E-4	1.42E-4	1.40E-4	1.40E-4
0.50	1.82E-4	1.83E-4	1.83E-4	1.83E-4	1.83E-4	1.83E-4	1.84E-4	1.84E-4	1.69E-4	1.69E-4	1.81E-4	1.78E-4	1.79E-4
0.75	2.45E-4	2.45E-4	2.45E-4	2.46E-4	2.46E-4	2.46E-4	2.47E-4	2.47E-4	2.27E-4	2.27E-4	2.44E-4	2.40E-4	2.41E-4
1.00	6.72E-3	6.73E-3	6.72E-3	6.69E-3	6.72E-3	6.70E-3	6.72E-3	6.81E-3	6.86E-3	6.84E-3	6.74E-3	6.72E-3	6.73E-3
1.50	2.68E-2	2.67E-2	2.68E-2	2.69E-2	2.71E-2	2.72E-2	2.74E-2	2.77E-2	2.72E-2	2.78E-2	2.71E-2	2.67E-2	2.68E-2
2.00	5.08E-2	5.09E-2	5.10E-2	5.14E-2	5.18E-2	5.27E-2	5.31E-2	5.36E-2	5.23E-2	5.30E-2	5.20E-2	5.02E-2	5.08E-2
3.00	9.93E-2	9.98E-2	1.00E-1	1.01E-1	1.02E-1	1.03E-1	1.03E-1	1.03E-1	9.99E-2	1.00E-1	1.01E-1	9.58E-2	9.75E-2
4.00	1.37E-1	1.39E-1	1.39E-1	1.40E-1	1.41E-1	1.42E-1	1.43E-1	1.44E-1	1.36E-1	1.37E-1	1.40E-1	1.32E-1	1.35E-1
	SAF (*Small Intestine Wall* ← *Upper Large Intestine Contents*) **in kg^{-1} for Photon**												
0.01	1.35E-2	1.35E-2	1.36E-2	1.36E-2	1.37E-2	1.38E-2	1.39E-2	1.40E-2	1.39E-2	1.40E-2	1.37E-2	1.33E-2	1.35E-2
0.015	9.31E-2	9.36E-2	9.39E-2	9.43E-2	9.48E-2	9.55E-2	9.60E-2	9.64E-2	9.17E-2	9.20E-2	9.43E-2	8.96E-2	9.11E-2
0.02	1.72E-1	1.72E-1	1.72E-1	1.72E-1	1.72E-1	1.72E-1	1.72E-1	1.72E-1	1.72E-1	1.72E-1	1.72E-1	1.72E-1	1.72E-1
0.03	1.88E-1	1.88E-1	1.88E-1	1.88E-1	1.89E-1	1.89E-1	1.89E-1	1.89E-1	1.72E-1	1.72E-1	1.87E-1	1.83E-1	1.84E-1
0.05	1.20E-1	1.20E-1	1.20E-1	1.20E-1	1.20E-1	1.20E-1	1.20E-1	1.20E-1	1.10E-1	1.10E-1	1.19E-1	1.17E-1	1.18E-1
0.10	7.43E-2	7.44E-2	7.44E-2	7.45E-2	7.45E-2	7.46E-2	7.46E-2	7.47E-2	6.87E-2	6.87E-2	7.38E-2	7.32E-2	7.34E-2
0.20	6.74E-2	6.74E-2	6.75E-2	6.75E-2	6.76E-2	6.77E-2	6.77E-2	6.78E-2	6.23E-2	6.23E-2	6.70E-2	6.64E-2	6.66E-2
0.35	6.57E-2	6.58E-2	6.58E-2	6.59E-2	6.59E-2	6.60E-2	6.61E-2	6.61E-2	6.07E-2	6.07E-2	6.53E-2	6.48E-2	6.49E-2
0.50	6.42E-2	6.42E-2	6.43E-2	6.43E-2	6.44E-2	6.45E-2	6.45E-2	6.46E-2	5.92E-2	5.92E-2	6.38E-2	6.32E-2	6.34E-2
0.75	6.11E-2	6.11E-2	6.11E-2	6.12E-2	6.13E-2	6.13E-2	6.14E-2	6.15E-2	5.64E-2	5.63E-2	6.07E-2	7.46E-2	7.50E-2
1.00	5.79E-2	5.80E-2	5.80E-2	5.80E-2	5.81E-2	5.82E-2	5.82E-2	5.83E-2	5.35E-2	5.36E-2	5.76E-2	5.71E-2	5.72E-2
1.50	5.29E-2	5.30E-2	5.30E-2	5.31E-2	5.31E-2	5.32E-2	5.32E-2	5.33E-2	4.89E-2	4.90E-2	5.26E-2	5.22E-2	5.23E-2
2.00	4.89E-2	4.90E-2	4.90E-2	4.91E-2	4.91E-2	4.92E-2	4.91E-2	4.93E-2	4.52E-2	4.53E-2	4.87E-2	4.82E-2	4.83E-2
3.00	4.31E-2	4.32E-2	4.32E-2	4.32E-2	4.33E-2	4.33E-2	4.32E-2	4.33E-2	3.98E-2	3.98E-2	4.28E-2	4.25E-2	4.26E-2
4.00	3.95E-2	3.97E-2	3.96E-2	3.96E-2	3.97E-2	3.97E-2	3.97E-2	3.97E-2	3.66E-2	3.65E-2	3.93E-2	3.90E-2	3.91E-2

Table B2. Continued.

Source Energy (MeV)	**SAF** (*Small Intestine Wall* ← *Lower Large Intestine Contents*) **in kg^{-1} for Electron**												
	At Mean Position (cm) in the Small Intestine Wall Measured Outward from Contents-Wall Interface.										Average to the		
	0.025	**0.0625**	**0.085**	**0.1125**	**0.1475**	**0.1825**	**0.2125**	**0.2375**	**0.2625**	**0.2875**	**Wall**	**Contents**	**Wall+Contents**
0.01[a]	1.02E-9	1.02E-9	1.02E-9	1.02E-9	1.02E-9	1.02E-9	1.02E-9	1.02E-9	1.03E-9	1.05E-9	1.02E-9	1.01E-9	1.01E-9
0.015	2.00E-8	2.00E-8	2.00E-8	2.04E-8	2.06E-8	2.06E-8	2.09E-8	2.10E-8	2.29E-8	2.35E-8	2.07E-8	1.92E-8	1.97E-8
0.02	9.44E-8	9.50E-8	9.57E-8	9.67E-8	9.71E-8	9.80E-8	9.85E-8	9.99E-8	1.11E-7	1.14E-7	9.86E-8	9.13E-8	9.36E-8
0.03	4.07E-7	4.11E-7	4.11E-7	4.12E-7	4.15E-7	4.18E-7	4.19E-7	4.21E-7	4.75E-7	4.79E-7	4.21E-7	3.95E-7	4.03E-7
0.05	1.31E-6	1.32E-6	1.32E-6	1.32E-6	1.33E-6	1.33E-6	1.34E-6	1.34E-6	1.52E-6	1.52E-6	1.35E-6	1.28E-6	1.30E-6
0.10	3.55E-6	3.55E-6	3.55E-6	3.56E-6	3.58E-6	3.57E-6	3.57E-6	3.58E-6	3.97E-6	3.98E-6	3.61E-6	3.46E-6	3.51E-6
0.20	7.25E-6	7.28E-6	7.27E-6	7.27E-6	7.28E-6	7.31E-6	7.30E-6	7.32E-6	8.00E-6	8.00E-6	7.36E-6	7.12E-6	7.20E-6
0.35	1.19E-5	1.19E-5	1.19E-5	1.20E-5	1.20E-5	1.20E-5	1.20E-5	1.20E-5	1.29E-5	1.30E-5	1.21E-5	1.18E-5	1.19E-5
0.50	1.63E-5	1.63E-5	1.63E-5	1.64E-5	1.64E-5	1.64E-5	1.64E-5	1.64E-5	1.75E-5	1.75E-5	1.65E-5	1.61E-5	1.62E-5
0.75	2.29E-5	2.29E-5	2.29E-5	2.29E-5	2.30E-5	2.30E-5	2.30E-5	2.31E-5	2.45E-5	2.44E-5	2.31E-5	2.25E-5	2.27E-5
1.00	2.21E-4	2.25E-4	2.22E-4	2.22E-4	2.16E-4	2.29E-4	2.24E-4	2.22E-4	2.24E-4	2.24E-4	2.23E-4	2.22E-4	2.22E-4
1.50	1.08E-3	1.08E-3	1.10E-3	1.10E-3	1.12E-3	1.12E-3	1.10E-3	1.10E-3	1.12E-3	1.28E-3	1.11E-3	1.07E-3	1.09E-3
2.00	2.21E-3	2.22E-3	2.26E-3	2.36E-3	2.37E-3	2.39E-3	2.39E-3	2.47E-3	2.83E-3	2.72E-3	2.38E-3	2.19E-3	2.25E-3
3.00	4.89E-3	5.08E-3	5.14E-3	5.11E-3	5.10E-3	5.17E-3	5.20E-3	5.24E-3	5.91E-3	6.12E-3	5.20E-3	4.55E-3	4.76E-3
4.00	7.17E-3	7.38E-3	7.48E-3	7.60E-3	7.58E-3	7.73E-3	7.67E-3	7.83E-3	8.84E-3	8.79E-3	7.68E-3	6.76E-3	7.05E-3
	SAF (*Small Intestine Wall* ← *Lower Large Intestine Contents*) **in kg^{-1} for Photon**												
0.01	5.53E-4	5.55E-4	5.58E-4	5.61E-4	5.66E-4	5.73E-4	5.81E-4	5.90E-4	6.43E-4	6.64E-4	5.76E-4	5.42E-4	5.53E-4
0.015	4.65E-3	4.68E-3	4.70E-3	4.72E-3	4.75E-3	4.79E-3	4.83E-3	4.86E-3	5.45E-3	5.53E-3	4.83E-3	4.41E-3	4.54E-3
0.02	8.99E-3	9.01E-3	9.03E-3	9.07E-3	9.11E-3	9.14E-3	9.17E-3	9.22E-3	1.05E-2	1.06E-2	9.25E-3	8.72E-3	8.89E-3
0.03	1.09E-2	1.09E-2	1.09E-2	1.09E-2	1.09E-2	1.09E-2	1.10E-2	1.10E-2	1.25E-2	1.25E-2	1.11E-2	1.07E-2	1.08E-2
0.05	1.04E-2	1.04E-2	1.04E-2	1.04E-2	1.04E-2	1.04E-2	1.04E-2	1.04E-2	1.11E-2	1.11E-2	1.05E-2	1.02E-2	1.03E-2
0.10	8.84E-3	8.83E-3	8.85E-3	8.84E-3	8.84E-3	8.85E-3	8.86E-3	8.87E-3	9.19E-3	9.17E-3	8.88E-3	8.74E-3	8.79E-3
0.20	8.08E-3	8.08E-3	8.09E-3	8.06E-3	8.07E-3	8.08E-3	8.10E-3	8.12E-3	8.40E-3	8.41E-3	8.12E-3	8.02E-3	8.05E-3
0.35	7.83E-3	7.83E-3	7.85E-3	7.82E-3	7.83E-3	7.85E-3	7.85E-3	7.87E-3	8.18E-3	8.19E-3	7.88E-3	7.76E-3	7.80E-3
0.50	7.65E-3	7.64E-3	7.65E-3	7.62E-3	7.63E-3	7.63E-3	7.65E-3	7.66E-3	7.95E-3	7.98E-3	7.68E-3	7.56E-3	7.60E-3
0.75	7.30E-3	7.32E-3	7.32E-3	7.28E-3	7.28E-3	7.34E-3	7.34E-3	7.34E-3	7.63E-3	7.67E-3	7.35E-3	7.23E-3	7.27E-3
1.00	7.01E-3	7.02E-3	7.04E-3	7.00E-3	7.00E-3	7.04E-3	7.05E-3	7.04E-3	7.31E-3	7.36E-3	7.06E-3	6.94E-3	6.98E-3
1.50	6.60E-3	6.61E-3	6.66E-3	6.65E-3	6.63E-3	6.65E-3	6.63E-3	6.65E-3	6.84E-3	6.95E-3	6.66E-3	6.58E-3	6.61E-3
2.00	6.23E-3	6.25E-3	6.29E-3	6.26E-3	6.26E-3	6.26E-3	6.27E-3	6.27E-3	6.44E-3	6.52E-3	6.28E-3	6.20E-3	6.22E-3
3.00	6.55E-3	6.56E-3	6.60E-3	6.58E-3	6.56E-3	6.58E-3	6.59E-3	6.60E-3	6.80E-3	6.87E-3	6.60E-3	6.53E-3	6.55E-3
4.00	5.18E-3	5.24E-3	5.24E-3	5.19E-3	5.18E-3	5.23E-3	5.36E-3	5.32E-3	5.50E-3	5.60E-3	5.27E-3	5.17E-3	5.20E-3

Table B2. Continued.

Source Energy (MeV)	**SAF** (*Upper Large Intestine Wall* ← *Esophagus Contents*) **in kg^{-1} for Electron**							
	At Mean Position (cm) in the Upper Large Intestine Wall Measured Outward from Contents-Wall Interface.							Average to the
	0.02	**0.06**	**0.1**	**0.14**	**0.1775**	**0.2125**	**0.24**	**Wall**
0.01	0.0	0.0	0.0	0.0	0.0	0.0	0.0	0.0
0.015	0.0	0.0	0.0	0.0	0.0	0.0	0.0	0.0
0.02	0.0	0.0	0.0	0.0	0.0	0.0	0.0	0.0
0.03[g]	2.07E-10	2.03E-10	1.98E-10	1.94E-10	1.90E-10	0.0	0.0	1.80E-10
0.05[b]	2.80E-08	2.70E-08	2.74E-08	2.99E-08	2.97E-08	2.81E-09	4.04E-09	2.66E-08
0.10	3.30E-07	3.24E-07	3.20E-07	3.27E-07	3.19E-07	3.87E-08	4.19E-08	3.04E-07
0.20	1.17E-06	1.18E-06	1.16E-06	1.15E-06	1.17E-06	1.60E-07	1.57E-07	1.10E-06
0.35	2.45E-06	2.44E-06	2.42E-06	2.44E-06	2.42E-06	3.49E-07	3.45E-07	2.30E-06
0.50	3.86E-06	3.83E-06	3.80E-06	3.81E-06	3.83E-06	6.03E-07	5.88E-07	3.62E-06
0.75	5.99E-06	5.87E-06	5.80E-06	5.81E-06	5.88E-06	9.54E-07	9.25E-07	5.57E-06
1.00	8.00E-06	7.95E-06	7.99E-06	7.94E-06	7.91E-06	1.28E-06	1.26E-06	7.95E-06
1.50	1.31E-05	1.31E-05	1.32E-05	1.31E-05	1.30E-05	2.19E-06	2.19E-06	1.31E-05
2.00	1.89E-05	1.92E-05	1.89E-05	1.91E-05	1.89E-05	3.28E-06	3.23E-06	1.90E-05
3.00	2.98E-05	3.06E-05	2.98E-05	3.02E-05	3.00E-05	5.18E-06	5.08E-06	3.00E-05
4.00	4.21E-05	4.25E-05	4.20E-05	4.22E-05	4.15E-05	8.37E-06	8.06E-06	4.21E-05
	SAF (*Upper Large Intestine Wall* ← *Esophagus Contents*) **in kg^{-1} for Photon**							
0.01	0.0	0.0	0.0	0.0	0.0	0.0	0.0	0.0
0.015	0.0	0.0	0.0	0.0	0.0	0.0	0.0	0.0
0.02	0.0	0.0	0.0	0.0	0.0	0.0	0.0	0.0
0.03[a]	2.59E-04	2.58E-04	2.54E-04	2.65E-04	2.58E-04	1.32E-05	1.34E-05	2.59E-04
0.05	1.91E-03	1.92E-03	1.94E-03	1.95E-03	1.93E-03	2.18E-04	2.10E-04	1.93E-03
0.10	2.78E-03	2.81E-03	2.80E-03	2.78E-03	2.79E-03	4.10E-04	4.17E-04	2.79E-03
0.20	2.81E-03	2.76E-03	2.77E-03	2.76E-03	2.77E-03	4.33E-04	4.48E-04	2.77E-03
0.35	2.79E-03	2.79E-03	2.80E-03	2.81E-03	2.82E-03	5.17E-04	5.12E-04	2.80E-03
0.50	2.78E-03	2.78E-03	2.82E-03	2.78E-03	2.80E-03	5.12E-04	5.11E-04	2.79E-03
0.75	2.87E-03	2.78E-03	2.76E-03	2.76E-03	2.75E-03	5.57E-04	5.31E-04	2.78E-03
1.00	2.86E-03	2.80E-03	2.75E-03	2.78E-03	2.74E-03	5.50E-04	5.25E-04	2.78E-03
1.50	2.79E-03	2.81E-03	2.74E-03	2.72E-03	2.71E-03	5.11E-04	5.00E-04	2.74E-03
2.00	2.69E-03	2.60E-03	2.62E-03	2.62E-03	2.55E-03	4.94E-04	4.82E-04	2.61E-03
3.00	2.43E-03	2.41E-03	2.48E-03	2.51E-03	2.43E-03	5.48E-04	5.59E-04	2.45E-03
4.00	2.49E-03	2.39E-03	2.47E-03	2.42E-03	2.42E-03	4.79E-04	5.10E-04	2.43E-03

Table B2. Continued.

Source Energy (MeV)	SAF (*Upper Large Intestine Wall* ← *Stomach Contents*) in kg^{-1} for Electron										
	At Mean Position (cm) in the Upper Large Intestine Wall Measured Outward from Contents-Wall Interface.										Average to the
	0.025	**0.06**	**0.075**	**0.085**	**0.1**	**0.13**	**0.1625**	**0.185**	**0.21**	**0.2375**	**Wall**
0.01	0.0	0.0	0.0	0.0	0.0	0.0	0.0	0.0	0.0	0.0	0.0
0.015	0.0	0.0	0.0	0.0	0.0	0.0	0.0	0.0	0.0	0.0	0.0
0.02[a]	4.11E-10	4.10E-10	4.15E-10	4.00E-10	3.97E-10	4.04E-10	4.34E-10	4.23E-10	0.0	0.0	3.74E-10
0.03	3.38E-08	3.43E-08	3.46E-08	3.49E-08	3.48E-08	3.49E-08	3.51E-08	3.47E-08	9.41E-10[a]	8.22E-10[a]	3.15E-08
0.05	5.06E-07	5.07E-07	5.11E-07	5.09E-07	5.11E-07	5.09E-07	5.14E-07	5.14E-07	2.56E-08	2.63E-08	4.69E-07
0.10	2.50E-06	2.49E-06	2.51E-06	2.50E-06	2.50E-06	2.52E-06	2.51E-06	2.52E-06	1.90E-07	1.91E-07	2.32E-06
0.20	6.90E-06	6.88E-06	6.93E-06	6.90E-06	6.89E-06	6.91E-06	6.89E-06	6.87E-06	6.23E-07	6.14E-07	6.41E-06
0.35	1.26E-05	1.25E-05	1.26E-05	1.26E-05	1.26E-05	1.26E-05	1.26E-05	1.28E-05	1.26E-06	1.28E-06	1.17E-05
0.50	1.76E-05	1.76E-05	1.76E-05	1.77E-05	1.76E-05	1.76E-05	1.76E-05	1.76E-05	1.88E-06	1.83E-06	1.64E-05
0.75	2.52E-05	2.52E-05	2.54E-05	2.55E-05	2.54E-05	2.53E-05	2.54E-05	2.54E-05	2.68E-06	2.70E-06	2.36E-05
1.00	3.20E-5	3.57E-5	3.33E-5	3.18E-5[a]	3.17E-5	3.42E-5	3.24E-5	3.53E-5	3.94E-6[a]	3.97E-6[a]	3.33E-5
1.50	5.13E-5	5.14E-5	5.15E-5	5.15E-5	5.13E-5	5.13E-5	5.16E-5	5.15E-5	6.17E-6	6.17E-6	5.14E-5
2.00	6.92E-05	6.91E-05	6.89E-05	6.90E-05	6.88E-05	6.91E-05	6.91E-05	6.92E-05	8.43E-06	8.50E-06	6.90E-05
3.00	1.05E-04	1.05E-04	1.05E-04	1.04E-04	1.04E-04	1.04E-04	1.04E-04	1.03E-04	1.35E-05	1.36E-05	1.04E-04
4.00	1.38E-04	1.39E-04	1.39E-04	1.40E-04	1.39E-04	1.39E-04	1.39E-04	1.39E-04	1.82E-05	1.82E-05	1.39E-04
	SAF (*Upper Large Intestine Wall* ← *Stomach Contents*) **in kg^{-1} for Photon**										
0.01	0.0	0.0	0.0	0.0	0.0	0.0	0.0	0.0	0.0	0.0	0.0
0.015[b]	5.09E-06	5.08E-06	5.31E-06	5.25E-06	7.45E-06	5.87E-06	6.21E-06	5.71E-06	0.00E+00	0.00E+00	5.19E-06
0.02	5.33E-04	5.36E-04	5.28E-04	5.22E-04	5.31E-04	5.44E-04	5.44E-04	5.51E-04	6.73E-06[b]	6.88E-06[b]	4.89E-04
0.03	6.56E-03	6.60E-03	6.51E-03	6.55E-03	6.61E-03	6.46E-03	6.48E-03	6.52E-03	2.50E-04	2.52E-04	5.98E-03
0.05	1.34E-02	1.35E-02	1.34E-02	1.35E-02	1.34E-02	1.34E-02	1.34E-02	1.34E-02	1.10E-03	1.09E-03	1.24E-02
0.10	1.18E-02	1.19E-02	1.19E-02	1.18E-02	1.18E-02	1.19E-02	1.19E-02	1.19E-02	1.39E-03	1.40E-03	1.11E-02
0.20	1.03E-02	1.03E-02	1.03E-02	1.03E-02	1.03E-02	1.03E-02	1.03E-02	1.03E-02	1.30E-03	1.30E-03	9.67E-03
0.35	9.97E-03	9.99E-03	9.92E-03	9.87E-03	9.93E-03	9.82E-03	9.87E-03	9.88E-03	1.27E-03	1.26E-03	9.30E-03
0.50	9.59E-03	9.65E-03	9.50E-03	9.49E-03	9.51E-03	9.61E-03	9.70E-03	9.65E-03	1.38E-03	1.33E-03	9.06E-03
0.75	9.30E-03	9.36E-03	9.27E-03	9.29E-03	9.28E-03	9.35E-03	9.44E-03	9.40E-03	1.41E-03	1.34E-03	8.83E-03
1.00	9.02E-03	9.06E-03	8.92E-03	8.93E-03	8.85E-03	8.97E-03	9.12E-03	9.01E-03	1.41E-03	1.32E-03	8.51E-03
1.50	8.33E-03	8.32E-03	8.23E-03	8.28E-03	8.31E-03	8.36E-03	8.52E-03	8.51E-03	1.48E-03	1.38E-03	7.96E-03
2.00	7.61E-03	7.63E-03	7.48E-03	7.58E-03	7.51E-03	7.57E-03	7.65E-03	7.65E-03	1.27E-03	1.21E-03	7.21E-03
3.00	6.90E-03	6.76E-03	6.65E-03	6.61E-03	6.73E-03	6.78E-03	6.80E-03	6.91E-03	1.07E-03	1.02E-03	6.44E-03
4.00	6.36E-03	6.32E-03	6.25E-03	6.24E-03	6.31E-03	6.31E-03	6.31E-03	6.45E-03	9.90E-04	9.48E-04	5.99E-03

Table B2. Continued.

SAF (*Upper Large Intestine Wall* ← *Small Intestine Contents*) **in kg^{-1}**														
Source Particle Energy (MeV)														
0.01			**0.015**			**0.02**			**0.03**			**0.05**		
Depth (cm)	**Electron SAF[c]**	**Photon SAF[a]**	**Depth (cm)**	**Electron SAF[a]**	**Photon SAF**	**Depth (cm)**	**Electron SAF**	**Photon SAF**	**Depth (cm)**	**Electron SAF**	**Photon SAF**	**Depth (cm)**	**Electron SAF**	**Photon SAF**
0.0025	1.32E-9	2.16E-03	**0.0025**	1.07E-07	3.91E-02	**0.0025**	8.05E-07	9.68E-02	**0.0025**	3.37E-06	1.30E-01	**0.0025**	1.34E-05	9.35E-02
0.0075	1.38E-9	2.18E-03	**0.0075**	1.10E-07	3.91E-02	**0.0075**	8.02E-07	9.68E-02	**0.0075**	3.34E-06	1.30E-01	**0.0075**	1.33E-05	9.38E-02
0.0125	1.43E-9	2.21E-03	**0.0125**	1.10E-07	3.94E-02	**0.0125**	8.22E-07	9.95E-02	**0.0125**	3.38E-06	1.32E-01	**0.0125**	1.34E-05	9.47E-02
0.0175	1.49E-9	2.24E-03	**0.0175**	1.12E-07	3.95E-02	**0.0175**	8.28E-07	9.80E-02	**0.0175**	3.45E-06	1.32E-01	**0.0175**	1.33E-05	9.44E-02
0.0225	1.53E-9	2.27E-03	**0.0225**	1.12E-07	4.00E-02	**0.0225**	8.29E-07	9.70E-02	**0.0225**	3.38E-06	1.33E-01	**0.0225**	1.32E-05	9.42E-02
0.0275	1.59E-9	2.31E-03	**0.0275**	1.16E-07	3.98E-02	**0.0275**	8.51E-07	9.81E-02	**0.0275**	3.36E-06	1.32E-01	**0.0275**	1.32E-05	9.42E-02
0.0325	1.65E-9	2.35E-03	**0.0325**	1.16E-07	4.04E-02	**0.0325**	8.38E-07	9.91E-02	**0.0325**	3.45E-06	1.33E-01	**0.0325**	1.35E-05	9.45E-02
0.0375	1.71E-9	2.39E-03	**0.0375**	1.16E-07	4.01E-02	**0.0375**	8.46E-07	9.81E-02	**0.0375**	3.41E-06	1.33E-01	**0.0375**	1.36E-05	9.45E-02
0.0425	1.77E-9	2.43E-03	**0.0425**	1.17E-07	4.02E-02	**0.0425**	8.46E-07	9.78E-02	**0.0425**	3.39E-06	1.32E-01	**0.0425**	1.35E-05	9.44E-02
0.0475	1.85E-9	2.47E-03	**0.0475**	1.18E-07	4.02E-02	**0.0475**	8.49E-07	9.92E-02	**0.0475**	3.55E-06	1.31E-01	**0.0475**	1.34E-05	9.38E-02
0.0525	1.95E-9	2.51E-03	**0.0525**	1.19E-07	4.02E-02	**0.0525**	8.49E-07	9.84E-02	**0.0525**	3.50E-06	1.30E-01	**0.0525**	1.34E-05	9.36E-02
0.0575	2.02E-9	2.56E-03	**0.0575**	1.21E-07	4.04E-02	**0.0575**	8.53E-07	9.84E-02	**0.0575**	3.48E-06	1.30E-01	**0.0575**	1.33E-05	9.33E-02
0.0625	2.10E-9	2.60E-03	**0.0625**	1.22E-07	4.10E-02	**0.0625**	8.59E-07	9.83E-02	**0.0625**	3.54E-06	1.31E-01	**0.0625**	1.33E-05	9.36E-02
0.0675	2.21E-9	2.66E-03	**0.0675**	1.30E-07	4.12E-02	**0.0675**	8.61E-07	9.85E-02	**0.0675**	3.51E-06	1.31E-01	**0.0675**	1.34E-05	9.38E-02
0.0725	2.32E-9	2.71E-03	**0.0725**	1.31E-07	4.17E-02	**0.0725**	8.88E-07	9.89E-02	**0.0725**	3.48E-06	1.32E-01	**0.0725**	1.34E-05	9.43E-02
0.0775	2.44E-9	2.77E-03	**0.0775**	1.30E-07	4.25E-02	**0.0775**	8.79E-07	1.01E-01	**0.0775**	3.58E-06	1.33E-01	**0.0775**	1.38E-05	9.39E-02
0.0825	2.57E-9	2.83E-03	**0.0825**	1.33E-07	4.38E-02	**0.0825**	8.79E-07	1.04E-01	**0.0825**	3.57E-06	1.32E-01	**0.0825**	1.37E-05	9.42E-02
0.0875	2.70E-9	2.89E-03	**0.0875**	1.33E-07	4.30E-02	**0.0875**	8.83E-07	1.01E-01	**0.0875**	3.55E-06	1.32E-01	**0.0875**	1.36E-05	9.40E-02
0.0925	2.83E-9	2.96E-03	**0.0925**	1.34E-07	4.29E-02	**0.0925**	8.86E-07	1.01E-01	**0.0925**	3.53E-06	1.30E-01	**0.0925**	1.37E-05	9.35E-02
0.0975	2.97E-9	3.02E-03	**0.0975**	1.35E-07	4.28E-02	**0.0975**	8.89E-07	9.99E-02	**0.0975**	3.63E-06	1.30E-01	**0.0975**	1.36E-05	9.33E-02
0.1025	3.10E-9	3.10E-03	**0.1025**	1.37E-07	4.31E-02	**0.1025**	9.15E-07	1.01E-01	**0.1025**	3.63E-06	1.30E-01	**0.1025**	1.36E-05	9.35E-02
0.1075	3.27E-9	3.17E-03	**0.1075**	1.39E-07	4.41E-02	**0.1075**	9.11E-07	1.07E-01	**0.1075**	3.62E-06	1.34E-01	**0.1075**	1.38E-05	9.40E-02
0.1125	3.44E-9	3.24E-03	**0.1125**	1.40E-07	4.45E-02	**0.1125**	9.15E-07	1.08E-01	**0.1125**	3.61E-06	1.34E-01	**0.1125**	1.38E-05	9.40E-02
0.1175	3.60E-9	3.32E-03	**0.1175**	1.42E-07	4.42E-02	**0.1175**	9.29E-07	1.05E-01	**0.1175**	3.68E-06	1.32E-01	**0.1175**	1.40E-05	9.43E-02
0.1225	3.80E-9	3.40E-03	**0.1225**	1.43E-07	4.42E-02	**0.1225**	9.29E-07	1.04E-01	**0.1225**	3.63E-06	1.31E-01	**0.1225**	1.38E-05	9.39E-02
0.1275	4.02E-9	3.47E-03	**0.1275**	1.46E-07	4.44E-02	**0.1275**	9.33E-07	1.05E-01	**0.1275**	3.63E-06	1.33E-01	**0.1275**	1.43E-05	9.45E-02
0.135	4.38E-9	3.60E-03	**0.135**	1.51E-07	4.46E-02	**0.135**	9.49E-07	1.03E-01	**0.135**	3.62E-06	1.33E-01	**0.135**	1.40E-05	9.41E-02
0.15	5.20E-9	3.90E-03	**0.15**	1.55E-07	4.63E-02	**0.15**	9.73E-07	1.06E-01	**0.15**	3.76E-06	1.33E-01	**0.15**	1.41E-05	9.45E-02
0.1775	7.20E-9	4.53E-03	**0.1775**	1.74E-07	4.79E-02	**0.1775**	1.03E-06	1.09E-01	**0.1775**	4.03E-06	1.35E-01	**0.1775**	1.45E-05	9.50E-02
0.2225	2.15E-9	3.70E-03	**0.2225**	1.57E-07	3.90E-02	**0.2225**	8.24E-07	8.83E-02	**0.2225**	3.36E-06	1.08E-01	**0.2225**	1.29E-05	7.80E-02

Table B2. Continued.

SAF (*Upper Large Intestine Wall* ← *Small Intestine Contents*) **in kg^{-1}**														
Source Particle Energy (MeV)														
0.10			**0.20**			**0.35**			**0.50**			**0.75**		
Depth (cm)	**Electron SAF**	**Photon SAF**	**Depth (cm)**	**Electron SAF**	**Photon SAF**	**Depth (cm)**	**Electron SAF**	**Photon SAF**	**Depth (cm)**	**Electron SAF**	**Photon SAF**	**Depth (cm)**	**Electron SAF**	**Photon SAF**
0.0025	3.56E-05	6.03E-02	**0.0025**	6.60E-05	5.30E-02	**0.0025**	1.00E-04	5.15E-02	**0.0025**	1.30E-04	4.97E-02	**0.0025**	1.79E-04	4.76E-02
0.0075	3.58E-05	6.02E-02	**0.0075**	6.63E-05	5.31E-02	**0.0075**	1.01E-04	5.18E-02	**0.0075**	1.30E-04	4.96E-02	**0.0075**	1.78E-04	4.74E-02
0.0125	3.59E-05	6.07E-02	**0.0125**	6.63E-05	5.31E-02	**0.0125**	1.01E-04	5.21E-02	**0.0125**	1.31E-04	4.97E-02	**0.0125**	1.79E-04	4.73E-02
0.0175	3.56E-05	6.09E-02	**0.0175**	6.65E-05	5.31E-02	**0.0175**	1.01E-04	5.21E-02	**0.0175**	1.31E-04	5.00E-02	**0.0175**	1.79E-04	4.76E-02
0.0225	3.57E-05	6.12E-02	**0.0225**	6.65E-05	5.31E-02	**0.0225**	1.01E-04	5.20E-02	**0.0225**	1.31E-04	5.00E-02	**0.0225**	1.79E-04	4.77E-02
0.0275	3.57E-05	6.06E-02	**0.0275**	6.66E-05	5.33E-02	**0.0275**	1.01E-04	5.22E-02	**0.0275**	1.31E-04	4.99E-02	**0.0275**	1.79E-04	4.76E-02
0.0325	3.57E-05	6.13E-02	**0.0325**	6.66E-05	5.32E-02	**0.0325**	1.02E-04	5.20E-02	**0.0325**	1.30E-04	4.99E-02	**0.0325**	1.80E-04	4.77E-02
0.0375	3.57E-05	6.16E-02	**0.0375**	6.67E-05	5.32E-02	**0.0375**	1.01E-04	5.17E-02	**0.0375**	1.31E-04	4.96E-02	**0.0375**	1.80E-04	4.76E-02
0.0425	3.58E-05	6.11E-02	**0.0425**	6.66E-05	5.33E-02	**0.0425**	1.01E-04	5.16E-02	**0.0425**	1.31E-04	4.97E-02	**0.0425**	1.80E-04	4.74E-02
0.0475	3.60E-05	6.09E-02	**0.0475**	6.67E-05	5.31E-02	**0.0475**	1.01E-04	5.09E-02	**0.0475**	1.32E-04	4.96E-02	**0.0475**	1.80E-04	4.74E-02
0.0525	3.60E-05	6.06E-02	**0.0525**	6.67E-05	5.29E-02	**0.0525**	1.01E-04	5.10E-02	**0.0525**	1.32E-04	4.95E-02	**0.0525**	1.80E-04	4.74E-02
0.0575	3.60E-05	6.06E-02	**0.0575**	6.67E-05	5.33E-02	**0.0575**	1.01E-04	5.11E-02	**0.0575**	1.31E-04	4.95E-02	**0.0575**	1.80E-04	4.76E-02
0.0625	3.59E-05	6.06E-02	**0.0625**	6.68E-05	5.31E-02	**0.0625**	1.02E-04	5.15E-02	**0.0625**	1.32E-04	4.96E-02	**0.0625**	1.80E-04	4.76E-02
0.0675	3.58E-05	6.09E-02	**0.0675**	6.66E-05	5.35E-02	**0.0675**	1.02E-04	5.19E-02	**0.0675**	1.32E-04	5.00E-02	**0.0675**	1.81E-04	4.78E-02
0.0725	3.58E-05	6.10E-02	**0.0725**	6.66E-05	5.33E-02	**0.0725**	1.02E-04	5.21E-02	**0.0725**	1.31E-04	4.99E-02	**0.0725**	1.81E-04	4.79E-02
0.0775	3.60E-05	6.09E-02	**0.0775**	6.68E-05	5.31E-02	**0.0775**	1.02E-04	5.17E-02	**0.0775**	1.31E-04	4.96E-02	**0.0775**	1.81E-04	4.78E-02
0.0825	3.60E-05	6.11E-02	**0.0825**	6.70E-05	5.32E-02	**0.0825**	1.02E-04	5.22E-02	**0.0825**	1.31E-04	4.97E-02	**0.0825**	1.82E-04	4.77E-02
0.0875	3.62E-05	6.09E-02	**0.0875**	6.69E-05	5.32E-02	**0.0875**	1.02E-04	5.22E-02	**0.0875**	1.32E-04	4.99E-02	**0.0875**	1.81E-04	4.79E-02
0.0925	3.62E-05	6.07E-02	**0.0925**	6.69E-05	5.33E-02	**0.0925**	1.03E-04	5.19E-02	**0.0925**	1.32E-04	4.97E-02	**0.0925**	1.81E-04	4.78E-02
0.0975	3.62E-05	6.03E-02	**0.0975**	6.72E-05	5.35E-02	**0.0975**	1.02E-04	5.22E-02	**0.0975**	1.32E-04	4.99E-02	**0.0975**	1.82E-04	4.80E-02
0.1025	3.63E-05	6.05E-02	**0.1025**	6.73E-05	5.35E-02	**0.1025**	1.03E-04	5.21E-02	**0.1025**	1.32E-04	4.99E-02	**0.1025**	1.82E-04	4.81E-02
0.1075	3.61E-05	6.12E-02	**0.1075**	6.72E-05	5.36E-02	**0.1075**	1.03E-04	5.24E-02	**0.1075**	1.32E-04	5.02E-02	**0.1075**	1.82E-04	4.81E-02
0.1125	3.62E-05	6.10E-02	**0.1125**	6.73E-05	5.35E-02	**0.1125**	1.03E-04	5.18E-02	**0.1125**	1.32E-04	5.00E-02	**0.1125**	1.82E-04	4.79E-02
0.1175	3.64E-05	6.07E-02	**0.1175**	6.73E-05	5.35E-02	**0.1175**	1.03E-04	5.16E-02	**0.1175**	1.32E-04	4.96E-02	**0.1175**	1.81E-04	4.79E-02
0.1225	3.67E-05	6.09E-02	**0.1225**	6.81E-05	5.34E-02	**0.1225**	1.03E-04	5.15E-02	**0.1225**	1.32E-04	4.96E-02	**0.1225**	1.82E-04	4.77E-02
0.1275	3.67E-05	6.05E-02	**0.1275**	6.79E-05	5.34E-02	**0.1275**	1.03E-04	5.20E-02	**0.1275**	1.33E-04	4.99E-02	**0.1275**	1.82E-04	4.79E-02
0.135	3.67E-05	6.07E-02	**0.135**	6.80E-05	5.33E-02	**0.135**	1.03E-04	5.15E-02	**0.135**	1.32E-04	4.97E-02	**0.135**	1.83E-04	4.79E-02
0.15	3.71E-05	6.07E-02	**0.15**	6.80E-05	5.35E-02	**0.15**	1.03E-04	5.19E-02	**0.15**	1.33E-04	4.98E-02	**0.15**	1.83E-04	4.81E-02
0.1775	3.74E-05	6.14E-02	**0.1775**	6.87E-05	5.40E-02	**0.1775**	1.04E-04	5.22E-02	**0.1775**	1.34E-04	5.03E-02	**0.1775**	1.85E-04	4.84E-02
0.2225	3.01E-05	5.21E-02	**0.2225**	5.67E-05	4.51E-02	**0.2225**	8.53E-05	4.50E-02	**0.2225**	1.11E-04	4.30E-02	**0.2225**	1.53E-04	4.10E-02

Table B2. Continued.

SAF (*Upper Large Intestine Wall* ← *Small Intestine Contents*) **in kg^{-1}**														
Source Particle Energy (MeV)														
1.00			**1.50**			**2.00**			**3.00**			**4.00**		
Depth (cm)	**Electron SAF**	**Photon SAF**	**Depth (cm)**	**Electron SAF**	**Photon SAF**	**Depth (cm)**	**Electron SAF**	**Photon SAF**	**Depth (cm)**	**Electron SAF**	**Photon SAF**	**Depth (cm)**	**Electron SAF**	**Photon SAF**
0.0025	2.27E-04	4.49E-02	**0.0025**	2.00E-03[c]	4.14E-02	**0.0025**	1.15E-02[a]	3.83E-02	**0.0025**	3.22E-02	3.46E-02	**0.0025**	5.53E-02	3.08E-02
0.0075	2.28E-04	4.48E-02	**0.0075**	2.01E-03[c]	4.12E-02	**0.0075**	1.18E-02[a]	3.85E-02	**0.0075**	3.13E-02	3.45E-02	**0.0075**	6.16E-02	3.08E-02
0.0125	2.27E-04	4.49E-02	**0.0125**	2.24E-03[c]	4.13E-02	**0.0125**	1.02E-02[a]	3.86E-02	**0.0125**	3.36E-02	3.46E-02	**0.0125**	5.18E-02	3.08E-02
0.0175	2.27E-04	4.49E-02	**0.0175**	2.08E-03[c]	4.14E-02	**0.0175**	1.07E-02[a]	3.87E-02	**0.0175**	3.30E-02	3.46E-02	**0.0175**	5.90E-02	3.10E-02
0.0225	2.28E-04	4.50E-02	**0.0225**	1.91E-03[c]	4.14E-02	**0.0225**	1.01E-02[a]	3.86E-02	**0.0225**	3.29E-02	3.47E-02	**0.0225**	6.04E-02	3.10E-02
0.0275	2.27E-04	4.52E-02	**0.0275**	2.30E-03[c]	4.16E-02	**0.0275**	1.13E-02[a]	3.88E-02	**0.0275**	3.53E-02	3.50E-02	**0.0275**	6.08E-02	3.11E-02
0.0325	2.27E-04	4.52E-02	**0.0325**	2.27E-03[c]	4.15E-02	**0.0325**	1.21E-02[a]	3.90E-02	**0.0325**	3.44E-02	3.46E-02	**0.0325**	6.07E-02	3.10E-02
0.0375	2.27E-04	4.50E-02	**0.0375**	2.46E-03[c]	4.14E-02	**0.0375**	1.09E-02[a]	3.87E-02	**0.0375**	3.84E-02	3.44E-02	**0.0375**	6.06E-02	3.10E-02
0.0425	2.28E-04	4.50E-02	**0.0425**	2.09E-03[c]	4.14E-02	**0.0425**	1.24E-02[a]	3.85E-02	**0.0425**	3.59E-02	3.39E-02	**0.0425**	5.99E-02	3.09E-02
0.0475	2.28E-04	4.50E-02	**0.0475**	2.64E-03[c]	4.13E-02	**0.0475**	1.21E-02[a]	3.84E-02	**0.0475**	3.69E-02	3.39E-02	**0.0475**	5.98E-02	3.10E-02
0.0525	2.28E-04	4.49E-02	**0.0525**	2.42E-03[c]	4.12E-02	**0.0525**	1.30E-02[a]	3.83E-02	**0.0525**	3.71E-02	3.40E-02	**0.0525**	6.09E-02	3.09E-02
0.0575	2.28E-04	4.50E-02	**0.0575**	1.99E-03[c]	4.13E-02	**0.0575**	1.33E-02[a]	3.86E-02	**0.0575**	3.73E-02	3.42E-02	**0.0575**	5.55E-02	3.08E-02
0.0625	2.28E-04	4.49E-02	**0.0625**	2.51E-03[b]	4.13E-02	**0.0625**	1.34E-02[a]	3.84E-02	**0.0625**	3.81E-02	3.45E-02	**0.0625**	6.12E-02	3.09E-02
0.0675	2.28E-04	4.51E-02	**0.0675**	3.07E-03[b]	4.15E-02	**0.0675**	1.24E-02[a]	3.86E-02	**0.0675**	3.79E-02	3.45E-02	**0.0675**	6.16E-02	3.10E-02
0.0725	2.29E-04	4.50E-02	**0.0725**	3.20E-03[b]	4.16E-02	**0.0725**	1.38E-02	3.87E-02	**0.0725**	3.69E-02	3.44E-02	**0.0725**	6.32E-02	3.10E-02
0.0775	2.29E-04	4.47E-02	**0.0775**	4.18E-03[b]	4.16E-02	**0.0775**	1.49E-02	3.86E-02	**0.0775**	3.87E-02	3.42E-02	**0.0775**	6.43E-02	3.10E-02
0.0825	2.29E-04	4.48E-02	**0.0825**	4.58E-03[b]	4.13E-02	**0.0825**	1.40E-02	3.85E-02	**0.0825**	3.95E-02	3.41E-02	**0.0825**	6.64E-02	3.09E-02
0.0875	2.29E-04	4.53E-02	**0.0875**	4.85E-03[b]	4.15E-02	**0.0875**	1.51E-02	3.86E-02	**0.0875**	3.78E-02	3.45E-02	**0.0875**	6.20E-02	3.10E-02
0.0925	2.30E-04	4.50E-02	**0.0925**	4.47E-03[b]	4.16E-02	**0.0925**	1.49E-02	3.87E-02	**0.0925**	3.58E-02	3.43E-02	**0.0925**	6.69E-02	3.11E-02
0.0975	2.30E-04	4.51E-02	**0.0975**	4.34E-03[b]	4.20E-02	**0.0975**	1.25E-02	3.89E-02	**0.0975**	3.90E-02	3.48E-02	**0.0975**	6.49E-02	3.12E-02
0.1025	2.30E-04	4.51E-02	**0.1025**	5.02E-03[b]	4.19E-02	**0.1025**	1.49E-02	3.87E-02	**0.1025**	4.15E-02	3.45E-02	**0.1025**	6.64E-02	3.12E-02
0.1075	2.30E-04	4.54E-02	**0.1075**	5.83E-03[b]	4.19E-02	**0.1075**	1.40E-02	3.88E-02	**0.1075**	3.93E-02	3.48E-02	**0.1075**	6.87E-02	3.11E-02
0.1125	2.30E-04	4.56E-02	**0.1125**	5.00E-03[a]	4.19E-02	**0.1125**	1.45E-02	3.86E-02	**0.1125**	3.89E-02	3.46E-02	**0.1125**	6.44E-02	3.11E-02
0.1175	2.30E-04	4.53E-02	**0.1175**	5.26E-03[a]	4.23E-02	**0.1175**	1.58E-02	3.87E-02	**0.1175**	4.20E-02	3.43E-02	**0.1175**	6.48E-02	3.11E-02
0.1225	3.43E-04[a]	4.51E-02	**0.1225**	5.28E-03[a]	4.19E-02	**0.1225**	1.49E-02	3.85E-02	**0.1225**	4.40E-02	3.44E-02	**0.1225**	6.70E-02	3.10E-02
0.1275	4.43E-04[a]	4.53E-02	**0.1275**	5.11E-03[a]	4.18E-02	**0.1275**	1.49E-02	3.84E-02	**0.1275**	4.45E-02	3.48E-02	**0.1275**	6.89E-02	3.12E-02
0.135	6.34E-04[a]	4.50E-02	**0.135**	5.46E-03[a]	4.18E-02	**0.135**	1.67E-02	3.84E-02	**0.135**	4.47E-02	3.43E-02	**0.135**	6.79E-02	3.11E-02
0.15	6.52E-04[a]	4.51E-02	**0.15**	6.48E-03[a]	4.20E-02	**0.15**	1.58E-02	3.88E-02	**0.15**	4.61E-02	3.46E-02	**0.15**	6.93E-02	3.12E-02
0.1775	1.19E-03[a]	4.55E-02	**0.1775**	8.66E-03[a]	4.23E-02	**0.1775**	1.79E-02	3.93E-02	**0.1775**	4.62E-02	3.51E-02	**0.1775**	6.95E-02	3.14E-02
0.2225	1.92E-04	3.91E-02	**0.2225**	4.74E-03[a]	3.58E-02	**0.2225**	5.73E-04	3.33E-02	**0.2225**	4.35E-02	3.11E-02	**0.2225**	5.66E-02	2.63E-02

Table B2. Continued.

SAF (*Upper Large Intestine Wall* ← *Upper Large Intestine Contents*) **in kg^{-1}**														
Source Particle Energy (MeV)														
0.01			**0.015**			**0.02**			**0.03**			**0.05**		
Depth (cm)	**Electron SAF**	**Photon SAF**	**Depth (cm)**	**Electron SAF**	**Photon SAF**	**Depth (cm)**	**Electron SAF**	**Photon SAF**	**Depth (cm)**	**Electron SAF**	**Photon SAF**	**Depth (cm)**	**Electron SAF**	**Photon SAF**
0.00005	1.68E-01	5.46E-01	**0.00005**	2.20E-01	5.01E-01	**0.00010**	2.15E-01	4.08E-01	**0.00010**	2.57E-01	2.33E-1	**0.0005**	2.93E-01	1.04E-1
0.00020	1.83E-02	5.43E-01	**0.00020**	8.85E-02	4.99E-01	**0.00035**	9.47E-02	4.07E-01	**0.00035**	1.64E-01	2.33E-1	**0.0015**	1.26E-01	1.04E-1
0.00040	1.88E-05	5.40E-01	**0.00040**	1.04E-02	4.99E-01	**0.00075**	7.02E-03	4.06E-01	**0.00075**	7.60E-02	2.33E-1	**0.003**	2.19E-02	1.04E-1
0.00060	2.11E-05	5.37E-01	**0.00060**	3.60E-05	4.98E-01	**0.00150**	5.22E-05	4.05E-01	**0.00150**	7.28E-03	2.32E-1	**0.005**	1.38E-04	1.04E-1
0.00085	1.80E-05	5.35E-01	**0.00085**	3.64E-05	4.97E-01	**0.00250**	2.97E-05	4.04E-01	**0.00250**	6.54E-05	2.32E-1	**0.0075**	9.92E-05	1.04E-1
0.00300	1.88E-05	5.14E-01	**0.00300**	3.74E-05	4.91E-01	**0.00550**	5.71E-05	4.00E-01	**0.00550**	8.57E-05	2.31E-1	**0.0105**	1.07E-04	1.03E-1
0.01000	1.49E-05	4.60E-01	**0.01000**	3.69E-05	4.72E-01	**0.01150**	4.52E-05	3.93E-01	**0.01150**	8.05E-05	2.28E-1	**0.0135**	9.10E-05	1.03E-1
0.02000	5.57E-06	4.04E-01	**0.02000**	1.58E-05	4.49E-01	**0.02000**	2.90E-05	3.85E-01	**0.02000**	5.24E-05	2.26E-1	**0.02**	8.94E-05	1.03E-1
0.03000	3.86E-06	3.59E-01	**0.03000**	1.28E-05	4.29E-01	**0.03000**	2.37E-05	3.75E-01	**0.03000**	4.55E-05	2.23E-1	**0.03**	7.89E-05	1.02E-1
0.04000	2.77E-06	3.22E-01	**0.04000**	1.07E-05	4.11E-01	**0.04000**	2.13E-05	3.67E-01	**0.04000**	4.12E-05	2.20E-1	**0.04**	7.47E-05	1.01E-1
0.05000	2.08E-06	2.91E-01	**0.05000**	8.82E-06	3.95E-01	**0.05000**	1.80E-05	3.59E-01	**0.05000**	3.88E-05	2.18E-1	**0.05**	6.66E-05	1.00E-1
0.06000	1.70E-06	2.64E-01	**0.06000**	7.94E-06	3.81E-01	**0.06000**	1.74E-05	3.51E-01	**0.06000**	3.54E-05	2.15E-1	**0.06**	6.59E-05	9.94E-2
0.06750	1.40E-06	2.46E-01	**0.06750**	6.94E-06	3.70E-01	**0.06750**	1.63E-05	3.45E-01	**0.06750**	3.34E-05	2.14E-1	**0.0675**	6.28E-05	9.90E-2
0.07250	1.26E-06	2.35E-01	**0.07250**	6.67E-06	3.64E-01	**0.07250**	1.52E-05	3.42E-01	**0.07250**	3.30E-05	2.13E-1	**0.0725**	6.41E-05	9.86E-2
0.07750	1.17E-06	2.25E-01	**0.07750**	6.45E-06	3.57E-01	**0.07750**	1.39E-05	3.39E-01	**0.07750**	3.17E-05	2.12E-1	**0.0775**	5.83E-05	9.82E-2
0.08250	1.05E-06	2.15E-01	**0.08250**	6.07E-06	3.51E-01	**0.08250**	1.34E-05	3.35E-01	**0.08250**	3.00E-05	2.10E-1	**0.0825**	5.66E-05	9.80E-2
0.08750	1.02E-06	2.06E-01	**0.08750**	5.80E-06	3.45E-01	**0.08750**	1.30E-05	3.32E-01	**0.08750**	2.94E-05	2.09E-1	**0.0875**	5.73E-05	9.76E-2
0.09250	8.13E-07	1.98E-01	**0.09250**	5.45E-06	3.39E-01	**0.09250**	1.26E-05	3.29E-01	**0.09250**	2.89E-05	2.08E-1	**0.0925**	5.62E-05	9.73E-2
0.10000	8.19E-07	1.85E-01	**0.10000**	5.02E-06	3.31E-01	**0.10000**	1.19E-05	3.24E-01	**0.10000**	2.80E-05	2.07E-1	**0.1**	5.41E-05	9.69E-2
0.11000	6.44E-07	1.71E-01	**0.11000**	4.63E-06	3.20E-01	**0.11000**	1.16E-05	3.18E-01	**0.11000**	2.60E-05	2.05E-1	**0.11**	5.13E-05	9.63E-2
0.12000	6.17E-07	1.57E-01	**0.12000**	4.28E-06	3.10E-01	**0.12000**	1.05E-05	3.13E-01	**0.12000**	2.53E-05	2.02E-1	**0.12**	5.30E-05	9.59E-2
0.13000	4.75E-07	1.46E-01	**0.13000**	3.90E-06	3.00E-01	**0.13000**	9.82E-06	3.07E-01	**0.13000**	2.36E-05	2.01E-1	**0.13**	4.84E-05	9.53E-2
0.14500	3.87E-07	1.31E-01	**0.14500**	3.41E-06	2.87E-01	**0.14500**	8.84E-06	3.00E-01	**0.14500**	2.34E-05	1.98E-1	**0.145**	4.70E-05	9.44E-2
0.16500	3.66E-07	1.13E-01	**0.16500**	3.00E-06	2.71E-01	**0.16500**	8.52E-06	2.90E-01	**0.16500**	2.14E-05	1.94E-1	**0.165**	4.45E-05	9.35E-2
0.18500	3.26E-07	9.90E-02	**0.18500**	2.75E-06	2.56E-01	**0.18500**	7.55E-06	2.80E-01	**0.18500**	1.98E-05	1.91E-1	**0.185**	4.16E-05	9.24E-2
0.20500	2.05E-07	1.00E-01	**0.20500**	2.70E-06	2.92E-01	**0.20500**	8.30E-06	3.30E-01	**0.20500**	2.25E-05	2.25E-1	**0.205**	4.65E-05	1.06E-1
0.22500	1.44E-07	8.66E-02	**0.22500**	2.33E-06	2.75E-01	**0.22500**	7.05E-06	3.18E-01	**0.22500**	2.04E-05	2.20E-1	**0.225**	4.62E-05	1.05E-1
0.24250	1.04E-07	7.59E-02	**0.24250**	2.37E-06	2.61E-01	**0.24250**	6.99E-06	3.10E-01	**0.24250**	1.96E-05	2.17E-1	**0.2425**	4.30E-05	1.04E-1

Table B2. Continued.

SAF (*Upper Large Intestine Wall* ← *Upper Large Intestine Contents*) **in kg^{-1}**														
Source Particle Energy (MeV)														
0.10			**0.20**			**0.35**			**0.50**			**0.75**		
Depth (cm)	**Electron SAF**	**Photon SAF**	**Depth (cm)**	**Electron SAF**	**Photon SAF**	**Depth (cm)**	**Electron SAF**	**Photon SAF**	**Depth (cm)**	**Electron SAF**	**Photon SAF**	**Depth (cm)**	**Electron SAF**	**Photon SAF**
0.0005	4.49E-01	6.11E-02	**0.0025**	4.51E-01	5.85E-02	**0.0025**	5.13E-01	5.84E-02	**0.005**	5.07E-01	5.71E-02	**0.005**	5.26E-01	5.44E-02
0.0015	3.50E-01	6.10E-02	**0.0075**	3.03E-01	5.81E-02	**0.0075**	4.14E-01	5.80E-02	**0.015**	3.88E-01	5.65E-02	**0.015**	4.41E-01	5.38E-02
0.003	2.47E-01	6.10E-02	**0.0125**	2.00E-01	5.78E-02	**0.0125**	3.51E-01	5.77E-02	**0.025**	3.15E-01	5.59E-02	**0.025**	3.80E-01	5.33E-02
0.005	1.50E-01	6.08E-02	**0.0175**	1.30E-01	5.75E-02	**0.0175**	2.98E-01	5.75E-02	**0.035**	2.55E-01	5.54E-02	**0.035**	3.39E-01	5.28E-02
0.0075	6.51E-02	6.08E-02	**0.0225**	7.76E-02	5.73E-02	**0.0225**	2.58E-01	5.71E-02	**0.045**	2.08E-01	5.49E-02	**0.045**	3.00E-01	5.22E-02
0.0105	1.17E-02	6.06E-02	**0.0275**	3.62E-02	5.71E-02	**0.0275**	2.18E-01	5.68E-02	**0.055**	1.65E-01	5.44E-02	**0.055**	2.66E-01	5.18E-02
0.0135	6.67E-04	6.04E-02	**0.0325**	1.32E-02	5.68E-02	**0.0325**	1.78E-01	5.66E-02	**0.065**	1.31E-01	5.40E-02	**0.065**	2.38E-01	5.14E-02
0.02	1.40E-04	6.02E-02	**0.0375**	2.26E-03	5.66E-02	**0.0375**	1.46E-01	5.63E-02	**0.075**	1.01E-01	5.35E-02	**0.075**	2.10E-01	5.10E-02
0.03	1.25E-04	5.98E-02	**0.0425**	3.28E-04	5.64E-02	**0.0425**	1.16E-01	5.61E-02	**0.085**	7.56E-02	5.31E-02	**0.085**	1.81E-01	5.06E-02
0.04	1.20E-04	5.93E-02	**0.0475**	1.62E-04	5.61E-02	**0.0475**	8.91E-02	5.58E-02	**0.095**	5.35E-02	5.27E-02	**0.095**	1.60E-01	5.03E-02
0.05	1.17E-04	5.89E-02	**0.05375**	1.55E-04	5.59E-02	**0.05375**	6.37E-02	5.56E-02	**0.105**	3.54E-02	5.24E-02	**0.105**	1.42E-01	4.99E-02
0.06	1.06E-04	5.84E-02	**0.06125**	1.52E-04	5.56E-02	**0.06125**	4.03E-02	5.52E-02	**0.115**	2.41E-02	5.20E-02	**0.115**	1.24E-01	4.95E-02
0.0675	1.13E-04	5.81E-02	**0.0675**	1.59E-04	5.53E-02	**0.0675**	2.73E-02	5.49E-02	**0.125**	1.42E-02	5.18E-02	**0.125**	1.06E-01	4.93E-02
0.0725	9.75E-05	5.80E-02	**0.0725**	1.42E-04	5.50E-02	**0.0725**	1.56E-02	5.48E-02	**0.135**	7.93E-03	5.14E-02	**0.135**	9.21E-02	4.90E-02
0.0775	9.91E-05	5.78E-02	**0.0775**	1.59E-04	5.48E-02	**0.0775**	9.02E-03	5.45E-02	**0.1475**	5.88E-03	5.09E-02	**0.1475**	7.63E-02	4.86E-02
0.0825	9.62E-05	5.75E-02	**0.0825**	1.45E-04	5.46E-02	**0.0825**	4.26E-03	5.43E-02	**0.165**	5.80E-03	5.03E-02	**0.165**	5.64E-02	4.80E-02
0.0875	1.05E-04	5.74E-02	**0.0875**	1.49E-04	5.45E-02	**0.0875**	2.44E-03	5.41E-02	**0.185**	8.04E-03	4.97E-02	**0.185**	3.94E-02	4.74E-02
0.0925	9.70E-05	5.71E-02	**0.0925**	1.44E-04	5.42E-02	**0.0925**	7.00E-04	5.40E-02	**0.2075**	2.10E-04	5.80E-02	**0.2075**	1.69E-02	5.53E-02
0.1	9.46E-05	5.70E-02	**0.1**	1.40E-04	5.40E-02	**0.1**	2.83E-04	5.37E-02	**0.235**	2.21E-04	5.71E-02	**0.235**	5.50E-03	5.44E-02
0.11	8.90E-05	5.66E-02	**0.11**	1.39E-04	5.36E-02	**0.11**	1.85E-04	5.32E-02						
0.12	9.25E-05	5.62E-02	**0.12**	1.29E-04	5.33E-02	**0.12**	2.82E-04	5.29E-02						
0.13	8.99E-05	5.60E-02	**0.13**	1.32E-04	5.30E-02	**0.13**	2.83E-04	5.26E-02						
0.145	8.27E-05	5.56E-02	**0.145**	1.26E-04	5.25E-02	**0.145**	8.52E-04	5.21E-02						
0.165	8.04E-05	5.49E-02	**0.165**	2.45E-04	5.19E-02	**0.165**	2.77E-03	5.14E-02						
0.185	3.07E-04	5.43E-02	**0.185**	2.26E-03	5.12E-02	**0.185**	5.57E-03	5.08E-02						
0.205	8.75E-05	6.22E-02	**0.205**	1.45E-04	5.93E-02	**0.205**	1.86E-04	5.90E-02						
0.225	8.31E-05	6.18E-02	**0.225**	1.24E-04	5.87E-02	**0.225**	1.71E-04	5.83E-02						
0.2425	8.16E-05	6.12E-02	**0.2425**	1.35E-04	5.82E-02	**0.2425**	1.79E-04	5.79E-02						

Table B2. Continued.

SAF (*Upper Large Intestine Wall* ← *Upper Large Intestine Contents*) **in kg^{-1}**														
Source Particle Energy (MeV)														
1.00			**1.50**			**2.00**			**3.00**			**4.00**		
Depth (cm)	**Electron SAF**	**Photon SAF**	**Depth (cm)**	**Electron SAF**	**Photon SAF**	**Depth (cm)**	**Electron SAF**	**Photon SAF**	**Depth (cm)**	**Electron SAF**	**Photon SAF**	**Depth (cm)**	**Electron SAF**	**Photon SAF**
0.0100	5.09E-01	5.17E-02	**0.0100**	5.26E-01	5.31E-02	**0.0100**	5.29E-01	5.17E-02	**0.0200**	4.89E-01	3.75E-02	**0.0200**	4.65E-01	3.45E-02
0.0300	4.09E-01	5.07E-02	**0.0300**	4.53E-01	5.19E-02	**0.0300**	4.72E-01	5.07E-02	**0.0600**	4.22E-01	3.61E-02	**0.0600**	4.20E-01	3.33E-02
0.0500	3.39E-01	4.97E-02	**0.0500**	4.03E-01	5.08E-02	**0.0500**	4.27E-01	4.97E-02	**0.1000**	3.79E-01	3.51E-02	**0.1000**	3.77E-01	3.23E-02
0.0700	2.90E-01	4.90E-02	**0.0700**	3.55E-01	4.98E-02	**0.0700**	3.89E-01	4.90E-02	**0.1400**	3.42E-01	3.41E-02	**0.1400**	3.51E-01	3.13E-02
0.0900	2.48E-01	4.82E-02	**0.0900**	3.23E-01	4.90E-02	**0.0900**	3.63E-01	4.82E-02	**0.1775**	3.06E-01	3.33E-02	**0.1775**	3.26E-01	3.05E-02
0.1100	2.09E-01	4.76E-02	**0.1100**	2.90E-01	4.81E-02	**0.1100**	3.37E-01	4.76E-02	**0.2125**	3.40E-01	3.87E-02	**0.2125**	3.64E-01	3.55E-02
0.1300	1.75E-01	4.69E-02	**0.1300**	2.60E-01	4.73E-02	**0.1300**	3.13E-01	4.69E-02	**0.2400**	3.15E-01	3.83E-02	**0.2400**	3.46E-01	3.50E-02
0.1500	1.50E-01	4.63E-02	**0.1500**	2.40E-01	4.67E-02	**0.1500**	2.93E-01	4.63E-02						
0.1700	1.25E-01	4.56E-02	**0.1700**	2.21E-01	4.60E-02	**0.1700**	2.70E-01	4.56E-02						
0.1875	1.07E-01	4.51E-02	**0.1875**	2.00E-01	4.54E-02	**0.1875**	2.53E-01	4.51E-02						
0.2025	9.92E-02	5.28E-02	**0.2025**	2.15E-01	6.01E-02	**0.2025**	2.85E-01	5.28E-02						
0.2200	7.65E-02	5.22E-02	**0.2200**	1.94E-01	5.93E-02	**0.2200**	2.66E-01	5.22E-02						
0.2400	5.97E-02	5.17E-02	**0.2400**	1.72E-01	5.84E-02	**0.2400**	2.48E-01	5.17E-02						

Table B2. Continued.

Source Energy (MeV)	SAF (*Upper Large Intestine Wall* ← *Lower Large Intestine Contents*) in kg^{-1} for Electron							
	At Mean Position (cm) in the Upper Large Intestine Wall Measured Outward from Contents-Wall Interface.							Average to the
	0.02	**0.06**	**0.1**	**0.14**	**0.1775**	**0.2125**	**0.24**	**Wall**
0.01	4.81E-10[h]	1.03E-09[d]	2.22E-09[c]	2.98E-09[b]	6.67E-09[a]	0.0	0.0	2.39E-09[b]
0.015	1.79E-08[a]	2.04E-08[a]	2.38E-08	2.86E-08	3.64E-08	0.00E+00	0.00E+00	2.29E-08
0.02	5.46E-08	5.39E-08	5.41E-08	5.82E-08	6.84E-08	0.00E+00	0.00E+00	5.23E-08
0.03	1.37E-07	1.41E-07	1.44E-07	1.51E-07	1.66E-07	5.05E-10[h]	4.90E-10[h]	1.34E-07
0.05	3.85E-07	3.88E-07	3.93E-07	4.04E-07	4.14E-07	1.31E-08[a]	1.71E-08[a]	3.63E-07
0.10	1.22E-06	1.24E-06	1.23E-06	1.23E-06	1.25E-06	1.77E-07	1.72E-07	1.16E-06
0.20	2.96E-06	3.26E-06	2.80E-06	2.95E-06	5.62E-05[i]	6.06E-07	6.05E-07	1.29E-05[h]
0.35	5.42E-06	4.91E-06	5.17E-06	5.64E-05[i]	1.15E-03[c]	1.26E-06	1.27E-06	2.31E-04[c]
0.50	5.32E-06[d]	6.34E-06	6.79E-05[h]	6.73E-04[c]	1.53E-03[b]	1.96E-06	1.91E-06	4.44E-04[b]
0.75	3.12E-04[e]	5.03E-04[d]	9.98E-04[c]	1.55E-03[b]	1.70E-03[a]	2.88E-06	2.91E-06	1.01E-03[a]
1.00	6.86E-04[c]	8.66E-04[c]	9.94E-04[b]	1.22E-03[b]	1.70E-03[a]	3.96E-06	3.98E-06	1.09E-03
1.50	1.68E-03[c]	1.98E-03[b]	2.58E-03[a]	2.79E-03[a]	2.52E-03[a]	6.34E-06	6.28E-06	2.32E-03[a]
2.00	2.88E-03[a]	2.51E-03[a]	3.05E-03[a]	2.91E-03[a]	2.79E-03[a]	8.46E-06	8.45E-06	2.84E-03[a]
3.00	2.73E-03[a]	3.13E-03[a]	2.99E-03[a]	2.79E-03[a]	2.51E-03[a]	1.43E-05	1.41E-05	2.85E-03[a]
4.00	2.71E-03[a]	2.99E-03[a]	2.89E-03[a]	3.22E-03[a]	3.55E-03[a]	1.87E-05	1.89E-05	3.09E-03[a]
	SAF (*Upper Large Intestine Wall* ← *Lower Large Intestine Contents*) **in kg^{-1} for Photon**							
0.01	6.49E-04	6.89E-04	7.64E-04	8.57E-04	9.53E-04	0.0	0.0	7.81E-04
0.015	1.74E-03	1.75E-03	1.82E-03	1.75E-03	1.77E-03	0.0	0.0	1.76E-03
0.02	2.29E-03	2.21E-03	2.25E-03	2.27E-03	2.29E-03	0.0	0.0	2.26E-03
0.03[a]	2.75E-03	2.75E-03	2.74E-03	2.73E-03	2.77E-03	1.79E-04	1.74E-04	2.75E-03
0.05	4.12E-03	4.13E-03	4.14E-03	4.13E-03	4.12E-03	1.05E-03	1.03E-03	4.13E-03
0.10	4.53E-03	4.55E-03	4.53E-03	4.51E-03	4.50E-03	1.45E-03	1.43E-03	4.52E-03
0.20	4.17E-03	4.14E-03	4.15E-03	4.19E-03	4.15E-03	1.38E-03	1.39E-03	4.16E-03
0.35	4.10E-03	4.11E-03	4.08E-03	4.08E-03	4.14E-03	1.43E-03	1.44E-03	4.10E-03
0.50	4.06E-03	4.09E-03	3.98E-03	3.97E-03	3.99E-03	1.38E-03	1.39E-03	4.01E-03
0.75	3.90E-03	3.91E-03	3.84E-03	3.85E-03	3.92E-03	1.33E-03	1.35E-03	3.88E-03
1.00	3.76E-03	3.68E-03	3.68E-03	3.71E-03	3.73E-03	1.26E-03	1.28E-03	3.70E-03
1.50	3.61E-03	3.67E-03	3.63E-03	3.63E-03	3.67E-03	1.28E-03	1.32E-03	3.64E-03
2.00	3.42E-03	3.44E-03	3.42E-03	3.41E-03	3.44E-03	1.19E-03	1.22E-03	3.42E-03
3.00	3.09E-03	3.15E-03	3.17E-03	3.09E-03	3.13E-03	1.11E-03	1.15E-03	3.12E-03
4.00	2.83E-03	2.80E-03	2.96E-03	2.94E-03	3.15E-03	1.04E-03	1.07E-03	2.95E-03

Table B2. Continued.

Source Energy (MeV)	SAF (*Lower Large Intestine Wall* ← *Esophagus Contents*) in kg^{-1} for Electron							
	At Mean Position (cm) in the Lower Large Intestine Wall Measured Outward from Contents-Wall Interface.							Average to the
	0.01	**0.035**	**0.07**	**0.11**	**0.15**	**0.19**	**0.23**	**Wall**
0.01	0.0	0.0	0.0	0.0	0.0	0.0	0.0	0.0
0.015	0.0	0.0	0.0	0.0	0.0	0.0	0.0	0.0
0.02	0.0	0.0	0.0	0.0	0.0	0.0	0.0	0.0
0.03[i]	3.56E-10	3.47E-10	3.36E-10	3.24E-10	3.12E-10	3.02E-10	2.92E-10	3.20E-10
0.05[b]	9.87E-09	8.05E-09	9.05E-09	7.72E-09	8.26E-09	7.62E-09	6.65E-09	8.04E-09
0.10	1.02E-07	9.49E-08	9.26E-08	1.01E-07	9.64E-08	9.56E-08	9.83E-08	9.73E-08
0.20	1.17E-06	1.18E-06	1.16E-06	1.15E-06	1.17E-06	1.60E-07	1.57E-07	1.10E-06
0.35	9.15E-07	9.03E-07	9.46E-07	9.01E-07	8.51E-07	8.27E-07	8.21E-07	8.82E-07
0.50	1.31E-06	1.28E-06	1.33E-06	1.30E-06	1.29E-06	1.25E-06	1.23E-06	1.29E-06
0.75	2.29E-06	2.37E-06	2.34E-06	2.24E-06	2.22E-06	2.42E-06	2.38E-06	2.34E-06
1.00	3.03E-06	3.20E-06	2.99E-06	2.94E-06	2.99E-06	2.93E-06	2.89E-06	3.01E-06
1.50	5.22E-06	5.22E-06	5.22E-06	5.22E-06	5.22E-06	5.22E-06	5.22E-06	5.22E-06
2.00	7.71E-06	7.99E-06	7.40E-06	7.27E-06	7.01E-06	7.23E-06	7.32E-06	7.46E-06
3.00	1.32E-05	1.31E-05	1.33E-05	1.30E-05	1.23E-05	1.20E-05	1.22E-05	1.28E-05
4.00	1.90E-05	1.86E-05	1.92E-05	2.14E-05	2.04E-05	1.94E-05	1.84E-05	1.98E-05
SAF (*Lower Large Intestine Wall* ← *Esophagus Contents*) **in kg^{-1} for Photon**								
0.01	0.0	0.0	0.0	0.0	0.0	0.0	0.0	0.0
0.015	0.0	0.0	0.0	0.0	0.0	0.0	0.0	0.0
0.02	0.0	0.0	0.0	0.0	0.0	0.0	0.0	0.0
0.03[a]	7.44E-05	7.16E-05	6.75E-05	6.35E-05	6.03E-05	6.19E-05	5.75E-05	7.20E-05
0.05	5.87E-04	5.93E-04	5.93E-04	5.92E-04	5.82E-04	5.71E-04	5.78E-04	6.82E-04
0.10	1.02E-03	1.01E-03	1.01E-03	1.00E-03	9.75E-04	9.74E-04	9.93E-04	1.00E-03
0.20	1.12E-03	1.09E-03	1.09E-03	1.13E-03	1.10E-03	1.05E-03	1.06E-03	1.38E-03
0.35	1.17E-03	1.26E-03	1.23E-03	1.22E-03	1.20E-03	1.20E-03	1.23E-03	1.58E-03
0.50	1.41E-03	1.49E-03	1.41E-03	1.43E-03	1.42E-03	1.33E-03	1.33E-03	1.86E-03
0.75	1.28E-03	1.21E-03	1.12E-03	1.22E-03	1.25E-03	1.21E-03	1.22E-03	1.59E-03
1.00	1.16E-03	1.16E-03	1.20E-03	1.21E-03	1.21E-03	1.17E-03	1.34E-03	1.74E-03
1.50	1.35E-03	1.32E-03	1.27E-03	1.28E-03	1.26E-03	1.21E-03	1.22E-03	1.81E-03
2.00	1.20E-03	1.24E-03	1.18E-03	1.14E-03	1.25E-03	1.17E-03	1.16E-03	1.70E-03
3.00	1.28E-03	1.23E-03	1.32E-03	1.40E-03	1.33E-03	1.26E-03	1.24E-03	1.80E-03
4.00	1.00E-03	1.00E-03	1.02E-03	1.15E-03	1.12E-03	1.14E-03	1.20E-03	1.61E-03

Table B2. Continued.

Source Energy (MeV)	SAF (*Lower Large Intestine Wall* ← *Stomach Contents*) in kg^{-1} for Electron									
	At Mean Position (cm) in the Lower Large Intestine Wall Measured Outward from Contents-Wall Interface.									Average to the
	0.025	**0.06**	**0.075**	**0.085**	**0.11**	**0.15**	**0.19**	**0.22**	**0.24**	**Wall**
0.01	0.0	0.0	0.0	0.0	0.0	0.0	0.0	0.0	0.0	0.0
0.015	0.0	0.0	0.0	0.0	0.0	0.0	0.0	0.0	0.0	0.0
0.02	2.32E-11[f]	2.43E-11[f]	2.61E-11[f]	2.60E-11[f]	1.72E-11[f]	1.28E-11[f]	8.35E-12[f]	6.69E-12[f]	6.62E-12[f]	1.56E-11[e]
0.03	5.20E-09	5.22E-09	5.20E-09	5.38E-09	5.36E-09	5.13E-09	4.78E-09	4.80E-09	4.68E-09	5.08E-09
0.05	1.22E-07	1.21E-07	1.19E-07	1.19E-07	1.20E-07	1.14E-07	1.13E-07	1.11E-07	1.11E-07	1.17E-07
0.10	7.11E-07	7.07E-07	6.98E-07	6.96E-07	6.84E-07	6.73E-07	6.62E-07	6.64E-07	6.55E-07	6.84E-07
0.20	2.19E-06	2.14E-06	2.12E-06	2.12E-06	2.12E-06	2.07E-06	2.04E-06	2.00E-06	2.01E-06	2.10E-06
0.35	4.14E-06	4.17E-06	4.37E-06	4.27E-06	4.20E-06	4.11E-06	4.08E-06	4.07E-06	4.01E-06	4.16E-06
0.50	6.36E-06	6.18E-06	6.16E-06	6.28E-06	6.11E-06	5.94E-06	5.90E-06	5.88E-06	5.83E-06	6.10E-06
0.75	9.30E-06	9.42E-06	9.52E-06	9.51E-06	9.20E-06	9.32E-06	9.06E-06	8.92E-06	8.83E-06	9.26E-06
1.00	1.26E-05	1.26E-05	1.26E-05	1.25E-05	1.24E-05	1.22E-05	1.21E-05	1.24E-05	1.23E-05	1.25E-05
1.50	2.01E-05	1.99E-05	1.97E-05	1.97E-05	1.95E-05	1.90E-05	1.89E-05	1.87E-05	1.86E-05	1.95E-05
2.00	2.66E-05	2.67E-05	2.80E-05	2.72E-05	2.67E-05	2.59E-05	2.55E-05	2.54E-05	2.54E-05	2.65E-05
3.00	4.26E-05	4.15E-05	4.23E-05	4.14E-05	4.11E-05	4.01E-05	3.96E-05	3.90E-05	3.87E-05	4.11E-05
4.00	5.76E-05	5.92E-05	5.83E-05	5.75E-05	5.96E-05	5.68E-05	5.75E-05	5.65E-05	5.57E-05	5.82E-05
	SAF (*Lower Large Intestine Wall* ← *Stomach Contents*) **in kg^{-1} for Photon**									
0.01	0.0	0.0	0.0	0.0	0.0	0.0	0.0	0.0	0.0	0.0
0.015	0.0	0.0	0.0	0.0	0.0	0.0	0.0	0.0	0.0	0.0
0.02	5.05E-05	5.19E-05	4.92E-05	4.65E-05	4.44E-05	4.56E-05	4.32E-05	4.16E-05	4.15E-05	4.59E-05
0.03	1.37E-03	1.32E-03	1.34E-03	1.29E-03	1.27E-03	1.27E-03	1.20E-03	1.20E-03	1.20E-03	1.27E-03
0.05	3.96E-03	3.88E-03	3.88E-03	3.88E-03	3.86E-03	3.80E-03	3.75E-03	3.80E-03	3.74E-03	3.85E-03
0.10	4.42E-03	4.40E-03	4.35E-03	4.29E-03	4.33E-03	4.26E-03	4.21E-03	4.23E-03	4.19E-03	4.32E-03
0.20	4.13E-03	4.18E-03	4.09E-03	4.08E-03	4.06E-03	3.96E-03	3.92E-03	3.87E-03	3.89E-03	4.05E-03
0.35	4.23E-03	5.16E-03	4.21E-03	4.24E-03	4.33E-03	4.05E-03	3.91E-03	3.83E-03	3.81E-03	4.20E-03
0.50	4.34E-03	4.16E-03	4.05E-03	4.42E-03	4.24E-03	4.52E-03	4.41E-03	4.15E-03	4.07E-03	4.34E-03
0.75	4.53E-03	4.32E-03	4.15E-03	4.88E-03	4.47E-03	4.74E-03	4.70E-03	4.29E-03	4.19E-03	4.56E-03
1.00	4.52E-03	4.28E-03	4.07E-03	4.70E-03	4.36E-03	4.63E-03	4.63E-03	4.25E-03	4.17E-03	4.49E-03
1.50	4.29E-03	4.02E-03	3.91E-03	4.85E-03	4.31E-03	4.47E-03	4.63E-03	4.21E-03	4.16E-03	4.39E-03
2.00	4.00E-03	3.75E-03	3.57E-03	4.34E-03	3.92E-03	4.19E-03	4.20E-03	3.86E-03	3.89E-03	4.04E-03
3.00	2.89E-03	2.88E-03	2.79E-03	2.75E-03	2.94E-03	2.62E-03	2.77E-03	2.85E-03	2.67E-03	2.85E-03
4.00	2.71E-03	2.55E-03	2.51E-03	2.50E-03	2.69E-03	2.37E-03	2.54E-03	2.63E-03	2.46E-03	2.61E-03

Table B2. Continued.

SAF (*Lower Large Intestine Wall* ← *Small Intestine Contents*) **in kg^{-1}**														
Source Particle Energy (MeV)														
0.01			**0.015**			**0.02**			**0.03**			**0.05**		
Depth (cm)	**Electron SAF**	**Photon SAF**	**Depth (cm)**	**Electron SAF**	**Photon SAF**	**Depth (cm)**	**Electron SAF**	**Photon SAF**	**Depth (cm)**	**Electron SAF**	**Photon SAF**	**Depth (cm)**	**Electron SAF**	**Photon SAF**
0.0025	4.58E-10[b]	1.29E-03	**0.0025**	7.66E-08[a]	3.04E-02	**0.0025**	5.88E-07	6.32E-2	**0.0025**	2.69E-06	8.58E-2	**0.0025**	9.39E-06	6.44E-2
0.0075	4.63E-10[b]	1.29E-03	**0.0075**	7.67E-08[a]	3.00E-02	**0.0075**	5.86E-07	6.35E-2	**0.0075**	2.80E-06	8.62E-2	**0.0075**	9.54E-06	6.46E-2
0.0125	4.69E-10[b]	1.30E-03	**0.0125**	7.67E-08[a]	3.05E-02	**0.0125**	5.85E-07	6.77E-2	**0.0125**	2.75E-06	8.66E-2	**0.0125**	9.43E-06	6.48E-2
0.0175	4.80E-10[b]	1.30E-03	**0.0175**	7.67E-08[a]	3.07E-02	**0.0175**	5.83E-07	6.49E-2	**0.0175**	2.70E-06	8.74E-2	**0.0175**	9.29E-06	6.50E-2
0.0225	4.87E-10[b]	1.31E-03	**0.0225**	7.67E-08[a]	3.05E-02	**0.0225**	5.83E-07	6.44E-2	**0.0225**	2.72E-06	8.70E-2	**0.0225**	9.43E-06	6.50E-2
0.0275	5.00E-10[b]	1.33E-03	**0.0275**	7.65E-08[a]	3.02E-02	**0.0275**	5.91E-07	6.40E-2	**0.0275**	2.77E-06	8.75E-2	**0.0275**	9.35E-06	6.50E-2
0.0325	5.04E-10[b]	1.33E-03	**0.0325**	7.64E-08[a]	3.00E-02	**0.0325**	5.91E-07	6.35E-2	**0.0325**	2.70E-06	8.66E-2	**0.0325**	9.44E-06	6.46E-2
0.0375	4.92E-10[b]	1.34E-03	**0.0375**	7.67E-08[a]	3.03E-02	**0.0375**	5.88E-07	6.31E-2	**0.0375**	2.68E-06	8.67E-2	**0.0375**	9.38E-06	6.47E-2
0.0425	4.94E-10[b]	1.35E-03	**0.0425**	8.01E-08[a]	3.06E-02	**0.0425**	5.86E-07	6.48E-2	**0.0425**	2.67E-06	8.91E-2	**0.0425**	9.54E-06	6.50E-2
0.0475	4.96E-10[b]	1.36E-03	**0.0475**	7.89E-08[a]	3.10E-02	**0.0475**	5.86E-07	6.62E-2	**0.0475**	2.65E-06	8.83E-2	**0.0475**	9.35E-06	6.45E-2
0.0525	5.01E-10[b]	1.38E-03	**0.0525**	7.88E-08[a]	3.06E-02	**0.0525**	5.84E-07	6.60E-2	**0.0525**	2.65E-06	8.78E-2	**0.0525**	9.54E-06	6.46E-2
0.0575	5.11E-10[b]	1.39E-03	**0.0575**	7.90E-08[a]	3.06E-02	**0.0575**	5.83E-07	6.52E-2	**0.0575**	2.63E-06	8.78E-2	**0.0575**	9.47E-06	6.40E-2
0.0625	5.26E-10[b]	1.42E-03	**0.0625**	7.89E-08[a]	3.03E-02	**0.0625**	5.85E-07	6.47E-2	**0.0625**	2.63E-06	8.76E-2	**0.0625**	9.53E-06	6.38E-2
0.0675	5.45E-10[b]	1.44E-03	**0.0675**	7.93E-08[a]	3.07E-02	**0.0675**	5.94E-07	6.60E-2	**0.0675**	2.63E-06	8.68E-2	**0.0675**	9.51E-06	6.40E-2
0.0725	5.67E-10[b]	1.46E-03	**0.0725**	8.00E-08[a]	3.18E-02	**0.0725**	5.91E-07	6.74E-2	**0.0725**	2.63E-06	8.81E-2	**0.0725**	9.39E-06	6.49E-2
0.0775	5.83E-10[b]	1.47E-03	**0.0775**	8.13E-08[a]	3.13E-02	**0.0775**	5.89E-07	6.58E-2	**0.0775**	2.62E-06	8.86E-2	**0.0775**	9.63E-06	6.48E-2
0.0825	5.92E-10[b]	1.49E-03	**0.0825**	8.20E-08[a]	3.08E-02	**0.0825**	5.90E-07	6.50E-2	**0.0825**	2.62E-06	8.81E-2	**0.0825**	9.45E-06	6.53E-2
0.0875	6.09E-10[b]	1.51E-03	**0.0875**	8.21E-08[a]	3.17E-02	**0.0875**	5.90E-07	7.00E-2	**0.0875**	2.69E-06	8.95E-2	**0.0875**	9.35E-06	6.53E-2
0.0925	6.48E-10[b]	1.54E-03	**0.0925**	8.25E-08[a]	3.13E-02	**0.0925**	5.91E-07	6.77E-2	**0.0925**	2.74E-06	9.06E-2	**0.0925**	9.74E-06	6.51E-2
0.0975	6.44E-10[b]	1.57E-03	**0.0975**	8.27E-08[a]	3.11E-02	**0.0975**	6.01E-07	6.63E-2	**0.0975**	2.69E-06	9.01E-2	**0.0975**	9.44E-06	6.49E-2
0.1025	6.66E-10[b]	1.59E-03	**0.1025**	8.31E-08[a]	3.10E-02	**0.1025**	6.07E-07	6.56E-2	**0.1025**	2.67E-06	8.94E-2	**0.1025**	9.37E-06	6.47E-2
0.1075	6.86E-10[b]	1.62E-03	**0.1075**	8.38E-08	3.11E-02	**0.1075**	6.39E-07	6.50E-2	**0.1075**	2.66E-06	8.89E-2	**0.1075**	9.35E-06	6.44E-2
0.115	7.16E-10[b]	1.67E-03	**0.115**	8.46E-08	3.14E-02	**0.115**	6.33E-07	6.69E-2	**0.115**	2.65E-06	8.94E-2	**0.115**	9.41E-06	6.38E-2
0.125	7.62E-10[b]	1.73E-03	**0.125**	8.60E-08	3.14E-02	**0.125**	6.20E-07	6.52E-2	**0.125**	2.76E-06	8.94E-2	**0.125**	9.71E-06	6.40E-2
0.16	1.09E-09[b]	2.27E-03	**0.16**	1.06E-07	3.63E-02	**0.16**	7.24E-07	7.60E-2	**0.16**	3.17E-06	1.00E-1	**0.16**	1.08E-05	7.15E-2
0.22	1.72E-09[a]	3.04E-03	**0.22**	1.28E-07	3.84E-02	**0.22**	7.70E-07	7.33E-2	**0.22**	3.20E-06	1.02E-1	**0.22**	1.11E-05	7.22E-2

Table B2. Continued.

SAF(*Lower Large Intestine Wall* ← *Small Intestine Contents*) **in kg^{-1}**														
Source Particle Energy (MeV)														
0.10			**0.20**			**0.35**			**0.50**			**0.75**		
Depth (cm)	**Electron SAF**	**Photon SAF**	**Depth (cm)**	**Electron SAF**	**Photon SAF**	**Depth (cm)**	**Electron SAF**	**Photon SAF**	**Depth (cm)**	**Electron SAF**	**Photon SAF**	**Depth (cm)**	**Electron SAF**	**Photon SAF**
0.0025	2.57E-05	4.21E-2	**0.0025**	4.78E-05	3.87E-2	**0.0025**	7.28E-05	3.66E-2	**0.0025**	9.47E-05	3.60E-2	**0.0025**	1.29E-04	3.42E-2
0.0075	2.56E-05	4.24E-2	**0.0075**	4.77E-05	3.87E-2	**0.0075**	7.32E-05	3.63E-2	**0.0075**	9.42E-05	3.61E-2	**0.0075**	1.29E-04	3.42E-2
0.0125	2.56E-05	4.23E-2	**0.0125**	4.81E-05	3.86E-2	**0.0125**	7.27E-05	3.63E-2	**0.0125**	9.43E-05	3.60E-2	**0.0125**	1.29E-04	3.43E-2
0.0175	2.58E-05	4.24E-2	**0.0175**	4.80E-05	3.88E-2	**0.0175**	7.28E-05	3.66E-2	**0.0175**	9.35E-05	3.62E-2	**0.0175**	1.29E-04	3.45E-2
0.0225	2.59E-05	4.31E-2	**0.0225**	4.78E-05	3.85E-2	**0.0225**	7.27E-05	3.66E-2	**0.0225**	9.47E-05	3.62E-2	**0.0225**	1.29E-04	3.44E-2
0.0275	2.57E-05	4.32E-2	**0.0275**	4.76E-05	3.86E-2	**0.0275**	7.32E-05	3.69E-2	**0.0275**	9.47E-05	3.64E-2	**0.0275**	1.30E-04	3.46E-2
0.0325	2.55E-05	4.24E-2	**0.0325**	4.79E-05	3.87E-2	**0.0325**	7.30E-05	3.69E-2	**0.0325**	9.48E-05	3.67E-2	**0.0325**	1.30E-04	3.49E-2
0.0375	2.57E-05	4.23E-2	**0.0375**	4.77E-05	3.87E-2	**0.0375**	7.34E-05	3.65E-2	**0.0375**	9.43E-05	3.64E-2	**0.0375**	1.30E-04	3.48E-2
0.0425	2.58E-05	4.28E-2	**0.0425**	4.79E-05	3.88E-2	**0.0425**	7.29E-05	3.69E-2	**0.0425**	9.39E-05	3.67E-2	**0.0425**	1.30E-04	3.49E-2
0.0475	2.58E-05	4.27E-2	**0.0475**	4.80E-05	3.90E-2	**0.0475**	7.27E-05	3.67E-2	**0.0475**	9.36E-05	3.66E-2	**0.0475**	1.30E-04	3.50E-2
0.0525	2.56E-05	4.24E-2	**0.0525**	4.78E-05	3.88E-2	**0.0525**	7.24E-05	3.67E-2	**0.0525**	9.42E-05	3.65E-2	**0.0525**	1.30E-04	3.49E-2
0.0575	2.56E-05	4.22E-2	**0.0575**	4.76E-05	3.89E-2	**0.0575**	7.30E-05	3.63E-2	**0.0575**	9.42E-05	3.64E-2	**0.0575**	1.30E-04	3.48E-2
0.0625	2.57E-05	4.26E-2	**0.0625**	4.78E-05	3.92E-2	**0.0625**	7.30E-05	3.65E-2	**0.0625**	9.47E-05	3.64E-2	**0.0625**	1.30E-04	3.48E-2
0.0675	2.58E-05	4.25E-2	**0.0675**	4.82E-05	3.92E-2	**0.0675**	7.31E-05	3.63E-2	**0.0675**	9.40E-05	3.66E-2	**0.0675**	1.29E-04	3.46E-2
0.0725	2.56E-05	4.32E-2	**0.0725**	4.82E-05	3.89E-2	**0.0725**	7.32E-05	3.65E-2	**0.0725**	9.40E-05	3.65E-2	**0.0725**	1.29E-04	3.43E-2
0.0775	2.56E-05	4.25E-2	**0.0775**	4.82E-05	3.89E-2	**0.0775**	7.33E-05	3.65E-2	**0.0775**	9.48E-05	3.64E-2	**0.0775**	1.30E-04	3.43E-2
0.0825	2.56E-05	4.29E-2	**0.0825**	4.81E-05	3.90E-2	**0.0825**	7.33E-05	3.66E-2	**0.0825**	9.48E-05	3.67E-2	**0.0825**	1.30E-04	3.46E-2
0.0875	2.57E-05	4.32E-2	**0.0875**	4.82E-05	3.88E-2	**0.0875**	7.38E-05	3.66E-2	**0.0875**	9.43E-05	3.64E-2	**0.0875**	1.29E-04	3.44E-2
0.0925	2.58E-05	4.29E-2	**0.0925**	4.79E-05	3.88E-2	**0.0925**	7.37E-05	3.71E-2	**0.0925**	9.50E-05	3.64E-2	**0.0925**	1.30E-04	3.45E-2
0.0975	2.59E-05	4.30E-2	**0.0975**	4.78E-05	3.90E-2	**0.0975**	7.38E-05	3.69E-2	**0.0975**	9.48E-05	3.61E-2	**0.0975**	1.30E-04	3.43E-2
0.1025	2.59E-05	4.29E-2	**0.1025**	4.76E-05	3.91E-2	**0.1025**	7.44E-05	3.68E-2	**0.1025**	9.45E-05	3.63E-2	**0.1025**	1.29E-04	3.42E-2
0.1075	2.60E-05	4.25E-2	**0.1075**	4.78E-05	3.90E-2	**0.1075**	7.41E-05	3.70E-2	**0.1075**	9.44E-05	3.68E-2	**0.1075**	1.30E-04	3.45E-2
0.115	2.61E-05	4.29E-2	**0.115**	4.80E-05	3.91E-2	**0.115**	7.38E-05	3.68E-2	**0.115**	9.47E-05	3.71E-2	**0.115**	1.30E-04	3.47E-2
0.125	2.63E-05	4.31E-2	**0.125**	4.79E-05	3.89E-2	**0.125**	7.38E-05	3.68E-2	**0.125**	9.50E-05	3.68E-2	**0.125**	1.30E-04	3.45E-2
0.16	2.93E-05	4.75E-2	**0.16**	5.44E-05	4.32E-2	**0.16**	8.27E-05	4.09E-2	**0.16**	1.06E-04	4.07E-2	**0.16**	1.45E-04	3.85E-2
0.22	2.97E-05	4.78E-2	**0.22**	5.47E-05	4.31E-2	**0.22**	8.30E-05	4.14E-2	**0.22**	1.06E-04	4.05E-2	**0.22**	1.47E-04	3.88E-2

Table B2. Continued.

SAF(*Lower Large Intestine Wall* ← *Small Intestine Contents*) **in kg^{-1}**														
Source Particle Energy (MeV)														
1.00			**1.50**			**2.00**			**3.00**			**4.00**		
Depth (cm)	**Electron SAF**	**Photon SAF**	**Depth (cm)**	**Electron SAF**[b]	**Photon SAF**	**Depth (cm)**	**Electron SAF**	**Photon SAF**	**Depth (cm)**	**Electron SAF**	**Photon SAF**	**Depth (cm)**	**Electron SAF**	**Photon SAF**
0.0025	1.65E-04	3.23E-2	**0.0025**	2.36E-4	2.95E-2	**0.0025**	1.02E-03[b]	2.74E-2	**0.0025**	2.30E-02	2.36E-2	**0.0025**	5.10E-02	2.25E-2
0.0075	1.65E-04	3.25E-2	**0.0075**	2.36E-4	2.95E-2	**0.0075**	1.53E-03[b]	2.72E-2	**0.0075**	2.57E-02	2.34E-2	**0.0075**	4.96E-02	2.24E-2
0.0125	1.64E-04	3.24E-2	**0.0125**	2.38E-4	2.93E-2	**0.0125**	1.39E-03[c]	2.71E-2	**0.0125**	2.67E-02	2.34E-2	**0.0125**	5.07E-02	2.24E-2
0.0175	1.65E-04	3.25E-2	**0.0175**	2.90E-4	2.96E-2	**0.0175**	1.25E-03[c]	2.73E-2	**0.0175**	2.82E-02	2.39E-2	**0.0175**	4.94E-02	2.25E-2
0.0225	1.65E-04	3.27E-2	**0.0225**	2.71E-4	2.95E-2	**0.0225**	1.14E-03[b]	2.76E-2	**0.0225**	2.60E-02	2.40E-2	**0.0225**	4.98E-02	2.26E-2
0.0275	1.66E-04	3.27E-2	**0.0275**	2.81E-4	2.97E-2	**0.0275**	1.52E-03[c]	2.75E-2	**0.0275**	2.57E-02	2.38E-2	**0.0275**	4.97E-02	2.27E-2
0.0325	1.67E-04	3.28E-2	**0.0325**	3.07E-4	3.00E-2	**0.0325**	2.43E-03[b]	2.79E-2	**0.0325**	2.22E-02	2.43E-2	**0.0325**	4.85E-02	2.27E-2
0.0375	1.66E-04	3.27E-2	**0.0375**	4.99E-4	2.97E-2	**0.0375**	2.40E-03[b]	2.78E-2	**0.0375**	2.33E-02	2.38E-2	**0.0375**	4.70E-02	2.28E-2
0.0425	1.67E-04	3.30E-2	**0.0425**	3.53E-4	2.99E-2	**0.0425**	2.47E-03[b]	2.78E-2	**0.0425**	2.48E-02	2.39E-2	**0.0425**	5.31E-02	2.27E-2
0.0475	1.66E-04	3.28E-2	**0.0475**	3.52E-4	3.00E-2	**0.0475**	3.20E-03[b]	2.78E-2	**0.0475**	2.36E-02	2.35E-2	**0.0475**	4.63E-02	2.27E-2
0.0525	1.66E-04	3.27E-2	**0.0525**	3.53E-4	2.99E-2	**0.0525**	3.01E-03[b]	2.76E-2	**0.0525**	2.51E-02	2.35E-2	**0.0525**	4.85E-02	2.27E-2
0.0575	1.66E-04	3.24E-2	**0.0575**	4.01E-4	2.99E-2	**0.0575**	2.96E-03[b]	2.78E-2	**0.0575**	2.57E-02	2.32E-2	**0.0575**	5.38E-02	2.27E-2
0.0625	1.65E-04	3.25E-2	**0.0625**	3.82E-4	2.98E-2	**0.0625**	2.36E-03[b]	2.76E-2	**0.0625**	2.37E-02	2.34E-2	**0.0625**	5.28E-02	2.26E-2
0.0675	1.66E-04	3.29E-2	**0.0675**	3.90E-4	2.99E-2	**0.0675**	3.07E-03[b]	2.79E-2	**0.0675**	2.52E-02	2.36E-2	**0.0675**	4.82E-02	2.27E-2
0.0725	1.65E-04	3.29E-2	**0.0725**	3.67E-4	2.98E-2	**0.0725**	2.93E-03[b]	2.76E-2	**0.0725**	2.67E-02	2.36E-2	**0.0725**	5.06E-02	2.27E-2
0.0775	1.65E-04	3.26E-2	**0.0775**	4.59E-4	2.98E-2	**0.0775**	2.60E-03[b]	2.75E-2	**0.0775**	2.49E-02	2.32E-2	**0.0775**	5.56E-02	2.27E-2
0.0825	1.66E-04	3.31E-2	**0.0825**	6.71E-4	3.00E-2	**0.0825**	3.09E-03[b]	2.78E-2	**0.0825**	2.29E-02	2.35E-2	**0.0825**	5.24E-02	2.27E-2
0.0875	1.66E-04	3.26E-2	**0.0875**	4.80E-4	2.99E-2	**0.0875**	2.81E-03[b]	2.75E-2	**0.0875**	2.44E-02	2.38E-2	**0.0875**	5.04E-02	2.26E-2
0.0925	1.67E-04	3.26E-2	**0.0925**	3.60E-4	3.00E-2	**0.0925**	3.30E-03[a]	2.74E-2	**0.0925**	2.45E-02	2.39E-2	**0.0925**	5.25E-02	2.27E-2
0.0975	1.67E-04	3.26E-2	**0.0975**	2.75E-4	3.00E-2	**0.0975**	3.19E-03[b]	2.73E-2	**0.0975**	2.21E-02	2.34E-2	**0.0975**	4.75E-02	2.27E-2
0.1025	1.67E-04	3.25E-2	**0.1025**	3.42E-4	2.98E-2	**0.1025**	3.82E-03[a]	2.73E-2	**0.1025**	2.44E-02	2.36E-2	**0.1025**	5.32E-02	2.25E-2
0.1075	1.67E-04	3.28E-2	**0.1075**	6.39E-4	3.01E-2	**0.1075**	3.87E-03[a]	2.76E-2	**0.1075**	2.63E-02	2.41E-2	**0.1075**	5.03E-02	2.26E-2
0.115	1.67E-04	3.32E-2	**0.115**	3.52E-4	3.01E-2	**0.115**	4.17E-03[a]	2.77E-2	**0.115**	2.50E-02	2.37E-2	**0.115**	4.75E-02	2.28E-2
0.125	1.67E-04	3.28E-2	**0.125**	4.63E-4	3.00E-2	**0.125**	4.60E-03[a]	2.74E-2	**0.125**	2.52E-02	2.38E-2	**0.125**	5.25E-02	2.26E-2
0.16	1.85E-04	3.63E-2	**0.16**	1.27E-3	3.34E-2	**0.16**	6.74E-03	3.07E-2	**0.16**	3.11E-02	2.70E-2	**0.16**	5.79E-02	2.50E-2
0.22	1.87E-04	3.65E-2	**0.22**	3.13E-3	3.35E-2	**0.22**	1.19E-02	3.10E-2	**0.22**	3.38E-02	2.71E-2	**0.22**	5.97E-02	2.51E-2

Table B2. Continued.

Source Energy (MeV)	**SAF** $(Lower\ Large\ Intestine\ Wall \leftarrow Upper\ Large\ Intestine\ Contents)$ **in kg^{-1} for Electron**									
	At Mean Position (cm) in the Lower Large Intestine Wall Measured Outward from Contents-Wall Interface.									Average to the
	0.025	**0.06**	**0.075**	**0.085**	**0.11**	**0.15**	**0.19**	**0.22**	**0.24**	**Wall**
0.01	0.0	0.0	0.0	0.0	0.0	0.0	0.0	0.0	0.0	0.0
0.015[b]	5.47E-09	5.02E-09	5.19E-09	3.94E-09	3.93E-09	3.85E-09	3.64E-09	3.58E-09	3.76E-09	4.25E-09
0.02[a]	3.49E-08	3.36E-08	3.31E-08	3.32E-08	3.47E-08	3.21E-08	3.39E-08	3.76E-08	3.53E-08	3.43E-08
0.03	2.36E-07	2.26E-07	2.38E-07	2.29E-07	2.18E-07	2.18E-07	2.05E-07	1.98E-07	1.99E-07	2.18E-07
0.05	1.07E-06	1.07E-06	1.09E-06	1.06E-06	1.05E-06	1.03E-06	1.05E-06	1.05E-06	1.03E-06	1.05E-06
0.10	4.03E-06	4.01E-06	3.97E-06	3.99E-06	4.01E-06	3.94E-06	3.96E-06	3.88E-06	3.84E-06	3.99E-06
0.20	9.18E-06	9.13E-06	9.12E-06	9.07E-06	9.04E-06	8.90E-06	8.83E-06	8.80E-06	8.76E-06	9.05E-06
0.35	1.53E-05	1.53E-05	1.54E-05	1.54E-05	1.54E-05	1.50E-05	1.50E-05	1.51E-05	1.49E-05	1.53E-05
0.50	2.17E-05	2.18E-05	2.16E-05	2.16E-05	2.16E-05	2.11E-05	2.09E-05	2.10E-05	2.11E-05	2.16E-05
0.75	3.10E-05	3.08E-05	3.09E-05	3.08E-05	3.07E-05	3.00E-05	3.00E-05	2.99E-05	2.97E-05	3.07E-05
1.00	1.77E-04[g]	4.48E-05	2.68E-05[c]	4.62E-05[a]	3.91E-05	4.01E-05	1.07E-04[f]	3.82E-05	3.68E-05	9.31E-05[c]
1.50	6.94E-04[d]	3.22E-04[e]	4.86E-04[e]	8.12E-04[g]	1.74E-04[f]	3.14E-04[g]	6.05E-05[a]	5.75E-05	1.26E-04[e]	3.50E-04[c]
2.00	1.37E-03[c]	1.97E-04[e]	5.39E-04[g]	3.51E-04[e]	5.46E-04[e]	4.87E-04[e]	6.05E-04[d]	2.28E-04[c]	7.59E-05	6.39E-04[b]
3.00	2.88E-03[a]	2.21E-03[b]	1.09E-03[f]	2.80E-03[b]	2.91E-03[b]	2.44E-03[b]	1.98E-03[b]	1.30E-03[b]	1.08E-03[b]	2.72E-03[a]
4.00	1.91E-03[c]	1.64E-03[c]	1.28E-03[b]	1.12E-03[c]	1.53E-03[c]	1.87E-03[c]	1.43E-03[c]	1.22E-03[b]	1.33E-03[b]	1.90E-03[b]
	SAF $(Lower\ Large\ Intestine\ Wall \leftarrow Upper\ Large\ Intestine\ Contents)$ **in kg^{-1} for Photon**									
0.01[b]	1.87E-04	1.56E-04	1.48E-04	1.37E-04	1.25E-04	1.07E-04	9.03E-05	8.15E-05	7.86E-05	1.24E-04
0.015	2.02E-03	1.85E-03	1.84E-03	1.79E-03	1.69E-03	1.64E-03	1.53E-03	1.49E-03	1.47E-03	1.70E-03
0.02	5.54E-03	5.45E-03	5.46E-03	5.34E-03	5.22E-03	5.06E-03	4.87E-03	4.81E-03	4.74E-03	5.15E-03
0.03	1.25E-02	1.24E-02	1.24E-02	1.23E-02	1.22E-02	1.21E-02	1.21E-02	1.21E-02	1.20E-02	1.22E-02
0.05	1.57E-02	1.56E-02	1.56E-02	1.57E-02	1.56E-02	1.54E-02	1.53E-02	1.54E-02	1.53E-02	1.56E-02
0.10	1.29E-02	1.29E-02	1.29E-02	1.29E-02	1.29E-02	1.26E-02	1.25E-02	1.25E-02	1.25E-02	1.29E-02
0.20	1.14E-02	1.14E-02	1.14E-02	1.14E-02	1.13E-02	1.09E-02	1.09E-02	1.09E-02	1.10E-02	1.13E-02
0.35	1.08E-02	1.08E-02	1.07E-02	1.07E-02	1.07E-02	1.04E-02	1.04E-02	1.04E-02	1.04E-02	1.07E-02
0.50	1.04E-02	1.04E-02	1.03E-02	1.02E-02	1.02E-02	9.89E-03	9.91E-03	1.00E-02	1.01E-02	1.03E-02
0.75	9.94E-03	9.97E-03	9.91E-03	9.83E-03	9.81E-03	9.49E-03	9.56E-03	9.59E-03	9.73E-03	9.90E-03
1.00	9.43E-03	9.43E-03	9.55E-03	9.46E-03	9.40E-03	8.96E-03	9.03E-03	8.99E-03	9.02E-03	9.38E-03
1.50	8.78E-03	8.63E-03	8.58E-03	8.60E-03	8.62E-03	8.26E-03	8.31E-03	8.23E-03	8.30E-03	8.63E-03
2.00	8.31E-03	7.95E-03	7.90E-03	8.00E-03	7.98E-03	7.76E-03	7.82E-03	7.76E-03	7.89E-03	8.11E-03
3.00	7.44E-03	7.45E-03	7.38E-03	7.31E-03	7.27E-03	7.08E-03	7.20E-03	7.16E-03	7.15E-03	7.41E-03
4.00	7.24E-03	7.20E-03	7.05E-03	7.14E-03	6.82E-03	6.72E-03	6.88E-03	6.79E-03	6.64E-03	7.06E-03

Table B2. Continued.

SAF (*Lower Large Intestine Wall* ← *Lower Large Intestine Contents*) **in kg^{-1}**														
Source Particle Energy (MeV)														
0.01			**0.015**			**0.02**			**0.03**			**0.05**		
Depth (cm)	**Electron SAF**	**Photon SAF**	**Depth (cm)**	**Electron SAF**	**Photon SAF**	**Depth (cm)**	**Electron SAF**	**Photon SAF**	**Depth (cm)**	**Electron SAF**	**Photon SAF**	**Depth (cm)**	**Electron SAF**	**Photon SAF**
0.00005	2.87E-01[f]	7.78E-1	**0.00005**	3.66E-1[a]	6.89E-1	**0.00010**	3.67E-1	5.36E-1	**0.00010**	4.62E-1[a]	2.86E-1	**0.0005**	4.37E-1	1.24E-1
0.00020	2.96E-02	7.75E-1	**0.00020**	1.40E-1[a]	6.88E-1	**0.00035**	1.42E-1[c]	5.36E-1	**0.00035**	2.85E-1[b]	2.86E-1	**0.0015**	1.80E-1[a]	1.23E-1
0.00040	3.86E-05	7.71E-1	**0.00040**	1.62E-2[b]	6.87E-1	**0.00075**	9.28E-3[b]	5.35E-1	**0.00075**	1.33E-1[c]	2.86E-1	**0.003**	3.19E-2[a]	1.23E-1
0.00060	4.68E-05	7.68E-1	**0.00060**	4.84E-4[d]	6.86E-1	**0.0015**	8.06E-5	5.32E-1	**0.0015**	1.04E-2[a]	2.85E-1	**0.005**	2.22E-4[a]	1.22E-1
0.00085	3.11E-05	7.64E-1	**0.00085**	5.84E-5	6.85E-1	**0.003**	6.92E-5	5.29E-1	**0.003**	1.08E-4[a]	2.84E-1	**0.0075**	1.44E-4	1.22E-1
0.00300	2.47E-05	7.33E-1	**0.00300**	4.79E-5	6.74E-1	**0.006**	6.31E-5	5.24E-1	**0.006**	9.97E-5	2.82E-1	**0.0105**	1.34E-4	1.22E-1
0.01000	1.34E-05	6.57E-1	**0.01000**	3.33E-5	6.46E-1	**0.0115**	1.91E-4[d]	5.15E-1	**0.0115**	8.55E-5	2.79E-1	**0.0135**	1.30E-4	1.21E-1
0.02000	8.06E-06	5.74E-1	**0.02000**	2.36E-5	6.13E-1	**0.02**	4.17E-5	5.03E-1	**0.02**	7.15E-5	2.76E-1	**0.02**	1.18E-4	1.21E-1
0.03000	5.27E-06	5.09E-1	**0.03000**	1.83E-5	5.84E-1	**0.03**	3.36E-5	4.90E-1	**0.03**	1.69E-4[d]	2.71E-1	**0.03**	1.07E-4	1.19E-1
0.04000	3.96E-06	4.55E-1	**0.04000**	1.49E-5	5.58E-1	**0.04**	2.88E-5	4.77E-1	**0.04**	5.80E-5	2.67E-1	**0.04**	1.01E-4	1.18E-1
0.05000	2.77E-06	4.09E-1	**0.05000**	1.31E-5	5.35E-1	**0.05**	2.61E-5	4.65E-1	**0.05**	5.24E-5	2.64E-1	**0.05**	8.97E-5	1.17E-1
0.05750	2.61E-06	3.79E-1	**0.05750**	1.11E-5	5.19E-1	**0.0575**	2.30E-5	4.56E-1	**0.0575**	5.07E-5	2.61E-1	**0.0575**	8.79E-5	1.17E-1
0.06250	2.12E-06	3.61E-1	**0.06250**	1.08E-5	5.08E-1	**0.0625**	2.31E-5	4.51E-1	**0.0625**	5.47E-5	2.59E-1	**0.0625**	7.64E-5[a]	1.16E-1
0.06750	1.95E-06	3.44E-1	**0.06750**	1.02E-5	4.99E-1	**0.0675**	2.17E-5	4.45E-1	**0.0675**	4.59E-5	2.57E-1	**0.0675**	8.15E-5[b]	1.16E-1
0.07250	1.90E-06	3.27E-1	**0.07250**	1.02E-5	4.89E-1	**0.0725**	2.11E-5	4.40E-1	**0.0725**	4.52E-5	2.56E-1	**0.0725**	9.20E-5[a]	1.15E-1
0.07750	1.63E-06	3.13E-1	**0.07750**	8.52E-6	4.80E-1	**0.0775**	1.92E-5	4.36E-1	**0.0775**	4.22E-5	2.54E-1	**0.0775**	8.06E-5	1.15E-1
0.08250	1.49E-06	2.99E-1	**0.08250**	9.27E-6[a]	4.72E-1	**0.0825**	1.86E-5	4.31E-1	**0.0825**	4.21E-5	2.52E-1	**0.0825**	7.20E-5	1.14E-1
0.08750	1.47E-06	2.85E-1	**0.08750**	7.23E-6[b]	4.63E-1	**0.0875**	1.75E-5	4.27E-1	**0.0875**	3.78E-5	2.51E-1	**0.0875**	7.53E-5	1.14E-1
0.09250	1.18E-06	2.73E-1	**0.09250**	7.66E-6	4.54E-1	**0.0925**	1.66E-5	4.22E-1	**0.0925**	3.71E-5	2.49E-1	**0.0925**	7.57E-5	1.13E-1
0.09750	1.05E-06	2.61E-1	**0.09750**	6.92E-6	4.46E-1	**0.0975**	1.67E-5	4.18E-1	**0.0975**	3.88E-5	2.48E-1	**0.0975**	7.38E-5	1.13E-1
0.10250	9.89E-07	2.50E-1	**0.10250**	6.27E-6	4.38E-1	**0.1025**	1.60E-5	4.14E-1	**0.1025**	3.65E-5	2.46E-1	**0.1025**	6.25E-5[a]	1.12E-1
0.10750	9.85E-07	2.39E-1	**0.10750**	6.91E-6	4.30E-1	**0.1075**	1.39E-5[c]	4.10E-1	**0.1075**	3.57E-5	2.45E-1	**0.1075**	7.19E-5[a]	1.12E-1
0.11500	8.42E-07	2.24E-1	**0.11500**	6.07E-6	4.19E-1	**0.115**	1.60E-5	4.03E-1	**0.115**	3.62E-5	2.43E-1	**0.115**	6.15E-5[a]	1.11E-1
0.12500	6.53E-07	2.06E-1	**0.12500**	5.34E-6	4.05E-1	**0.125**	1.36E-5	3.95E-1	**0.125**	3.16E-5	2.40E-1	**0.125**	6.89E-5[a]	1.11E-1
0.14000	2.64E-07	1.04E-1	**0.14000**	1.99E-6	2.25E-1	**0.14**	5.62E-6	2.27E-1	**0.14**	1.47E-5	1.45E-1	**0.14**	3.14E-5	7.22E-2
0.17500	1.35E-07	7.84E-2	**0.17500**	1.67E-6	2.01E-1	**0.175**	4.63E-6	2.13E-1	**0.175**	1.27E-5	1.41E-1	**0.175**	2.68E-5	7.09E-2
0.22500	7.24E-08	5.30E-2	**0.22500**	1.17E-6	1.73E-1	**0.225**	3.79E-6	1.95E-1	**0.225**	1.04E-5	1.34E-1	**0.225**	2.35E-5	6.92E-2

Table B2. Continued.

SAF (*Lower Large Intestine Wall* ← *Lower Large Intestine Contents*) **in kg^{-1}**														
Source Particle Energy (MeV)														
0.10			**0.20**			**0.35**			**0.50**			**0.75**		
Depth (cm)	**Electron SAF**	**Photon SAF**	**Depth (cm)**	**Electron SAF**	**Photon SAF**	**Depth (cm)**	**Electron SAF**	**Photon SAF**	**Depth (cm)**	**Electron SAF**	**Photon SAF**	**Depth (cm)**	**Electron SAF**	**Photon SAF**
0.0005	6.75E-01	7.42E-2	**0.002**	6.71E-1	7.22E-2	**0.002**	7.57E-1	7.28E-2	**0.002**	8.21E-1	7.20E-2	**0.005**	7.63E-1	6.82E-2
0.0015	5.18E-01	7.40E-2	**0.0065**	4.57E-1	7.18E-2	**0.0065**	6.10E-1	7.21E-2	**0.0065**	7.09E-1	7.13E-2	**0.015**	6.32E-1	6.72E-2
0.003	3.74E-01	7.39E-2	**0.012**	3.16E-1	7.14E-2	**0.012**	5.20E-1	7.17E-2	**0.012**	6.12E-1	7.07E-2	**0.025**	5.53E-1	6.62E-2
0.005	2.31E-01	7.36E-2	**0.02**	1.51E-1	7.08E-2	**0.02**	4.01E-1	7.11E-2	**0.02**	5.15E-1	6.98E-2	**0.035**	4.88E-1	6.53E-2
0.0075	8.86E-02[a]	7.33E-2	**0.03**	3.20E-2	6.99E-2	**0.03**	2.73E-1	7.03E-2	**0.03**	4.15E-1	6.89E-2	**0.045**	4.34E-1	6.46E-2
0.0105	1.74E-02[b]	7.31E-2	**0.04**	1.80E-3	6.93E-2	**0.04**	1.83E-1	6.93E-2	**0.04**	3.34E-1	6.82E-2	**0.055**	3.95E-1	6.41E-2
0.0135	9.68E-04	7.30E-2	**0.05**	2.15E-4	6.86E-2	**0.05**	1.17E-1	6.89E-2	**0.05**	2.67E-1	6.74E-2	**0.065**	3.45E-1	6.35E-2
0.02	1.83E-04	7.24E-2	**0.0575**	1.98E-4	6.81E-2	**0.0575**	7.44E-2	6.82E-2	**0.0575**	2.32E-1	6.69E-2	**0.075**	3.09E-1	6.27E-2
0.03	1.80E-04	7.18E-2	**0.0625**	1.98E-4	6.78E-2	**0.0625**	5.13E-2	6.79E-2	**0.0625**	2.02E-1	6.65E-2	**0.085**	2.64E-1	6.18E-2
0.04	1.75E-04	7.12E-2	**0.0675**	1.87E-4	6.74E-2	**0.0675**	3.24E-2	6.73E-2	**0.0675**	1.73E-1	6.60E-2	**0.095**	2.22E-1	6.14E-2
0.05	1.59E-04	7.08E-2	**0.0725**	1.96E-4	6.72E-2	**0.0725**	2.16E-2	6.70E-2	**0.0725**	1.50E-1	6.57E-2	**0.105**	2.00E-1	6.08E-2
0.0575	1.37E-04[b]	7.02E-2	**0.0775**	1.91E-4	6.69E-2	**0.0775**	9.52E-3	6.66E-2	**0.0775**	1.27E-1	6.53E-2	**0.115**	1.74E-1	6.04E-2
0.0625	1.32E-04	6.99E-2	**0.0825**	2.09E-4	6.66E-2	**0.0825**	6.10E-3	6.64E-2	**0.0825**	1.07E-1	6.49E-2	**0.125**	1.50E-1	6.02E-2
0.0675	1.41E-04	6.96E-2	**0.0875**	1.57E-4	6.63E-2	**0.0875**	2.83E-3	6.61E-2	**0.0875**	9.43E-2	6.47E-2	**0.135**	5.44E-2	3.86E-2
0.0725	1.14E-04[a]	6.93E-2	**0.0925**	1.73E-4	6.60E-2	**0.0925**	1.29E-3	6.57E-2	**0.0925**	7.41E-2	6.44E-2	**0.145**	4.42E-2	3.83E-2
0.0775	1.45E-04[a]	6.90E-2	**0.0975**	1.80E-4	6.55E-2	**0.0975**	4.06E-4	6.54E-2	**0.0975**	6.42E-2	6.41E-2	**0.155**	3.32E-2	3.82E-2
0.0825	1.21E-04[b]	6.89E-2	**0.1025**	1.76E-4	6.52E-2	**0.1025**	2.40E-4	6.51E-2	**0.1025**	5.24E-2	6.39E-2	**0.165**	2.46E-2	3.82E-2
0.0875	1.13E-04[a]	6.86E-2	**0.1075**	1.87E-4	6.49E-2	**0.1075**	2.43E-4	6.46E-2	**0.1075**	4.47E-2	6.38E-2	**0.175**	1.93E-2	3.79E-2
0.0925	1.43E-04	6.82E-2	**0.115**	1.62E-4	6.47E-2	**0.115**	2.90E-4	6.43E-2	**0.115**	2.75E-2	6.32E-2	**0.185**	1.42E-2	3.76E-2
0.0975	1.17E-04	6.79E-2	**0.125**	1.62E-4	6.45E-2	**0.125**	2.82E-4	6.43E-2	**0.125**	1.41E-2	6.31E-2	**0.195**	1.10E-2	3.73E-2
0.1025	1.15E-04	6.76E-2	**0.14**	8.36E-5	4.24E-2	**0.14**	1.10E-4	4.16E-2	**0.14**	2.01E-3	4.06E-2	**0.205**	7.78E-3	3.71E-2
0.1075	1.17E-04	6.74E-2	**0.175**	7.68E-5	4.17E-2	**0.175**	1.05E-4	4.07E-2	**0.175**	1.36E-4	3.97E-2	**0.215**	7.15E-3	3.69E-2
0.115	1.14E-04	6.71E-2	**0.225**	6.96E-5	4.07E-2	**0.225**	9.46E-5	3.99E-2	**0.225**	1.23E-4	3.89E-2	**0.225**	2.56E-3	3.68E-2
0.125	1.13E-04	6.67E-2										**0.235**	1.74E-3	3.67E-2
0.14	5.39E-05	4.51E-2										**0.245**	1.67E-3	3.63E-2
0.175	4.90E-05	4.43E-2												
0.225	4.38E-05	4.32E-2												

Table B2. Continued.

SAF (*Lower Large Intestine Wall* ← *Lower Large Intestine Contents*) **in kg^{-1}**														
Source Particle Energy (MeV)														
1.00			**1.50**			**2.00**			**3.00**			**4.00**		
Depth (cm)	**Electron SAF**	**Photon SAF**	**Depth (cm)**	**Electron SAF**	**Photon SAF**	**Depth (cm)**	**Electron SAF**	**Photon SAF**	**Depth (cm)**	**Electron SAF**	**Photon SAF**	**Depth (cm)**	**Electron SAF**	**Photon SAF**
0.005	7.88E-1	6.49E-2	**0.005**	7.86E-1	5.86E-2	**0.005**	7.71E-1	5.41E-2	**0.01**	7.04E-1	4.69E-2	**0.01**	6.79E-1	4.29E-2
0.015	6.91E-1	6.40E-2	**0.02**	6.79E-1	5.76E-2	**0.02**	6.87E-1	5.30E-2	**0.035**	6.28E-1	4.56E-2	**0.035**	6.05E-1	4.18E-2
0.025	6.14E-1	6.31E-2	**0.04**	5.73E-1	5.62E-2	**0.04**	6.19E-1	5.19E-2	**0.07**	5.49E-1	4.41E-2	**0.07**	5.44E-1	4.06E-2
0.035	5.68E-1	6.24E-2	**0.06**	5.09E-1	5.49E-2	**0.06**	5.67E-1	5.08E-2	**0.11**	4.82E-1	4.25E-2	**0.11**	4.83E-1	3.91E-2
0.045	5.08E-1	6.18E-2	**0.08**	4.61E-1	5.37E-2	**0.08**	5.12E-1	4.96E-2	**0.15**	2.11E-1	2.63E-2	**0.15**	2.21E-1	2.45E-2
0.055	4.55E-1	6.11E-2	**0.1**	4.05E-1	5.27E-2	**0.1**	4.70E-1	4.86E-2	**0.19**	1.86E-1	2.57E-2	**0.19**	2.02E-1	2.39E-2
0.065	4.09E-1	6.07E-2	**0.12**	3.74E-1	5.24E-2	**0.12**	4.25E-1	4.84E-2	**0.23**	1.64E-1	2.54E-2	**0.23**	1.83E-1	2.33E-2
0.075	3.71E-1	6.01E-2	**0.14**	1.51E-1	3.30E-2	**0.14**	1.76E-1	3.05E-2						
0.085	3.48E-1	5.93E-2	**0.16**	1.37E-1	3.27E-2	**0.16**	1.67E-1	3.00E-2						
0.095	3.14E-1	5.87E-2	**0.18**	1.19E-1	3.26E-2	**0.18**	1.57E-1	2.98E-2						
0.105	2.80E-1	5.81E-2	**0.2**	1.04E-1	3.21E-2	**0.2**	1.39E-1	2.95E-2						
0.115	2.63E-1	5.81E-2	**0.22**	8.63E-2	3.16E-2	**0.22**	1.28E-1	2.93E-2						
0.125	2.40E-1	5.75E-2	**0.24**	7.61E-2	3.13E-2	**0.24**	1.16E-1	2.90E-2						
0.135	9.33E-2	3.68E-2												
0.145	9.12E-2	3.69E-2												
0.155	8.32E-2	3.65E-2												
0.165	7.26E-2	3.65E-2												
0.175	6.20E-2	3.64E-2												
0.185	6.42E-2	3.59E-2												
0.195	5.25E-2	3.59E-2												
0.205	4.45E-2	3.57E-2												
0.215	4.11E-2	3.54E-2												
0.225	3.29E-2	3.52E-2												
0.235	3.10E-2	3.50E-2												
0.245	2.48E-2	3.47E-2												

APPENDIX C

RADIONUCLIDES WHICH HAVE A SECTION OF THE GASTROINTESTINAL TRACT AS A LIMITING FOR EXPOSURE

Table C1. Radionuclides of concern, annual limits on intake, ALI (Bq) and derived air concentrations, DAC (Bq/m^3) (40h/wk) for isotopes of different radionuclides critical to the GIT (ICRP 1979).

No.	Radio-nuclide	Oral (ALI)			No.	Radio-nuclide	Oral (ALI)		
		f_1	ST Wall	LLI Wall			f_1	ST Wall	LLI Wall
1	^{18}F	1	2×10^{9} (2×10^{9})	-	24	^{104}Tc	8×10^{-1}	8×10^{8} (1×10^{9})	-
2	^{35}S	1×10^{-1}	-	2×10^{8} (3×10^{8})	25	^{106}Ru	5×10^{-2}	-	7×10^{6} (9×10^{6})
3	^{38}Cl	1	6×10^{8} (9×10^{8})	-	26	^{102m}Rh	5×10^{-2}	-	5×10^{7} (5×10^{7})
4	^{39}Cl	1	8×10^{8} (1×10^{9})	-	27	^{105}Rh	5×10^{-2}	-	1×10^{8} (1×10^{8})
5	^{44}K	1	8×10^{8} (1×10^{9})	-	28	^{107}Rh	5×10^{-2}	3×10^{9} (3×10^{9})	-
6	^{45}K	1	1×10^{9} (2×10^{9})	-	29	^{102}Ag	5×10^{-2}	2×10^{9} (2×10^{9})	-
7	^{60}Cu	5×10^{-1}	1×10^{9} (1×10^{9})	-	30	^{106}Ag	5×10^{-2}	2×10^{9} (2×10^{9})	-
8	^{63}Zn	5×10^{-1}	9×10^{8} (9×10^{9})	-	31	^{111}Ag	5×10^{-2}	-	3×10^{7} (4×10^{7})
9	^{74m}Br	1	5×10^{8} (8×10^{8})	-	32	^{115}Ag	5×10^{-2}	1×10^{9} (1×10^{9})	-
10	^{74}Br	1	8×10^{8} (1×10^{9})	-	33	^{115}Cd	5×10^{-2}	-	3×10^{7} (4×10^{7})
11	^{75}Br	1	1×10^{9} (1×10^{9})	-	34	^{112}In	2×10^{-2}	6×10^{9} (9×10^{9})	-
12	^{80}Br	1	2×10^{9} (3×10^{9})	-	35	^{114m}In	2×10^{-2}	-	1×10^{7} (1×10^{7})
13	^{83}Br	1	2×10^{9} (3×10^{9})	-	36	^{119m}In	2×10^{-2}	1×10^{9} (2×10^{9})	-
14	^{84}Br	1	7×10^{8} (1×10^{9})	-	37	^{131m}Ba	1×10^{-1}	1×10^{10} (2×10^{10})	-
15	^{79}Rb	1	1×10^{9} (2×10^{9})	-	38	^{133m}Ba	1×10^{-1}	-	9×10^{7} (1×10^{8})
16	^{81m}Br	1	9×10^{9} (1×10^{10})	-	39	^{140}Ba	1×10^{-1}	-	2×10^{7} (2×10^{7})
17	^{88}Rb	1	7×10^{8} (1×10^{9})	-	40	^{177}Re	8×10^{-1}	4×10^{9} (4×10^{9})	-
18	^{89}Rb	1	1×10^{9} (2×10^{9})	-	41	^{178}Re	8×10^{-1}	3×10^{9} (4×10^{9})	-
19	^{90}Y	1×10^{-4}	-	2×10^{7} (2×10^{7})	42	^{186m}Re	8×10^{-1}	5×10^{7} (6×10^{7})	-
20	^{91}Y	1×10^{-4}	-	2×10^{7} (2×10^{7})	43	^{191}Os	1×10^{-2}	-	8×10^{7} (9×10^{7})
21	^{94}Y	1×10^{-4}	8×10^{8} (1×10^{9})	-	44	^{193}Os	1×10^{-2}	-	6×10^{7} (6×10^{7})
22	^{95}Y	1×10^{-4}	1×10^{9} (2×10^{9})	-	45	^{194}Os	1×10^{-2}	-	2×10^{7} (2×10^{7})
23	^{101}Tc	8×10^{-1}	3×10^{9} (5×10^{9})	-	46	^{182}Ir	1×10^{-2}	2×10^{9} (2×10^{9})	-

Table C1. Continued.

No.	Radionu-clide	Oral (ALI)			No.	Radio-nuclide	Oral (ALI)		
		f_1	ST Wall	LLI Wall			f_1	ST Wall	LLI Wall
47	^{189}Ir	1×10^{-1}	-	2×10^{8} (2×10^{8})	70	^{138}Cs	1	7×10^{8} (1×10^{9})	-
48	^{199}Au	1×10^{-1}	-	1×10^{8} (1×10^{8})	71	^{134}Ce	3×10^{-4}	-	2×10^{7} (2×10^{7})
49	^{201}Au	1×10^{-1}	3×10^{9} (3×10^{9})	-	72	^{137m}Ce	3×10^{-4}	-	9×10^{7} (9×10^{7})
50	^{199m}Hg	1	2×10^{9} (4×10^{9})	-	73	^{141}Ce	3×10^{-4}	-	6×10^{7} (7×10^{7})
51	^{199m}Hg	4×10^{-1}	2×10^{9} (2×10^{9})	-	74	^{143}Ce	3×10^{-4}	-	4×10^{7} (4×10^{7})
52	^{214}Bi	5×10^{-2}	6×10^{8} (8×10^{8})	-	75	^{144}Ce	3×10^{-4}	-	8×10^{6} (9×10^{6})
53	^{239}Np	1×10^{-2}	-	6×10^{7} (6×10^{7})	76	^{226}Th	2×10^{-4}	2×10^{8} (2×10^{8})	-
54	^{52m}Mn	1×10^{-1}	1×10^{9} (1×10^{9})	-	77	^{234}Th	2×10^{-4}	-	1×10^{7} (1×10^{7})
55	^{60m}Co	5×10^{-2}	4×10^{10} (5×10^{10})	-	78	^{234}Th	2×10^{-4}	-	1×10^{7} (1×10^{7})
56	^{60m}Co	3×10^{-1}	4×10^{10} (5×10^{10})	-	79	^{231}U	5×10^{-2}	-	2×10^{8} (2×10^{8})
57	^{62m}Co	5×10^{-2}	1×10^{9} (2×10^{9})	-	80	^{231}U	2×10^{-3}	-	2×10^{8} (2×10^{8})
58	^{62m}Co	3×10^{-1}	1×10^{9} (2×10^{9})	-	81	^{237}U	5×10^{-2}	-	6×10^{7} (7×10^{7})
59	^{89}Sr	1×10^{-2}	-	2×10^{7} (2×10^{7})	82	^{237}U	2×10^{-3}	-	6×10^{7} (7×10^{7})
60	^{88}Nb	1×10^{-2}	2×10^{9} (3×10^{9})	-	83	^{246m}Am	5×10^{-4}	2×10^{9} (2×10^{9})	-
61	^{93m}Nb	1×10^{-2}	-	3×10^{8} (4×10^{8})	84	^{244}Cf	5×10^{-4}	9×10^{8} (1×10^{9})	-
62	^{95m}Nb	1×10^{-2}	-	8×10^{7} (9×10^{7})	85	^{246}Cf	5×10^{-4}	-	1×10^{7} (2×10^{7})
63	^{99}Mo	5×10^{-2}	-	4×10^{7} (4×10^{7})	86	^{10}Be	5×10^{-3}	-	4×10^{7} (4×10^{7})
64	^{101}Mo	8×10^{-1}	2×10^{9} (2×10^{9})	-	87	^{32}Si	1×10^{-2}	-	8×10^{7} (1×10^{8})
65	^{101}Mo	5×10^{-2}	2×10^{9} (2×10^{9})	-	88	^{47}Sc	1×10^{-4}	-	8×10^{7} (1×10^{8})
66	^{128}I	1	2×10^{9} (2×10^{9})	-	89	^{47}V	1×10^{-2}	1×10^{9} (1×10^{9})	-
67	^{125}Cs	1	2×10^{9} (3×10^{9})	-	90	^{49}V	1×10^{-2}	-	3×10^{9} (3×10^{9})
68	^{130}Cs	1	2×10^{9} (4×10^{9})	-	91	^{66}Ni	5×10^{-2}	-	1×10^{7} (2×10^{7})
69	^{134m}Cs	1	4×10^{9} (4×10^{9})	-	92	^{65}Ga	1×10^{-3}	2×10^{9} (2×10^{9})	-

Table C1. Continued.

No.	Radio-nuclide	Oral (ALI)			No.	Radio-nuclide	Oral (ALI)		
		f_1	ST Wall	LLI Wall			f_1	ST Wall	LLI Wall
93	^{70}Ga	1×10^{-3}	2×10^{9} (3×10^{9})	-	116	^{120}Sb	1×10^{-2}	-	3×10^{7} (3×10^{7})
94	^{67}Ge	1.0	1×10^{9} (2×10^{9})	-	117	^{124m}Sb	1×10^{-1}	9×10^{9} (1×10^{10})	-
95	^{75}Ge	1.0	2×10^{9} (3×10^{9})	-	118	^{126m}Sb	1×10^{-1}	2×10^{9} (2×10^{9})	-
96	^{78}Ge	1.0	8×10^{8} (9×10^{8})	-	119	^{126m}Sb	1×10^{-2}	2×10^{9} (2×10^{10})	-
97	^{69}As	5×10^{-1}	1×10^{9} (2×10^{9})	-	120	^{127}Sb	1×10^{-1}	-	3×10^{7} (3×10^{7})
98	^{77}As	5×10^{-1}	-	2×10^{8} (2×10^{8})	121	^{127}Sb	1×10^{-2}	-	3×10^{7} (3×10^{7})
99	^{81}Se	8×10^{-1}	2×10^{9} (3×10^{9})	-	122	^{128}Sb	1×10^{-1}	3×10^{9} (4×10^{9})	-
100	^{81}Se	5×10^{-2}	2×10^{9} (3×10^{9})	-	123	^{128}Sb	1×10^{-2}	3×10^{9} (4×10^{9})	-
101	^{83}Se	8×10^{-1}	2×10^{9} (2×10^{9})	-	124	^{143}La	1×10^{-3}	1×10^{9} (1×10^{9})	-
102	^{103}Pd	5×10^{-3}	-	2×10^{8} (3×10^{8})	125	^{136}Pr	3×10^{-4}	2×10^{9} (3×10^{9})	-
103	^{107}Pd	5×10^{-3}	-	1×10^{9} (1×10^{9})	126	^{143}Pr	3×10^{-4}	-	3×10^{7} (4×10^{7})
104	^{113}Sn	2×10^{-2}	-	6×10^{7} (7×10^{7})	127	^{144}Pr	3×10^{-4}	1×10^{9} (2×10^{9})	-
105	^{117m}Sn	2×10^{-2}	-	6×10^{7} (7×10^{7})	128	^{147}Pr	3×10^{-4}	2×10^{9} (3×10^{9})	-
106	^{119m}Sn	2×10^{-2}	-	1×10^{8} (2×10^{8})	129	^{147}Nd	3×10^{-4}	-	4×10^{7} (5×10^{7})
107	^{121m}Sn	2×10^{-2}	-	1×10^{8} (1×10^{8})	130	^{141}Pm	3×10^{-4}	2×10^{9} (2×10^{9})	-
108	^{121}Sn	2×10^{-2}	-	2×10^{8} (2×10^{8})	131	^{147}Pm	3×10^{-4}	-	2×10^{8} (2×10^{8})
109	^{123}Sn	2×10^{-2}	-	2×10^{7} (2×10^{7})	132	^{148}Pm	3×10^{-4}	-	2×10^{7} (2×10^{7})
110	^{125}Sn	2×10^{-2}	-	1×10^{7} (2×10^{7})	133	^{149}Pm	3×10^{-4}	-	4×10^{7} (5×10^{7})
111	^{116}Sb	1×10^{-1}	3×10^{9} (3×10^{9})	-	134	^{141}Sm	3×10^{-4}	2×10^{9} (2×10^{9})	-
112	^{116}Sb	1×10^{-2}	3×10^{9} (3×10^{9})	-	135	^{151}Sm	3×10^{-4}	-	5×10^{8} (5×10^{8})
113	^{120}Sb	1×10^{-1}	4×10^{9} (6×10^{9})	-	136	^{153}Sm	3×10^{-4}	-	6×10^{7} (7×10^{7})
114	^{120}Sb	1×10^{-2}	4×10^{9} (6×10^{9})	-	137	^{155}Sm	3×10^{-4}	2×10^{9} (3×10^{9})	-
115	^{120}Sb	1×10^{-1}	-	3×10^{7} (3×10^{7})	138	^{145}Gd	3×10^{-4}	2×10^{9} (2×10^{9})	-

Table C1. Continued.

No.	Radio-nuclide	Oral (ALI)			No.	Radio-nuclide	Oral (ALI)		
		f_1	ST Wall	LLI Wall			f_1	ST Wall	LLI Wall
139	^{157}Tb	3×10^{-4}	-	2×10^{9} (2×10^{9})	162	^{185}W	3×10^{-1}	-	1×10^{8} (1×10^{8})
140	^{161}Tb	3×10^{-4}	-	6×10^{7} (7×10^{7})	163	^{188}W	1×10^{-2}	-	1×10^{7} (2×10^{7})
141	^{166}Dy	3×10^{-4}	-	2×10^{9} (3×10^{9})	164	^{188}W	3×10^{-1}	-	2×10^{7} (3×10^{7})
142	^{162}Ho	3×10^{-4}	2×10^{10} (3×10^{10})	-	165	^{193m}Pt	1×10^{-2}	-	9×10^{7} (1×10^{8})
143	^{164}Ho	3×10^{-4}	7×10^{9} (8×10^{9})	-	166	^{193}Pt	1×10^{-2}	-	1×10^{9} (2×10^{8})
144	^{166}Ho	3×10^{-4}	-	3×10^{7} (3×10^{7})	167	^{195m}Pt	1×10^{-2}	-	7×10^{7} (8×10^{7})
145	^{169}Er	3×10^{-4}	-	1×10^{8} (1×10^{8})	168	^{194m}Tl	1.0	2×10^{9} (3×10^{9})	-
146	^{172}Er	3×10^{-4}	-	4×10^{7} (5×10^{7})	169	^{194}Tl	1.0	9×10^{9} (1×10^{10})	-
147	^{162}Tm	3×10^{-4}	2×10^{9} (3×10^{9})	-	170	^{224}Ac	1×10^{-3}	-	7×10^{7} (7×10^{7})
148	^{167}Tm	3×10^{-4}	-	8×10^{7} (9×10^{7})	171	^{225}Ac	1×10^{-3}	-	2×10^{6} (2×10^{6})
149	^{170}Tm	3×10^{-4}	-	3×10^{7} (4×10^{7})	172	^{226}Ac	1×10^{-3}	-	5×10^{6} (5×10^{6})
150	^{171}Tm	3×10^{-4}	-	4×10^{8} (5×10^{8})	173	^{233}Pa	1×10^{-3}	-	5×10^{7} (6×10^{7})
151	^{172}Tm	3×10^{-4}	-	3×10^{7} (3×10^{7})	174	^{253}Es	5×10^{-4}	-	8×10^{6} (8×10^{6})
152	^{175}Tm	3×10^{-4}	2×10^{9} (3×10^{9})	-	175	^{254m}Es	5×10^{-4}	-	1×10^{7} (1×10^{7})
153	^{175}Yb	3×10^{-4}	-	1×10^{8} (1×10^{8})	176	^{253}Fm	5×10^{-4}	-	5×10^{7} (5×10^{7})
154	^{174m}Lu	3×10^{-4}	-	8×10^{7} (1×10^{8})	177	^{235}Np	1×10^{-3}	-	8×10^{8} (9×10^{8})
155	^{177}Lu	3×10^{-4}	-	8×10^{7} (9×10^{7})	178	^{239}Np	1×10^{-3}	-	6×10^{7} (6×10^{7})
156	^{178m}Lu	3×10^{-4}	2×10^{9} (2×10^{9})	-	179	^{246}Pu	1×10^{-3}	-	1×10^{7} (1×10^{7})
157	^{178}Lu	3×10^{-4}	1×10^{9} (2×10^{9})	-	180	^{246}Pu	1×10^{-4}	-	1×10^{7} (1×10^{7})
158	^{182m}Ta	1×10^{-3}	6×10^{9} (8×10^{9})	-	181	^{246}Pu	1×10^{-5}	-	1×10^{7} (1×10^{7})
159	^{183}Ta	1×10^{-3}	-	3×10^{7} (4×10^{7})	182	^{244m}Am	1×10^{-3}	2×10^{9} (3×10^{9})	-
160	^{186}Ta	1×10^{-3}	2×10^{9} (3×10^{9})	-	183	^{246m}Am	1×10^{-3}	2×10^{9} (2×10^{9})	-
161	^{185}W	1×10^{-2}	-	8×10^{7} (1×10^{8})	184	^{244}Cf	1×10^{-3}	9×10^{8} (1×10^{9})	-

Table C1. Continued.

No.	Radio-nuclide	Oral (ALI)			No.	Radio-nuclide	Oral (ALI)		
		f_1	ST Wall	LLI Wall			f_1	ST Wall	LLI Wall
185	^{154m}Es	1×10^{-3}	-	1×10^{7} (1×10^{7})					
186	^{82}Sr	1×10^{-2}	-	7×10^{6} (9×10^{6})					
187	^{116}Sb	1×10^{-1}	3×10^{9} (3×10^{9})	-					
188	^{116}Sb	1×10^{-2}	3×10^{9} (3×10^{9})	-					

VITA

Md. Nasir Uddin Bhuiyan is the son of Ali Ahmed Bhuiyan and Salma Ali of Chandpur, Bangladesh. He received a B.Sc. and M.Sc. in physics from the University of Dhaka, Dhaka, Bangladesh, in 1985 and 1986, respectively. The Bangladesh Atomic Energy Commission then employed him as a Health Physicist until he entered the health physics graduate program in the Department of Nuclear Engineering at Texas A&M University, College Station, Texas in September 1998.

Mr. Bhuiyan received his M.S. in health physics and Ph.D. in nuclear engineering from Texas A&M University in August 2000 and August 2003, respectively. He became a member of the faculty in the Department of Radiology at Baylor College of Medicine, Houston, Texas in January 2003.

Mr. Bhuiyan can be reached through his work place at One Baylor Plaza, Department of Radiology, BCM 360, Houston, Texas, 77030-3498.